UNIVERSIDADE FEDERAL DE SANTA CATARINA
CENTRO TECNOLÓGICO
PROGRAMA DE PÓS-GRADUAÇÃO EM ENGENHARIA AMBIENTAL

Magali Teresinha Ritter

Soluções ambientalmente amigáveis para o tratamento de meios aquosos contendo corantes têxteis: Zeólitas procedentes de resíduos e biomassa bacteriana

Florianópolis
2024

Programa de Doctorado en Química Aplicada
Departamento de Geología y Geoquímica
Facultad de Ciencias de la Universidad Autónoma de Madrid

Soluciones ambientalmente amigables para el tratamiento de medios acuosos conteniendo colorantes textiles: Zeolitas procedentes de residuos y biomasa bacteriana

TESIS DOCTORAL

Tesis doctoral presentada a la Universidade Federal de Santa Catarina y a la Universidad Autónoma de Madrid en cumplimiento parcial de los requisitos para el grado de Doctor en Ingeniería Ambiental y Química Aplicada

Magali Teresinha Ritter

Supervisores:
Dr. María Ángeles Lobo Recio
Dr. Isabel Padilla Rodríguez

Co-supervisor:
Maria Eliza Nagel Hassemer

Tutor:
Jaime Fernando Cuevas Rodríguez

Instituto de Ciencias de la Construcción EDUARDO TORROJA
CSIC
Consejo Superior de Investigaciones Científicas

Instituto de Ciencias de la Construcción Eduardo Torroja
Consejo Superior de Investigaciones Científicas

Florianópolis/Madrid
2024

Magali Teresinha Ritter

Soluções ambientalmente amigáveis para o tratamento de meios aquosos contendo corantes têxteis: Zeólitas procedentes de resíduos e biomassa bacteriana

Tese submetida ao Programa de Pós-Graduação em Engenharia Ambiental da Universidade Federal de Santa Catarina e ao Programa de Química Aplicada da Universidad Autónoma de Madrid em regime de cotutela para a obtenção do título de Doutora em Engenharia Ambiental e em Química Aplicada.

Orientadoras: Profa. María Ángeles Lobo Recio, Dra. (Universidade Federal de Santa Catarina – UFSC) e Isabel Padilla Rodríguez, Dra. (Consejo Superior de Investigaciones Científicas – CSIC)

Coorientadora: Profa. Maria Eliza Nagel Hassemer, Dra. (UFSC)

Supervisor: Prof. Jaime Fernando Cuevas Rodríguez, Dr. (Universidad Autónoma de Madrid – UAM)

Florianópolis/Madrid

2024

Magali Teresinha Ritter

Environmentally friendly solutions for the treatment of aqueous media containing textile dyes: Waste-based zeolites and bacterial biomass

Thesis submitted to the Postgraduate Program in Environmental Engineering at the Federal University of Santa Catarina and the Applied Chemistry Program at the Autonomous University of Madrid on a co-tutorial basis to obtain a PhD in Environmental Engineering and Applied Chemistry.
Advisors: Prof. María Ángeles Lobo Recio, Dr. (Universidade Federal de Santa Catarina – UFSC) e Isabel Padilla Rodríguez, Dr. (Superior Council for Scientific Research – CSIC)
Co-advisor: Prof. Maria Eliza Nagel Hassemer, Dr. (UFSC)
Supervisor: Prof. Jaime Fernando Cuevas Rodríguez, Dr. (Autonomous University of Madrid – UAM)

Florianópolis/Madrid
2024

Ficha catalográfica gerada por meio de sistema automatizado gerenciado pela BU/UFSC.
Dados inseridos pelo próprio autor.

Ritter, Magali Teresinha
Soluções ambientalmente amigáveis para o tratamento de meios aquosos contendo corantes têxteis : Zeólitas procedentes de resíduos e biomassa bacteriana / Magali Teresinha Ritter ; orientadora, María Ángeles Lobo-Recio, coorientadora, Isabel Padilla, coorientadora, Maria Eliza Nagel-Hassemer, 2024.
230 p.

Tese (doutorado) - Universidade Federal de Santa Catarina, Centro Tecnológico, Programa de Pós-Graduação em Engenharia Ambiental, Florianópolis, 2024.

Inclui referências.

1. Engenharia Ambiental. 2. Soluções de tratamento. 3. Corantes têxteis. 4. Adsorção usando zeólitas baseadas em resíduos. 5. Células de Combustível Microbianas (CCMs). I. Lobo-Recio, María Ángeles. II. Padilla, Isabel. III. Nagel Hassemer, Maria Eliza IV. Universidade Federal de Santa Catarina. Programa de Pós-Graduação em Engenharia Ambiental. V. Título.

Magali Teresinha Ritter

Environmentally friendly solutions for the treatment of aqueous media containing textile dyes: Waste-based zeolites and bacterial biomass

This work at doctoral level was evaluated and approved on November 22, 2024, by the examining board composed of the following members:

Prof. José Manuel Moreno Maroto, Dr.
Autonomous University of Madrid – UAM

Prof. Flávio Rubens Lapolli, Dr.
Federal University of Santa Catarina – UFSC

Prof. Elise Sommer Watzko, Dr.
Federal University of Santa Catarina – UFSC

Prof. Dr. Luisa Barbieri
University of Modena and Reggio Emilia – UNIMORE

Prof. Sol López Andrés, Dr.
Complutense University of Madrid – UCM

We certify that this is the original and final version of the final work that was deemed suitable for obtaining the title of Doctor of Environmental Engineering and Applied Chemistry.

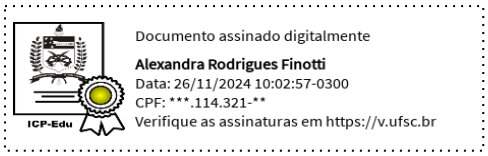

Postgraduate Program Coordination

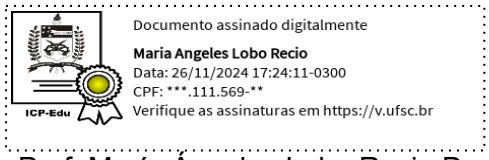

Prof. María Ángeles Lobo Recio Dr.
Supervisor

Florianópolis/Madrid
2024.

I dedicate this work to my dear supervisors María Ángeles, Isabel, Aurora and Maria Eliza.

ACKNOWLEDGMENTS

To my greatest encourager, friend, companion, my great love, my husband Allan Rabello, who from the very first moment pushed me to keep studying, to believe in myself, to grow. This achievement is also yours! Thank you for dreaming and making this dream come true with me!

To all my family, especially my siblings Monalisa and Matheus, my nephew Davi and above all my parents, Márcia and Milton, for their support and unconditional love, for the education they gave me and for always being with me in my happiest and most difficult moments.

To my dear friends, those who make life more beautiful, lighter, and happier, especially Amanda Schimdt, Luciana Malfussi, Diandra Teixeira, Cristiane de Souza, Natália Silvério, Jéssica Prats, Luciana Vieira and Joacir Marques, who are true gifts that life has given me.

To the entire Rabello family, who have always been there for me.

To María Maqueda, Sandra, Raúl and Janeth who welcomed me so warmly and were my family during my stay in Madrid. Os quiero!

To my dear supervisor, Prof. Dr. María Ángeles Lobo Recio, for all her guidance and immense dedication over the years, helping me at all times to do my best. Thank you so much for believing in my potential, for supporting me, for correcting me and for constantly encouraging me. Without you, none of this would have been possible and I will be grateful for that all my life!

To my co-supervisor, dear Prof. Dr. Maria Eliza Nagel Hassemer, who has been by my side since I was an undergraduate, encouraging me and helping me to reach higher heights. Thank you for being with me on this journey.

To my co-supervisor Dr. Isabel Padilla, for all the teachings shared, for all her guidance and help, which were fundamental to perfecting my research. I will never forget her efforts to help me obtain the co-tutorship agreement with the UAM, or her loving hugs every morning.

To Dr. Aurora López Delgado for all the guidance, teachings and knowledge shared. For welcoming me to the IETcc and introducing me to the fantastic world of zeolites. For all her patience, support and help so that I could carry out my research in the best possible way.

To Dr. Maximina Romero, for all the shared experiences and teachings. For all the support and help in polishing my work.

Those fantastic women, mothers, friends and professionals with whom I had the pleasure of living, and who took me in, taught me and shared so many lessons with me. You are examples that I want to follow in my life. Thank you for everything!

To the CSIC, the IETcc and especially the MEDES Group for welcoming me with open doors during my stay in Spain, for providing all the necessary infrastructure, equipment and materials, making it possible to carry out my doctoral research. I would also like to thank the other members of the IETcc, especially Esther Garrido, Rafael Carrizosa, Virginia Martín, Sara Mateo and Jefferson Adrian for all their help. Also to Dr. Ana Guerrero, Belén Merino, Cristina Carrillo, Hector Cruz and José Manuel Llueca, for their help in analyzing the samples.

To the members of LaRA who have been part of the research group over the years, especially Ketley Costa, Thamires Custodio, Ana Carla Sorgato, Carlos Eduardo Lach, Gabriel Tochetto and Amanda Dalalibera, for all their help. I would also like to thank Prof. Dr. Daniele da Silveira for sharing her experience, helping with the analysis of the microbial community.

To GemBac, especially Amanda Hecktheuer and Professor Ricardo Mazzon for introducing me to the world of microbiology and for making it possible to carry out an important stage of my research.

To Eliel Romancini and Prof. Dr. Ricardo Moraes, from the Department of Energy and Sustainability at UFSC, Araranguá Campus, for their help in setting up the electronic device for measuring and recording the MFC's electrical parameters.

To the Universidad Autónoma de Madrid, the Department of Geology and Geochemistry and the Doctoral Program in Applied Chemistry, especially the director Prof. Dr. Miguel Remacha Moreno and the coordinator Prof. Dr. Jesús Procopio Rodríguez for all their guidance and for helping me during the registration process and the signing of the co-tutorship agreement.

To my tutor, Prof. Dr. Jaime Cuevas, for accepting the invitation to be my tutor and for all his help in assessing and validating the necessary documentation and also for his contributions to improving the thesis.

To the Postgraduate Program in Environmental Engineering, the Department of Sanitary and Environmental Engineering and the Federal University of Santa Catarina for all the infrastructure made available.

CASAN for supplying the anaerobic sludge samples. To Herba Ricemills S.L.U. (Spain) for providing the rice husk ash sample and Alusigma S.A. (Spain) for supplying the salt slag sample and also to Industrias Químicas del Ebro, S.A. (Spain) for giving the commercial sample of LTA zeolite used as a reference sample.

To the members of the thesis examination board, for accepting the invitation and for the time they dedicated to evaluating and contributing to the improvement of this research.

To the National Council for Scientific and Technological Development (CNPq) for granting me a doctoral scholarship and to the Coordination for the Improvement of Higher Education Personnel (CAPES) for funding the research project under the Capes-PrInt Program, process no. 88887.310573/2018-00, which made my sandwich doctoral exchange possible.

RESUMO

A contaminação dos recursos hídricos por águas residuais poluídas com corantes é uma grande preocupação ambiental. No intento de contribuir com soluções para minimizar a depleção das fontes de água e a contaminação do meio ambiente, este estudo reporta a aplicação de tecnologias de tratamento ambientalmente amigáveis desenvolvidas a partir de fontes renováveis e sustentáveis, na descoloração de diferentes corantes têxteis, Índigo Carmim (IC) e Safranina-T (ST) como modelos de corante aniônico e catiônico, respectivamente. Para esse propósito foram utilizadas *i)* tecnologia de adsorção a partir de zeólitas adsorventes sintetizadas à base resíduos industriais e agrícolas como fontes de alumínio e silício e *ii)* biomassa bacteriana e tecnologia bioeletroquímica usando Célula de Combustível Microbiana (CCM). Na primeira etapa desta pesquisa, diferentes tipos de zeólitas altamente cristalinas, NaP, LTA e SOD, foram sintetizadas a partir da combinação exclusiva, pela primeira vez, dos resíduos de escórias salinas de alumínio e cinzas de casca de arroz (CCA) como matérias-primas não convencionais de baixo custo. As zeólitas foram obtidas mediante distintas condições experimentais de síntese hidrotermal e sol-gel, demonstrando seu papel fundamental no desenvolvimento e cristalização de fases específicas de zeólita. A zeólita NaP foi obtida por síntese hidrotermal e as zeólitas LTA e SOD via síntese sol-gel. Enquanto maiores concentrações de sódio resultaram na obtenção da zeólita SOD, a formação da zeólita LTA foi favorecida em temperaturas mais elevadas e tempos de envelhecimento prolongados. A aplicação da zeólita LTA à base de resíduos de alumínio como agente de tratamento neste estudo demonstrou sua elevada eficiência (>98%) e celeridade (<1 min) na descoloração do corante catiônico ST de soluções aquosas. Esses resultados foram superiores inclusive aos da zeólita LTA comercial, o que destaca suas excelentes propriedades adsorventes, representando uma alternativa promissora e sustentável ao uso de adsorventes produzidos a partir de reativos químicos comerciais. Além disso, o mecanismo de remoção identificado como sendo fisissorção, sugere interações fracas e reversíveis entre as moléculas do corante e a superfície da zeólita, permitindo regenerações sucessivas do material adsorvente via dessorção. Na segunda etapa do estudo, a remoção biológica bem-sucedida (>96%) do corante aniônico IC foi alcançada usando a cultura bacteriana *Pseudomonas aeruginosa*. Enquanto isso, na CCM de câmara única inoculada com lodo anaeróbio, o corante IC, embora tenha gerado maiores potenciais de bioeletricidade, teve um desempenho de descoloração aquém ao do corante ST, o qual superou notáveis 93% de eficiência de remoção. Os resultados evidenciaram o excelente desempenho das estratégias de tratamento empregadas, especialmente na eliminação do corante catiônico, destacando a grande influência da estrutura molecular e da natureza iônica desses poluentes nos processos de tratamento. A interação eletrostática das partículas negativamente carregadas das zeólitas e também da biomassa bacteriana com as cargas superficiais positivas do corante ST em solução possibilitaram a remoção via adsorção, enquanto a eliminação do corante IC só foi alcançada via biodegradação, devido ao seu caráter aniônico. O desenvolvimento e a aplicação dessas tecnologias emergentes e inovadoras representam um avanço para a área ambiental, oferecendo alternativas complementares aos métodos convencionais de tratamento e contribuindo para a preservação ambiental, a economia circular e a sustentabilidade.

Palavras-chave: soluções de tratamento; corantes têxteis; adsorção; zeólitas baseadas em resíduos; Célula de Combustível Microbiana (CCM); descoloração.

ABSTRACT

The contamination of water resources by dye-polluted wastewater is a major environmental concern. In an attempt to contribute to solutions to minimize the depletion of water sources and the environmental contamination, this study reports on the application of eco-friendly treatment technologies developed from renewable and sustainable sources, in the decolorization of different textile dyes, Indigo Carmine (IC) and Safranine-T (ST) as anionic and cationic dye models, respectively. For this purpose, *i)* adsorption technology using adsorbent zeolites synthesized from industrial and agricultural waste as sources of aluminum and silicon and *ii)* bacterial biomass and bioelectrochemical technology using the Microbial Fuel Cell (MFC) were used. In the first stage of this research, different types of highly crystalline zeolites, NaP, LTA and SOD, were synthesized from the exclusive combination, for the first time, of aluminum salt slag waste and rice husk ash (RHA) as unconventional, low-cost raw materials. The zeolites were obtained using different experimental conditions of hydrothermal and sol-gel synthesis, demonstrating their fundamental role in the development and crystallization of specific zeolite phases. The NaP zeolite was obtained by hydrothermal synthesis and the LTA and SOD zeolites via sol-gel synthesis. While higher sodium concentrations resulted in the SOD zeolite, the formation of the LTA zeolite was favored at higher temperatures and longer aging times. The application of LTA zeolite based on aluminum waste as a treatment agent in this study demonstrated its high efficiency (>98%) and speed (<1 min) in decolorizing the cationic dye ST from aqueous solutions. These results were even superior to those of commercial LTA zeolite, which highlights its excellent adsorbent properties, representing a promising and sustainable alternative to the use of adsorbents produced from commercial chemical reagents. In addition, the removal mechanism identified as physisorption suggests weak and reversible interactions between the dye molecules and the zeolite surface, allowing successive regenerations of the adsorbent material via desorption. In the second stage of the study, successful biological removal (>96%) of the anionic IC dye was achieved using the bacterial culture *Pseudomonas aeruginosa*. Meanwhile, in the single chamber MFC inoculated with anaerobic sludge, the IC dye, although it generated higher bioelectricity potentials, had a lower decolorization performance than the ST dye, which exceeded a remarkable 93% removal efficiency. The results showed the excellent performance of the treatment strategies employed, especially in the elimination of cationic dye, highlighting the great influence of the molecular structure and ionic nature of these pollutants on the treatment processes. The electrostatic interaction of the negatively charged particles of the zeolites and also of the bacterial biomass with the positive surface charges of the ST dye in solution enabled removal via adsorption, while elimination of the IC dye was only achieved via biodegradation, due to its anionic character. The development and application of these emerging and innovative technologies represents a breakthrough for the environmental field, offering complementary alternatives to conventional treatment methods and contributing to environmental preservation, the circular economy and sustainability.

Keywords: treatment solutions; textile dyes; adsorption; waste-based zeolites; Microbial Fuel Cell (MFC); decolorization.

RESUMEN

La contaminación de los recursos hídricos debida a las aguas residuales contaminadas con colorantes es una gran preocupación medioambiental. Con el objetivo de aportar soluciones para minimizar la disminución de las fuentes de agua y la contaminación ambiental, este estudio aborda la aplicación de tecnologías de tratamiento ambientalmente amigables desarrolladas a partir de fuentes renovables y sostenibles, para la decoloración de diferentes colorantes textiles, Índigo Carmín (IC) y Safranina-T (ST) como modelos de colorante aniónico y catiónico, respectivamente. Para ello, se utilizaron *i)* tecnología de adsorción utilizando zeolitas adsorbentes sintetizadas a partir de residuos industriales y agrícolas como fuentes de aluminio y silicio y *ii)* biomasa bacteriana y tecnología bioelectroquímica utilizando una Celda de Combustible Microbiana (CCM). En la primera etapa de esta investigación, se sintetizaron diferentes tipos de zeolitas altamente cristalinas, NaP, LTA y SOD, a partir de la combinación exclusiva, por primera vez, de residuos de escorias salinas de aluminio y cenizas de cáscara de arroz (CCA) como materias primas no convencionales y de bajo coste. Las zeolitas se obtuvieron bajo diferentes condiciones experimentales mediante síntesis hidrotermal y sol-gel, demostrando su papel fundamental en el desarrollo y cristalización de fases específicas de zeolita. La zeolita NaP se obtuvo mediante síntesis hidrotermal y las zeolitas LTA y SOD se obtuvieron mediante síntesis sol-gel. Mientras que las concentraciones más altas de sodio dieron lugar a la zeolita SOD, la formación de la zeolita LTA se vio favorecida a temperaturas más altas y tiempos de envejecimiento más largos. La aplicación de la zeolita LTA obtenida mediante a partir de residuos de aluminio como agente de tratamiento en este estudio demostró su alta eficiencia (>98%) y rapidez (<1 min) en la decoloración del colorante catiónico ST en disoluciones acuosas. Estos resultados fueron incluso superiores a los obtenidos con una zeolita LTA comercial, lo que pone de manifiesto sus excelentes propiedades adsorbentes, y la convierte en una alternativa prometedora y sostenible frente a los adsorbentes obtenidos a partir de reactivos químicos comerciales. Además, el mecanismo de eliminación identificado como fisisorción sugiere interacciones débiles y reversibles entre las moléculas de colorante y la superficie de la zeolita, permitiendo sucesivas regeneraciones del material adsorbente mediante desorción. En la segunda etapa del estudio, se logró la eliminación biológica con éxito (>96%) del colorante aniónico IC utilizando la bacteria *Pseudomonas aeruginosa*. Mientras tanto, en la CCM de cámara única inoculada con lodo anaerobio, el colorante IC, aunque generó mayores potenciales de bioelectricidad, su rendimiento de decoloración fue inferior al del colorante ST, que superó la notable eficiencia de eliminación del 93%. Los resultados mostraron el excelente rendimiento de las estrategias de tratamiento empleadas, especialmente en la eliminación del colorante catiónico, destacando la gran influencia de la estructura molecular y la naturaleza iónica de estos contaminantes en los procesos de tratamiento. La interacción electrostática de las partículas cargadas negativamente de las zeolitas y también de la biomasa bacteriana con las cargas superficiales positivas del colorante ST en disolución permitió la eliminación mediante adsorción, mientras que la eliminación del colorante IC sólo se consiguió mediante biodegradación, debido a su carácter aniónico. El desarrollo y aplicación de estas tecnologías emergentes e innovadoras representan un gran avance para el campo medioambiental, ofreciendo alternativas complementarias a los métodos de tratamiento convencionales y contribuyendo a la preservación del medio ambiente, la economía circular y la sostenibilidad.

Palabras clave: disoluciones de tratamiento; colorantes textiles; adsorción; zeolitas a base de residuos; Celda de Combustible Microbiana (CCM); decoloración.

RESUMO EXPANDIDO

Introdução

A poluição dos recursos hídricos devida às águas residuais contaminadas com corantes é uma grande preocupação ambiental. Os corantes figuram entre os principais contaminantes presentes nos efluentes devido à sua produção em larga escala e ampla aplicação em diversas áreas, especialmente no setor têxtil. Destaque no cenário econômico mundial, nacional e também catarinense, as indústrias têxteis têm uma cadeia produtiva conhecida pelo elevado consumo de água e pela geração de grandes volumes de efluentes com elevado potencial poluidor, sendo apontadas como uma das principais poluidoras dos recursos de água doce. A descarga de corantes nos ecossistemas aquáticos, mesmo em pequenas concentrações, pode acarretar sérios impactos ao meio ambiente e aos seres vivos, tendo em vista a natureza tóxica, xenobiótica e recalcitrante da maioria desses compostos. A elevada solubilidade, complexidade estrutural e baixa biodegradabilidade dos corantes torna inefetivos os métodos convencionais de tratamento comumente utilizados. Além disso, diferentes tipos de corantes podem requerer a aplicação de tecnologias distintas para sua efetiva remoção. Nesse contexto, os esforços das pesquisas têm se concentrado na busca por soluções de tratamento alternativas para a eliminação desses componentes tóxicos e biologicamente prejudiciais dos efluentes antes da sua disposição no meio ambiente, com particular ênfase nos processos desenvolvidos sob bases renováveis e sustentáveis. Dentre essas tecnologias, a adsorção é considerada uma das mais promissoras para a remediação de águas residuais contendo corantes. Embora já consolidada e com vantagens bastante conhecidas, como design e operação simplificados, baixo custo e elevada eficiência, essa técnica tem ganhado crescente atenção apoiada no conceito de “tratar resíduos com resíduos”, a partir do desenvolvimento de novos materiais adsorventes de baixo custo, com destaque para as zeólitas (SHU et al., 2023). As zeólitas são materiais microporosos cristalinos que devido às suas propriedades únicas têm sido extensivamente utilizadas em diversas aplicações industriais como adsorventes, trocadores iônicos, catalisadores, peneiras moleculares, materiais de membranas, sensores químicos, entre outros (ABDEL HAMEED et al., 2020). Embora disponíveis na natureza, as zeólitas podem ser sintetizadas a partir de uma grande variedade de fontes de alumínio e silício, preservando assim os recursos minerais e resultando na obtenção de materiais sob medida com características mais uniformes, maior grau de pureza e de capacidade de troca iônica (EL BOJADDAYNI et al., 2023). Nos últimos anos, em lugar de reativos químicos comerciais, diversos resíduos têm sido testados como matérias-primas não convencionais na produção de zeólitas com o intuito de reduzir os custos de produção, oferecer uma alternativa sustentável para a gestão desses resíduos e ainda mitigar os impactos ambientais associados. Considerando as suas ricas composições, as escórias salinas e as CCA são consideradas potenciais candidatas a precursoras de alumínio e silício, respectivamente, na síntese de diferentes zeólitas. As escórias salinas são o principal subproduto gerado pela indústria de reciclagem do alumínio, sendo consideradas um resíduo perigoso devido especialmente às suas características tóxicas, inflamáveis, lixiviáveis e altamente reativas. Enormes quantidades deste resíduo são produzidas todos os anos, e a sua disposição é um sério problema ambiental. Elencadas no Catálogo Europeu de Resíduos Perigosos (EWC, 2001), quando em contato com a água ou até mesmo com a umidade do ar, as escórias salinas liberam gases tóxicos como H_2, H_2S, PH_3, NH_3 and CH_4, cujas emissões na atmosfera são extremamente prejudiciais. As CCA, por sua vez, são o mais abundante resíduo agro-indrustrial e, embora não sejam consideradas perigosas

como as escórias salinas, sua deposição em aterros e lenta biodegradação também causam impactos ao meio ambiente. Por se tratar de um material rico em silício, a sua utilização como componente na síntese de zeólitas representa uma nova e mais adequada rota ao seu gerenciamento. Assim, a partir da co-reciclagem desses resíduos podem ser obtidos materiais adsorventes úteis e que não requerem um processamento físico prévio (separação, pulverização, etc.) para aplicação como agentes de tratamento (LOBO-RECIO et al., 2021). Mais recentemente, outra estratégia de tratamento que tem atraído grande interesse dos pesquisadores é o uso de cepas específicas de bactérias ou de consórcios microbianos para a biodegradação de substâncias poluentes. Surgem então as tecnologias bioeletroquímicas com o uso de Células de Combustível Microbianas (CCMs). As CCMs são biorreatores capazes de converter a energia química contida nas ligações de compostos orgânicos e inorgânicos diretamente em energia elétrica através de reações catalisadas por microrganismos (LOGAN; REGAN, 2006). Uma das aplicações mais promissoras desses dispositivos é, justamente, no tratamento de efluentes, usando os poluentes contidos nos efluentes como substrato para o metabolismo bacteriano. Os mecanismos envolvidos no processo de geração de energia são bastante complexos e dependem de muitos fatores, dentre eles o design da célula, materiais dos eletrodos, substrato e condições experimentais (GUL et al., 2021). Ademais, os microrganismos eletroativos desempenham um papel central atuando como biocatalisadores responsáveis tanto pela degradação dos poluentes quanto pela transferência de elétrons, possibilitando assim a produção de eletricidade. Apesar de limitações relacionadas aos potenciais de energia gerados, custos dos componentes e escalabilidade, as CCMs apresentam inúmeras vantagens sobre as tecnologias usuais de tratamento de águas residuais, oferecendo uma combinação de processos biológicos e eletroquímicos, elevado desempenho na remoção de corantes e geração mínima de lodo, além de serem sistemas autossustentáveis, permitindo a geração de eletricidade de maneira limpa e sustentável a partir de fontes renováveis. O desenvolvimento e implementação das tecnologias mencionadas abre novos caminhos em direção a soluções mais ambientalmente amigáveis para a eliminação de corantes das águas residuais, contribuindo à preservação ambiental, à economia circular e à sustentabilidade.

Objetivos

O objetivo principal deste estudo consistiu na avaliação da performance de tratamento de duas soluções inovativas e promissoras, a adsorção utilizando zeólitas sintetizadas a partir de resíduos e tecnologias biológicas de tratamento, via biorremediação (usando a bactéria *Pseudomonas aeruginosa*) e tecnologia bioeletroquímica (usando uma CCM inoculada com lodo anaeróbio), aplicadas ao tratamento de diferentes tipos de corantes têxteis, o corante aniônico Índigo Carmim (IC) e o corante catiônico Safranina-T (ST).

Metodologia

A presente pesquisa foi desenvolvida em duas etapas principais. A primeira etapa concentrou-se na síntese de zeólitas a partir de resíduos e nos estudos de adsorção aplicando as zeólitas sintetizadas a meios aquosos contendo IC ou ST. A segunda foi dedicada a estudos de biodescoloração dos corantes por meio de uma cepa de *P. aeruginosa* e a estudos bioeletroquímicos usando uma CCM para tratamento das soluções de corantes e geração simultânea de energia elétrica limpa. Para tanto, inicialmente foi realizado o processamento dos resíduos de escórias salinas e CCA,

utilizados como precursores alternativos de alumínio e silício, respectivamente, à síntese das zeólitas. As escórias salinas foram hidrolisadas para remover o excesso de sal e as CCA calcinadas para eliminar o material carbonáceo. Soluções de aluminato e silicato foram produzidas a partir da dissolução alcalina das escórias hidrolisadas e das CCA calcinadas usando hidróxido de sódio (NaOH) 5M e 3M, respectivamente. As zeólitas foram produzidas através de dois diferentes processos: síntese hidrotermal usando as escórias de alumínio hidrolisadas e o silicato e, síntese sol-gel a partir das soluções de silicato e aluminato. Distintas condições experimentais de síntese foram testadas. Após a obtenção e caracterização das zeólitas adsorventes, aplicando a zeólita à base de resíduos do tipo LTA, foram conduzidos os estudos cinéticos e isotérmicos de adsorção dos corantes IC e ST em regime de batelada. Na segunda etapa da pesquisa, foi realizado o tratamento biológico dos corantes através de um estudo cinético de biorremediação usando uma cultura pura bacteriana de *P. aeruginosa*, examinando o efeito de diferentes tipos e concentrações de corantes, agitações e concentrações do meio de crescimento. Além disso, a remoção biológica dos corantes também foi avaliada através da aplicação da tecnologia bioeletroquímica utilizando uma CCM de câmara única inoculada com lodo anaeróbio. Além da performance de descoloração de diferentes concentrações dos corantes, também foram determinadas as remoções de matéria orgânica, o potencial de geração de bioeletricidade, a fitotoxicidade e a análise da comunidade microbiana.

Resultados e Discussão

No estágio inicial desta pesquisa, diferentes tipos de zeólitas altamente cristalinas, NaP, LTA e SOD, foram sintetizadas sob condições moderadas a partir da combinação, pela primeira vez, de escórias salinas de alumínio e CCA como matérias-primas não convencionais. A obtenção das diferentes fases de zeólitas foi alcançada usando distintas condições experimentais de síntese. A zeólita do tipo NaP foi sintetizada através de um processo hidrotermal e as condições experimentais ótimas que levaram a sua formação foram 105 ºC de temperatura durante 20 horas. A síntese sol-gel resultou nas zeólitas LTA e SOD, ambas obtidas a 70 ºC, e foram necessárias 6 e 24 horas para a formação da zeólita SOD e LTA, respectivamente. Os resultados indicaram que as condições experimentais desempenham um papel crucial no desenvolvimento de uma fase específica de zeólita. Concentrações mais elevadas de sódio promoveram a formação da zeólita SOD, enquanto a zeólita LTA foi obtida a temperaturas mais elevadas e tempos de envelhecimento prolongados. A zeólita do tipo LTA a base de resíduos apresentou um perfil mineralógico muito semelhante ao da zeólita comercial, com picos de Difração de Raios-X (DRX) bem desenvolvidos e intensidades ligeiramente superiores, demonstrando sua promissora aplicabilidade como material adsorvente. A aplicação da zeólita LTA produzida a partir de resíduos de alumínio como agente de tratamento neste estudo demonstrou sua elevada eficiência (>98%) na descoloração do corante catiônico ST de soluções aquosas. Nas condições experimentais ótimas de agitação (147 rpm) e dosagem de zeólita (21.5 g L^{-1}), além de eficiente, o processo de adsorção, que seguiu uma cinética de pseudo-primeira ordem, foi extremamente rápido, alcançando a remoção quase completa do corante em apenas 1 minuto de tempo de contato. O melhor ajuste dos dados experimentais ao modelo isotérmico de Sips sugeriu que o mecanismo de remoção foi a fisissorção, indicando interações fracas e reversíveis entre as moléculas do corante e a superfície da zeólita, o que é vantajoso do ponto de vista de reutilização do material adsorvente uma vez que facilita o processo de dessorção. Isso indica que o mecanismo de remoção do corante catiônico ST está intimamente ligado à natureza

das interações eletrostáticas estabelecidas com a superfície da zeólita, que tem uma superfície carregada negativamente. A zeólita LTA a base de resíduos mostrou resultados superiores em comparação a outros tipos de zeólitas testadas, inclusive à zeólita LTA comercial, destacando as excelentes propriedades adsorventes da zeólita sintetizada para o tratamento de águas residuais contendo corantes, provendo, dessa forma, uma alternativa sustentável ao uso de adsorventes produzidos com reativos comerciais, reduzindo o consumo de recursos e, ao mesmo tempo, ajudando a melhorar a qualidade da água e a mitigar a poluição ambiental. A segunda etapa desta pesquisa produziu informações valiosas, especialmente relacionadas ao efeito das estruturas moleculares dos diferentes tipos de corantes na sua degradação por meio de processos biológicos e bioeletroquímicos. Com relação à biodescoloração dos corantes têxteis usando cultura microbiana pura, foi observado que *P. aeruginosa* se comportaram de maneira oposta na remoção do IC e ST. Enquanto a eficiência de remoção do corante catiônico diminuiu à medida que crescentes concentrações iniciais foram aplicadas, o corante aniônico IC seguiu a tendência de aumento e alcançou eficiências de remoção notáveis (> 96%), mesmo quando testadas as maiores cargas de corante (500 mg L^{-1}). A efetiva descoloração do IC foi atingida em 8 horas, embora 90% da remoção tenha ocorrido nas primeiras 3 horas. Os resultados foram atribuídos aos mecanismos de remoção empregados pelas bactérias nos diferentes corantes: via biodegradação para o corante aniônico e via biossorção para o catiônico. Inferiu-se que a descoloração do corante IC teve lugar por meio da atividade enzimática de *P. aeruginosa,* cuja capacidade de clivagem de ligações (C-S) é reconhecida, beneficiada pela presença de grupos sulfonados na estrutura do mesmo. A biossorção do corante IC não é favorecida considerando o seu caráter aniônico, que dificulta a interação eletrostática com a biomassa bacteriana, cuja superfície celular é igualmente negativamente carregada. Em contraste, as partículas positivamente carregadas do corante ST em solução, são atraídas pelas cargas elétricas e aderidas às paredes celulares da biomassa microbiana, levando à descoloração via biossorção, evidenciada pela presença de um precipitado de células fortemente coloridas após a centrifugação das amostras. Com relação às condições experimentais, para ambos os corantes, melhores resultados foram obtidos sob agitação, o que se explica pelo fato de que ambos os mecanismos de remoção são favorecidos nessa circunstância, tanto a atividade enzimática (biodegradação) quanto a transferência de massa externa (biossorção). A concentração do meio de crescimento bacteriano, por sua vez, não exerceu um efeito estatisticamente significativo no processo de biodescoloração dos corantes. Por fim, a avaliação do desempenho da tecnologia bioeletroquímica usando CCM de câmara única inoculada com uma cultura mista de lodo anaeróbio demonstrou sua excelente habilidade no tratamento de altas concentrações do corante catiônico ST, alcançando uma taxa de remoção > 93% em 24 horas. Por outro lado, a remoção da Demanda Química de Oxigênio (DQO), a geração de bioeletricidade e os resultados da análise fitotóxica foram melhores na presença do corante aniônico IC. Durante o tratamento do corante IC, as máximas voltagem de saída, densidade de corrente e densidade de potência foram 300 mV, 210,58 mA m^{-2} e 34,54 mW m^{-2}, respectivamente. As grandes diferenças registradas em resposta ao tratamento dos corantes sugeriram que a capacidade de tratamento do sistema CCM foi severamente afetada pelas diferenças estruturais moleculares dos corantes. Assim como na biodescoloração, as CCMs também dependem de microrganismos para catalisar os processos de descoloração e transferência eletrônica, o que, em última instância, promove a geração de bioenergia. Nesse sentido, a maior afinidade entre as partículas superficias

negativamente carregadas (devido aos fosfolipídios e lipopolissacarídeos) da biomassa microbiana mista (assim como na cultura pura) e a forma iônica carregada positivamente do corante ST em solução, embora permita seu excelente desempenho de descoloração por meio da biossorção, desfavorece o mecanismo de transferência de elétrons, reduzindo as densidades de corrente e energia produzidas. Enquanto isso, o potencial redox mais alto do corante aniônico IC e a presença de grupos sulfonados (fortes aceptores de elétrons) levaram à sua redução eletroquímica e à transferência de uma densidade maior de elétrons para o ânodo, proporcionando um aumento na geração de corrente na CCM. Isso também explica os diferentes efeitos fitotóxicos dos corantes, uma vez que a natureza eletrostática permite que a ST interaja mais facilmente com as membranas celulares das sementes de *Lactuca sativa* usadas como bioindicadores, sendo seus efeitos tóxicos potencialmente maiores em comparação com o IC. A análise da comunidade microbiana revelou que os gêneros mais abundantes encontrados no biofilme da CCM ao final dos experimentos foram *Rhodopseudomonas* (46%), pertencentes ao filo *Proteobacteria* (62%), reconhecidas como bactérias eletroativas capazes de degradar uma ampla gama de compostos complexos, inclusive corantes. Os índices de diversidade e riqueza microbiana foram menores no biofilme aclimatado do que no inóculo, evidenciando que o compartimento anódico da CCM e a presença de IC e ST proporcionaram um ambiente oportuno ao desenvolvimento de microrganismos exoeletrogênicos e degradadores de corantes, o que favoreceu significativamente o desempenho da descoloração e a geração de bioeletricidade do sistema.

Considerações Finais

Esta pesquisa destaca a valorização de resíduos industriais, especialmente os resíduos perigosos de alumínio e as CCA, através da sua conversão em zeólitas, como uma alternativa sustentável ao seu gerenciamento, minimizando o uso de recursos naturais e contribuindo para a economia circular por meio da simbiose entre diferentes segmentos industriais. Além disso, a excelente capacidade adsorvente demonstrada pela zeólita LTA sintetizada representa uma solução ambientalmente amigável para a remediação de águas residuais contaminadas com corantes, especialmente os corantes catiônicos. Nesse sentido, este estudo evidenciou que tanto a tecnologia de adsorção quanto o tratamento bioeletroquímico usando a CCM culminaram na descoloração mais bem-sucedida do corante catiônico enquanto que o melhor desempenho de remoção do corante aniônico foi obtido por meio da descoloração biológica usando uma cultura pura de *P. aeruginosa*. Isso confirma a influência da estrutura molecular e da natureza iônica dos corantes como elementos fundamentais para o aprimoramento dos processos de tratamento de águas residuais têxteis. Dessa forma, as estratégias de tratamento apresentadas representam alternativas atraentes, promissoras e sustentáveis, fornecendo soluções de baixo custo e ambientalmente amigáveis em comparação aos métodos convencionais.

Palavras-chave: tratamento de efluentes; corantes têxteis; adsorção; zeólitas baseadas em resíduos; Célula de Combustível Microbiana (CCM); descoloração.

RESUMEN AMPLIADO

Introducción

La contaminación de los recursos hídricos debida a las aguas residuales contaminadas con colorantes es una gran preocupación ambiental. Los colorantes se encuentran entre los principales contaminantes presentes en los efluentes debido a su producción a gran escala y a su amplia aplicación en diversas áreas, especialmente en el sector textil. Las industrias textiles, que tienen un papel destacado en la economía mundial, nacional y también en la de Santa Catarina, se caracterizan por presentar una cadena productiva conocida por su elevado consumo de agua y por generar grandes volúmenes de efluentes con alto potencial contaminante, siendo identificadas como una de las principales fuentes de contaminación de los recursos de agua dulce. El vertido de colorantes en los ecosistemas acuáticos, incluso en pequeñas concentraciones, puede causar un grave impacto al medio ambiente y a los seres vivos, debido a la naturaleza tóxica, xenobiótica y persistente de la mayoría de estos compuestos. La elevada solubilidad, la complejidad estructural y la baja biodegradabilidad de los colorantes hacen que los métodos convencionales de tratamiento sean ineficaces. Además, los distintos tipos de colorantes pueden requerir la aplicación de tecnologías diferentes para su eliminación eficaz. En este contexto, los esfuerzos de investigación se han centrado en la búsqueda de soluciones alternativas para la eliminación de estos componentes tóxicos y biológicamente nocivos de los efluentes antes de su vertido en el medio ambiente, haciendo especial hincapié en los procesos desarrollados sobre bases renovables y sostenibles. Entre estas tecnologías, la adsorción se considera una de las más prometedoras para la remediación de las aguas residuales que contienen colorantes. Aunque ya está totalmente consolidada y cuenta con ventajas bien conocidas, como su diseño y operación simplificados, bajo coste y alta eficiencia, esta técnica ha recibido una creciente atención basada en el concepto de “tratar residuos con residuos”, mediante el desarrollo de nuevos materiales adsorbentes de bajo coste, particularmente zeolitas (SHU et al., 2023). Las zeolitas son materiales microporosos cristalinos que, debido a sus propiedades únicas, se han utilizado ampliamente en diversas aplicaciones industriales como adsorbentes, intercambiadores de iones, catalizadores, tamices moleculares, materiales de membrana, sensores químicos, entre otros (ABDEL HAMEED et al., 2020). Aunque están disponibles en la naturaleza, las zeolitas pueden ser sintetizadas a partir de una gran variedad de fuentes de aluminio y silicio, preservando así los recursos minerales y dando lugar a la obtención de materiales a medida con características más uniformes, un mayor grado de pureza y capacidad de intercambio iónico (EL BOJADDAYNI et al., 2023). En los últimos años, en lugar de reactivos químicos comerciales, se han utilizado diversos residuos como materias primas no convencionales en la producción de zeolitas con el objetivo de reducir los costes de producción, ofrecer una alternativa sostenible para la gestión de estos residuos y mitigar también los impactos ambientales asociados. Considerando su composición, las escorias salinas y las cenizas de cáscara de arroz (CCA) se pueden considerar candidatos potenciales como precursores de aluminio y silicio, respectivamente, para la síntesis de diferentes zeolitas. Las escorias salinas son el principal subproducto generado por la industria de reciclado de aluminio y se consideran un residuo peligroso debido a sus características tóxicas, inflamables, lixiviables y altamente reactivas. Cada año se producen enormes cantidades de estos residuos, y su disposición constituye un grave problema medioambiental. Incluidas en el Catálogo Europeo de Residuos Peligrosos (EWC, 2001), cuando las escorias

salinas entran en contacto con el agua o incluso con la humedad del aire, liberan gases tóxicos como H_2, H_2S, PH_3, NH_3 y CH_4, cuyas emisiones a la atmósfera son extremadamente nocivas. Las CCA, por su parte, son el residuo agroindustrial más abundante y, aunque no se considera tan peligrosas como la escoria salina, su disposición en vertederos y su lenta biodegradación también causan un grave impacto medioambiental. Al tratarse de un material rico en silicio, su utilización como componente en la síntesis de zeolitas representa una nueva y más adecuada vía para su gestión. Así, mediante el co-reciclado de estos residuos, se pueden obtener materiales adsorbentes útiles que no requieren un procesado físico previo (separación, pulverización, etc.) para su aplicación como agentes de tratamiento (LOBO-RECIO et al., 2021). Más recientemente, otra estrategia de tratamiento que ha atraído gran interés entre los investigadores es el uso de cepas específicas de bacterias o consorcios microbianos para la biodegradación de sustancias contaminantes. Surgen así las tecnologías bioelectroquímicas con el uso de las Celdas de Combustible Microbianas (CCM). Las CCM son biorreactores capaces de convertir la energía química contenida en los enlaces de compuestos orgánicos e inorgánicos directamente en energía eléctrica mediante reacciones catalizadas por microorganismos (LOGAN; REGAN, 2006). Una de las aplicaciones más prometedoras de estos dispositivos es, precisamente, el tratamiento de efluentes, utilizando los contaminantes contenidos en los efluentes como sustrato para el metabolismo bacteriano. Los mecanismos implicados en el proceso de generación de energía son bastante complejos y dependen de muchos factores, entre ellos el diseño de la célula, los materiales de los electrodos, el sustrato y las condiciones experimentales (GUL et al., 2021). Además, los microorganismos electroactivos desempeñan un papel central al actuar como biocatalizadores responsables tanto de la degradación de contaminantes como de la transferencia de electrones, permitiendo así la producción de electricidad. A pesar de las limitaciones relacionadas con el potencial energético generado, los costes de los componentes y la escalabilidad, las CCM presentan numerosas ventajas frente a las tecnologías convencionales de tratamiento de aguas residuales, ofreciendo una combinación de procesos biológicos y electroquímicos, un alto rendimiento en la eliminación de colorantes y una mínima generación de lodos, además de ser sistemas autosuficientes que permiten generar electricidad de forma limpia y sostenible a partir de fuentes renovables. El desarrollo e implementación de estas tecnologías abre nuevos caminos hacia soluciones más respetuosas con el medio ambiente para la eliminación de colorantes de las aguas residuales, contribuyendo a la preservación del medio ambiente, la economía circular y la sostenibilidad.

Objetivos

El objetivo principal de este estudio consistió en evaluar el rendimiento del tratamiento de dos soluciones innovadoras y prometedoras: la adsorción utilizando zeolitas sintetizadas a partir de residuos y las tecnologías de tratamiento biológico, mediante biorremediación (utilizando la bacteria *Pseudomonas aeruginosa*) y tecnología bioelectroquímica (utilizando un CCM inoculada con lodo anaerobio). Estas tecnologías se aplicaron para la eliminación de diferentes tipos de colorantes textiles, el colorante aniónico Índigo Carmín (IC) y el colorante catiónico Safranina-T (ST).

Metodología

La presente investigación se desarrolló en dos etapas principales. La primera etapa se centró en la síntesis de zeolitas a partir de residuos y en los estudios de adsorción

aplicando las zeolitas sintetizadas a medios acuosos conteniendo IC o ST. La segunda etapa se dedicó a los estudios de biodecoloración de los colorantes mediante una cepa de *P. aeruginosa* y a estudios bioelectroquímicos utilizando una CCM para el tratamiento de las disoluciones de colorantes y la generación simultánea de electricidad limpia. Para ello, inicialmente se procesaron los residuos de escorias salinas y CCA, utilizados como precursores alternativos de aluminio y silicio, respectivamente, para la síntesis de zeolitas. La escoria salina se hidrolizó para eliminar el exceso de sal y el CCA se calcinó para eliminar el material carbonáceo. Las disoluciones de aluminato y silicato se obtuvieron a partir de la disolución alcalina de las escorias hidrolizadas y las CCA calcinadas utilizando hidróxido de sodio(NaOH) 5M y 3M, respectivamente. Las zeolitas se sintetizaron mediante dos procesos diferentes: síntesis hidrotermal utilizando la escoria de aluminio hidrolizada y silicato, y síntesis sol-gel a partir de dos disoluciones de silicato y aluminato. Se ensayaron diferentes condiciones experimentales de síntesis. Tras la obtención y caracterización de las zeolitas adsorbentes, se utilizó la zeolita tipo LTA para realizar estudios cinéticos e isotérmicos de adsorción de los colorantes IC y ST en régimen discontinuo. En la segunda etapa de la investigación, se llevó a cabo el tratamiento biológico de los colorantes mediante un estudio cinético de biorremediación utilizando un cultivo bacteriano puro de *P. aeruginosa*, examinando el efecto de diferentes tipos y concentraciones de colorantes, agitación y concentraciones del medio de crecimiento. Además, también se evaluó la eliminación biológica de los colorantes mediante la aplicación de la tecnología bioelectroquímica utilizando un CCM de cámara única inoculada con lodo anaerobio. Además del rendimiento de decoloración a diferentes concentraciones de los colorantes, también se determinaron la eliminación de materia orgánica, el potencial de generación de bioelectricidad, la fitotoxicidad y el análisis de la comunidad microbiana.

Resultados y discusión

En la fase inicial de esta investigación, se sintetizaron diferentes tipos de zeolitas altamente cristalinas, NaP, LTA y SOD, bajo condiciones moderadas a partir de la combinación, por primera vez, de escoria salina de aluminio y CCA como materias primas no convencionales. La obtención de las distintas fases de zeolitas se logró utilizando diferentes condiciones experimentales de síntesis. La zeolita de tipo NaP se sintetizó mediante un proceso hidrotermal y las condiciones experimentales óptimas para su formación fueron 105 ºC de temperatura durante 20 horas. La síntesis sol-gel dio lugar a las zeolitas LTA y SOD, ambas obtenidas a 70 ºC, se necesitaron 6 y 24 horas para la formación de la zeolita SOD y LTA, respectivamente. Los resultados indicaron que las condiciones experimentales desempeñan un papel crucial en el desarrollo de una fase específica de zeolita. Concentraciones más altas de sodio promovieron la formación de la zeolita SOD, mientras que la zeolita LTA se obtuvo a temperaturas más altas y tiempos de envejecimiento prolongados. La zeolita LTA obtenida a partir de residuos presentó un perfil mineralógico muy similar al de la zeolita comercial, con picos de Difracción de Rayos X (DRX) bien desarrollados e intensidades ligeramente superiores, lo que demuestra su prometedora aplicabilidad como material adsorbente. La aplicación de la zeolita LTA producida a partir de residuos de aluminio como agente de tratamiento demostró su alta eficiencia (>98%) en la decoloración del colorante catiónico ST en disoluciones acuosas. En las condiciones experimentales óptimas de agitación (147 rpm) y dosis de zeolita (21,5 g L^{-1}), el proceso de adsorción, siguió una cinética de pseudo-primer orden, fue extremadamente rápido, alcanzando una eliminación casi completa del colorante en

tan sólo 1 minuto de tiempo de contacto. El mejor ajuste de los datos experimentales al modelo de isoterma de Sips sugirió que el mecanismo de eliminación fue la fisisorción, indicando interacciones débiles y reversibles entre las moléculas de colorante y la superficie de la zeolita, lo cual es muy ventajoso desde el punto de vista de la reutilización del material adsorbente, ya que facilita el proceso de desorción. Esto indica que el mecanismo de eliminación del colorante catiónico ST está estrechamente relacionado con la naturaleza de las interacciones electrostáticas con la superficie de la zeolita, que tiene una superficie cargada negativamente. La zeolita LTA obtenida a partir de residuos presenta una capacidad de intercambio catiónico mayor en comparación con otros tipos de zeolitas ensayadas, incluida la zeolita LTA comercial, destacando así las excelentes propiedades adsorbentes de la zeolita sintetizada para el tratamiento de aguas residuales que contienen colorantes, proporcionando una alternativa sostenible al uso de adsorbentes producidos con reactivos comerciales, reduciendo el consumo de recursos y, al mismo tiempo, contribuyendo a mejorar la calidad del agua y a mitigar la contaminación ambiental. La segunda etapa de esta investigación proporcionó información valiosa, especialmente relacionada con el efecto de las estructuras moleculares de los diferentes tipos de colorantes sobre su degradación mediante procesos biológicos y bioelectroquímicos. En cuanto a la biodecoloración de los colorantes textiles utilizando cultivos microbianos puros, se observó que *P. aeruginosa* se comportó de forma opuesta en la eliminación de IC y ST. Mientras que la eficiencia de eliminación del colorante catiónico disminuyó a medida que se aplicaban concentraciones iniciales crecientes, el colorante aniónico IC mostró una tendencia ascendente y alcanzó eficiencias de eliminación notables (>96%), incluso con las cargas de colorante más altas (500 mg L^{-1}). La decoloración efectiva del IC se logró en 8 horas, aunque el 90% de la eliminación se produjo en las 3 primeras horas. Los resultados se atribuyeron a los mecanismos de eliminación empleados por las bacterias en los distintos colorantes: biodegradación para el colorante aniónico y biosorción para el colorante catiónico. Se dedujo que la decoloración del colorante IC tuvo lugar mediante la actividad enzimática de *P. aeruginosa*, cuya capacidad de romper enlaces (C-S) es conocida, y se ve potenciada por la presencia de grupos sulfonados en la estructura del colorante. La biosorción del colorante IC no se encuentra favorecida debido a su naturaleza aniónica, lo que dificulta la interacción electrostática con la biomasa bacteriana, cuyas partículas superficiales también están cargadas negativamente. Por el contrario, las partículas cargadas positivamente del colorante ST en disolución son atraídas por las cargas eléctricas de las bacterias y se adhieren a las paredes celulares de la biomasa microbiana, conduciendo a la decoloración mediante biosorción, evidenciada por la presencia de un precipitado de células fuertemente coloreadas tras centrifugar las muestras. En cuanto a las condiciones experimentales, para ambos colorantes, los mejores resultados se obtuvieron bajo agitación, que se explica por el hecho de que ambos mecanismos de eliminación, tanto la actividad enzimática (biodegradación) como la transferencia de masa externa (biosorción), se encuentran favorecidos en esta circunstancia. Por otra parte, la concentración del medio de crecimiento bacteriano no tuvo un efecto estadísticamente significativo en el proceso de biodecoloración de los colorantes. Por último, la evaluación del rendimiento de la tecnología bioelectroquímica utilizando CCM de cámara única inoculada con un cultivo mixto de lodo anaerobio demostró su excelente capacidad para tratar altas concentraciones del colorante catiónico ST, alcanzando una tasa de eliminación > 93% en 24 horas. Por otro lado, la eliminación de Demanda Química de Oxígeno (DQO), la generación de bioelectricidad y los resultados del análisis fitotóxico fueron

mejores en presencia del colorante aniónico IC. Durante el tratamiento del colorante IC, el voltaje de salida máximo, la densidad de corriente y la densidad de potencia fueron de 300 mV, 210,58 mA m^{-2} y 34,54 mW m^{-2}, respectivamente. Las grandes diferencias registradas en respuesta al tratamiento de los colorantes sugirieron que la capacidad de tratamiento del sistema CCM se vio severamente afectada por las diferencias estructurales moleculares de los colorantes. Así como en la biodecoloración, la CCM también dependen de los microorganismos para catalizar los procesos de decoloración y transferencia de electrones, lo que en última instancia, promueve la generación de bioenergía. En este sentido, la mayor afinidad entre las partículas superficiales cargadas negativamente (debido a los fosfolípidos y lipopolisacáridos) de la biomasa microbiana mixta (así como en el cultivo puro) y la forma iónica cargada positivamente del colorante ST en disolución da lugar a un excelente rendimiento de decoloración mediante biosorción; no obstante, se desfavorece el mecanismo de transferencia de electrones, se reducen las densidades de corriente y, también, la energía producida. Por otra parte, el mayor potencial redox del colorante aniónico IC y la presencia de grupos sulfonados (fuertes aceptores de electrones) llevaron a su reducción electroquímica y a la transferencia de una mayor densidad de electrones al ánodo, proporcionando un aumento en la generación de corriente en la CCM. Esto también explica los diferentes efectos fitotóxicos de los colorantes, ya que la naturaleza electrostática permite que la ST interactúe más fácilmente con las membranas celulares de las semillas de *Lactuca sativa*, utilizadas como bioindicadores, siendo sus efectos tóxicos potencialmente mayores en comparación con IC. El análisis de la comunidad microbiana reveló que los géneros más abundantes encontrados en el biofilm de la CCM al final de los experimentos fueron *Rhodopseudomonas* (46%), pertenecientes al filo *Proteobacteria* (62%), reconocidas como bacterias electroactivas capaces de degradar una amplia gama de compuestos complejos, incluidos los colorantes. Los índices de diversidad y riqueza microbiana fueron menores en el biofilm aclimatado que en el inóculo, lo que demuestra que el compartimento anódico de la CCM y la presencia de IC y ST proporcionaron un entorno propicio para el desarrollo de microorganismos exoelectrogénicos y degradadores de colorantes, lo que favoreció significativamente el rendimiento de decoloración y la generación de bioelectricidad del sistema.

Consideraciones finales

Esta investigación destaca la valorización de residuos industriales, especialmente los residuos peligrosos de aluminio y CCA, a través de su conversión en zeolitas, como una alternativa sostenible para su gestión, minimizando el uso de recursos naturales y contribuyendo a la economía circular mediante la simbiosis entre diferentes sectores industriales. Además, la excelente capacidad de adsorción demostrada por la zeolita LTA sintetizada representa una solución respetuosa con el medio ambiente para la remediación de aguas residuales contaminadas con colorantes, especialmente por colorantes catiónicos. En este sentido, este estudio demostró que tanto la tecnología de adsorción como el tratamiento bioelectroquímico utilizando una CCM resultaron en la decoloración del colorante catiónico, mientras que el mejor rendimiento para la eliminación del colorante aniónico se obtuvo mediante decoloración biológica utilizando un cultivo puro de *P. aeruginosa*. Esto confirma la influencia de la estructura molecular y la naturaleza iónica de los colorantes como elementos fundamentales para mejorar los procesos de tratamiento de aguas residuales textiles. De este modo, las estrategias de tratamiento presentadas representan alternativas atractivas,

prometedoras y sostenibles, proporcionando soluciones de bajo coste y respetuosas con el medio ambiente frente a los métodos convencionales.

Palabras clave: tratamiento de aguas residuales; colorantes textiles; adsorción; zeolitas a base de residuos; Celda de Combustible Microbiana (CCM); decoloración.

LIST OF FIGURES

LIST OF TABLES

LIST OF ABBREVIATIONS AND ACRONYMS

ANOVA – Analysis of Variance
APHA – American Public Health Association
ARE – Average Relative Error
ASS – Aluminum Salt Slag
ATCC – American Type Culture Collection
BJH – Barrett-Joyner-Halenda Method
BOD – Biochemical Oxygen Demand
CAPES – Foundation for the Improvement of Higher Education Personnel
CAS – Chemical Abstracts Service
CASAN – Santa Catarina Water and Sanitation Company
CCRD – Central Composite Rotational Design
CE – Coulombic Efficiency
CEC – Cation Exchange Capacity
CI – Colour Index
CND – Coefficient of Nondetermination
CNPq – National Council for Scientific and Technological Development
COD – Chemical Oxygen Demand
CRHA – Calcined Rice Husk Ash
CSIC – Superior Council for Scientific Research
D-R – Dubinin-Radushkevish
EDS – Energy Dispersive Spectroscopy
EWC – European Waste Catalogue and Hazardous Waste List
FAO – Organization of the United Nations for Food and Agriculture
FTIR – Fourier Transform Infrared Spectroscopy
FWHM – Full Width at Half Maximum
GDE – Gas Diffusion Electrode
GDL – Gas Diffusion Layer
GemBac – Laboratory of Molecular Genetics of Bacteria
HRT – Hydraulic Retention Time
HS – Hydrolyzed Slag
IC – Indigo Carmine
ICDD – International Centre for Diffraction Data

ICP-OES – Inductively Coupled Plasma Optical Emission Spectrometer

ID – Intraparticle Diffusion

IETcc – Eduardo Torroja Institute for Construction Sciences

IUPAC – International Union of Pure and Applied Chemistry

LaRA – Water Reuse Laboratory

LB – Luria Bertani Broth

LOI – Loss of Ignition

LTA – Linde Type-A

MEA – Membrane Electrode Assembly

MFC – Microbial Fuel Cell

NaP – Sodium Zeolite P-type

NaX – Sodium Zeolite X-type

OD – Optical density

OTU – Number of Unique Species

PBS – Phosphate Buffer Solution

PDF – Powder Diffraction File

PFO – Pseudo First Order

PrInt – Institutional Internationalization Programme

PROPG – Rectorate of Postgraduate Studies

PTFE – Polytetrafluoroethylene

PSO – Pseudo Second Order

RHA – Rice Husk Ash

R-P – Redlich-Peterson

RPM – Rotation per Minute

RRG – Relative Root Growth

rRNA – Ribosomal Ribonucleic Acid

RT – Room Temperature

SEM – Scanning Electron Microscopy

SG – Seed Germination

SNE – Sum of Normalized Errors

SOD – Sodalite

SS – Salt Slag

ST – Safranine-T

TG/DTA – Thermogravimetric Analysis and Differential Thermal Analysis

UAM – Autonomous University of Madrid

UFSC – Federal University of Santa Catarina

UN – United Nations

UNEP – United Nations Environment Programme

UV-Vis – Ultraviolet/Visible Radiation

XRD – X-Ray Diffraction

XRF – X-Ray Fluorescence

ZCOM – Commercial Zeolite

LIST OF SYMBOLS

® - Registered trademark

3D – Three-dimensional

A – Ampere

Å – Amstrong

Al_2MgO_4 – Spinel

D – Crystallite size

J – Joule

M – Molar

meq – Milliequivalent

$Na_{12}Al_{12}Si_{12}O_{48}.27H_2O$ – LTA zeolite

$Na_6Al_6Si_{10}O_{32}.12H_2O$ – NaP zeolite

$Na_8Al_6Si_6O_{24}.(OH)_2.2H_2O$ – SOD zeolite

nm - Nanometer

Pz – Zeta potential

R^2 – Coefficient of determination

Rad – Radian

R_{ext} – External resistance

S_{BET} – Brunauer-Emmett-Teller surface area

S_{Ext} – External surface area

™ – Unregistered trademark

UV-H_2O_2 – Ultraviolet radiation/Hydrogen peroxide

V - Volts

W – Watts

Wt.% – Weight percent

λ – Wavelength

μm – Micrometer

Ω – Ohm

TABLE OF CONTENTS

1 CHAPTER I: INTRODUCTORY REMARKS

1.1 CONTEXT AND JUSTIFICATION

The scarcity of drinking water is already an alarming reality in contemporary society, and the demand for fresh water is expected to increase by up to 30% by 2050 (SINGH; DAHIYA; MISHRA, 2021). Even earlier, in 2030, it is estimated that approximately 47% of the world's population will have to deal with a shortage of clean water (AL-TOHAMY et al., 2022).

Contributing to this scenario are population growth and rapid industrial development, which have led to an increase in energy demand, unbridled use of natural resources and an ever-increasing generation of polluting waste and effluents, which end up in the environment, contaminating water sources.

Water pollution due to dye-containing wastewater is a major environmental issue. The presence of dyes as one of the main pollutants in effluents is due to their large-scale production and widespread application in many areas, such as the textile, cosmetics, food and pulp and paper sectors (KAMEL et al., 2021; SIEREN et al., 2020).

Standing out as one of the main players on the world economic scene, the textile sector is considered the largest consumer of freshwater resources for its production chain and generates large volumes of highly polluting effluents, releasing around 200 billion liters of dye-contaminated wastewater into the environment every year (N LOTHA et al., 2024; TKACZYK; MITROWSKA; POSYNIAK, 2020). This sector alone consumes 80% of the annual global production of around 1,000,000 tons of dyes and accounts for approximately 20% of global water pollution, ranking second among water-polluting industries, leaded by petrochemicals (LIN et al., 2023; PERIYASAMY, 2024; UNEP, 2018).

In textile production, the enormous waste of dyes varies between 5% and 50% from the total used, depending on the type of dye and fabric, so it is estimated that a staggering 280,000 tons of dyes are lost to the environment every year worldwide (DUTTA et al., 2024; MISHRA; MAITI, 2018; TKACZYK; MITROWSKA; POSYNIAK, 2020).

When discharged into aquatic ecosystems, even in small amounts (concentrations above 1 mg L^{-1} are visually noticeable), textile dyes result in the

deterioration of water quality, affecting its aesthetic value, reducing oxygen availability, light penetration, impairing photosynthetic function and, finally, triggering biomagnification, which significantly impacts aquatic life (HOLKAR et al., 2016; LI et al., 2021; SINGH; DAHIYA; MISHRA, 2021).

In addition, due to their xenobiotic nature and the presence of aromatic compounds such as naphthalene, benzamine and other intermediates, dyes are associated with many risks when they enter the human body, ranging from skin allergies, reproductive disorders, alterations to the immune system and central nervous system, to DNA damage, chromosomal aberrations and genetic dysfunctions (SINGH; DAHIYA; MISHRA, 2021; TARA et al., 2020).

According to Fallah et al. (FALLAH et al., 2021), in recent years, the concentration of organic pollutants, including dyes, has increased considerably, from nano to micrograms per liter in effluents, fresh- and drinking water. Data from the World Health Organization (WHO) demonstrate that around 80% of illnesses are due to water contamination (VAN DEN BERG et al., 2019). Thus, the discharge of wastewater containing dyes into water bodies increases the risk of exposure to these compounds, posing a threat to human health.

This has prompted environmental protection agencies and the relevant legislation, especially in developed countries, to become increasingly strict and restrict the permissible limits, requiring the complete elimination of dyes from wastewater before they are discharged into the environment (SULEMAN et al., 2021).

However, as conventional treatment technologies are unable to meet the established criteria without compromising the economic benefits, the majority of textile industries are currently located in developing countries (ISMAIL; SAKAI, 2022), where around 80% of textile effluents continue to be disposed without adequate treatment or used directly in farm irrigation, causing contamination of soil, ground- and surface water (LIN et al., 2023).

Synthetic dyes have been designed to resist the effects of time, exposure to light, perspiration and washing, among others. However, the color fastness, resistance and stability of dyes, while conferring greater quality to textile products, also make it extremely difficult to remove them from wastewater, rendering commonly used treatments ineffective (VALLI NACHIYAR; SUSEELA RAJAKUMAR, 2004). In addition, modifications to the molecular structure of dyes, such as the introduction of

sulphonic acid groups to increase their solubility in water, make them more resistant to biological degradation (VALLI NACHIYAR; SUSEELA RAJAKUMAR, 2004).

Owing to their high solubility, complex chemistry and low biodegradability, the decolorization of dyes is quite challenging. The physical-chemical methods conventionally used (coagulation-flocculation, membrane filtration, ozonation, electrolysis, etc.) have several limitations, are inefficient, cost-intensive, generate secondary pollutants and large volumes of sludge to be managed (SRIVASTAVA et al., 2022; TACAS et al., 2021). Furthermore, there are numerous types of dyes, which may require the employment of different technologies for their effective removal. In this regard, among the various ways of classifying dyes, the most influential is based on the ionic form of the dyes when in solution, differentiating them into anionic (direct, acidic and reactive dyes), cationic (all basic dyes) and non-ionic (disperse dyes) (YAGUB et al., 2014).

Anionic dyes carry a negative charge in their molecule and produce colored anions in solution, while cationic dyes give rise to positive ions (SALLEH et al., 2011). This interferes, for example, with coagulation-flocculation processes, which are one of the most widely used in wastewater treatment plants; since the method is based on neutralizing the surface charges of suspended particles by adding positively charged coagulating agents, it proves inefficient for removing cationic dyes (ISMAIL; SAKAI, 2022; SRIVASTAVA et al., 2022).

In this sense, it is necessary and urgent to propose alternative strategies. However, more than efficient and economical, the new demand calls for ecologically acceptable solutions developed under the aegis of sustainability (RAMYA; SENTHIL KUMAR, 2022). In view of this, and with the intention of adding pieces of knowledge to help curb the depletion of water resources, this research focused on more environmentally friendly treatment solutions developed on a renewable and sustainable basis to eradicate different types of dyes, both anionic and cationic, from wastewater. To this end, two different wastewater treatment technologies were studied: firstly, adsorption using zeolites synthesized from waste and secondly, biotechnological techniques, using bioremediation and the bioelectrochemical technology of the Microbial Fuel Cell (MFC).

Adsorption is one of the most potentially attractive alternatives for the separation and elimination of dyes from wastewater, due to its high efficiency,

operational simplicity and low cost (CHOWDHURY et al., 2020; YADAV et al., 2022b). Although already widespread, this technology has become even more promising in recent years, based on the concept of "treating waste with waste" and the development of new low-cost adsorbent materials (SHU et al., 2023). As a result, a wide range of materials have been studied for this function, with particular emphasis on zeolites, as they are highly stable and crystalline materials with a large surface area and pore volume, and can be produced in an environmentally friendly way (SIVALINGAM; SEN, 2018).

In this context, and considering the structure and presentation of this research as a compendium of publications, the first two articles comprising this thesis deal with the synthesis of zeolites using only waste as raw material precursors. For this purpose, hazardous salt slag (industrial aluminum waste) and rice husk ash (agri-food waste) served as sources of aluminum and silicon, respectively, in the manufacture of adsorbent zeolites. Regarding waste, their choices were primarily based on the composition rich in aluminum and silicon, the main components of zeolites, avoiding the use of commercial chemical reagents. Furthermore, converting these waste into useful value-added products is immeasurable for environmental protection (SHU et al., 2023). Rice husk ash (RHA) is one of the most abundantly available agro-industrial wastes, and when disposed of in landfills it takes a long time to biodegrade (ISLAM et al., 2018). Salt slag, in turn, is the main waste derived from the aluminum recycling industry, whose global consumption is estimated to exceed 100 million tons by 2025 (LÓPEZ-DELGADO et al., 2020). For every ton of aluminum recycled, half a ton of salt slag is generated (PADILLA et al., 2022). In addition to the enormous amount produced, its biggest problem lies in its harmful, toxic, irritating, flammable and leachable nature, which has incorporated it into the European Catalogue of Hazardous Waste (EWC, 2001) under code 100308 - Toxic and Hazardous Waste, making its management a global environmental dilemma.

In the first article, entitled "**Salt slag and rice husk ash as raw materials in zeolite synthesis: Process optimization using central composite rotational design**" (https://doi.org/10.1016/j.scp.2024.101599), statistical factorial design was applied to optimize the experimental synthesis conditions for obtaining highly crystalline NaP-type zeolites from these wastes.

However, among the various types, the LTA zeolite is the most widely used and marketed, and it is also the most sought-after in synthesis processes, due to its extraordinary structural arrangement as a space-specific catalysis supercage, i.e. an internal cavity large enough to support a variety of reactions and small pores allowing the entry of specific structures, thus providing the best adsorption and ion exchange capacities (PANGAN et al., 2021). Along these lines, the second article, entitled "**Waste symbiosis through the synthesis of highly crystalline LTA and SOD zeolites**" (https://doi.org/10.3390/ma17174310), examines how the sodium concentration in the solutions for sol-gel synthesis and the different aging conditions (time and temperature) influence the formation of LTA- and SOD-type zeolites.

Having obtained the adsorbent materials, the adsorption method was then applied using an aluminum slag-based LTA zeolite. The textile dyes chosen as models for this study were the anionic dye Indigo Carmine (IC) and the cationic dye Safranine-T (ST), some of the most traditional dyes used in the textile industry. Preliminary tests confirmed the importance of the ionic nature of the dyes for the treatment processes when the anionic one was not able to be removed by the zeolite (data not shown). The increase in adsorption capacity for the anionic dye could have been achieved by modifying the surface of the zeolite (TURP et al., 2020), but this would have detracted from the target, adding costs, chemicals and time-consuming steps that were not intended.

Thus, the third article "**Adsorption of Safranine-T dye using a waste-based zeolite: Optimization, kinetic and isothermal study**" (https://doi.org/10.1016/j.jiec.2024.02.005) discusses the best treatment conditions, determined through statistical planning, for the adsorption of the cationic ST dye onto the waste-based LTA zeolite.

On the other hand, bioelectrochemical treatment technology based on the use of MFC devices has attracted increasing attention in recent environmental research. According to Singh et al. (SINGH; DAHIYA; MISHRA, 2021), the implementation of this technology offers a suitable option for the removal of various types of dyes, which is attributed to the occurrence of oxidative and reductive reactions simultaneously in a single module, in addition to providing direct energy production, minimal sludge generation, low greenhouse gas emissions and high efficiency when compared to the traditional technologies. MFC represents a promising new energy-saving platform for

wastewater treatment, as well as having great potential in a number of other applications, such as hydrogen production, biosensors and remote power supply (YONG et al., 2017). Time magazine ranked MFCs as one of the 50 most important inventions of the year in 2009 (FRANKS; NEVIN, 2010).

In this technique, the polluting dyes in wastewater are served as substrates for the metabolism of electrochemically active microorganisms, thus coupling these bioremediation systems with the generation of bioelectricity (KARDI et al., 2017; RATHOUR et al., 2019). The system consists of electroactive microorganisms, also called exoelectrogens, oxidizing available organic matter and donating or receiving electrons from an anode to a cathode as terminal acceptor (FERNÁNDEZ, 2015). The electrons (e^-) produced by these bacteria from the degradation of organic and inorganic compounds are transferred (via different mechanisms) to the anode (negative terminal) and flow to the cathode (positive terminal) via an external circuit, while the protons (H^+) diffuse to the cathode via the proton exchange membrane (LOGAN; REGAN, 2006).

Exoelectrogenic microorganisms act as indispensable biocatalysts for the functioning of MFCs (CAO et al., 2019). Several studies have shown that, among all of them, *Pseudomonas aeruginosa* is one of the dominant species present in the sludge of textile wastewater treatment plants, capable of surviving in aerobic and anoxic environments and competing in complex ecosystems with substrate limitations (BAGCHI; BEHERA, 2021; NARAYANASAMY; JAYAPRAKASH, 2018; SHEN et al., 2014). Moreover, its distinct ability to bioremove different dyes has been reported by several authors (BORAN et al., 2019; JIALIANG et al., 2012; KALYANI et al., 2009; KHAN et al., 2022; MAQBOOL et al., 2016; MISHRA; MAITI, 2018).

In this sense, the fourth article presented in this thesis under the title "**Influence of the chemical structure of textile dyes on their biodecolorization by *Pseudomonas aeruginosa*: Indigo Carmine and Safranine-T as model dyes in bioremoval experiments**" (submitted to ACS Omega) reports on the preliminary studies conducted using this pure bacterial culture in the bioremoval of the textile IC and ST dyes. Again, due to the molecular structures of the dyes, dissimilar results were obtained; this time, the proposed treatment showed excellent performance in removing the anionic dye, but not the cationic one. For this reason, plus the need to ensure strict aseptic conditions for inoculation with pure culture, it was decided to populate the MFC with a mixed microbial community. In addition, recent evidence has shown that

although most microorganisms are electrochemically inactive, the symbiosis developed by these mixed bacterial communities in MFCs improves stress resistance, stability and nutritional adaptability, leading to the generation of higher energy potentials compared to pure cultures (SOLANKI; SUBRAMANIAN; BASU, 2013; ZHOU et al., 2022).

Finally, the fifth and last article, entitled "**Eco-friendly decolorization of Indigo Carmine and Safranine-T dyes with simultaneous bioenergy generation using an air-cathode single-chamber microbial fuel cell**", investigates the treatment performance of IC and ST dyes and the simultaneous production of bioelectricity using a single-chamber MFC equipped with a membrane electrode assembly (MEA) and inoculated with anaerobic sludge.

It is important to emphasize the original contributions of this study to the field of research. From this perspective, it is worth mentioning that in the synthesis of zeolites, the combination of hazardous aluminum salt slag waste and rice husk ash agri-food waste had not previously been explored. Most studies reporting the use of waste in zeolite production provide a single source of aluminum or silicon from waste, supplementing the required content of the other precursor with chemical reagents. Therefore, to our knowledge, this study reports for the first time the obtaining of highly crystalline LTA, SOD and NaP zeolites synthesized exclusively from these two aforementioned wastes. Furthermore, this research applied the strategy of optimization through statistical experimental planning, which is underestimated by researchers in the field of materials synthesis, and which represents an important tool in the simultaneous analysis of the factors and levels influencing the process, thus reducing the number of experiments required and with it the time spent and the costs involved.

As far as adsorption is concerned, the LTA zeolite synthesized from aluminum waste was used by the research group to treat acid mine drainage (AMD) (CHOSTAK et al., 2023a, 2023b) and now, for the first time, it has been applied to the removal of textile dyes. What's more, the novelty of this work also extends to the dyes used as models, anionic IC and cationic ST dyes, whose comparison in biological decolorization and bioelectrochemical processes using MFC had never been performed, and as it is well known, is a crucial point for the development and improvement of textile wastewater treatment technologies.

Advancing the development for future application of the above-mentioned treatment solutions adds a step towards reducing environmental contamination by dyes, improving the wastewater treatment quality and helping to reduce the issue of clean water scarcity. The progress of these innovative green technologies based on the use of waste to treat effluents will favor the symbiosis between the different industrial sectors, thus creating solutions for recovering and adding value to waste, reducing landfill disposal, minimizing management and process costs and avoiding damage to environmental ecosystems. At the same time, promoting strategies for the production of clean, renewable energy from polluting effluents cooperates to contain the current global warming crisis by diminishing greenhouse gas emissions, thus contributing to the United Nations Sustainable Development Goals (UN, 2015), especially Goals 6, 7, 12 and 13, which relate to the water-energy nexus, respectively, Clean Water and Sanitation, Affordable and Clean Energy, Responsible Consumption and Production and Action against Global Climate Change.

This research follows on from previous studies carried out at the Water Reuse Laboratory (LaRA) of the Graduate Program in Environmental Engineering at the Federal University of Santa Catarina (UFSC), related to the treatment of textile effluents (DALBOSCO, 2021; RAVADELLI, 2021; SCHALLEMBERGER, 2021), adsorption (CHOSTAK, 2023; DALARI, 2022; LACH, 2023; NÚÑEZ-GÓMEZ, 2018; TOMASSONI, 2019) and bioelectrochemical technology (SORGATO, 2022), as well as other ongoing research at master's, doctoral and post-doctoral level.

1.2 HYPOTHESES

I. Using only wastes, salt slag and rice husk ash as alternative precursors of aluminum and silicon, respectively, it is possible to synthesize adsorbent zeolites.
II. The experimental synthesis conditions determine the zeolite phases obtained.
III. Cationic dyes can be sorbed by zeolites due to their negative superficial charge, whereas anionic dyes must be requiring other removal techniques.

IV. The performance of *P. aeruginosa* in the biodecolorization of dyes should be influenced by the experimental conditions (type and concentration of dye, agitation conditions, concentration of the bacterial growth medium).

V. The relative abundance of the microbial community in an MFC is expected to be reduced during acclimatization, favoring the development of exoelectrogenic microorganisms.

1.3 OBJECTIVES

1.3.1 General Objective

The main objective of this study was to evaluate the treatment performance of solutions containing different types of dyes, the anionic IC and cationic ST dyes, by applying adsorption technology using waste-based zeolites and biotechnological techniques via bioremediation and bioelectrochemical technology using a single-chamber microbial fuel cell.

1.3.2 Specific Objectives

1.3.2.1 Adsorption Studies

- Co-recycling hazardous waste from the aluminum recycling industry (salt slag) and agri-food waste (RHA), as sources of aluminum and silicon, respectively, through the synthesis of zeolites, in order to reduce the environmental problems associated with their disposal;
- Synthesizing adsorbent zeolites using wastes as alternative raw materials to preserve natural resources;
- Establish the experimental conditions for obtaining different types of zeolites with adequate characteristics for application as adsorbent materials;
- Characterize the waste-based zeolites mineralogically, morphologically, structurally and texturally, in addition to thermal behavior and cation exchange capacity;

- Determine the best treatment conditions for textile dye removal by the LTA zeolite using batch tests and statistical methods;
- Establish the removal rate and the ideal contact time between the adsorbent material (zeolite) and the adsorbate (synthetic textile dyes) by means of kinetic studies;
- Determine the adsorption equilibrium, maximum adsorption capacity and removal mechanisms through isothermal studies;
- Correlate the treatment efficiency using LTA zeolite as an adsorbent material with the structure and surface charge of the dyes.

1.3.2.2 Biotechnological Studies

- Evaluate the influence of experimental parameters on the biodecolorization of dye-containing solutions, using a pure culture of *P. aeruginosa*;
- Assess the performance of a MFC inoculated with anaerobic sludge in the decolorization of dye-containing solutions, regarding color and COD removal efficiency, and bioelectricity generation;
- Determine the maximum current and power densities of the MFC for both dyes at different initial concentrations and external resistances using polarization curves;
- Correlate the effectiveness of the biotreatments with the structure and surface charge of the dyes;
- Evaluate the phytotoxicity of synthetic dye solutions before and after treatment in the MFC using lettuce seeds (*Lactuca sativa*) as a bioindicator;
- Analyze the diversity and richness of the microbial community in the inoculum and in the MFC biofilm using 16S rRNA sequencing.

1.4 METHODOLOGICAL STRUCTURING

The development of this research was conducted in two major stages which involved carrying out numerous independent and sequential steps linked to the objectives specified in Section 1.3.

The first major stage was the adsorption studies using zeolites synthesized from wastes. This stage was carried out at the Instituto Eduardo Torroja de Ciencias de la Construcción - IETcc, belonging to the Consejo Superior de Investigaciones Científicas - CSIC, in Madrid, Spain, over the course of a year, between November 2022 and October 2023, as part of the studies related to the sandwich doctorate scholarship, awarded through Call Nº. 02/2022/PROPG - PrInt-CAPES/UFSC.

The second stage, referring to bioelectrochemical studies, was conducted at the Water Reuse Laboratory - LaRA, belonging to the Department of Environmental Engineering, and at the Laboratory of Molecular Genetics of Bacteria - GemBac, belonging to the Department of Microbiology, Immunology and Parasitology, both at the Federal University of Santa Catarina, in Florianópolis, Brazil.

The general methodological flowchart covering all the steps of the research is shown in Figure 1.1. The results of the methodological stages have been gathered into thematic axes, each corresponding to a chapter of this study and also to an article published (1, 2 and 3) or submitted (4 and 5) to a prestigious international scientific journal. They are presented as follows:

- **Article 1**: Salt slag and rice husk ash as raw materials in zeolite synthesis: Process optimization using central composite rotational design;
- **Article 2**: Waste symbiosis through the synthesis of highly crystalline LTA and SOD zeolites;
- **Article 3**: Adsorption of Safranine-T dye using a waste-based zeolite: Optimization, kinetic and isothermal study;
- **Article 4**: Influence of the chemical structure of textile dyes on their biodecolorization by *Pseudomonas aeruginosa*: Indigo Carmine and Safranine-T as model dyes in bioremoval experiments;
- **Article 5**: Eco-friendly decolorization of Indigo Carmine and Safranine-T dyes with simultaneous bioenergy generation using an air-cathode single-chamber microbial fuel cell.

By structuring the thesis as a compendium of articles, it is worth highlighting the existence of different summaries and conclusions based on the partial results of each one. Some information may have been presented in different ways or repeatedly, in order to contextualize and maintain the coherence of the chapters/articles. Thus, considering the theoretical framework included in each of the chapters according to

the topic studied, a general literature review is not presented, although the introduction and conclusions of this research provide the information that allows for a general and consolidated perception of the topic addressed.

Figure 1.1 – General flowchart of the research highlighting the thematic axes referring to the chapters/articles.

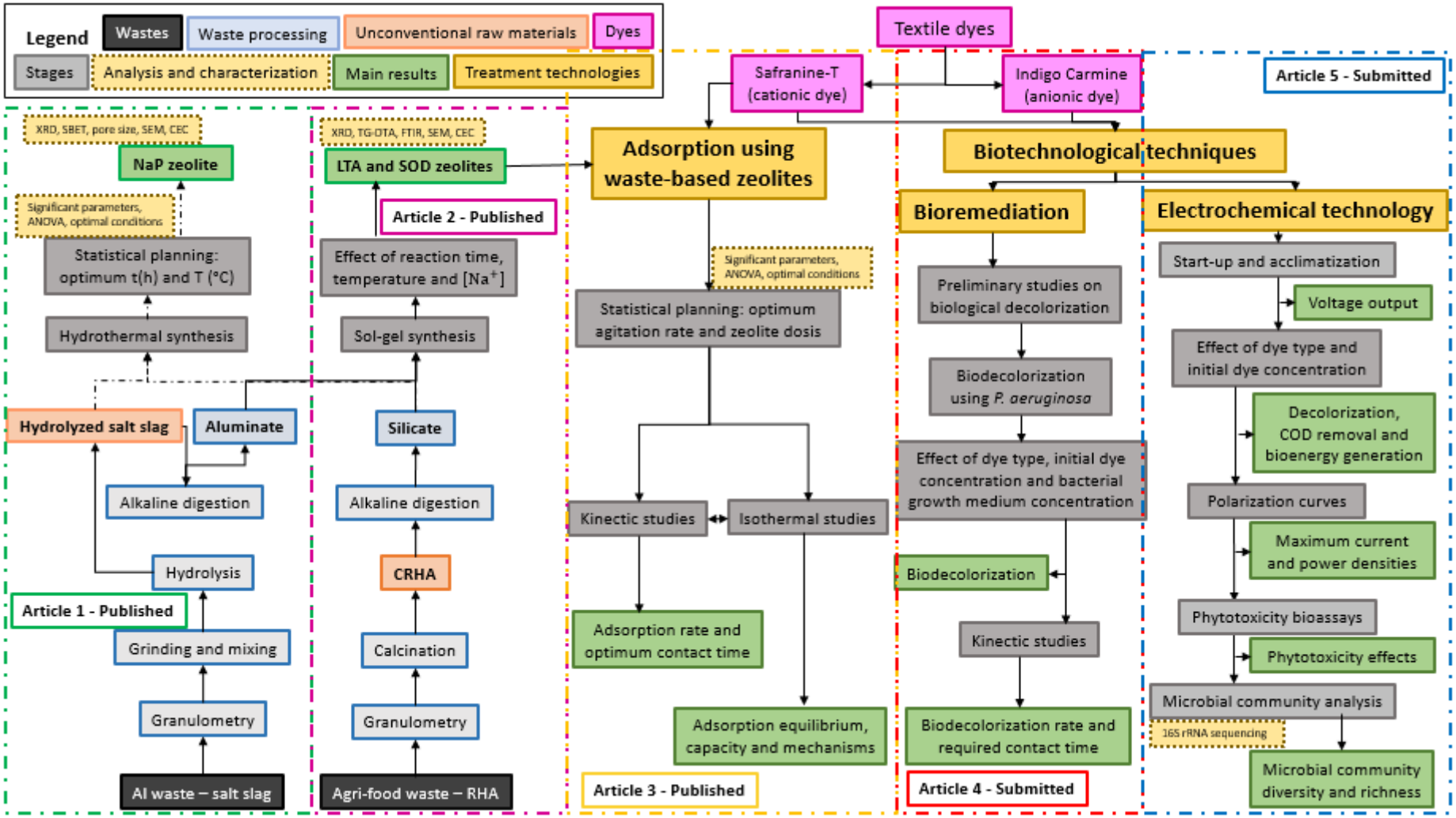

Source: created by the author

2 CHAPTER II: SALT SLAG AND RICE HUSK ASH AS RAW MATERIALS IN ZEOLITE SYNTHESIS: PROCESS OPTIMIZATION USING CENTRAL COMPOSITE ROTATIONAL DESIGN[1]

Sustainable Chemistry and Pharmacy 39 (2024) 101599

Contents lists available at ScienceDirect

Sustainable Chemistry and Pharmacy

journal homepage: www.elsevier.com/locate/scp

Salt slag and rice husk ash as raw materials in zeolite synthesis: Process optimization using central composite rotational design

Magali Teresinha Ritter[a, b], María Ángeles Lobo-Recio[b, c], Isabel Padilla[a, *], Maximina Romero[a], Aurora López-Delgado[a]

[a] Department of Materials, Eduardo Torroja Institute for Construction Sciences (IETcc-CSIC), Serrano Galvache Street, 4, 28033, Madrid, Spain
[b] Department of Sanitary and Environmental Engineering, Federal University of Santa Catarina (UFSC), Campus Reitor João David Ferreira Lima, 88040-900, Florianópolis, SC, Brazil
[c] Department of Energy and Sustainability, Federal University of Santa Catarina (UFSC), Campus Araranguá, Rod. Gov. Jorge Lacerda, 3201, Jardim das Avenidas, 88.906-072, Araranguá, SC, Brazil

HIGHLIGHTS

- Co-recycling of a hazardous aluminum waste and an agri-food waste
- High-performance synthesis of zeolites from salt slag and rice husk ash
- Natural resources conservation by converting waste into secondary raw-materials
- Central Composite Rotational Design settles the values of synthesis key parameters
- Optimal synthesis conditions yield zeolites with high degree of crystallinity

[1] RITTER et al. (2024). Article published in the journal Sustainable Chemistry and Pharmacy (Impact factor 5.5 – Q1:2023) in May 2024.

GRAPHICAL ABSTRACT

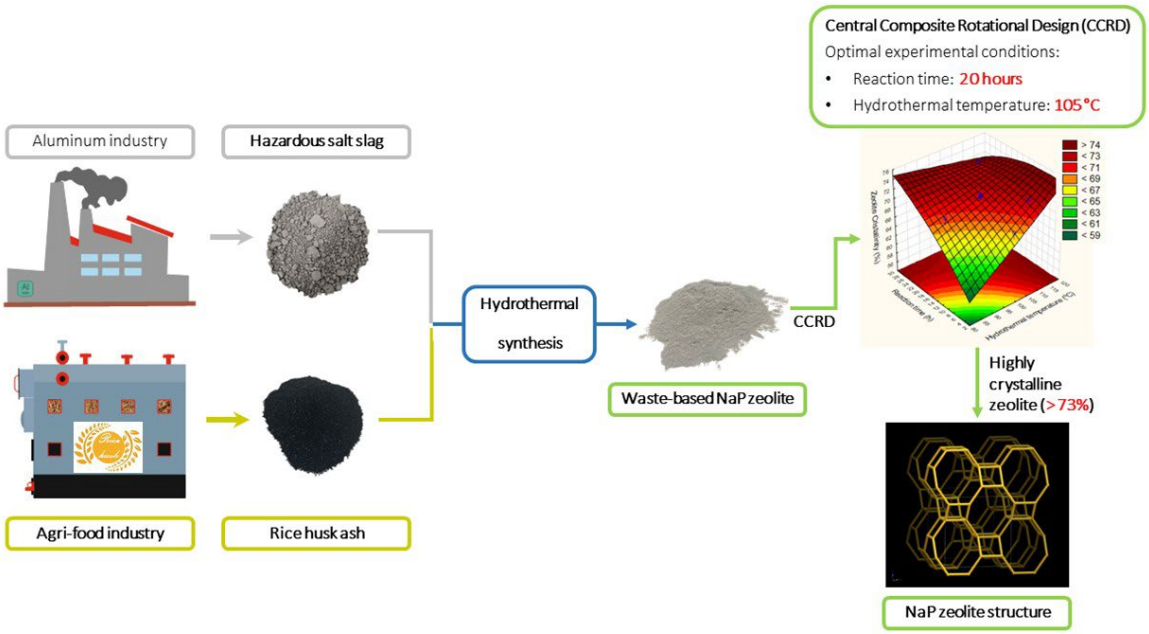

Source: created by the author

2.1 ABSTRACT

The growing demand of zeolites for many industrial applications has led to a search for eco-friendly alternatives for their production, in an attempt to reduce costs, save natural resources and alleviate the associated environmental impacts. In the present study, hazardous aluminum salt slag (aluminum source) and rice husk ash (silicon source) were used as secondary raw materials to synthesize sustainable NaP-type zeolites through a hydrothermal process. A central composite rotational experimental design was applied to evaluate the effect of the reaction time and hydrothermal temperature on the obtained zeolites crystallinity. Using the proposed experimental design, temperatures between 85 and 115 ºC and different reaction times (2 to 28 hours) were tested. It was found that the interaction between the variables (time and temperature) and both variables, independently, exerted a significant influence on the crystallinity of the zeolites. The optimal experimental conditions (105 ºC and 20 hours), statistically determined, enabled a high degree of crystallinity (>73%) to be achieved. Thus, the use of hazardous aluminum and agri-food wastes as unconventional precursors for the production of zeolites represents a sustainable

alternative to manage these wastes, by transforming them into secondary raw materials.

Keywords: waste-based zeolites, NaP zeolite, hazardous waste, salt slag, rice husk ash, central composite rotational design.

2.2 INTRODUCTION

Zeolites are crystalline materials with a three-dimensional structure composed of AlO_4 and SiO_4 tetrahedra. Due to their unique properties, they have been extensively used in many industrial applications as adsorbents, catalysts, membrane materials, ion exchangers, and chemical sensors, among others (Abdel-Hameed et al., 2020). Zeolites represent the most important group of microporous materials (Xu et al., 2007), and their global demand is increasing, especially stimulated by the detergent industry, where synthetic zeolites are employed as an alternative to replace contaminating phosphate agents, following more restrictive regulations implemented in several countries (Markets and Markets, 2023). Zeolites can be obtained from natural deposits or synthesized from a wide variety of aluminum and silicon sources (Xu et al., 2007). According to a recent report by Markets and Markets (2023), the global zeolite market was 4,872 metric tons (12.1 billion dollars) in 2021 and an estimated 5,453 metric tons (14.1 billion dollars) in 2026, of which 5.9 billion dollars correspond to synthetic zeolites.

Concerning synthetic zeolites, research efforts have recently focused on the production of zeolites using different wastes as unconventional raw materials. Converting waste into functional value-added products is of great importance for sustainability and environmental protection (Shu et al., 2023). A variety of wastes have been used in the zeolite synthesis, including coal fly ash, waste glass, alum sludge, rice husk, bauxite residue, etc. (Collins et al., 2020).

Among aluminum waste, salt slag is the main solid waste, generated in large quantities by the secondary aluminum industry (~0.5 tons of salt slag per ton of recycled aluminum produced) (Padilla et al., 2022). By 2027, it is estimated that more than 26 million metric tons of recycled aluminum will be generated worldwide (Statista, 2023), representing approximately 13 million metric tons of slat slag. The management

of this waste is considered a major problem. The European Catalogue of Hazardous Waste (2001) classifies salt slag as a toxic and hazardous waste (code 10 03 08), and considered highly irritant, harmful, leachable and flammable (EWC, 2001). Salt slag contains a significant amount of harmful leachable salts and its disposal has negative effects on both the environment and human health, polluting soil and groundwater (Srivastava and Meshram, 2023). In addition, it is highly reactive in contact with water or even moisture in the air, leading to the formation of toxic gases, such as CH_4, NH_3, H_2, H_2S and PH_3, whose emissions into the atmosphere cause serious environmental damage (Tsakiridis, 2012). However, its aluminum-rich composition makes salt slag a potential candidate for zeolite synthesis. In this sense, in a preliminary study (Padilla et al., 2022), a NaP-type zeolite was synthesized using salt slag and a commercial sodium silicate as silicon source. The synthesis process was performed at 100 ºC for 24 hours. The as-obtained zeolite exhibited a specific surface area of 17 $m^2\ g^{-1}$, a cation exchange capacity (CEC) of 2.12 meq g^{-1} and a predominant pore size of 3.8 nm.

Regarding silicon waste, rice husk ash (RHA) is a silicon-rich material and is considered one of the most abundant agri-food wastes. It results from the thermal transformation of rice husks, a readily available and inexpensive material. The Organization of the United Nations for Food and Agriculture (FAO, 2022) estimated that more than 31 million tons of rice husk ash would be generated in the world by the end of 2023. Although RHA is not considered a hazardous waste, its landfill disposal and slow biodegradation cause several environmental impacts. Thus, zeolite synthesis from RHA opens a new route for the use of this waste, which is presented as an alternative and low-cost substitute for commercial silica (Mallapur and Oubagaranadin, 2017; Mohamed et al., 2015; Tan et al., 2011; Tran-Nguyen et al., 2021; Vasconcelos et al., 2023). In this way, Mohamed et al. (2015) reported the synthesis of NaY zeolite, using RHA and commercial aluminate. The process involved extracting silica from the RHA through acid washing and alkali activation (NaOH) followed by a two-step synthesis in which a feedstock solution and a seed gel were prepared, kept at room temperature for 24 hours and then mixed and stirred at 110 ºC for the same period of time. In a similar way to the aforementioned authors, Tan et al. (2011) obtained NaY and NaA zeolites using RHA and commercial aluminate. The process consisted of preparing the seed and feedstock solution by adding the required amounts of

reactants, stirring vigorously until completely mixed and then aging at room temperature for 24 hours. The mixture of both solutions forms a gel that was kept at room temperature for 24 hours and finally, using a Teflon bottle, heated to 100 ºC for a further 5 hours. The difference in the zeolitic material obtained was related to the silica extraction process; alkaline activation using NaOH pellets led to the formation of NaY-type zeolite, while with NaOH (1M) solution, NaA zeolite was formed. Tran-Nguyen et al. (2021) obtained a NaX zeolite using RHA and commercial aluminum powder. The silicate solution was prepared by treating RHA with a 5M NaOH solution at 90 ºC for 3 hours, and the aluminate solution was also produced by alkaline dissolution of the aluminum powder. The synthesis was carried out by mixing the two solutions under vigorous stirring (at 50 ºC for 2 hours) and heating the obtained gel at 90 ºC for 4 hours.

With regard to the methodologies used in zeolite synthesis, most studies report the use of processes involving several steps, as mentioned above. Furthermore, in most cases, zeolitic materials are synthesized from a single waste as a source of silicon or aluminum, supplementing the necessary content of the other precursor with chemical reagents. In this work, both hazardous salt slag and rice husk ash have been used as exclusive aluminum and silicon sources, respectively, and the hydrothermal synthesis of waste-based zeolites, more specifically NaP zeolite, was carried out in a single-step under mild conditions. To our knowledge, the combination of these two wastes has not been reported in the literature. Indeed, the process developed can be considered as a co-recycling of two different wastes. In order to determine the effect of the main synthesis parameters (time and temperature) on the crystallization of zeolites, a central composite rotational design (CCRD) was applied (Alaba et al., 2017). The use of experimental design is under-exploited by researchers but represents an important optimization strategy for determining the optimal synthesis parameters, allowing the simultaneous analysis of factors at different levels and reducing the number of required experiments. Optimizing the experimental conditions is a crucial point in the synthesis of crystalline zeolites. The conventional orthogonal method, although extensively employed for optimizing operational parameters in Various processes, is not capable of generating a clear functional relationship between factors and response values, posing challenges in identifying the ideal parameter combination (Yi et al., 2010). In the present investigation, the CCRD was used to

determine the optimal synthesis conditions and overcome these disadvantages of the traditional orthogonal method. The use of hazardous aluminum and agri-food wastes as less-common precursors for the production of zeolites is presented as a sustainable alternative to the waste management, generating value-added materials with promising applications, and greatly contributing to environmental preservation, circular economy, and industrial symbiosis.

2.3 MATERIALS AND METHODS

2.3.1 Characterization Techniques

A wavelength dispersive X-ray fluorescence (XRF) spectrometer (Bruker, S8 Tiger) was used to determine the chemical composition of the raw materials. The composition of the silicate solution extracted from the RHA was analyzed by an inductively coupled plasma optical emission spectrometer (ICP-OES) (Spectro Arcos). Mineralogical characterization of the wastes and obtained zeolites was performed by X-ray diffraction (XRD) using a Bruker D8 Advance Diffractometer with CuKα radiation, with 2θ from 5º to 60º, at a scan rate 2θ of 0.02º, 5 s per step. The crystallite sizes were calculated using the Scherrer equation (Equation 2.1) (Scherrer, 1918):

$$D_{hkl} = {K.\lambda}/{FWHM.cos\theta} \quad (2.1)$$

where K is the constant of Scherrer (0.9), λ is the x-ray wavelength (0.154 nm), FWHM is the Full Width at Half Maximum (in rad) and θ corresponds to the diffraction angle (in rad) of the most intense reflection centered around 28.1º (2θ), corresponding to the hkl [301]. The FWHM was determined by non-linear fit to the Gauss function, using OriginPro 8.5 software. The degree of crystallinity and semi-quantification of the crystalline phases of the zeolites was performed using Diffrac.Suite EVA software. The thermal behavior of rice husk ash was studied using thermogravimetric analysis and differential thermal analysis (TG/DTA) on a Thermoanalyzer model SDT-Q600 (TA Instruments), with a heating rate of 10 ºC min^{-1} under an air flow of 100 mL min^{-1}. The morphology of the zeolites was examined by Scanning Electron Microscopy (SEM), using a Hitachi S4800 microscope equipped with an energy dispersive X-ray

spectroscopy detector (EDS). The textural characterization of the zeolite was performed by determination of nitrogen adsorption/desorption isotherms at -196 ºC in an ASAP 2010 Micromeritics system. The sample was previously outgassed at 250 ºC in vacuum for 24 h. The specific surface area (S_{BET}) and pore size distribution was determined through multi-point measurements using the Brunauer-Emmett-Teller (BET) method and the Barrett-Joyner-Halenda (BJH) method, respectively. The external area (S_{Ext}) was calculated by the t-plot method from the slope of the linear fit in the thickness range (t) of 0.35–0.5 nm according to the Harkins-Jura equation. The NH_4^+ ion exchange method using a 1M NH_4Cl solution (pH ~ 7) was applied to determine the cation exchange capacity (CEC) of the zeolites, with tests conducted in duplicate (NC 626, 2008).

2.3.2 Raw Materials

Aluminum salt slag (ASS) and rice husk ash (RHA) were used as aluminum and silicon source, respectively, for the synthesis of zeolite type P ($Na_6Al_6Si_{10}O_{32}\cdot 12H_2O$).

The as-received ASS (Alusigma S.A, Gijón, Spain) consisted of a dark-grayish granular solid (Fig. 2.1a), with a particle size distribution ranging from very fine powder (< 0.5 mm) to granules larger than 5.7 mm, and the major fraction (53%) composed of coarse grain sizes (1–4 mm). Due to its granulometric and compositional heterogeneity, salt slag was subjected to a grinding process in order to standardize the particle size (< 0.25 mm) and enable a better reaction in the synthesis stage. A sample of around 3 kg of ASS was divided into eight representative aliquots using a Laborette 27 Rotary Cone Sample Divider, with one of these aliquots used in the experiments. This procedure aimed to guarantee the reproducibility and accuracy of the results.

Due to its high NaCl content, ASS was subjected to a hydrolysis process (see Section 2.5.3) before being used as a raw material in the synthesis of zeolites.

The as-received rice husk ash (RHA) (Herba Ricemills, Seville, Spain) consisted of a homogeneous dark powdery solid with some white fibers and a predominant particle size of 0.1 – 0.5 mm (Fig. 2.1c).

2.3.3 Pretreatment of Waste Materials

The salt slag was hydrolyzed in order to eliminate *(i)* excess salt that could interfere with the process of transforming the slag into zeolites and *(ii)* cause the reaction of the aluminum compounds, transforming them into oxides and thus releasing the corresponding gases (such as ammonia, hydrogen and hydrogen sulfide).

The hydrolysis of the aluminum salt slag was carried out by placing 300 g of sample in a volumetric flask and dripping distilled water using a peristaltic pump. After adding the corresponding volume of water, the suspension was maintained at a temperature of 90 ºC under continuous stirring for 2 hours. After filtering under pressure, the cake (hydrolyzed slag, HS) was dried for 24 hours at 100 ºC. HS (Fig. 2.1b) was the only source of aluminum used in the zeolite synthesis.

A silicate solution was prepared from calcined rice husk ash (Fig. 2.1d) in order to provide the silicon required for formation of zeolite. The extraction of silicon from CRHA was carried out by mixing 48 g of RHA with a 3M NaOH solution in a Teflon-lined autoclave reactor (Parr, 1 L volume) and kept under constant stirring for a reaction time of 3 hours at 120 ºC. After the reaction, the products were filtered to separate the sodium silicate solution. The composition of the silicate solution was analyzed by an inductively coupled plasma optical emission spectrometer (ICP-OES).

Figure 2.1 – Macroscopic appearance of the (a) aluminum salt slag (ASS), (b) hydrolyzed slag (HS), (c) rice husk ash (RHA) and (d) calcined rice husk ash (CRHA).

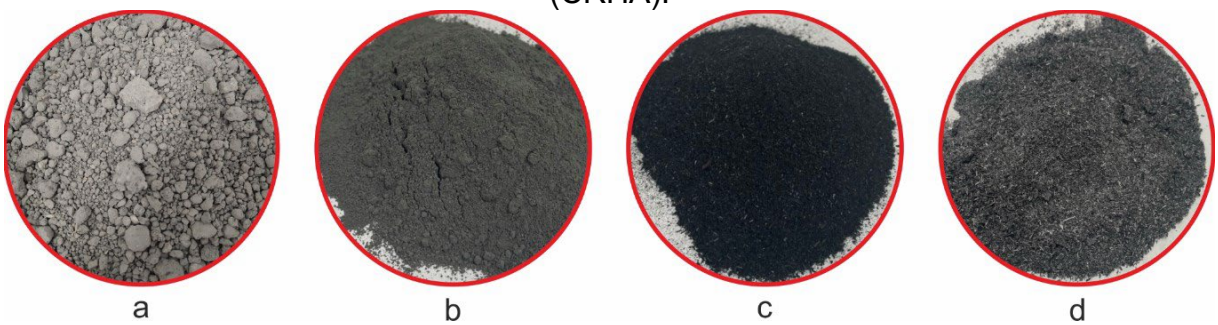

Source: author's collection

2.3.4 Synthesis of Zeolites

The waste-based zeolites were produced following the procedure shown in Figure 2.2. Synthesis was carried out in the Na_2O-Al_2O_3-SiO_2-H_2O system by the

conventional hydrothermal method. The reactants, solid aluminum hydrolyzed slag, and the silicate solution extracted from the CRHA, were mixed in appropriate proportions to provide the stoichiometric Si/Al ratio fot NaP-type zeolite ($Na_6Al_6Si_{10}O_{32}\cdot 12H_2O$), and they were placed, along with the corresponding volumes of 1M NaOH solution and distilled water, in the autoclave reactor. For the objective of synthesizing NaP type-zeolite, all the experiments were performed with continuous stirring and under autogenous pressure. Different temperatures (85-115 ºC) and reaction times (2 to 28 hours) were tested according to the experimental design (Table 2.1) presented in Section 2.5.5. After the synthesis, the solid products were separated by filtration, rinsed with distilled water, and subjected to drying at 100 ºC for 24 h.

Figure 2.2 – Schematic procedure for the synthesis of waste-based zeolite.

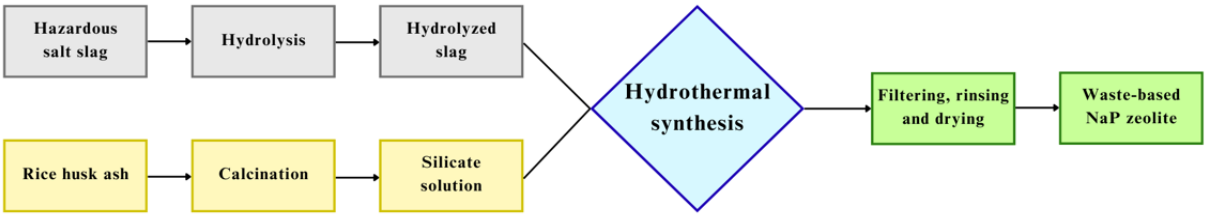

Source: created by the author

2.3.5 Experimental Design

Design of experiments is an important tool for modeling, developing, improving, and optimizing processes, determining the effects of factors on a response at different levels. Furthermore, this method minimizes the number of required experiments and allows the determination of the optimal factor values influencing the process (Kafshgari et al., 2017). In order to determine the optimal conditions for the hydrothermal synthesis of the zeolite, a central composite rotational design (CCRD) with two factors and two levels (2^2) was developed. Hydrothermal temperature and reaction time were considered as the independent variables influencing zeolite synthesis, and the degree of crystallinity of the obtained zeolites was chosen as the response (dependent variable). The CCRD was developed using the STATISTICA® 13.3 software. Eleven tests were carried out, using the factor scores (-1 and +1), which indicate the minimum and maximum level of each variable; 3 central points (0) and the axial portions (-1.414 and +1.414), calculated by Equation 2.2.

$$\alpha = (2^n)^{1/4} \quad (2.2)$$

where α is the axial distance from the central point and *n* is the number of independent variables (*n* = 2). Factor values at the central point (100 ºC and 15 hours) were determined based on preliminary tests. The variable levels used in this study are shown in Table 2.1. The statistical analysis of the experimental results were analyzed using the *p*-value, where values of 0.05 being statistically significant at the 95% confidence level. The optimal experimental conditions were determined based on the median of the statistical critical points.

Table 2.1 – Levels of variables used for CCRD.

Variable	**(-1.414)**	**(-1)**	**(0)**	**(+1)**	**(+1.414)**
Hydrothermal temperature (ºC)	85	90	100	110	115
Reaction time (h)	2	6	15	24	28

Source: created by the author

2.4 RESULTS AND DISCUSSION

2.4.1 Characterization of Raw and Processed Materials

The chemical composition of salt slag mainly consists of about 35 wt.% aluminum (expressed as Al_2O_3) and 18 wt.% Na_2O, along with chloride, according to the X-ray fluorescence (XRF) analysis presented in Table 2.2. The X-ray diffraction (XRD) pattern of the aluminum slag (Fig. 2.3), consistent with its chemical composition, shows the aluminum content distributed in different phases: corundum (Al_2O_3), aluminum nitride (AlN), metallic aluminum (Al) and spinel (Al_2MgO_4); and quartz (SiO_2). Salt slag exhibits pronounced peaks related to halite (NaCl), derived from the high amounts of salt used in the aluminum scrap melting process. The high background of the XRD pattern also suggests the existence of non-crystalline or amorphous phases, which may include metallic oxides such as iron oxide, among others. This presence may vary depending on the type of scrap used in the production of secondary aluminum.

Due to its high salt content, the salt slag was hydrolyzed before being used as a raw material. The main component of the hydrolyzed slag was aluminum oxide (Al_2O_3), and its content in relation to the initial composition of salt slag (Table 2.2) increased significantly, from 35.5% to 63.5%. This increase can be attributed to the

effectiveness of the hydrolysis process, which resulted in a reduction of more than 90% in NaCl content, along with the newly formed aluminum oxides from the reaction of metallic aluminum, aluminum nitride and other aluminum compounds with water.

Table 2.2 – Chemical composition (XRF, expressed as wt.% oxide) and loss of ignition (LOI) (%) of the aluminum salt slag (ASS), hydrolyzed slag (HS), as-received rice husk ash (RHA) and calcined rice husk ash (CRHA).

	Al_2O_3	SiO_2	Na_2O	Cl	MgO	CaO	Fe_2O_3	K_2O	ZnO	P_2O_5	TiO_2	CuO	LOI
ASS	35.5	6.4	18.3	16.7	5.1	3.9	1.7	0.5	0.4	<0.1	0.4	0.4	9.8
HS	63.5	7.7	1.6	1.5	7.9	4.5	3.0	0.2	0.8	<0.1	0.7	0.8	6.2
RHA	0.2	73.5	0.4	0.7	1.1	1.3	0.8	3.9	<0.1	1.4	-	<0.1	15.7
CRHA	0.3	89.7	0.4	<0.1	0.8	1.3	0.2	3.6	<0.1	1.7	-	-	0.2

Source: created by the author

Figure 2.3 – XRD pattern of the aluminum salt slag (ASS) and hydrolyzed slag (HS).

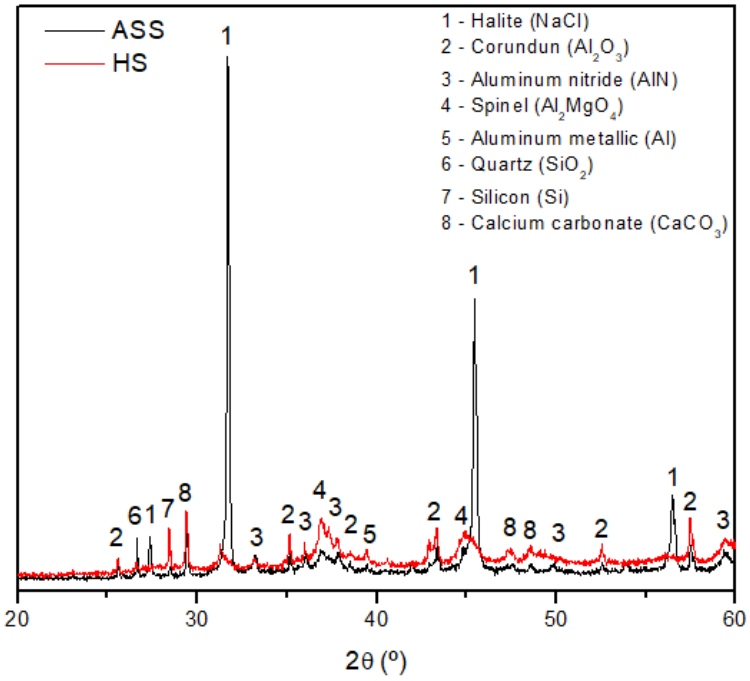

Source: created by the author

The chemical composition of the RHA (Table 2.2), shows that its main component is SiO_2 (73.5 wt.%), followed by small amounts of potassium, phosphorus, calcium, and magnesium. The XRD pattern (Fig. 2.4a) indicates that RHA is composed of silica in its crystalline form, cristobalite, due to the predominant presence of a peak located at 2θ = 21.8º (Shinohara and Kohyama, 2004). The amorphous, crystalline or combined forms of silica are related to the ash production method and its calcination temperature. The silica contained in the ash is predominantly crystalline when high temperatures are used to calcine the rice husk (Foletto et al., 2009; Melo et al., 2014).

Figure 2.4 – (a) XRD pattern of the rice husk ash (RHA) and calcined rice husk ash (CRHA), and (b) TG/DTA curves.

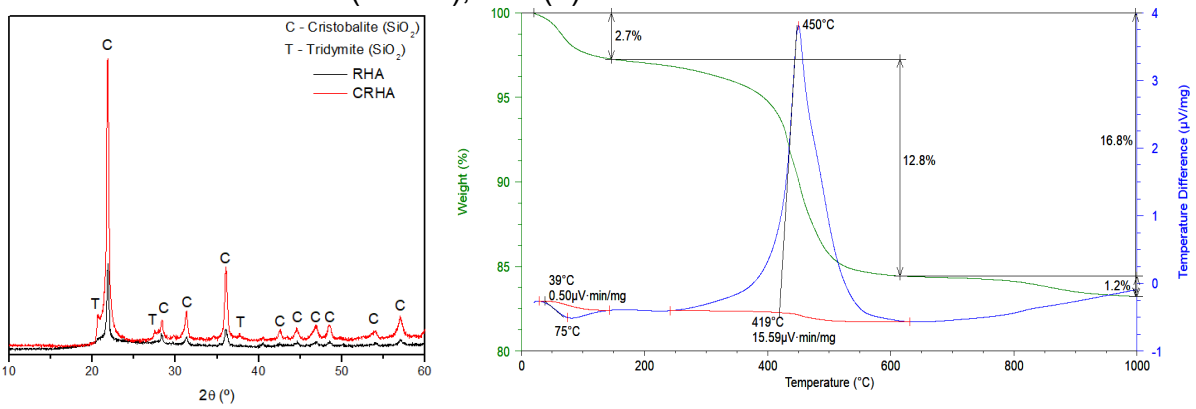

(a) (b)

Source: created by the author

Due to the high LOI value (Table 2.2), RHA was thermally treated to eliminate the carbonaceous material. Previously, a thermal analysis was carried out to determine the optimal calcination temperature. Figure 2.4b shows the TG/DTA curves. Three stages are clearly observed in the TG curve. The first one, at a temperature below 100 ºC, corresponds to the loss of water due to humidity (2.72 wt.%). Between 200 and 600 ºC, the greatest loss of mass takes place, with a value of 12.84 wt.%, which can be attributed to the combustion of carbonous material, as it is accompanied by a exothermic peak, centered around 450 ºC (associated energy of 15.46 μV min mg^{-1}). Finally, a small mass loss of 1.23 wt.% can be observed between 800-1000 ºC. This loss can be attributed to the decomposition of chlorinated compounds and/or the formation of gases containing chlorine, which occurs at high temperatures, since there is a decrease in the presence of this component, from 0.7 to <0.1 (Table 2.2). The total loss of mass was 16.79% obtained by thermal analysis is quite similar to the loss of ignition (LOI) of 15.69%. In this way, knowing the temperature required to remove the carbon content, the initial RHA was calcined at 800 ºC for 8 hours in a Thermo Concept furnace. The appearance of calcined RHA is shown in Figure 2.1d and its XRD pattern (Fig. 2.4a) indicates that cristobalite remains the predominant component of the CRHA, but it has increased in crystallinity and other SiO_2 phase, tridymite, has developed. The LOI reduction from 15.7 to 0.2% (Table 2.2) confirms the effectiveness of the calcination of the RHA.

To achieve the stoichiometric ratio of silicon for the synthesis of NaP zeolite, a silicate solution was produced from CRHA, since it is composed of high crystalline

cristobalite (Fig. 2.4a), which is a very stable form of SiO_2, and accordingly makes it difficult to react properly (especially at lower temperatures), with aluminate ions. The silicate solution consisted mainly of Na (69.7 g L^{-1}) and Si (58.3 g L^{-1}), with minor participation of other elements (Table 2.3).

Table 2.3 – Quantitative chemical composition of silicate solution from CRHA (ICP–OES, in g L^{-1}).

Na	Si	K	S	Al	Ca	Fe	Mg
69.7	58.3	4.1	0.27	0.14	0.007	0.006	<0.001

Source: created by the author

2.4.2 Statistical Analysis of the Waste-based Zeolite Synthesis

The synthesis of the waste-based zeolites was carried out using hydrolyzed slag and silicate solution from calcined rice husk ash as aluminum and silicon sources, respectively. The effect of the synthesis parameters on the zeolites crystallization was explored using a CCRD (Table 2.1). According to the experimental design proposed, hydrothermal temperatures between 85 and 115 ºC were tested using different reaction times (2 to 28 hours). The 2^2-CCRD data matrix with the sample names, factor values and responses is presented in Table 2.4.

Table 2.4 – Factorial design (2^2) results for waste-based zeolite synthesis using HS and CRHA.

Run nº	Factors				Sample	Responses
	Hydrothermal Temperature		Reaction Time			
	Factor Level	Temperature (ºC)	Factor Level	Time (h)		Crystallinity (%)
1	-1	90	-1	6	Z90-6	63.2
2	-1	90	1	24	Z90-24	71.4
3	1	110	-1	6	Z110-6	72.0
4	1	110	1	24	Z110-24	73.9
5	-1.414	85	0	15	Z85-15	70.3
6	1.414	115	0	15	Z115-15	72.1
7	0	100	-1.414	2	Z100-2	68.5
8	0	100	1.414	28	Z100-28	72.7
9	0	100	0	15	Z_A100-15	72.0
10	0	100	0	15	Z_B100-15	71.4
11	0	100	0	15	Z_C100-15	71.5

Source: created by the author

Most of the conditions tested showed a degree of crystallization of over 70% for the waste-based NaP zeolites, with the exception of runs 1 and 7, in which lower reaction times were used. In run 3, although a low reaction time (6 hours) was also

used, the hydrothermal temperature was higher (110 ºC), resulting in a sample with 72% crystallinity. Using a high hydrothermal temperature (110 ºC) for the longest reaction time (24 h), run 4 resulted in the highest crystallinity, 73.9%. The estimated effects, presented in Table 2.5, were based on the p-value. At a significance level of 95%, the planning determined that, in the implemented model, the interaction ($Q_1 vs Q_2$) between the variables (time and temperature) had a significant influence (p <0.05) on the crystallization of synthetic zeolites. In addition, the independent variables temperature (Q_1) in linear form, and time (Q_2) in both linear and quadratic form, were also significant (p <0.05) and influenced the crystallization process. The crystallinity of the waste-based zeolites is linearly dependent on the hydrothermal temperature and reaction time, and their effects are positive (3.2941 and 4.1572, respectively), i.e., when increasing temperature and time there is also an increase in the degree of crystallization of the zeolite. Coefficient of determination (R^2) provides the measure of the proportion of variation explained by the regression equation in relation to the variation in responses. For the zeolite crystallization, an R^2 = 0.8367 was obtained, indicating that the model is able to explain approximately 83.7% of the variations in the crystallization of the obtained zeolites. The variance analysis (ANOVA) was performed, and it was found that for the crystallization of the zeolites, $F_{calculated} > F_{tabulated}$ (Table 2.6), confirming the statistical representativeness of the sample distribution. Therefore, the ANOVA regarding the crystallization of the obtained zeolites demonstrated the validity of the model within the 95% confidence interval, indicating no need for adjustments within the examined range. This outcome indicates an excellent reproduction of the experimental samples.

According to (Núñez-Gómez et al., 2017), the linear and quadratic coefficients, along with their interactions, are part of the template employed to construct the surface that define the optimal conditions for maximizing the response. Response surface and contour curve graphics (Fig. 2.5) allow visualization of the optimal (or near optimal) values, in which the combination of variables led to these better responses. The results indicate that zeolite crystallization was maximum (> 74%) when the synthesis was performed at high temperatures (> 115 ºC), even with shorter reaction times of up to 18 hours (Fig. 2.5). In other conditions, the interaction between these two variables determines the degree of crystallization of the obtained zeolites. Using longer reaction times, high crystallinity can be obtained even at lower temperatures. At temperatures

of up to 100 ºC, synthesis times of over 24 hours are required to obtain crystallinity of up to 74%. The same occurs at shorter times using higher hydrothermal temperatures. A synthesis conducted for 6 hours can result in a zeolite with a degree of crystallinity of up to 72% when using a temperature of 110 ºC.

This indicates that there was variation in the crystallization process of the synthetic zeolites related to the hydrothermal temperature and reaction time, in agreement with the corresponding p-value discussed above (Table 2.5). The critical values statistically determined using the STATISTICA® 13.3 software, were a hydrothermal temperature of 105 ºC and a reaction time of 20 hours. An experiment with these determined factor values was conducted to assess the validity of the results, as other experimental factors were not taken into account in the statistical analysis. In this sample (named Z_{oc}105-20), a high degree of crystallinity was observed (73.4%), even though an intermediate temperature and reaction time were used. This value was only slightly below that of run 4, which resulted in a crystallinity of 73.9%. However, in this case, the synthesis was carried out at a higher temperature (110 ºC) and using a longer reaction time (24 hours). The observed difference in terms of crystallinity of the obtained zeolites is very small considering the energy and time savings between the two processes, so the results demonstrate the suitability of CCRD planning to determine the optimum synthesis conditions.

Table 2.5 – Estimated effects for the crystallization of the waste-based zeolites.

	Coefficient	**Effect**	**Standard error**	**t(2)**	***p*-value**
Temperature (L)	Q_1	*3.2941*	*0.2205*	*14.9382*	*0.0045*
Temperature (*Q*)	Q_{12}	-0.6844	0.2461	-2.7808	0.1086
Time (L)	Q_2	*4.1572*	*0.2301*	*18.0673*	*0.0030*
Time (Q)	Q_{22}	*-1.6467*	*0.2797*	*-5.8873*	*0.0277*
Temperature vs Time	$Q_1 vs Q_2$	*-3.1500*	*0.3214*	*-9.7992*	*0.0103*

L: Linear; Q: Quadratic; *p*-value significant at $p < 0.05$. Source: created by the author

Table 2.6 – Analysis of variance for the waste-based zeolite crystallization for the 2^2 factorial design.

Variation source	**SS**	**df**	**MS**	**F**		***p***
				Calc.	**Tab.[a]**	
Regression	68.0548	3	22.6849	11.153	4.347	<0.05
Sediments	14.2416	7	2.0345			
Total	82.2963	10				

SS: sum of square; df: degree of freedom; MS: mean of square; F: Fisher's ratio; *p*: probability; [a]Tabulated values (BOX; HUNTER; HUNTER, 1978). Source: created by the author

Figure 2.5 – (a) Response surface and (b) contour curve for waste-based zeolite crystallization.

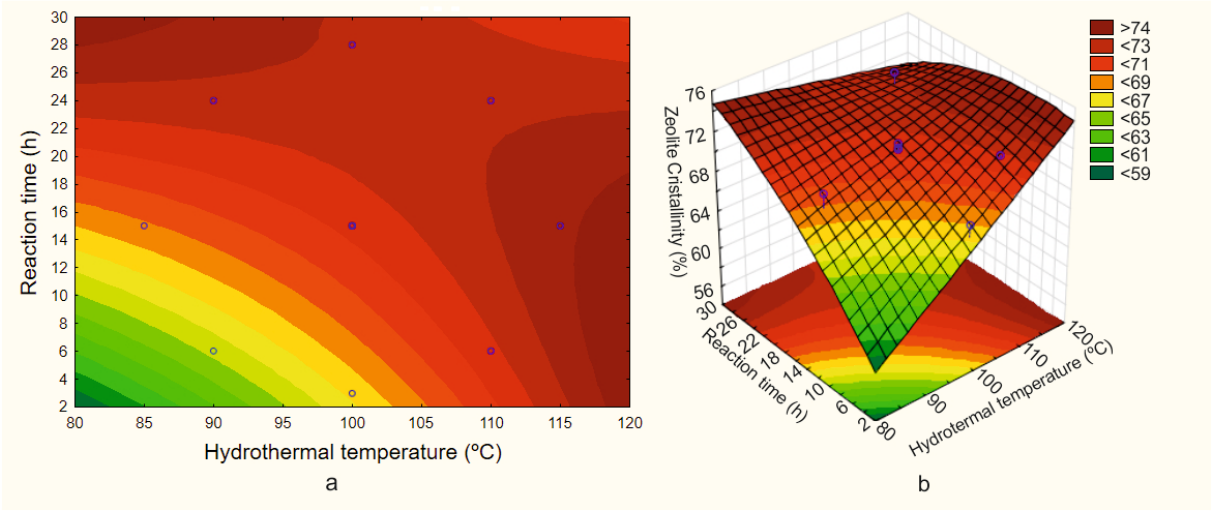

Source: created by the author

Equation 2.1 represents the model describing the degree of crystallization (%). A quadratic regression of the functional variable for the crystallinity response is proposed, where 't' represents the reaction time and 'T' denotes the hydrothermal temperature.

$$\text{Crystallinity (\%)} = 23.172 + 0.427 \cdot T + 2.240 \cdot t + 0.009 \cdot t^2 - 0.0175 \cdot t \cdot T \qquad (2.3)$$

2.4.3 Characterization of the Synthesized Waste-based Zeolites

The XRD spectra of the waste-based zeolites synthesized under different conditions (Runs 1 to 11, Table 2.4) are shown in Figure 2.6.

All samples presented a profile characteristic of tetragonal type P zeolite (NaP, $Na_6Al_6Si_{10}O_{32} \cdot 12H_2O$). According to Hansen et al. (1993), the different symmetries (cubic, tetragonal or orthorhombic) depend on the synthesis conditions. In this regard, Sánchez-Hernández et al. (Sánchez-Hernández et al., 2016) also obtained a NaP zeolite with tetragonal symmetry, using different aluminum waste (sleeve filter fine dust from slag milling) and commercial waterglass by hydrothermal synthesis at 120 ºC for 6 hours. Padilla et al. (2022) synthesized a NaP-type zeolite with cubic symmetry from salt slag and commercial silicate at 100 ºC for 24 hours. This corroborates the influence of the experimental synthesis conditions, but also indicates that the starting reagents used affect the symmetry of the zeolite crystals.

Figure 2.6 – XRD spectra of zeolite materials synthesized under various parameter settings: (a) Run 1-Run 6 and (b) Run 7-Run 11 and Z_{OC}105-20 (• = NaP zeolite, reference file ICDD PDF = 39-0219).

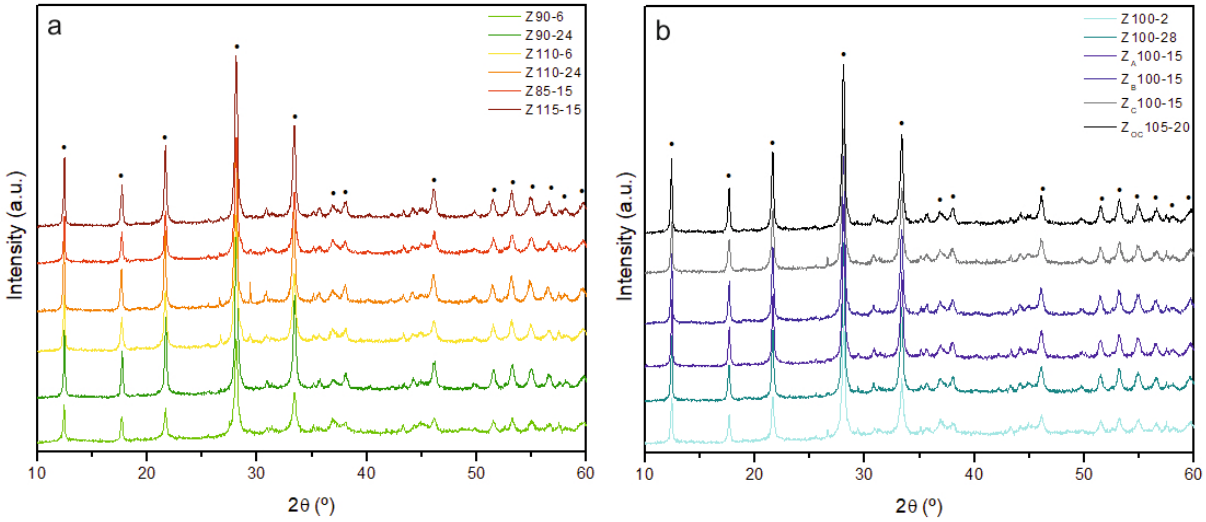

Source: created by the author

The XRD pattern of the obtained zeolites exhibits narrow, well-defined peaks, with the most intense reflection centered around 28.1º (2θ), corresponding to the hkl [301]. The difference in the intensity and FWHM of this peak with the synthesis conditions can be seen in Figure 2.7.

Figure 2.7 – Most intense reflection of the synthesized waste-based zeolites.

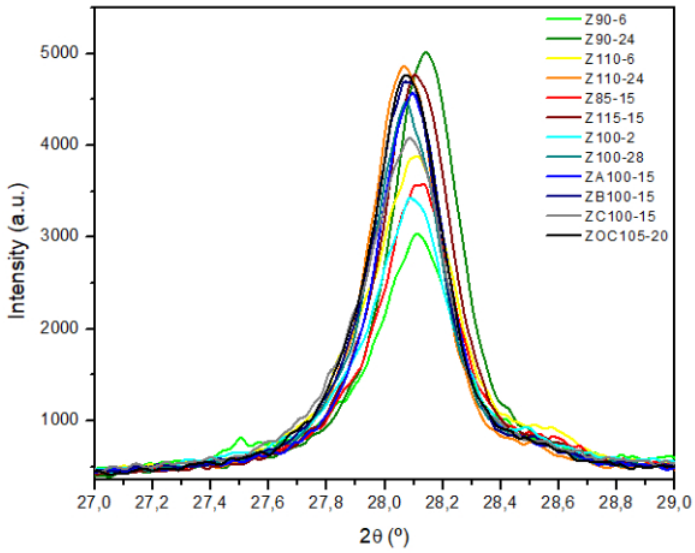

Source: created by the author

Table 2.7 shows the intensity, diffraction angle (2θ) and Full Width at Half Maximum (FWHM) of the most intense diffraction peak [301] for each waste-based zeolite synthesized, as well as the crystallite size (D_{hkl}) determined using the Scherrer

equation (Equation 2.1) (presented in Section 2.5.1). The obtained zeolites showed the most intense peak (3042 to 5063 counts) centered between 28.07º and 28.14º (2θ), and the crystallite sizes ranged from 21 to 28 nm. For the samples corresponding to the central points of the CCRD (Z_A100-15, Z_B100-15 and Z_C100-15), determined to assess the repeatability of the results, the average values of the peak parameters were calculated. A maximum intensity of 4490 ± 331 counts was observed, centered on the diffraction angle 28.08º ± 0.01º, with a FWHM of 0.33º ± 0.03º and a crystallite size of 25 nm ± 2 nm.

Table 2.7 – Peak parameters (intensity, 2θ and FWHM) and crystallite sizes (D_{hkl}) of the synthesized waste-based zeolites.

Sample	Intensity (counts)	2θ (º)	FWHM (º)	D_{hkl} (nm)
Z90-6	3042	28.11	0.3950	21
Z90-24	5063	28.14	0.3117	26
Z110-6	3910	28.09	0.3901	21
Z110-24	4892	28.07	0.2968	28
Z85-15	3270	28.11	0.3513	23
Z115-15	4821	28.11	0.3183	26
Z100-2	3456	28.09	0.3706	22
Z100-28	4509	28.07	0.3165	26
Z_A100-15	4619	28.09	0.3064	27
Z_B100-15	4738	28.07	0.3158	26
Z_C100-15	4114	28.07	0.3614	23
Z_{OC}105-20	4778	28.07	0.3280	25

Source: created by the author

In addition to the peak parameters and crystallite sizes, the semi-quantification of the most crystalline phases for the Z90-24, Z110-6, Z110-24 and Z_{OC}105-20 waste-based zeolites (obtained using the Diffrac.Suite EVA software) and the yield of the synthesis reaction are shown in Table 2.8.

Table 2.8 – Semi-quantification of the NaP zeolite (reference file ICDD PDF = 39-0219) and yield of the synthesis reaction.

Sample	NaP (%)	Yield ($Kg_{zeolite}/Kg_{HS}$)
Z90-24	89.1	1.70
Z110-6	82.6	1.69
Z110-24	83.6	1.75
Z_{OC}105-20	90.8	1.77

Source: created by the author

The semi-quantitative analysis of the samples shows that the waste-based zeolite synthesis resulted in the formation of materials with high NaP zeolite content, ranging from 82.6% (Z110-6) to 90.8% (Z_{OC}105-20). No other type of zeolite was observed. However, small amounts of compounds from salt slag that did not react completely could be tentatively identified in these samples, including corundum and

spinel. Furthermore, for each kg of hydrolyzed slag used in the synthesis process, between 1.69 and 1.77 kg of zeolites can be produced. The zeolite synthesized at 110 ºC for 24 hours (Z110-24) showed a slightly higher yield (1.75) and percentage of NaP zeolite (83.6%) compared to the synthesis carried out for 6 hours (Z110-6), which were 1.69 and 82.6%, respectively. Also, the longer reaction time increased the crystallinity of this sample (73.9%) compared to the previous one (72.0%) (Table 2.4). Despite the lower yield (1.70) and crystallinity (71.4%) compared to Z110-24, sample Z90-24 has significantly higher amounts of NaP zeolite, 89.1% compared to 83.6%. Comparing samples Z90-24 and Z110-6, it can be observed that a longer reaction time has a greater impact than temperature on crystallinity, resulting in a higher content of NaP zeolite in the synthesized material. Although the Z_{OC}105-20 sample presents a slightly lower degree of crystallinity (73.4%) than that obtained for Z110-24 (73.9%), it was the one that obtained the highest yield (1.77) and the highest content of NaP zeolite (90.8%). This confirms that the optimal experimental conditions for hydrothermal synthesis, obtained through CCRD, are a moderate temperature of 105 ºC and a reaction time of 20 hours.

The textural properties of the selected zeolites Z90-24, Z110-6, Z110-24 and Z_{OC}105-20, including specific surface area (S_{BET}), external surface area (S_{Ext}) and pore size, determined from adsorption isotherms/N_2 desorption (Fig. 2.8a), as well as their cation exchange capacity (CEC) are presented in Table 2.9.

Figure 2.8 – (a) Nitrogen adsorption/desorption isotherms and (b) distribution of pore diameter of the waste-based NaP zeolites.

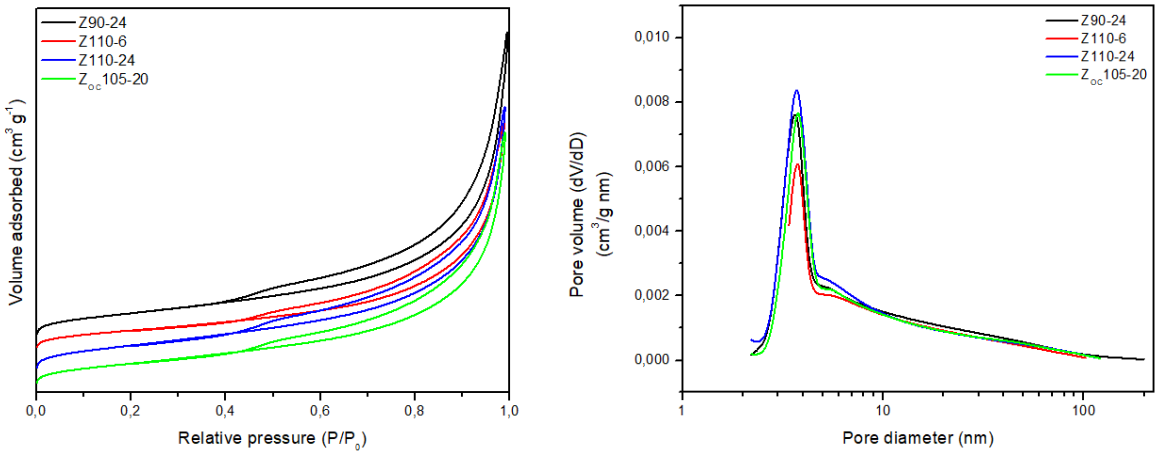

(a) (b)

Source: created by the author

The nitrogen adsorption/desorption isotherms of the zeolites showed the same type IV behavior typical of mesoporous materials (2-50 nm). The mesoporous characteristic of NaP zeolite possibly results from the assembly of nanometric crystallites that form its aggregates (Sayehi et al., 2020). In all cases, the hysteresis loop (H3 type – according to the IUPAC classification) was observed at P/P_0 range between 0.45 and 0.98 (maximum pressure) indicating the presence of many nanometer-sized pores and characterizing solid materials with slit-shaped pores of non-uniform sizes or shapes (Bandura et al., 2015). The pore size distribution curve, acquired by the BJH method (Fig. 2.8b) shows a mesoporous distribution with a predominant pore size of 3.8 nm observed in all samples. The smaller peaks located at 5.4 nm (Z90-24, Z110-6 and Z110-24) and 5.6 nm (Z_{OC}105-20) could indicate a secondary pore size.

Table 2.9 – Textural properties and CEC of the synthesized waste-based zeolites.

Sample	S_{BET} ($m^2\ g^{-1}$)	S_{Ext} ($m^2\ g^{-1}$)	Micropore volume ($x10^{-4}\ cm^3\ g^{-1}$)	Pore size (nm)	CEC (meq g^{-1})
Z90-24	22.45	22.11	1.86	3.80	3.55
Z110-6	18.49	17.53	4.82	3.79	2.86
Z110-24	23.18	23.57	Not determined	3.80	3.23
Z_{OC}105-20	21.11	20.77	1.89	3.80	3.67

Source: created by the author

In terms of S_{BET} (Table 2.9), values between 18.49 and 23.18 $m^2\ g^{-1}$ were obtained. The observation of tabulated values suggests that the difference in surface area of the obtained zeolites was influenced to a greater extent by the reaction time than by the synthesis temperature. The Z_{OC}105-20 zeolite, synthesized under optimal experimental conditions, showed a S_{BET} of 21.11 $m^2\ g^{-1}$ and S_{Ext} = 20.77 $m^2\ g^{-1}$. This small difference indicates the low micropore volume (1.89 $x10^{-4}\ cm^3\ g^{-1}$) of the zeolite. The small micropore volume observed in the samples is probably due to the shape (bottleneck) of the micropores, which interferes with the entry of the gas and, consequently, its determination (Sharma et al., 2016). S_{BET} values were higher when compared to those obtained for NaP-type zeolites using other aluminum waste (14.2 $m^2\ g^{-1}$) (Sánchez-Hernández et al., 2016), salt slag (17.0 $m^2\ g^{-1}$) (Padilla et al., 2022) and fly ash (18.5 $m^2\ g^{-1}$) (Liu et al., 2018). Although differences in the degasification conditions may affect these values of S_{BET}, the results obtained in this work indicate that the waste-based NaP zeolite owing potential characteristic to be used as an adsorbent material.

The CEC values for NH_4Cl ranged from 2.86 to 3.67 meq g^{-1} for the synthesized NaP zeolites. The highest CEC (3.67 meq g^{-1}) was obtained for the zeolite Z_{OC}105-20. This value is higher than those reported for waste-based NaP-type zeolites. Using aluminum waste, as already mentioned, Padilla et al. (2022) and Sánchez-Hernández et al. (2016), obtained a CEC of 2.12 and 2.73 meq g^{-1}, respectively. From coal fly ash, Cardoso et al. (2015) obtained CEC of 2.6 meq g^{-1} through hydrothermal synthesis with 3M NaOH at 100 ºC for 24 h. Musyoka et al. (2012) achieved a CEC of 2.98 meq g^{-1} in a two-step synthesis at 100 ºC for 48 h. Additionally, Zhou et al. (2023) reported a CEC of 2.58 meq g^{-1} for zeolite synthesized in a two-step process with a microwave reaction at 180 ºC for 2 h after 12 hours of stirring. This characteristic also enables zeolite to be used as an adsorbent.

The morphology of the Z90-24, Z110-6, and Z110-24 zeolites at different magnifications is shown in Figure 2.9. All the samples exhibited a homogeneous 'cauliflower-like' morphology, characteristic of NaP-type structures (Sánchez-Hernández et al., 2016). In the figure, it can be observed that the units constituting the aggregates are particles measuring between 420 and 990 nm, while the joining of these units forms conglomerates measuring between 2 and 5 μm.

Figure 2.9 – SEM images of the waste-based zeolites (a) Z90-24, (b) Z110-6 and (c) Z110-24, at different magnifications.

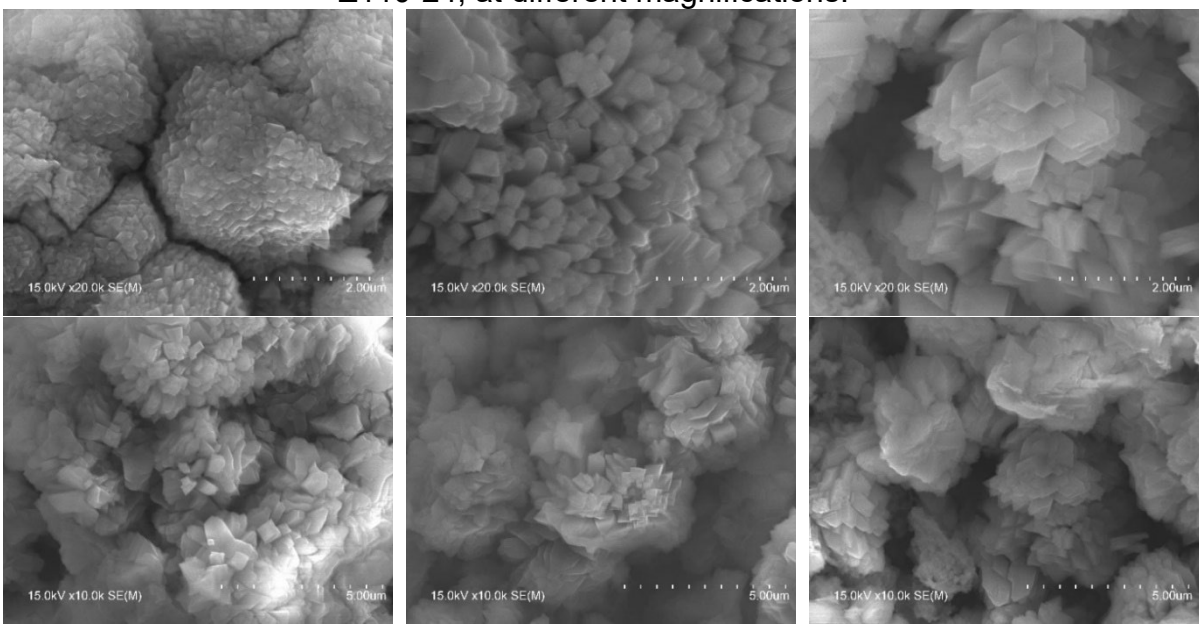

(a) (b) (c)

Source: author's collection

Figure 2.10 shows the SEM images at different magnifications of the Z_{OC}105-20 zeolite. This NaP zeolite exhibited a morphology composed by agglomerates of around 10–50 μm (Fig. 2.10a and b). As can be seen at high magnification (Fig. 2.10c and d), these clusters were formed by smaller secondary aggregates with defined contours growing in different directions.

Figure 2.10 – SEM images of the waste-based zeolite synthesized under the optimal conditions at different magnifications.

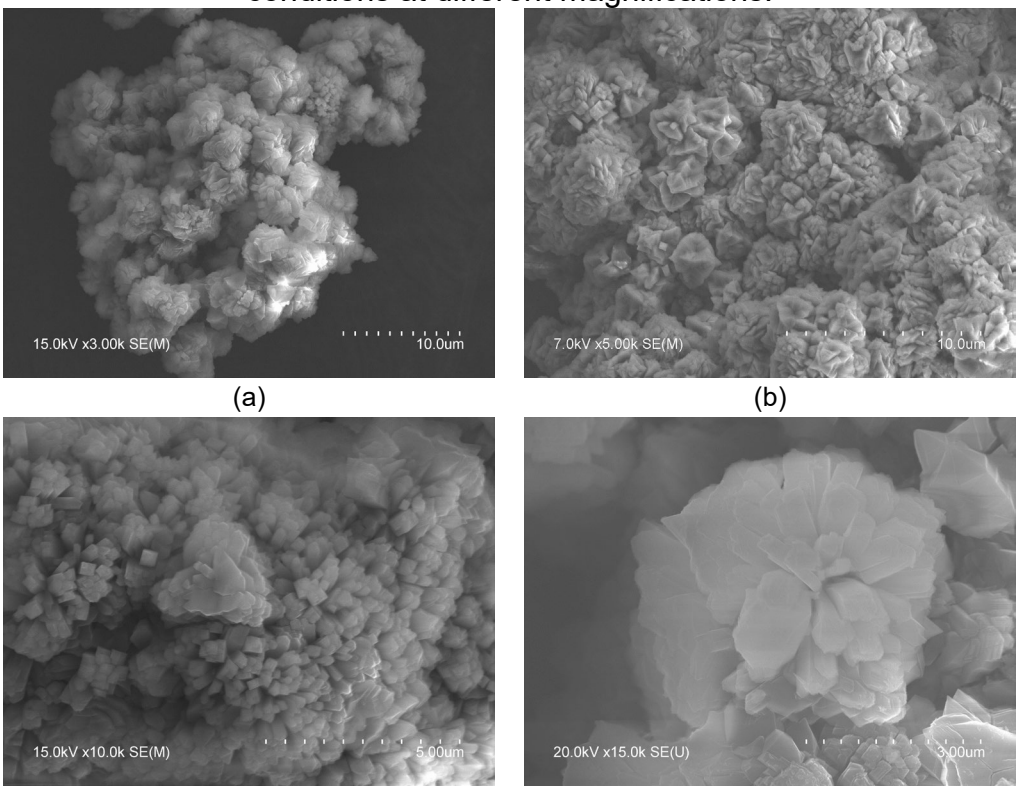

(a) (b)

(c) (d)

Source: author's collection

2.5 CONCLUSION

In this study, hazardous salt slag (aluminum source) and rice husk ash (silicon source) were valorized through their use as uncommon raw materials for the production of zeolites with excellent sorbent characteristics and promising applications. Almost all the tested synthesis conditions showed a degree of crystallization greater than 70% for the waste-based NaP zeolites. It was found that the variables of time and temperature, separately and the interaction between them, exerted a significant influence on the crystallization of the zeolites. The optimal experimental conditions (105 ºC and 20 hours), statistically determined, resulted in a zeolite with a high degree

of crystallinity (73.4%) and containing more than 90% zeolitic material. ANOVA analysis regarding the crystallization of the obtained zeolites indicated that the validity of the model was within the 95% confidence interval, and no adjustments were required within the evaluated range. This led to an outstanding reproducibility of experimental samples. Both S_{BET} (21.11 m^2 g^{-1}) and CEC (3.67 meq g^{-1}) showed higher values than those reported by other authors for the synthesis of NaP-type zeolites using different wastes, suggesting adequate properties of the waste-based NaP-zeolite for effluent treatments via adsorption and ion exchange mechanisms. The co-recycling of both hazardous aluminum and agri-food wastes into zeolites promotes an industrial symbiosis and can be considered a sustainable alternative in waste management, generating value-added materials and greatly contributing to environmental preservation.

3 CHAPTER III: WASTE SYMBIOSIS THROUGH THE SYNTHESIS OF HIGHLY CRYSTALLINE LTA AND SOD ZEOLITES[2]

materials

MDPI

Article

Waste Symbiosis through the Synthesis of Highly Crystalline LTA and SOD Zeolites

Magali Teresinha Ritter [1,2], Isabel Padilla [1], María Ángeles Lobo-Recio [2,3], Maximina Romero [1] and Aurora López-Delgado [1,*]

[1] Department of Materials, Eduardo Torroja Institute for Construction Sciences (IETcc-CSIC), Serrano Galvache Street, 4, 28033 Madrid, Spain; magali.ritter@posgrad.ufsc.br (M.T.R.); isabel.padilla@ietcc.csic.es (I.P.); mromero@ietcc.csic.es (M.R.)
[2] Department of Environmental Engineering, Federal University of Santa Catarina (UFSC), Campus Reitor João David Ferreira Lima, Florianópolis 88040-900, SC, Brazil; maria.lobo@ufsc.br
[3] Department of Energy and Sustainability, Federal University of Santa Catarina (UFSC), Campus Araranguá, Rodovia Governador Jorge Lacerda, 3201, Jardim das Avenidas, Araranguá 88906-072, SC, Brazil
* Correspondence: alopezdelgado@ietcc.csic.es

HIGHLIGHTS

- Synthesis of zeolites using wastes as unconventional raw materials
- Salt slag and rice husk ash used for the first time to produce LTA zeolites
- Eco-synthesis process for producing highly crystalline LTA and SOD zeolites
- Preserving natural resources through co-recycling wastes
- Influence of reaction time, temperature and Na^+ concentration on zeolites types

[2] RITTER et al. (2024c). Article published in the journal Materials (Impact factor 3.1 – Q1:2023) in August 2024.

GRAPHICAL ABSTRACT

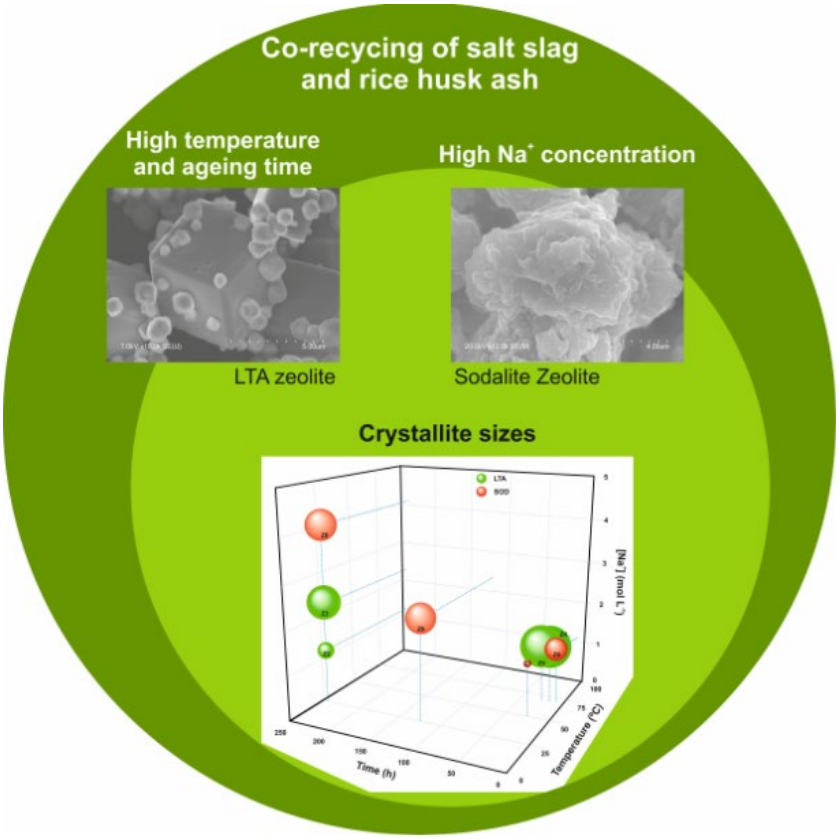

Source: created by the author

3.1 ABSTRACT

In recent years, the demand for natural and synthetic zeolites has surged due to their distinctive properties and myriad industrial applications. This research aims to synthesise crystalline zeolites by co-recycling two industrial wastes: salt slag (SS) and rice husk ash (RHA). Salt slag, a problematic by-product of secondary aluminium smelting, is classified as hazardous waste due to its reactive and leachable nature, though it is rich in aluminium. Conversely, RHA, an abundant and cost-effective by-product of the agro-food sector, boasts a high silicon content. These wastes were utilised as aluminium and silicon sources for synthesising various zeolites. This study examined the effects of temperature, ageing time, and sodium concentration on the formation of different zeolite phases and their crystallinity. Results indicated that increased Na^+ concentration favoured sodalite (SOD) zeolite formation, whereas Linde type-A (LTA) zeolite formation was promoted at higher temperatures and extended ageing times. The formation range of the different zeolites was defined and supported

by crystallographic, microstructural, and morphological analyses. Additionally, the thermal behaviour of the zeolites was investigated. This work underscores the potential to transform industrial waste, including hazardous materials like salt slag, into sustainable, high-value materials, fostering efficient waste co-recycling and promoting clean, sustainable industrial production through cross-sectoral industrial symbiosis.

Keywords: sol-gel synthesis, waste-based zeolites, LTA and SOD zeolites, hazardous waste, salt slag, rice husk ash.

3.2 INTRODUCTION

Demand for zeolites has grown considerably in recent years, driven mainly by the detergent industry, where synthetic zeolites have been used to replace phosphate-based agents, which are highly polluting to the environment. In addition to detergents, zeolites have been widely applied in several other areas, including petrochemicals, biotechnology, fertilisers, construction, gas separation, environmental remediation, and even biodiesel production (COLLINS et al., 2020).

A recent analysis by Markets and Markets (MARKETS AND MARKETS, 2023) predicts a 3.1% Compound Annual Growth Rate (CAGR) in the global zeolite market from 2021 to 2026, expanding from 4,872 metric tonnes to 5,453 metric tonnes, with synthetic zeolites comprising approximately 42% of the total. Despite the availability of natural zeolites, they are generally contaminated to varying degrees by other minerals, metals, or other zeolites, making them unsuitable for commercial and industrial applications that require high purity and uniformity (MALLAPUR; OUBAGARANADIN, 2017). Consequently, there is growing interest in the synthesis of zeolites, which allows the production of zeolitic structures with high purity, more uniform sizes, better ion exchange capacity, high selectivity, and higher thermal resistance (EL BOJADDAYNI et al., 2023).

With regard to synthetic zeolites, the Linde Type-A (LTA) zeolite is one of the most widely used, especially due to its three-dimensional structural arrangement, which provides high adsorption and ion exchange capacity. This makes it suitable for use as molecular sieves and adsorbents in cooling, cleansing, and water softening systems (COLLINS et al., 2020; EL BOJADDAYNI et al., 2023). The LTA zeolite

($Na_{12}Al_{12}Si_{12}O_{48}\cdot 27H_2O$) framework is formed by the so-called β-cages or sodalite cages (24 T atoms [T = Si^{4+} or Al^{3+}]), in which the primary units are SiO_4 and AlO_4 tetrahedra (Fig. 3.1). These units are connected to the six nearest neighbouring β-cages by double T4 rings [D4Rs]. When connected to neighbouring β-cages via single T4 rings [S4Rs], the sodalite zeolite structure is formed, which is the simplest structure among zeolites (PROKOF'EV; GORDINA, 2014). The cubic framework of the sodalite (SOD) zeolite ($Na_8Al_6Si_6O_{24}(OH)_2\cdot 2H_2O$) has small pore sizes and thus a low application potential for ion exchange and molecular sieving. However, it is considered a promising material as a membrane separator for small molecules of liquids and gases, including H_2 and He (SÁNCHEZ-HERNÁNDEZ et al., 2016).

Figure 3.1 – LTA- and SOD-type frameworks. The double D4R and single S4R bonds are in blue.

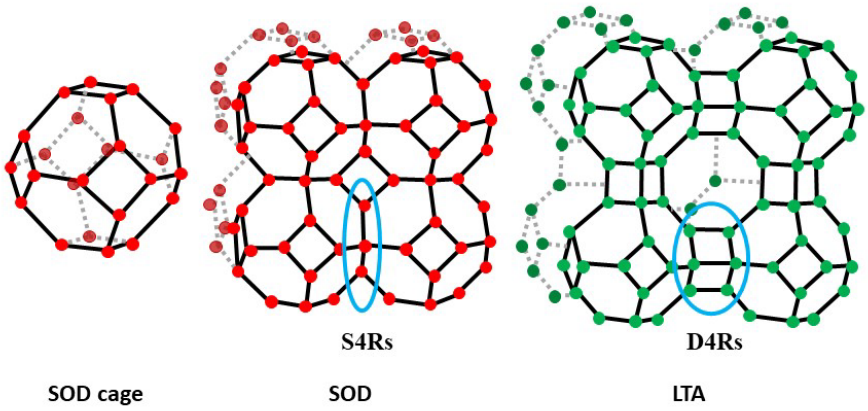

Source: created by the author

The formation of LTA or SOD zeolites is defined by the ideal synthesis condition, as the development of the desired zeolite phase depends on a specific temperature range, reaction time, and the molar ratio of the initial gel composition, which directly affect the nucleation and crystal growth processes (WANG et al., 2009).

In recent years, the synthesis of zeolites using secondary raw materials has attracted increasing attention in order to reduce production costs and mitigate the associated environmental impacts. In this sense, a great variety of wastes have been tested to produce LTA and SOD zeolites, including waste glass (KIM et al., 2015; LEE; LIN; LIN, 2022; MOUNA; HAJJI; TOUNSI, 2024), rice husks (BOHRA; KUNDU; NASKAR, 2014; MELO et al., 2014; SIMANJUNTAK et al., 2021; WAJIMA et al., 2009; WANG et al., 2018), fly ash (AL-DAHRI; ABDULRAZAK; ROHANI, 2022; BEHIN et al.,

2014; BELVISO et al., 2012; CAO; WANG; SUN, 2020; CARDOSO et al., 2015; KIM; LEE, 2009; LIU et al., 2024; SHABANI et al., 2022; SHOUMKOVA; STOYANOVA, 2013; XU et al., 2014; ZIEJEWSKA et al., 2023), alum sludge (ANUWATTANA; KHUMMONGKOL, 2009; ESPEJEL-AYALA et al., 2014; ROZHKOVSKAYA; RAJAPAKSE; MILLAR, 2021; WONGWICHIEN, 2014), and aluminium waste (ABDELRAHMAN et al., 2021; KUROKI et al., 2019; LÓPEZ-DELGADO et al., 2020; SÁNCHEZ-HERNÁNDEZ et al., 2016; SELIM et al., 2017; TERZANO et al., 2015; TOUNSI; MSEDDI; DJEMEL, 2009). The synthesis methods applied often involve several steps and high temperature or long reaction time. Melo et al. (MELO et al., 2014) reported the synthesis of LTA through a hydrothermal process, employing a commercial sodium aluminate solution and a sodium silicate derived from RHA treated at 1200 °C for 2 h. Abdelharam et al. (ABDELRAHMAN et al., 2021) employed a sol-gel process involving RHA and aluminium can waste at 150 °C for 12 h. RHA was also used by Simanjuntak et al. (SIMANJUNTAK et al., 2021) together with food-grade aluminium foil, in a process that entailed the alkaline dissolution of both wastes, followed by the ageing of the solution mixture for 24 h at room temperature, and a crystallisation stage at 100 °C for 72 h; the resulting product was then subjected to a calcination process at 550 °C for 8 h to form zeolite A.

Among aluminium waste, salt slag is the main waste produced by the secondary aluminium industry, generating approximately 0.5 tons of salt slag for every ton of recycled aluminium produced (PADILLA et al., 2022). Based on data published by Statista (2023) (STATISTA, 2023), it is estimated that more than 13 million metric tons of salt slag will be generated worldwide by 2027. This figure has almost tripled in 20 years and is on an upward trend due to the increased use and recycling of aluminium (HUANG et al., 2014). In addition to the large volumes, the management and disposal of this waste is a major concern due to its potential for environmental contamination. Salt slag is considered toxic and hazardous waste, highly harmful, flammable, irritating, and leachable, according to the European Catalogue of Hazardous Waste (EWC, 2001) code 10 03 08. Its irritant properties pose a threat to human health and can cause damage through contact with the skin or mucous membranes, ingestion, and inhalation. Disposal in landfills is an environmental catastrophe due to the leachable salts, which can cause irreversible impacts on groundwater and soil (ATTIA; HASSAN; HASSAN, 2018). Furthermore, the high

reactivity of salt slag in contact with water leads to the formation of toxic gases (NH_3, CH_4, H_2S, H_2, and PH_3), which also pollute the atmosphere (PADILLA et al., 2022). Nevertheless, its aluminium-rich composition makes salt slag a potential candidate for producing zeolites.

Although, as mentioned above, some authors have used different aluminium wastes as precursor materials in the synthesis of zeolites, few studies have been conducted with salt slag (JIMÉNEZ et al., 2021; PADILLA et al., 2022). In addition, commercial silicate solutions were used as the source of silicon in these works.

Concerning silicon waste, rice husk ash (RHA) has been identified as a promising low-cost alternative to commercial silica (PODE, 2016). It is a silicon-rich material resulting from the thermal transformation of rice husks and is considered to be one of the most abundant agro-food waste products. According to the Food and Agriculture Organization of the United Nations (FAO, 2024) more than 31 million tons of RHA were generated worldwide in 2023. Although rice husk ash is not hazardous waste as salt slag is, its high production, slow biodegradation, small particle size, and need to be disposed of in landfills cause several environmental problems.

In a previous paper, the authors studied the synthesis of NaP-type zeolite from salt slag and RHA by a hydrothermal method. Moreover, a central composite rotational design (CCRD) was applied to determine the best experimental conditions required to obtain NaP zeolite (RITTER et al., 2024a). This work reports for the first time the synthesis of LTA and SOD zeolites from two unconventional raw materials, such as hazardous aluminium salt slag and rice husk ash. The aim of this study was to promote the co-recycling of these two wastes via the sol-gel process as a way of minimising the environmental impacts associated with their management. The evolution in terms of crystallinity, microstructure, and morphology of zeolitic materials synthesised under different experimental conditions was evaluated, assessing the influence of reaction time, temperature, and alkalinity. In addition, the thermal behaviour of the zeolites and their cation exchange capacity were also studied. The novelty and applicability of this work fall under the development of a synthesis method under mild conditions that makes it possible to produce highly crystalline LTA- and SOD-type zeolites from the combination of two industrial wastes.

3.3 MATERIALS AND METHODS

3.3.1 Raw Materials

For the synthesis of zeolites, two different industrial wastes were employed: a hazardous waste from the secondary aluminium industry named salt slag (SS) and a waste from the agro-food industry, specifically rice husk ash (RHA). The wastes were selected for their respective contents of alumina (SS) and silicon (RHA), the two main components of zeolite composition. SS was supplied by Alusigma S.A (Gijón, Spain), and its chemical composition mainly consists of Al_2O_3 (63.5 wt.%) and smaller amounts of MgO (7.9 wt.%), SiO_2 (7.7 wt.%), CaO (4.5 wt.%), and Fe_2O_3 (3.0 wt.%). Rice husk ash (RHA) was used to provide the necessary amount of silicon for zeolite synthesis. The RHA sample was supplied by Herba Ricemills S.L.U. (Seville, Spain). The main component of RHA is SiO_2 (89.7 wt.%), followed by minor amounts of K_2O (3.6 wt.%), P_2O_5 (1.7 wt.%) and CaO (1.3 wt.%).

The complete characterisation of both wastes (SS and RHA) was reported in a previous work (RITTER et al., 2024a). Furthermore, a commercial sample of LTA zeolite, used for comparative purposes, was supplied by Industrias Químicas del Ebro, S.A. (Zaragoza, Spain).

3.3.2 Zeolite Synthesis

The waste-based zeolites were synthesised using a sol-gel process followed by an ageing step. Firstly, aluminate and silicate solutions were prepared by treating the initial SS and RHA in an alkaline medium (NaOH solution). Preliminary studies were conducted at different times (1–24 h), temperatures (room temperature–120 °C), and alkalinities (1–5 M) in order to determine the best conditions for obtaining aluminate and silicate solutions with the highest aluminium and silicon contents, respectively. The highest Al concentration, 19.88 g L^{-1}, was achieved by treating 0.15 g mL^{-1} of SS with a 5M NaOH solution for 1 h at 100 °C. Similarly, the highest silicon content (58.34 g L^{-1}) of the silicate solution prepared from RHA was achieved by treating 0.16 g mL^{-1} of RHA with a 3M NaOH solution, for 3 h at 120 °C. The Na

concentrations in the aluminate and silicate solutions were 105.3 and 69.66 g L^{-1}, respectively.

The sol-gel synthesis was performed by adding the silicate solution, in the required amounts to obtain a Si/Al ratio = 1, to the aluminate solution at room temperature with constant stirring. The resulting gel was kept under constant stirring under different ageing conditions (Table 3.1). Due to the high sodium content of the aluminate and silicate solutions, only distilled water in the appropriate volumes was added to the synthesis, and no additional NaOH solution was required. The different Na^+ concentrations used focused on obtaining the LTA zeolite phase, while the temperatures and ageing times tested aimed to increase the crystallinity of the resulting samples (JOHNSON; ARSHAD, 2014; PROKOF'EV; GORDINA, 2014). Nine experiments were carried out under different ageing conditions to evaluate their effect on the type and properties of the zeolites obtained. The samples obtained were labeled Z1 - Z9 (Table 3.1).

Table 3.1 – Experimental ageing conditions of the synthesised waste-based materials, and Na^+ concentration in the solution.

Samples	T (ºC)	t (h)	[Na^+] (mol L^{-1})
Z1	RT	24	1.27
Z2	RT	240	1.27
Z3	RT	240	2.36
Z4	70	15	1.27
Z5	70	24	1.27
Z6	RT	240	4.12
Z7	50	24	1.27
Z8	70	6	1.27
Z9	RT	120	2.36

RT: room temperature. Source: created by the author

After the tests, the resulting solid products were filtered, washed with distilled water, and dried at 100 °C for 24 h. The samples were then characterised by XRD, SEM, and FTIR according to the procedures described in the following section 3.5.3. In addition, their cation exchange capacity (CEC) and thermal behaviour (TG/DTA) were also determined.

3.3.3 Characterisation Techniques

The composition of the aluminate and silicate solutions extracted from salt slag and RHA, respectively, was analysed using an inductively coupled plasma optical

emission spectrometer, ICP-OES (Varian 725-ES, Agilent Technology, Santa Clara, CA, USA). The mineralogical characterisation of the zeolites was carried out by X-ray diffraction (XRD) using a Bruker D8 Advance diffractometer (Bruker, Champs–sur–Marne, France) with CuKα radiation, 2θ from 5º to 60º, and a scan rate of 2θ of 0.02º, 5 s per step. Diffrac.Suite EVA Plus 13.0 software (Bruker, AXS GmbH, Karlsruhe, Germany) was used to semi-quantify the crystalline phases of the zeolitic materials obtained. A crystallographic study of the zeolites was performed, which included the determination of interplanar spacings and network parameters. The interplanar spacing d (Å) was calculated by applying Bragg's law (Equation 3.1), where n is a natural number other than zero (n = 1), λ is the wavelength of the incident radiation (1.541 nm), and θ is the diffraction angle.

$$d = {}^{n.\lambda}/_{2.sen\theta} \tag{3.1}$$

The lattice parameter a was calculated according to the crystalline system (cubic) using Equation 3.2, where d corresponds to the interplanar spacing and hkl to the Müller indices relative to the diffraction planes.

$$a = d\sqrt{(h^2 + k^2 + l^2)} \tag{3.2}$$

Thermogravimetric and differential thermal analysis (TG-DTA) was carried out on a Thermoanalyzer model SDT-Q600 (TA Instruments, New Castle, DE, USA), under an air flow of 100 mL min^{-1} and a heating rate of 10 °C min^{-1}. The Fourier transform infrared (FTIR) spectra (Nicolet Nexus 670–870, Nexus, Singapur, Malaysia) were recorded on KBr discs in the 400–4000 cm^{-1} range. The cation exchange capacity (CEC) of the zeolites was determined by the ammonium ion exchange method using an NH_4Cl solution (1M), as described in the Standard number NC 626 (NC 626, 2008).

3.4 RESULTS AND DISCUSSION

3.4.1 Effect of Ageing Time, Temperature, and Alkali Concentration

The XRD patterns of the nine samples of the zeolites synthesised using aluminate and silicate solutions from SS and RHA, are shown in Figure 3.2a (samples

Z1 to Z5) and Figure 3.2b (samples Z6 to Z9), based on the predominant zeolitic material obtained, for better viewing. The crystallographic parameters, including the intensity, diffraction angle (2θ), and Full Width at Half Maximum (FWHM) of the most intense reflections are shown in Table 3.2. In addition, the semi-quantification of the most crystalline phases identified using Diffrac.Suite EVA software is presented, as is the crystallite size (D); determined from the most intense peak of the zeolite phase using the Scherrer equation: $D = (0.9 \cdot \lambda) / (FWHM \cdot \cos\theta)$, where λ is the X-ray wavelength (0.154 nm) and θ is the diffraction angle (in rad).

From Figure 3.2 and Table 3.2, it can be observed that, with the exception of sample Z1, in which no crystalline phase could be identified, and sample Z2, with an incipient appearance of peaks, all the other samples resulted in the formation of crystalline zeolites. By increasing the ageing time from 24 h (Z1) to 240 h (Z2), the XRD pattern shows the development of small peaks with a profile characteristic of the cubic zeolite LTA, with a crystallite size of 22 nm. Increasing the Na^+ concentration from 1.27 mol L^{-1} (Z2) to 2.36 mol L^{-1} (Z3) at 240 h and room temperature, resulted in the development of narrow, very intense, and well-defined peaks (> 4000 counts), which fit well with those of the XRD pattern of the LTA zeolite from the International Centre for Diffraction Data (ICDD), reference file PDF 73-2340. A crystallite size of 45 nm was calculated for this sample. This result highlights that a higher concentration of Na^+ promotes the formation of LTA when the ageing time is extended. Both samples Z4 and Z5, synthesised with a NaOH concentration of 1.27 mol L^{-1} at 70 ºC, resulted in 100% zeolitic material. However, for the sample synthesised over 15 h (Z4), several peaks corresponding to the SOD-type zeolite were observed along with corresponding ones to LTA, the latter with a crystallite size of 55 nm. By increasing the ageing time to 24 h (Z5), a single LTA zeolite phase was obtained with very intense, and well-defined peaks (> 5800 counts) and a crystallite size of 53 nm. This indicates that a longer ageing time favours the formation of LTA zeolite.

Regarding samples Z6, Z7, Z8, and Z9, the XRD patterns (Fig. 3.2b) principally showed peaks corresponding to the SOD-type zeolite (ICDD PDF 76-1639). A certain amorphous phase content, decreasing from Z6 (close to 40%) to Z9 (around 25%), is also consistent with the background of the patterns. At room temperature, 240 h, and 4.12 mol L^{-1} of Na^+ (Z6), SOD showed a peak intensity >1400 counts and a crystallite size of 45 nm. Increasing the temperature to 50 °C for 24 h while maintaining a Na^+

concentration of 1.27 mol L^{-1} (Z7) resulted in SOD with a peak intensity >1700 counts and a crystallite size of 10 nm. At 70 °C for 6 h (Z8), the percentage of crystalline SOD in the sample reached 81.3%, with a maximum peak intensity around 5000 counts and a crystallite size of 30 nm. Finally, sample Z9, synthesised at room temperature for 120 h with 2.36 mol L^{-1} of Na^{+}, resulted in the highest percentage of crystalline SOD and the highest peak intensity (> 6700 counts), with a crystallite size of 41 nm.

Figure 3.2 – XRD patterns of the waste-based materials (a) Z1 to Z5 and (b) Z6 to Z9, synthesised under different experimental conditions [A – LTA zeolite (PDF 73-2340) and S – SOD zeolite (PDF 76-1639)].

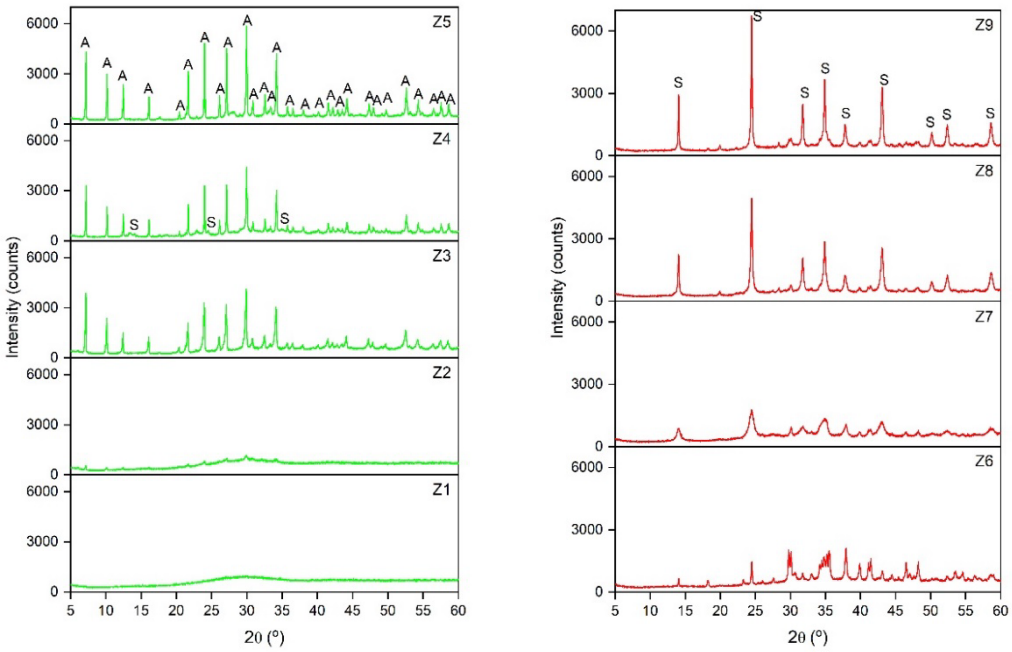

(a) (b)

Source: created by the author

Table 3.2 – Crystallographic parameters (intensity, 2θ, and FWHM), semi-quantification of the zeolite phases, and crystallite sizes (D) of the synthesised waste-based materials.

Samples	Phase	Zeolite (%)	Intensity (counts)	2θ (º)	FWHM (º)	D (nm)
Z1	Amorphous phase	-	-	-	-	-
Z2	LTA + amorphous phase	47.4	1162	29.92	0.3743	22
Z3	LTA	100	4101	29.88	0.1848	45
Z4	LTA	95.6	4423	29.96	0.1496	55
	SOD	4.4				
Z5	LTA	100	5864	29.96	0.1564	53
Z6	SOD	24.6	1464	24.49	0.1808	45
Z7	SOD	30.0	1783	24.48	0.7829	10
Z8	SOD	81.3	4955	24.48	0.2703	30
Z9	SOD	81.8	6723	24.47	0.1992	41

FWHM: Full Width at Half Maximum; D: crystallite size determined from the most intense reflection.

Source: created by the author

The crystallite sizes of the different zeolite phases synthesised as a function of the experimental conditions applied (ageing time, temperature, and Na^+ concentration) are shown in Figure 3.3.

Figure 3.3 – Zeolite phase and corresponding crystallite size obtained according to different experimental conditions (LTA in green and SOD in red).

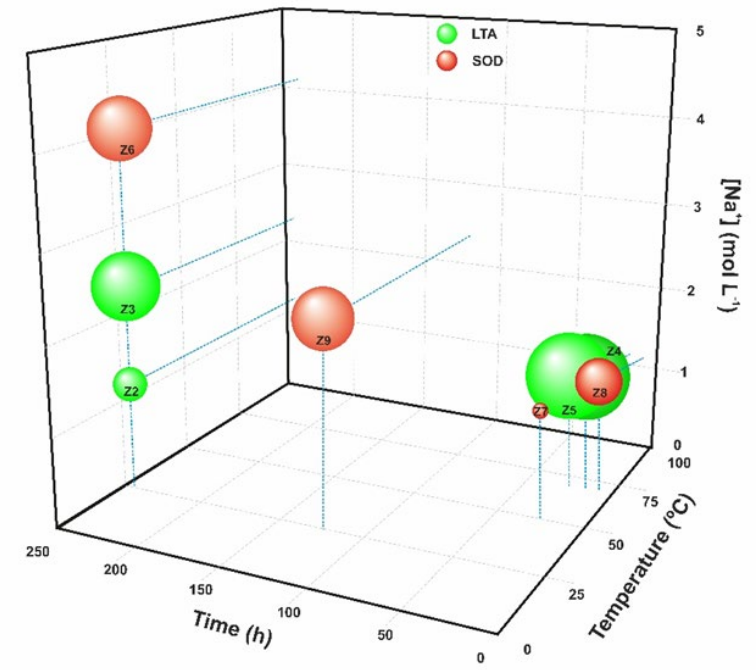

Source: created by the author

Several factors, including temperature, ageing, pressure, reagent sources, Si/Al ratio, and water content (JOHNSON; ARSHAD, 2014), influence not only the development of specific zeolite phases and their crystallinity but also the size of the crystals formed. Thus, increasing the ageing time from 24 to 240 h at room temperature resulted in the evolution from a geopolymer (Z1) to the incipient formation of LTA zeolite (Z2). However, this trend was not observed at a higher temperature; in the synthesis conducted at 70 °C, extending the reaction time from 15 to 24 hours resulted in similar crystallite sizes (samples Z4 and Z5). Sodium concentration had the most significant effect on crystallite size. Increasing the Na^+ concentration from 1.27 mol L^{-1} to 2.36 mol L^{-1} caused the crystallite size of the LTA zeolites to increase from 22 nm (Z2) to 45 nm (Z3). Nevertheless, obtaining a specific zeolite phase is defined by the alkali concentration in the mixing reaction and the crystallisation kinetics (PANGAN et al., 2021; TOUNSI; MSEDDI; DJEMEL, 2009). Comparing samples Z2, Z3, and Z6, synthesised under the same conditions of time (240 h) and temperature (RT), revealed

that increasing the sodium content resulted in the development of the SOD phase, known for its higher Na_2O/Al_2O_3 ratio (close to 1.33 for the stoichiometric phase) compared to the LTA zeolite (Na_2O/Al_2O_3 = 1). This conclusion is supported by the fact that a high concentration of NaOH solution (>3.5 M) destabilises the structure of the LTA zeolite, causing the destruction of double T4 rings [D4Rs] and leading to the binding of β-cages via single T4 rings [S4Rs] and the consequent formation of sodalite (JOHNSON; ARSHAD, 2014; PROKOF'EV; GORDINA, 2014).

According to the results, longer ageing times and higher temperatures led to the formation of LTA-type zeolites. This behaviour was observed by comparing Z7 and Z5, when the temperature was increased from 50 to 70 °C to a fixed Na^+ concentration of 1.27 mol L^{-1}, and with samples Z9 and Z3, which transitioned from an SOD zeolite to an LTA zeolite by doubling the ageing time (120 to 240 h). Shorter ageing times disproved this outcome when comparing samples Z8, Z4, and Z5, which transitioned from an SOD zeolite (6 h) to a mixture of LTA-SOD (15 h) and a pure LTA (24 h). This suggests that sodalite could serve as an intermediate phase that evolves into an LTA zeolite as the ageing time increases, as indicated by the mixture of zeolitic phases identified for an intermediate ageing time (Z4). Similar results were reported by other authors. Simanjuntak et al. (SIMANJUNTAK et al., 2021), who synthesised zeolites using RHA and aluminium foil as raw materials, corroborate the findings, also reporting that an SOD zeolite was obtained with a shorter reaction time (48 h) compared to a longer time (72 h) which resulted in an LTA-type zeolite. This result suggests that an increase in reaction temperature enhances the partial dissolution of silica and alumina components from the gel into the aqueous phase and subsequently promotes the formation of crystal nuclei within the gel matrix (TOUNSI; MSEDDI; DJEMEL, 2009). It can be inferred that different heating rates lead to the formation of slightly different initial gels and, consequently, to the development of different zeolite phases. Thus, the interplay between temperature and ageing time is key for obtaining highly crystalline single-phase LTA zeolites.

In regard to the crystallite size, the values obtained are quite similar to those reported by other authors who have synthesised LTA- and SOD-type zeolites from wastes. Al-Dahri et al. (AL-DAHRI; ABDULRAZAK; ROHANI, 2022) obtained LTA zeolite with a crystallite size of 45 nm from coal fly ash using a microwave-assisted method. The sol-gel synthesis performed by Asefa & Feyisa (ASEFA; FEYISA, 2022)

from aluminium foil waste and sugarcane bagasse ash resulted in LTA zeolite with a crystallite size of 49 nm. Meanwhile, the SOD zeolite produced by this same method had crystallites ranging from 46 to 64 nm when aluminium can waste was used (ABDELRAHMAN; HEGAZEY, 2019).

The reported differences in crystallinity and structure were also observed in the morphology of the waste-based zeolites obtained under different ageing conditions (Fig. 3.4). Corroborating the XRD analysis, the SEM micrograph of sample Z1 (Fig. 3.4Z1) shows agglomerates of tiny rounded particles (< 0.1 μm), characteristic of geopolymeric materials, whereas in the case of sample Z2 (Fig. 3.4Z2), larger particles (1-1.6 μm) have begun to develop which, although predominantly amorphous, present an incipient cubic morphology (1-1.6 μm), but without well defined edges and boundaries. The micrograph of sample Z3 (Fig. 3.4Z3) shows a stacking of particles with a cubic tendency and edges with a higher degree of definition than those observed in Z2, with sizes varying between 0.1 and 0.9 μm, indicating the formation of a more crystalline LTA zeolite. The lack of definition on the edges of the cubes is due to the low temperature during the ageing stage. The synthesis temperature affects the morphology of the zeolites, with low temperatures leading to the formation of rounder crystals and higher temperatures leading to more cubic shapes (BRAR; FRANCE; SMIRNIOTIS, 2001; COLLINS et al., 2020). This is corroborated by the predominant presence of well-defined cubic crystals in the SEM images of samples Z4 (Fig. 3.4Z4) and Z5 (Fig. 3.4Z5), characteristics of crystalline LTA zeolite. In the first sample, the largest cubes ranged in size from 2.5 to 5 μm and the smallest from 0.2 to 1.5 μm. As for sample Z5, the cubic crystals exhibit perfectly defined and slightly chamfered edges. In this sample, some cubic twinned crystals are also observed, along with very small cubes (500 to 900 nm) developed on top of the larger ones.

The morphology of the Z6-Z9 samples (Fig. 3.4Z6-Z9) confirms the XRD analysis by presenting structures consistent with sodalite-type zeolites, similar to those reported by other authors (ABDELRAHMAN; HEGAZEY, 2019; ANDRADES et al., 2020). SEM images of samples Z6 and Z9 show clusters (30-100 μm) of slightly rounded "flower-like" particles with average diameters of 2-10 μm, which are characteristic of the SOD-type structure (SHOUMKOVA; STOYANOVA, 2013).

Figure 3.4 – SEM images of the waste-based synthesised materials Z1–Z9.

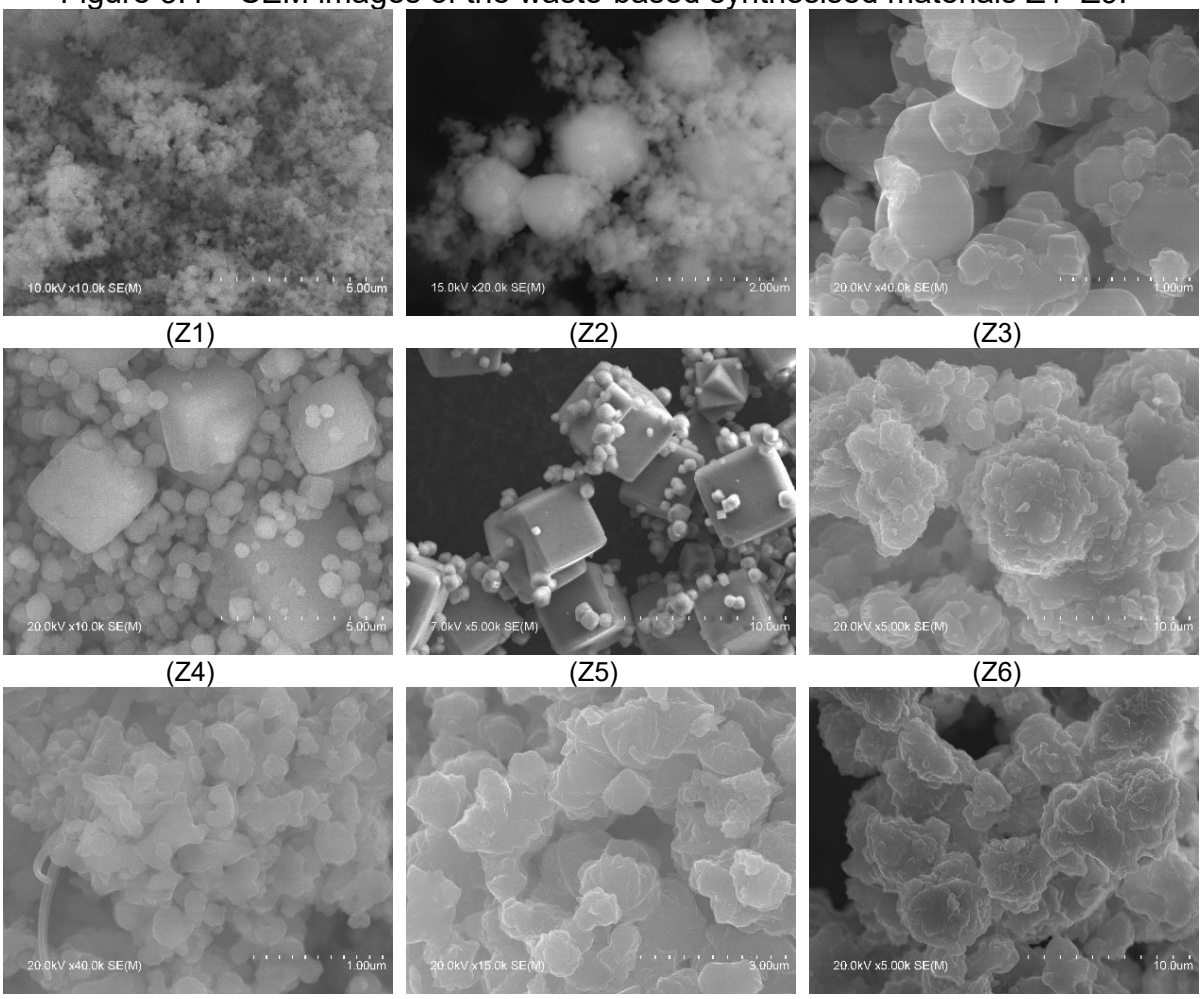

Source: author's collection

3.4.2 Study of LTA and SOD Zeolites

As mentioned above, samples Z5 and Z9 correspond to well-defined LTA- and SOD-type zeolites, respectively, so both samples were subjected to more in-depth analysis.

Due to the high crystallinity and well-defined peaks of LTA zeolite obtained from Z5, its XRD pattern and crystallographic parameters were compared with those of a commercial LTA zeolite (ZCOM) (Figure 3.5, Table 3.3).

The LTA zeolite synthesised from SS and RHA showed an XRD profile quite similar to that of the commercial zeolite, with well-developed peaks and slightly higher intensities (Fig. 3.5). The most significant peaks of the Z5 sample compared to the commercial LTA zeolite; the reference file PDF 73-2340 showed the similarity of the interplanar spacing values obtained as well as the relative intensities (I/I_0) (MILTON,

1953). The most intense reflection of the synthesised LTA zeolite, centred at 29.96 ° (2θ), corresponds to the diffraction hkl index [644], according to PDF 73-2340. In addition, the lattice parameter a, calculated according to Equation 3.2, which considers the cubic crystal system of the LTA zeolite, was 12.29 Å, very similar to the 12.32 Å reported in the reference ICDD files.

In the case of the SOD zeolite, the most significant peaks of the Z9 sample coincide completely with the reference file PDF 76-1639 (HASSAN; GRUNDY, 1983) (Table 3.4). The interplanar spacing and the relative intensities of the most intense reflections show practically identical values. The most intense reflection corresponding to the SOD phase was centred at 24.47° (2θ), which corresponds to the hkl index [211].

Figure 3.5 – XRD patterns of the waste-based LTA zeolite (Z5) in green and commercial LTA zeolite (ZCOM) in blue.

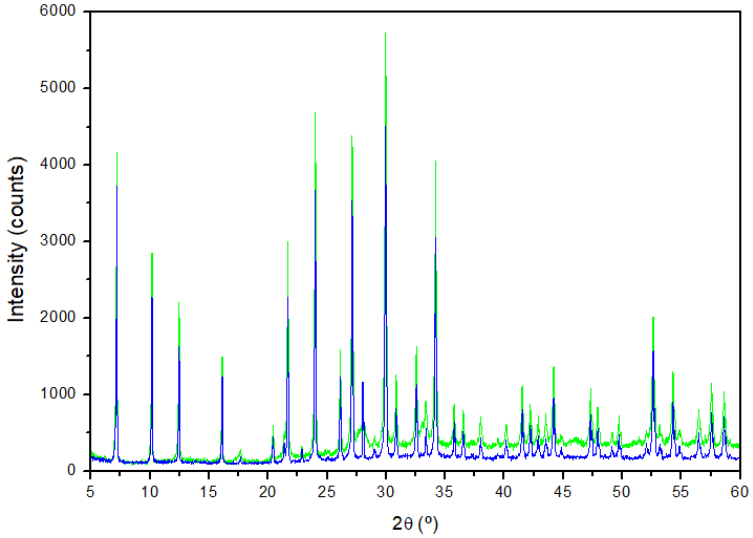

Source: created by the author

Table 3.3 – Crystallographic parameters of waste-based LTA zeolite, commercial LTA zeolite, and reference ICDD files.

Z5 (LTA)			**ZCOM**			**PDF 73-2340**			
d(Å)	**2θ (°)**	**I/I_0**	**d(Å)**	**2θ (°)**	**I/I_0**	**d(Å)**	**2θ (°)**	**I/I_0**	**hkl**
12.27	7.20	73	12.27	7.20	64	12.31	7.18	69	[2 0 0]
8.69	10.17	51	8.69	10.17	39	8.70	10.16	46	[2 2 0]
7.09	12.47	40	7.09	12.47	28	7.10	12.45	51	[2 2 2]
4.10	21.68	54	4.10	21.68	39	4.10	21.65	39	[6 0 0]
3.71	24.00	82	3.71	24.00	63	3.71	23.97	54	[6 2 2]
3.41	26.12	29	3.41	26.12	21	3.41	26.09	8	[6 4 0]
3.29	27.13	77	3.29	27.13	60	3.29	27.09	67	[6 4 2]
2.98	29.96	100	2.98	29.96	100	2.98	29.92	100	[6 4 4]
2.75	32.56	30	2.75	32.56	19	2.75	32.52	22	[8 4 0]
2.62	34.20	72	2.62	34.18	52	2.62	34.15	50	[6 6 4]

Source: created by the author

The calculated lattice parameter, which, as for the LTA zeolite, also considers the cubic-type crystal system of the SOD zeolite, was 8.90 Å, compared to 8.89 Å assigned by the reference file.

Table 3.4 – Crystallographic parameters of waste-based SOD zeolite.

Z9 (SOD)			**PDF 76-1639**			
d(Å)	**2θ (º)**	**I/I_0**	**d(Å)**	**2θ (º)**	**I/I_0**	**hkl**
6.30	14.05	44	6.29	14.08	44	[1 1 0]
3.64	24.47	100	3.63	24.51	100	[2 1 1]
2.81	31.79	37	2.81	31.81	40	[3 1 0]
2.57	34.88	55	2.57	34.93	48	[2 2 2]
2.10	43.10	49	2.10	43.14	56	[4 1 1]

Source: created by the author

The FTIR spectra of samples Z5 (LTA) and Z9 (SOD) (Fig. 3.6) were recorded in the mid-infrared wavenumber region (1200 to 400 cm^{-1}), where the fundamental vibrations of the framework (Si, Al)O_4 tetrahedra are located (FLANIGEN; SAND, 1974). The spectrum of sample Z5 shows the four absorption bands characteristic of LTA zeolite. The bands at 995 and 664 cm^{-1} are due to asymmetrical and symmetrical internal stretching vibrations, respectively. The band at 461 cm^{-1} corresponds to the Si-O-Al bending mode and the medium-intensity vibration at 552 cm^{-1} is attributed to the vibration of the secondary structural units [D4Rs] (TOUNSI; MSEDDI; DJEMEL, 2009). Similar FTIR values were reported by López-Delgado et al. (LÓPEZ-DELGADO et al., 2020) who also prepared LTA zeolite from an aluminium waste, as well as those reported by Vegere et al. (VEGERE et al., 2020) for zeolite 4A prepared from commercial raw materials. This points the high purity of the synthesised waste-based LTA zeolite. Sample Z9 showed the typical triplet of SOD zeolite, with bands at 735, 709 and 665 cm^{-1} corresponding to the symmetrical stretching mode. The two bands at 464 and 434 cm^{-1} represent the octahedral bending mode. In addition, two low-intensity bands are observed at 881 and 867 cm^{-1}, attributable to the symmetrical external stretching of T-O-T (T= Si and/or Al) (ABDELRAHMAN et al., 2021). These results are corroborated by Sánchez-Hernández et al. (SÁNCHEZ-HERNÁNDEZ et al., 2016) for SOD zeolite produced from an aluminium waste and commercial sodium silicate.

Figure 3.6 – FTIR spectra of LTA (Z5) in green and SOD (Z9) in red.

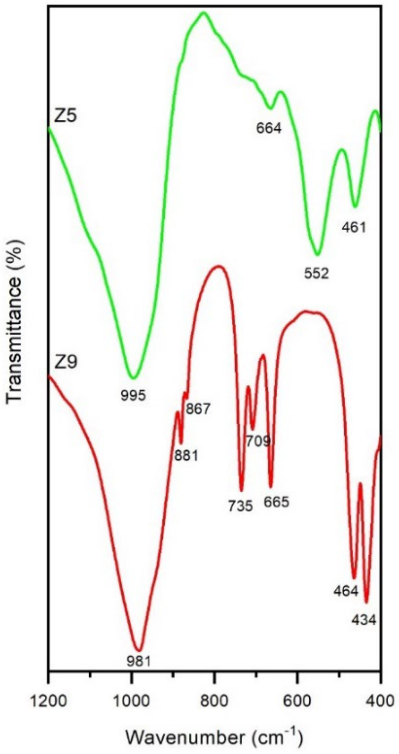

Source: created by the author

The TG-DTA curves of samples Z5 (LTA) and Z9 (SOD) are shown in Figure 3.7. Both samples exhibit endothermic effects below 250 °C. The structured profile of these bands indicates that the dehydration of both zeolites occurs in several overlapped steps, and is due to different types of water (absorbed, zeolitic, etc). Concerning LTA, a second mass loss takes place below 400 °C, and is associated with the loss of water due to a dehydroxylation process. The total mass loss for sample Z5, according to the TG curve, was 21.7%, similar to the loss observed for a commercial zeolite (MUSYOKA et al., 2015). This value corresponds to a loss of approximately 26 water molecules, which is quite similar to the corresponding one for the stoichiometric theoretical LTA zeolite ($Na_{12}Al_{12}Si_{12}O_{48}{\cdot}27H_2O$). After that, no mass loss is observed in the TG curve, but the DTA curve exhibits two exothermic peaks centred at 913 and 969 °C. These peaks were attributed to the topotactic transformation of the cubic framework of LTA zeolite into the hexagonal framework of nepheline ($NaAlSiO_4$). Several authors reported that this transformation occurs at temperatures higher than 700 °C (DIMITRIJEVIC et al., 2004). A temperature of 890 °C has also been reported for LTA zeolite obtained at pilot scale from an aluminium waste and commercial water glass (LÓPEZ-DELGADO et al., 2020). Selvaraj et al. (SELVARAJ, 2010) also

observed two exothermic peaks between 800 and 900 °C in the DTA curve of a commercial LTA zeolite, due to the transformation and recrystallisation of nepheline.

In the case of sample Z9 (SOD), a total mass loss of 27% took place from room temperature up to 800 °C, corresponding to the release of 22 water molecules. Between 400 and 800 °C the mass loss of 5.2 % can be attributed to the crystallisation and structural water, which fit well to the theoretical value for a sodalite stoichiometry of $Na_8Al_6Si_6O_{24}(OH)_2 \cdot 2H_2O$ (GÜNTHER et al., 2015). Above 790 °C, the DTA curve shows an inflection point without any corresponding mass loss. This observation suggests the onset of a gradual transformation from sodalite to nepheline, although the transformation remains incomplete at the test temperature.

Overall, the zeolites studied exhibit the ability to retain their structure and only lose water during thermal treatment at temperatures below 800 °C for both Z5 and Z9. This characteristic makes these zeolites useful in processes requiring high temperatures or those needing high-temperature treatment for regeneration (MUSYOKA et al., 2015).

Figure 3.7 – TG (dot line) and DTA (solid line) for the selected waste-based zeolites LTA (Z5) and SOD (Z9).

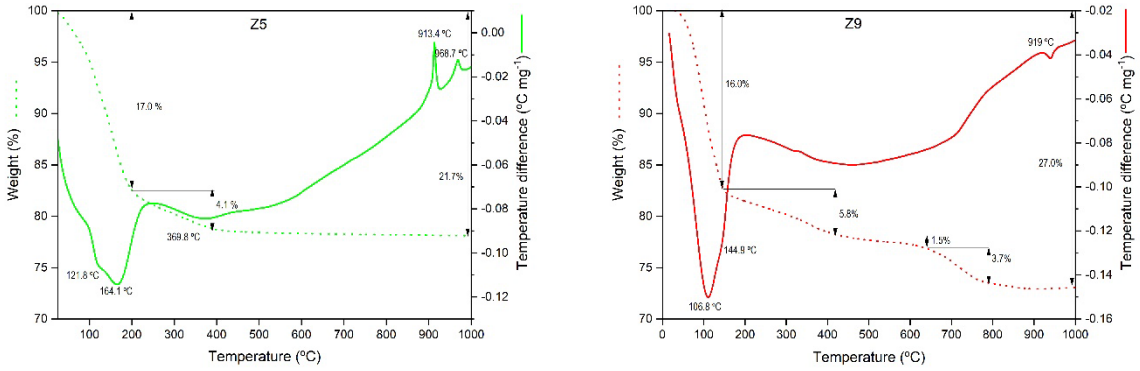

Source: created by the author

Concerning the cation exchange capacity (CEC), the value for Z5 was 3.40 meq g^{-1}, higher than that of Z9 (1.82 meq g^{-1}). The CEC is one of the main requirements for the use of zeolites, especially in detergent formulation and water decontamination (AYELE et al., 2015; QUEROL et al., 2002). The CEC results found in this study are remarkable when compared to the values reported by other authors who synthesised A-type zeolites using different wastes (BEHIN et al., 2014; LOBO-RECIO et al., 2021;

LÓPEZ-DELGADO et al., 2020; PANGAN et al., 2021; WONGWICHIEN, 2014). Pangan et al. (PANGAN et al., 2021) reported a CEC value of 2.44 meq g^{-1} for an LTA zeolite synthesised from corn straw ash by a hydrothermal method at 90 °C for 9 h, while other authors reported values of CEC lower than 2 meq g^{-1} for zeolites obtained from aluminium slag milling waste (LÓPEZ-DELGADO et al., 2020), fly ash by a microwave-assisted hydrothermal process [(BEHIN et al., 2014)], or alum sludge by hydrothermal synthesis at 90 °C for 9 h (WONGWICHIEN, 2014). The high CEC value of the LTA zeolite synthesised in this study suggests its promising application in processes such as the treatment of metal-contaminated wastewaters. The CEC of SOD zeolite, although lower than that of LTA, was higher than that reported by other authors (SÁNCHEZ-HERNÁNDEZ et al., 2016).

3.5 CONCLUSION

The co-recycling of hazardous aluminium salt slag and rice husk ash through a synthesis process under mild conditions resulted in highly crystalline LTA and SOD zeolites. A highly crystalline LTA zeolite was obtained at a temperature of 70 °C for 24 h, while under the same conditions, the SOD zeolite was synthesiszed in only 6 h. The results showed the great influence of the experimental conditions on the development of a specific zeolite phase. The increase in sodium concentration favours the formation of SOD zeolite. The effect of temperature on the crystallinity of the zeolites is much more significant than the effect of ageing time. A high value of cation exchange capacity of 3.40 meq g^{-1} was obtained for the LTA. This indicates that the LTA-type zeolite prepared from wastes could have potential applications in the same way as commercial zeolites. The synthesis of zeolites can be considered as a new alternative route to conventional waste management methods, especially for hazardous wastes such as salt slag, leading to the production of value-added materials, which are in increasing demand worldwide and have significant applications in several fields. The valorisation of these wastes through their conversion into advanced materials, such as LTA- and SOD-type zeolites, contributes above all to saving natural resources and preserving the environment. Finally, yet importantly, this approach favours the circular economy, creating a symbiosis between the different industrial segments, given that

many industries that generate aluminium and agro-food waste use zeolites in their industrial gas and effluent treatment systems.

4 CHAPTER IV: ADSORPTION OF SAFRANINE-T DYE USING A WASTE-BASED ZEOLITE: OPTIMIZATION, KINETIC AND ISOTHERMAL STUDY[3]

Journal of Industrial and Engineering Chemistry 136 (2024) 177–187

Contents lists available at ScienceDirect

Journal of Industrial and Engineering Chemistry

journal homepage: www.elsevier.com/locate/jiec

Adsorption of Safranine-T dye using a waste-based zeolite: Optimization, kinetic and isothermal study

Magali Teresinha Ritter [a,b], María Ángeles Lobo-Recio [b,c], Isabel Padilla [a,*], Maria Eliza Nagel-Hassemer [b], Maximina Romero [a], Aurora López-Delgado [a]

[a] Department of Materials, Eduardo Torroja Institute for Construction Sciences (IETcc)-CSIC, Serrano Galvache, 4, 28033 Madrid, Spain
[b] Departament of Environmental Engineering, Federal University of Santa Catarina (UFSC), Campus Reitor João David Ferreira Lima, 88040-900 Florianópolis, SC, Brazil
[c] Department of Energy and Sustainability, Federal University of Santa Catarina (UFSC), Campus Araranguá, Rod. Gov. Jorge Lacerda, 3201, Jardim das Avenidas, 88.906-072 Araranguá, SC, Brazil

HIGHLIGHTS

- A waste-based Linde Type-A (LTA) zeolite successfully used to remove a cationic dye
- A Composite Central Rotational Design (CCRD) allowed the determination of optimal adsorption parameters (zeolite dosage and agitation rate)
- Efficient removal of Safranine-T dye (> 98%) from colored aqueous solutions
- Nearly quantitative removal achieved with very short contact times
- High potential of aluminum waste-based LTA zeolites for treating textile wastewater

[3] RITTER et al. (2024b). Article published in the Journal of Industrial and Engineering Chemistry (Impact factor 5.9 – Q1:2023) in February 2024.

GRAPHICAL ABSTRACT

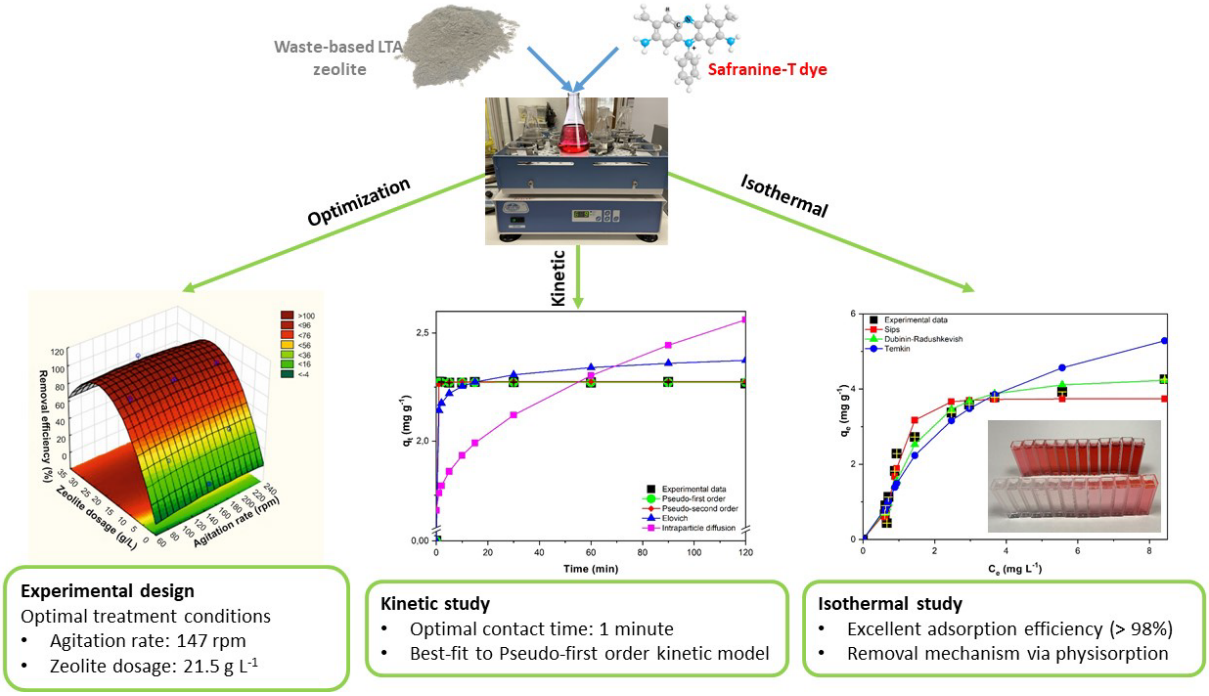

Source: created by the author

4.1 ABSTRACT

The global issue of water resource pollution due to wastewater containing dyes is a significant environmental concern. The proper treatment of these harmful wastewaters is a great challenge due to their characteristic structural complexity and low biodegradability. The present work reports the application of a Linde Type-A (LTA) zeolite synthesized from a hazardous aluminum waste as an adsorbent to remediate Safranine-T dye from aqueous solutions. The optimal experimental conditions (agitation rate and zeolite dosage of 147 rpm and 21.5 g L^{-1}, respectively) were determined through a central composite rotational design (CCRD), and enabled a removal efficiency of 98.12% of the textile dye. The model that showed the best fit to the experimental data and better explained the adsorption mechanism, according to the isothermal studies, was the Sips model. The kinetics followed the pseudo-first order model and revealed that Safranine-T dye removal was achieved in a contact time of just one minute. The waste-based LTA zeolite exhibited highly promising adsorbent properties with an efficient and extremely fast adsorption capacity. Its use as a treatment agent for dye-contaminated wastewater can significantly contribute to sustainability and the circular economy.

Keywords: adsorption, cationic dye, Safranine-T, LTA zeolite, aluminum waste, central composite rotational design.

4.2 INTRODUCTION

Contamination of water resources is a major environmental problem in the world today (AL-TOHAMY et al., 2022). Industrial development has led to an increasing generation of wastes and effluents containing various harmful and damaging components, which adversely affect water quality and human health when discharged into the environment without proper treatment (GHOLAMI et al., 2023). Dyes are one of the most commonly found pollutants in wastewater due to their large-scale production and widespread use in many areas, including the food, textile, cosmetic, paper and plastic industries (KAMEL et al., 2021; SIEREN et al., 2020).

The textile industry is a highly polluting industry for the aquatic resources due to the use of dyes. Throughout the different stages of the dyeing process, and depending on the type of fabric and dye used, dye losses can range between 5% and 50%, generating nearly 200 billion liters of dye-containing effluents every year (TKACZYK; MITROWSKA; POSYNIAK, 2020). Annually, around 280,000 tons of dyes are lost within the textile industry, ending up in aquatic ecosystems (MISHRA; MAITI, 2018).

In terms of environmental impacts, the textile industry requires a significant amount of freshwater to process its textile products, resulting in the discharge of highly contaminated effluents (HOLKAR et al., 2016; SARWAR et al., 2023). Thus, the textile industry ranks second among the most water-polluting industries, trailing behind the petroleum industry (UNEP, 2018).

Textile dyes discharged into aquatic ecosystems, even in small amounts, result in the deterioration of water quality, affecting its odor and color. Additionally, they reduce light penetration thereby impacting the efficiency of photosynthetic function and decreasing oxygen levels, leading to negative consequences for aquatic life (LI et al., 2021). Recent research has revealed that these toxic dyes can cause gene mutations and even trigger the development of cancer (SHU et al., 2023).

Safranine-T (ST) (Figure 4.1) is a synthetic cationic dye available as a powder or reddish crystals with the molecular formula $C_{20}H_{19}ClN_4$ (3,7-dimethyl-10-phenylphenazin-10-ium-2,8-diamine chloride).

Figure 4.1 – Molecular 3D structure of Safranine-T dye (a) Front view; (b) Side view.

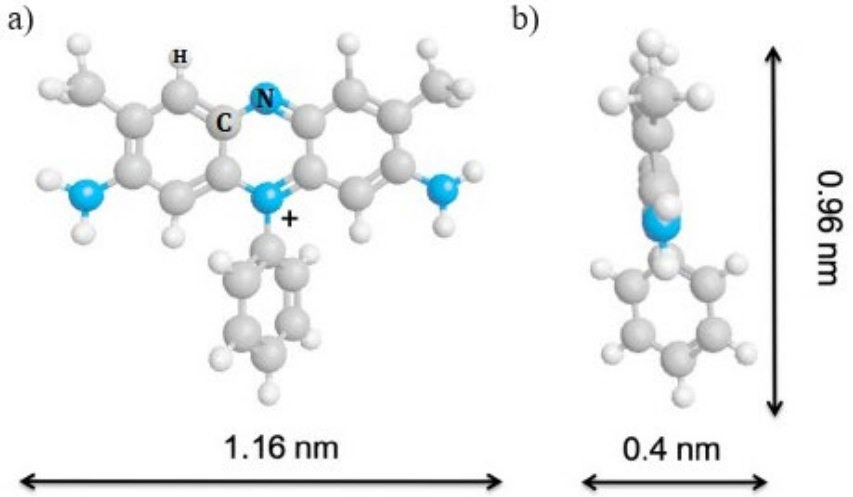

Source: adapted from SHI et al. (2021)

This dye is extensively used in dyeing cotton, silk, tannin, wool, leather, bast fibers and paper, and is considered a model compound representing the dyes released into the effluents of the textile industry (GUPTA et al., 2006). Due to their easy and strong interaction with negatively charged cell membranes, cationic dyes pose a higher risk compared to anionic dyes and can cause allergies and respiratory difficulties (SAHA et al., 2021). Contamination with dyes, especially with Safranine-T, can cause stomach discomfort, irritation of the respiratory tract, throat discomfort, as well as irritation and redness of the eyes and skin (KAMEL et al., 2021). Hence, environmental protection agencies and relevant legislation demand compliance with the established permissible limits for dye discharge in wastewater, necessitating their elimination before being discharged into mainstreams (SULEMAN et al., 2021).

ST is also classified as a nitrogenous heterocyclic dye, which is more difficult to degrade compared to the aromatic ones (JIALIANG et al., 2012). In this regard, the structural complexity and stability of these dyes significantly affect the decolorization process, making them difficult to treat by the methods normally utilized in wastewater treatment plants (GHOSH et al., 2021; SHARAFINIA; FARROKHNIA; LEMRASKI, 2022). Physicochemical methods commonly used in wastewater treatment, such as

membrane separation, coagulation-flocculation and advanced oxidation processes have several limitations related to their high cost, low versatility, limited efficiency, generation of secondary pollutants and waste management (SRIVASTAVA et al., 2022; TACAS et al., 2021). Thus, recently, a great deal of research has been focused on improving water treatment processes and expanding technologies to increase the quality of treated effluents, with the aim of eliminating these toxic and biologically harmful components (ASHRAFIVALA et al., 2022).

Among these technologies, adsorption stands out as the most extensively utilized technique for eliminating dyes from wastewater (YADAV et al., 2022b). In recent years, this method has garnered increased attention due to its ease of use and efficiency, particularly with the development of low-cost alternative adsorbents (LOBO-RECIO et al., 2021). A wide range of new adsorbent materials has been studied, with especial emphasis on zeolitic materials. Zeolites are aluminosilicates structured in a three-dimensional network formed by AlO_4 and SiO_4 tetrahedra interconnected through oxygen atoms, creating intracrystalline channels of atomic size (MALLAPUR; OUBAGARANADIN, 2017). Zeolites have been employed in various industrial applications due to their regular porous structure and unique properties, encompassing areas such as gas purification, water remediation, and catalysis, among other industrial uses (COLLINS et al., 2020).

Zeolites occur naturally or can be synthesized from various sources or silicon and aluminum. Currently, the authors have focused their research on producing zeolites from waste materials rich in silica and alumina, as an alternative to the use of pure chemical products and to preserve mineral resources. This approach leads to a reduction in process costs and environmental impact (LIN et al., 2022). According to López-Delgado et al. (LÓPEZ-DELGADO et al., 2020), the utilization of hazardous waste from aluminum industry is an uncommon choice for zeolite synthesis, offering an altenative while also reducing the generation and management of such waste.

In recent years, the adsorption of Safranine-T using zeolites has been widely investigated (ABUKHADRA; MOHAMED, 2019; ATUN et al., 2011; AYAR et al., 2015; DAS; BARMAN, 2013; PEREIRA et al., 2018; SÁNCHEZ-HERNÁNDEZ et al., 2016; SHI et al., 2021; SIEREN et al., 2020). In relation to the synthesized zeolite, Atun et al. (ATUN et al., 2011) conducted the synthesis of various zeolites using fly ash, varying the parameters of time and temperature. The zeolite that exhibited the most favorable

adsorption results for ST was obtained at a temperature of 90 ºC after 7 days. Throughout this process, the formation of a mixture of NaP, X, Y, Analcime, and Sodalite zeolites was achieved. The adsorption capacity at equilibrium, considering a equilibrium time of 60 minutes, reached 7.02 mg g^{-1}. Ayar et al. (AYAR et al., 2015) also investigated the adsorption of ST using a zeolite synthesized from fly ash at a temperature of up to 150 ºC for 1 day, resulting in a mixture of Analcime and Sodalite. The adsorption capacity was determined after 40 days, reaching a qe of 15.72 mg g^{-1}. Furthermore, Das et al. (DAS; BARMAN, 2013) conducted the synthesis of NaX and NaA zeolites from fly ash through alkali fusion at 650 ºC for 1 hour, followed by a hydrothermal treatment at 90º C for 6 hours, aimed at removing Safranine-T from water. The adsorption capacity at equilibrium was determined after 24 hours, reaching a value of 1.27 mg g^{-1}, and, finally, Pereira et al. (PEREIRA et al., 2018) synthesized LTA zeolite from metakaolin through a hydrothermal process at 80ºC for 24 hours. The obtained zeolite was utilized for the adsorption of Safranine-T, achieving a q_e of 9.4 mg g^{-1} after 5 minutes. However, as far as is known, there are no studies on the adsorption of dyes, including Safranine-T, using zeolites synthesized from aluminum waste.

In this context, this work was envisaged as an opportunity to create a symbiosis between two industrial sectors: on one hand, the aluminum industry produces a hazardous waste, which is transformed by a simple process into LTA zeolite. On the other hand, this waste-based zeolite is applied for the remediation of wastewater from the dyeing industry. After selecting the optimal temperature and pH for studying the adsorption of ST on LTA zeolite, a factorial planning based on central composite rotatable design (CCRD) was employed to model, assess, and enhance treatment efficiency, as well as to identify optimal parameters in the remediation process. Moreover, kinetic and isothermal studies were performed to investigate the zeolite sorption kinetics, and its adsorption capacity and mechanism. In addition, under the best experimental conditions, a comparison of ST dye adsorption using different zeolite types was also evaluated.

4.3 MATERIALS AND METHODS

4.3.1 Adsorbent Material

In this research, LTA zeolite obtained on a pilot scale through a moderate-temperature hydrothermal process, using hazardous aluminum waste as raw material, was employed (LÓPEZ-DELGADO et al., 2020). The aluminum waste used originates from the tertiary aluminum industry and consists of the finest power fraction captured in sleeve filters during the aluminum slag process. The chemical composition consists of about 77 wt% Al_2O_3 and 4 wt% SiO_2, while mineralogical composition is primarily distributed among metallic aluminum, aluminum nitride, corundum, spinel and alkaline salts (LÓPEZ-DELGADO et al., 2020).

LTA zeolite [$Na_{12}Al_{12}Si_{12}O_{48}(H_2O)_{27}$] consists of a homogeneous fine-grain solid with a particle size <100 μm. The textural characterization of the zeolite was carried out by determining the nitrogen adsorption/desorption isotherms at 77 K (ASAP 2010 Micromeritics) with the sample previously degassed (250 ºC in vacuum for 24 h). The specific surface area (S_{BET}) of 19.7 $m^2\ g^{-1}$ was determined through multi-point measurements using the Brunauer-Emmett-Teller (BET) method and the pore size distribution using the Barrett-Joyner-Halenda (BJH) method. The external area (S_{Ext}) (7.7 $m^2\ g^{-1}$) was calculated by the t-plot method from the slope of the linear fit in the thickness range (t) of 0.35-0.5 nm according to the Harkins-Jura equation. This zeolite presents a relatively high micropore area of 12 $m^2\ g^{-1}$, a micropore volume of 0.006 $cm^3\ g^{-1}$ and a predominant pore diameter of 3.8 nm (LÓPEZ-DELGADO et al., 2020). The cation exchange capacity (CEC), determined by the NH_4^+ ion exchange method using a 1 M NH_4Cl solution, was 170 meq 100 g^{-1}; and zeta potential (Pz), determined using a doppler laser electrophoresis analyzer (Zetasizer Nano, Malvern) shows that the zeolite exhibits a negatively charged surface at a pH higher than >5.6 (LOBO-RECIO et al., 2021). All these characteristics suggest that the waste-based LTA zeolite employed in this research possesses favorable adsorption properties for cationic dye removal. Preliminary studies carried out to assess the stability of the adsorbent material in response to pH variations showed that the zeolite was stable at pH >4.

4.3.2 Adsorbate

The Safranine-T (Neon Commercial, Brazil), herein named ST, is a basic dye, also known as Basic Red 2 (CAS nº 477-73-6). A ST stock solution (1.0 g L^{-1}) was prepared in distilled water and the pH values adjusted by using either 0.1 M HCl or NaOH solutions in a multiMeter (Crison MM41). The aqueous ST solutions for adsorption tests were prepared to the required concentrations by diluting the stock solution in distilled water. As with the adsorbent material, the pH stability of the adsorbate was also determined. Preliminary tests were conducted at pH 4 to 11. The stability of the ST was demonstrated, since there were no variations in the absorbance of the dye over the pH range evaluated.

4.3.3 Sorption Experiments

Batch adsorption experiments were performed using 100 mL conical flasks in which 50 mL of dye solution at the required concentration and the corresponding amount of zeolite were added. The pH of the dye solution was kept as obtained, approximately 7.5 (before mixing with the zeolite). All the experiments were carried out at room laboratory temperature, using a rotational shaker (Rotabit/SELECTA), reaching a maximum agitation speed of 230 rpm. The tests were conducted in duplicate and the results were expressed as the average of these values. Blank control trials were also performed. After treatment, the suspensions were centrifuged at a speed of 5300 rpm during 5 minutes (OrtoAlresa Digicen 21 Centrifuge), recovering the supernatant solution for measurement. The measurements of dye concentration were carried out in duplicate within the concentration range of 0.1 to 20.0 mg L^{-1}, using a HACH DR/3900 VIS spectrophotometer with a selected wavelength of 520 nm. The dye removal efficiency E (%) was calculated using Equation 4.1.

$$E(\%) = \left(\frac{C_0 - C_t}{C_0}\right).100 \quad (4.1)$$

where C_0 and C_t represent, respectively, the initial concentration and the concentration at the time t (min) of ST in (mg L^{-1}).

Adsorption essays were performed at different pH values (5, 7, 9 and 11) and temperatures (22, 35, 45 and 55 ºC ± 1 ºC). Moreover, three different types of zeolite,

namely a waste-based NaP zeolite (SÁNCHEZ-HERNÁNDEZ et al., 2016), a natural Mordenite type zeolite and a commercial LTA zeolite were also tested in the optimal experimental conditions determined, in order to verify their effectiveness on the adsorption process and complement the performed study.

4.3.4 Statistical Determination of the Optimal Treatment Conditions

In adsorption experiments, the sorbent adsorption capacity is dependent on various parameters, such as the nature of the adsorbate and the adsorbent, and the operational conditions (NASCIMENTO et al., 2014). In this context, statistical analysis serves as a valuable tool for comprehending the interactions among factors and for ascertaining the optimal conditions for dye removal, which, if required, can be extrapolated with fewer experiments compared to the traditional univariate method (BOX; HUNTER; HUNTER, 1978).

Thus, to determine the best treatment conditions and optimize the dye removal efficiency, a CCRD involving two factors, each composed of two levels (2^2), was developed. It was considered that the agitation rate and zeolite dosage were the independent variables and exerted influence on the treatment efficiency, and the percentage of ST removal was chosen as the response (dependent variable). Factorial scores (-1 and +1), indicating the minimum and maximum level for each variable, axial portions (-1.414 and +1.414) (calculated by Equation 4.2), and 4 central (0) points were used in the experiment, totaling 12 assays.

$$\alpha = (2^n)^{1/4} \tag{4.2}$$

where n is the number of independent variables (n = 2) and α is the axial distance from the central point.

Experiments were conducted using 50 mL of dye solution (C_0 50 mg L^{-1}), under optimal pH and temperature conditions. The contact time was 10 minutes. The values of the factors at the central point, which were 15 g L^{-1} of zeolite and 150 rpm, were established after conducting some preliminary tests. The experimental outcomes underwent statistical scrutiny using the STATISTICA® 13.3 software. This involved employing analysis of variance (ANOVA) in order to assess statistical parameters and appraise the predictive capabilities of the mathematical model.

4.3.5 Sorption Kinetics

The kinetic studies seek to ascertain the required contact time for treatment and the adsorption process rate. The rate was determined through nine assays (1, 2, 5, 10, 15, 30, 60, 90 and 120 min), using 50 mL of 50 mg L^{-1} ST solution, in the optimal pH and temperature conditions, and employing a zeolite dosage and agitation rate based on the data determined by the CCRD, (following the procedure described in Section 4.5.3). The adsorption kinetic process was assessed using the pseudo-first order (PFO), pseudo-second order (PSO), intraparticle diffusion (ID) and Elovich kinetic models. These models, presented in Table 4.1, were utilized to achieve a clearer understanding of the adsorption process, including aspects such as the type and rate of adsorption, saturation time and controlling steps (YADAV et al., 2022b).

Usually for determining the best fit of experimental data with the proposed assessment models, the linear regression method is employed, especially due to its simplicity. However, the process of linearization alters the variables considered independent or dependent, potentially leading to error propagation and inaccurate parameter estimations (WANG; GUO, 2020). Hence, to ensure consistent and accurate estimations for fitting the experimental data to the studied kinetic models, the non-linear regression method utilizing the Excel Solver add-in was utilized. Finally, several error functions (Table 4.2) were applied to determine the model with the best fit to the experimental data. However, since the adoption of different error criteria leads to obtaining different sets of parameters, the standard normalizing procedure (known as *Sum of Normalized Errors* – SNE) was applied following the proposed by Foo et al. (FOO; HAMEED, 2010). This process entails the following steps: (*i*) selecting the model and error function, identifying the parameters that can be adjusted to reduce the error function; (*ii*) identifying the remaining error functions based on the parameter set; (*iii*) computing the parameters and their respective error function values (restarting the process upon minimizing the error function); (*iv*) selecting the most significant parameters contributing to the highest error; and (*v*) summing the parameters contributing to the least error.

Table 4.1 – Equations for the models employed in the study of kinetics.

Model	Equation	Reference
Pseudo-first order	$q_t = q_e(1 - e^{(-K_1 t)})$	LAGERGREN (1898)
Pseudo-second order	$q_t = \frac{K_2 {q_e}^2 t}{1 + K_2 q_e t}$	HO; MCKAY (1999)
Intraparticle diffusion	$q_t = K_{int}\, t^{1/2} + C$	WEBER; MORRIS (1963)
Elovich	$q_t = \frac{1}{\beta}\ln(1 + \alpha\beta t)$	ELOVICH; LARINOV (1962)

q_t =dye amount sorbed at time t (mg g^{-1}); q_e =dye amount sorbed at equilibrium (mg g^{-1}); K_1 =rate constant of pseudo-first order sorption kinetics (L min^{-1}); K_2 = equilibrium rate constant of pseudo-second order sorption (g mg^{-1} min^{-1}); K_{int} = intraparticle diffusion rate constant (mg g^{-1} $min^{-0.5}$); C =constant indicative of the significant external mass transfer (mg g^{-1}); α =desorption constant; β =initial adsorption rate (mg g^{-1} min^{-1}) and t =time. Source: created by the author

Table 4.2 – Error functions used in the isothermal and kinetic analysis.

Error function	Equation
Sum Square of Errors (ERRSQ)	$ERRSQ = \sum_{i=1}^{n}\left(q_{e_{calc}} - q_{e_{exp}}\right)^2$
Hybrid Fractional Error Function (HYBRID)	$HYBRID = \frac{100}{n-p}\sum_{i=1}^{n}\left[\frac{\left(q_{e_{exp}} - q_{e_{calc}}\right)^2}{q_{e_{exp}}}\right]$
Average Relative Error (ARE)	$ARE = \frac{100}{n}\sum_{i=1}^{n}\left[\frac{q_{e_{calc}} - q_{e_{exp}}}{q_{e_{exp}}}\right]$
Marquardt's Percent Standard Deviation (MPSD)	$MPSD = \sqrt{\frac{1}{n-p}\sum_{i=1}^{n}\left(\frac{\left(q_{e_{exp}} - q_{e_{calc}}\right)}{q_{e_{exp}}}\right)^2}$
Sum of Absolute Errors (EABS)	$EABS = \sum_{i=1}^{n}\left[q_{e_{exp}} - q_{e_{calc}}\right]$
Coefficient of Determination (R^2)	$R^2 = \frac{\sum\left(q_{e_{calc}} - q_{m_{exp}}\right)^2}{\sum[\left(q_{e_{calc}} - q_{m_{exp}}\right)^2 + \left(q_{e_{calc}} - q_{e_{exp}}\right)^2]}$
Nonlinear Chi-Square Test (X^2)	$X^2 = \sum_{i=1}^{n}\frac{\left(q_{e_{calc}} - q_{e_{exp}}\right)^2}{q_{e_{exp}}}$
Coefficient of Nondetermination (CND)	$CND = 1 - R^2$

$q_{e\ calc}$ =dye amount sorbed at equilibrium (mg g^{-1}) (calculated/theoretical); $q_{e\ exp}$ =dye amount sorbed at equilibrium (mg g^{-1}) (experimentally determined); $q_{m\ exp}$ = average amount of dye sorbed at equilibrium (mg g^{-1}) (experimentally determined); n =number of the data points; p =number of the parameters and R^2 =coefficient of determination. Source: adapted from (AYAWEI; EBELEGI; WANKASI, 2017)

4.3.6 Sorption Isotherms

Adsorption equilibrium is an essential requirement in the analysis of an adsorption separation process. Isothermal studies were conducted to determine how much sorbate (ST dye) is sorbed per gram of adsorbent material (zeolite) after reaching equilibrium (q_e), and also the process mechanism. To obtain the adsorption isotherms, different dye solution concentrations (10-100 mg L^{-1}) were treated under optimal pH

and temperature conditions, using the agitation rate and zeolite dosage obtained from the CCRD. As described in Section 4.5.3, the experimental method was carried out, and through the execution of kinetic tests, the optimal contact time was determined. Equation 4.3 was used to calculate the adsorption capacity q_e (mg g^{-1}).

$$q_e = \frac{(C_0 - C_e).V}{m} \tag{4.3}$$

in which q_e = sorbent adsorption capacity ($mg_{sorbate}/g_{adsorbent}$) at the equilibrium; C_0 is the initial sorbate concentration (mg L^{-1}); C_e is the equilibrium sorbate concentration (mg L^{-1}); V is the ST solution volume (L); and m is the quantity of adsorbent applied (g).

In order to determine the mechanisms governing the adsorption process, several mathematical models were applied, such as Linear, Langmuir, Freundlich, Dubinin-Radushkevish (D-R), Sips, Toth, Redlich-Peterson (R-P) and Temkin. Their corresponding equations are presented in Table 4.3.

Table 4.3 – Equations for the models employed in the study of isothermal.

Model	Equation	Reference
Linear	$q_e = K_d\, C_e$	FREUNDLICH (1906)
Langmuir	$q_e = \frac{q_{max}\, K_L\, C_e}{1 + K_L\, C_e}$	LANGMUIR (1916)
Freundlich	$q_e = K_F\, {C_e}^{1/n}$	FREUNDLICH (1906)
Dubinin-Radushkevish	$q_e = q_{max} \exp(-K_{ads}\varepsilon^2)$ $\varepsilon = RTln\left(1 + \left(\frac{1}{C_e}\right)\right)$ $E = \frac{1}{\sqrt{2K_{ads}}}$	DUBININ; RADUSHKEVISH (1947)
Sips	$q_e = \frac{q_{max}\, K_S\, Ce^m}{1 + K_S\, Ce^m}$	SIPS (1948)
Toth	$q_e = \frac{K_T\, C_e}{(a_T + C_e)^{1/t}}$	TOTH (1971)
Redlich-Peterson	$q_e = \frac{K_R C_e}{1 + a_R {C_e}^n}$	REDLICH; PETERSON (1959)
Temkin	$q_e = \frac{RT}{b_T} ln(A_T C_e)$	TEMKIN; PYZHEV (1940)

q_{max} =maximum adsorption capacity (mg g^{-1}); K_d =sorbent distribution constant (L g^{-1}); K_L =Langmuir adsorption equilibrium constant (L mg^{-1}); K_F =Freundlich adsorption [(mg g^{-1}) (mg $L^{-1})^{1/n}$]; 1/n =empirical coefficient; K_S = Sips isotherm constant (L g^{-1}); m =Sips isotherm exponent; K_T =Toth isotherm constant (mg g^{-1}); t =exponent inverse of the Toth model; a_T =constant (L mg^{-1}); K_R =Redlich-Peterson isotherm constant (L g^{-1}); a_R =Redlich-Peterson constant (L mg^{-1}); n =exponent of Redlich-Peterson model; K_{ads} =Dubinin-Radushkevich isotherm constant (mol^2 kJ^{-2}); ε =mean adsorption energy (kJ mol^{-1}); R =gas constant (0.008314 kJ mol^{-1} K^{-1}); T =temperature (K); b_T =Temkin heat of adsorption constant and A_T =equilibrium binding constant (L mg^{-1}). Source: created by the author

As in the kinetic studies, nonlinear regression and the error functions (Table 4.2), with minimizing the error distributions through a standard normalization procedure was applied to evaluate the isothermal models.

4.4 RESULTS AND DISCUSSION

4.4.1 Effect of the pH and Temperature

The influence of initial pH and temperature was studied in the adsorption process of ST dye. The pH of the mixed solution (adsorbent + adsorbate) is a critical parameter that influences the removal of the adsorbate, affecting the structural stability of the adsorbent, the state of functional groups on the adsorbent surface, and the ionization of the sorbate within the solution (YADAV et al., 2022b). In this research, the effect of pH was investigated at room temperature, with a contact time of 1 minute at different pH values (5, 7, 9 and 11). This pH range was selected based on the fact that at pH values below 4, zeolites lose their stability, while at pH values above 11, Safranine-T evolves into its anionic structure, interfering with the colorimetric determination. It was found that more basic pH leads to a greater ability of the zeolite to remove the dye. The maximum removal was reported at pH 11, reaching 98.12% of removal. At pH 9, ST removal was 84.62%; at pH 7, 82.68% and, at pH 5, 78.71%. This is advantageous, since textile wastewaters are usually basic. The behavior of the zeolite in the adsorption process at different dye solution pH can be clarified by considering the relationship between the zeta potential (Pz) of LTA zeolite and the dissociated state of Safranine-T molecules. The Pz of the LTA zeolite was found to be negative when the pH values exceeded 5.6, indicating a negatively charged zeolite surface at these pH values, which facilitates the electrostatic interaction between the LTA zeolite and the cationic molecules of ST dye. Consequently, this leads to an increased percentage of removal (ABUKHADRA; MOHAMED, 2019). On the contrary, there was reduced dye adsorption at acidic pH, likely due to a higher concentration of free protons competing for the avaiable adsorption sites on the zeolite with the cationic groups on the dye (KAUR et al., 2015).

Temperature is another important factor in adsorption processes, especially when the system involves a solid adsorbent and a liquid or gaseous adsorbate. Temperature variations affect the kinetic energy of molecules, the adsorbate-adsorbent molecular affinity, adsorption capacity and changes in the adsorbate stability. The effect of the temperature was analyzed at 22, 35, 45 and 55 ºC ± 1 ºC. This temperature range was selected because 22 ºC represents the average ambient laboratory temperature, while temperature of 55 ºC was chosen as a possible extreme environmental condition. The result obtained showed a slight decrease in dye removal from 98.12% to 94.50%, as the temperature increased within the mentioned range. As a result, the optimal parameters selected for conducting the adsorption process include a pH equal to that of the adsorbate/adsorbent mixture (~11), at room laboratory temperature (22 ºC ± 1 ºC).

4.4.2 Statistical Analysis for ST Removal

In Table 4.4, the 2^2-CCRD data matrix is presented, which includes the levels of the factors, the corresponding values, and the obtained responses. The utilization of LTA zeolite for adsorbing dye-containing solutions proved to be highly efficient, as evidenced by the high levels of dye removal, higher than 95% in almost all the conditions evaluated, with the exception of runs 1, 3 and 7, in which small doses of zeolite were used.

The estimated effects were based on the *p*-value (Table 4.5). At a 95% confidence level, the only variable that significantly influenced (p <0.05) the dye removal efficiency was the dosage of zeolite, in both its linear (Q_2) and quadratic (Q_{22}) forms. ST removal is linearly dependent on the zeolite dosage and its effect is positive (59.0026), i.e., when increasing the zeolite dosage, the dye removal also increased. Agitation rate (linear (Q_1) and quadratic (Q_{12})) did not significantly (p >0.05) influence dye removal. Determination coefficient (R^2) quantifies the extent to which the regression equation accounts for the variability in responses compared to the overall variation. For the ST dye removal, a R^2 = 0.9927 was obtained. This value suggests a strong interrelationship between the values obtained through experimentation and those predicted by the model, both for the independent variables and for the

responses. That is, the model is able to explain approximately 99.27% of the variations in the final concentration of the dye.

Table 4.4 – Data matrix and responses of CCRD design (C_0 50 mg L^{-1}).

Run nº	Factors				Responses
	Agitation Rate		Zeolite Dosage		
	Factor Level	Agitation Rate (rpm)	Factor Level	Zeolite Dosage (g L^{-1})	Cf (mg L^{-1}) [Removal (%)]
1	-1	100	-1	5	29.45 ± 0.05 [41.10]
2	-1	100	1	25	1.25 ± 0.04 [97.51]
3	1	200	-1	5	27.40 ± 0.00 [45.20]
4	1	200	1	25	1.26 ± 0.02 [97.48]
5	-1.414	80	0	15	2.12 ± 0.05 [95.77]
6	1.414	220	0	15	2.09 ± 0.04 [95.83]
7	0	150	-1.414	0.85	46.54 ± 0.46 [6.92]
8	0	150	1.414	29.15	1.22 ± 0.09 [97.57]
9	0	150	0	15	2.00 ± 0.09 [96.01]
10	0	150	0	15	2.04 ± 0.06 [95.93]
11	0	150	0	15	2.09 ± 0.10 [95.82]
12	0	150	0	15	2.01 ± 0.01 [95.98]

Source: created by the author

Table 4.5 – Estimated effects for Safranine-T removal variables.

	Coefficient	Effect	Standard error	t(2)	*p*-value
Agitation (*L*)	Q_1	1.0490	2.540712	0.4129	0.694048
Agitation (*Q*)	Q_{12}	-2.0753	2.869380	-0.7233	0.496737
Zeolite dosage (L)	***Q_2***	***59.2070***	***2.527274***	***23.4272***	***0.000000***
Zeolite dosage (Q)	***Q_{22}***	***-45.4985***	***2.821168***	***-16.1275***	***0.000004***
Agitation *vs* Zeolite dosage	Q_1*vs*Q_2	-2.0650	3.575099	-0.5776	0.584538

Source: created by the author

The analysis of variance (ANOVA) showed that, for the removal efficiency of the ST dye, the $F_{calculated} > F_{tabulated}$ (Table 4.6), which confirms that the sample distribution is statistically representative. Thus, the ANOVA for ST removal indicated that the model is valid within the 95% confidence interval, and that no adjustment was required within this interval, resulting in an excellent reproduction of the experimental samples.

Table 4.6 – Analysis of variance for Safranine-T removal for the 2^2 factorial design.

Variation source	SS	df	MS	F		*p*
				Calc.	Tab.[a]	
Regression	10172.477	1	10172.477	1326.489	4.965	<0.05
Sediments	76.687	10	7.669			
Total	10249.164	11				

SS: sum of square; df: degree of freedom; MS: mean of square; F: Fisher's ratio; *p*: probability;
[a] Tabulated values (BOX; HUNTER; HUNTER, 1978). Source: created by the author

Furthermore, to reinforce the model's validity, a residual distribution graph (Fig. 4.2) was employed, which compares the percentage removal predicted by the model with the values obtained in the experimental tests. In this graph (Fig. 4.2), it is observed that the experimental values (represented by dots) are close to the line (predicted values), showing proportional negative and positive deviations. This may indicate a strong correlation and indicates the quality of fit between the predicted and the experimental values.

Figure 4.2 – Residual distribution for ST dye removal (R^2 = 0.9927) (observed values and values predicted by the model).

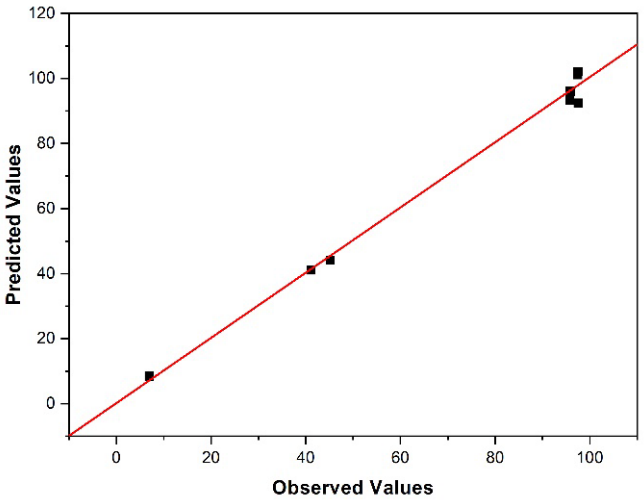

Source: created by the author

Figure 4.3 displays response surface plots and contour curves, enabling visualization of the optimal values where the combination of variables led to an improved response (NÚÑEZ-GÓMEZ et al., 2017). The results reveal that the highest removal of ST was achieved when an agitation rate within the range of 90-200 rpm and a zeolite dosage of 19-24 g L^{-1} were employed (Fig. 4.3). This indicates that there was no variation in the removal efficiency related to the agitation rate, in agreement with the corresponding *p*-value above discussed (Table 4.5). The critical values,

determined through statistical analysis using Statistica® 13.3 software, were established at 21.5 g of zeolite per liter and an agitation rate of 147 rpm. An experiment was conducted using the established factor values to assess the appropriateness of the results, as not all experimental factors could be considered in the statistical analysis. Due to the high removal of ST dye (97.61%), the suitability of the planning carried out by the CCRD for establishing the optimal treatment conditions is demonstrated.

Figure 4.3 – Response surface (left) and contour curve (right) for ST removal (%).

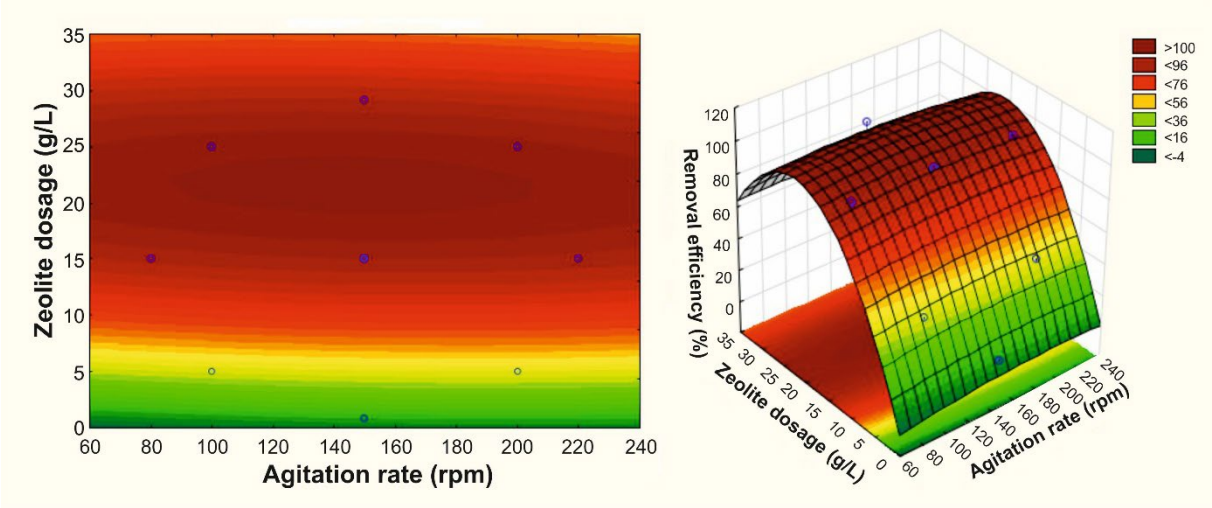

Source: created by the author

4.4.3 Sorption Kinetic Results

The kinetic study is a crucial point to evaluate the adsorption, allowing the determination of the appropriate contact time to control the process and assisting in identifying the predominant adsorption mechanism. Adsorption kinetics were conducted at 22 ºC ± 1 ºC, using a dye concentration of 50 mg L^{-1}, and operating with the optimal values of pH, zeolite dosage, and agitation rate. Different contact times (1-120 min) between the zeolite and textile dye solutions were tested. The experimental kinetic data and the calculated parameters are presented in Table 4.7. Dye removal efficiency reached 97.80% (C_e = 1.100 ± 0.000 mg L^{-1}) in the first minute of the test, and remained in this range for all tested contact times, indicating an extremely fast adsorption kinetics. This brief contact duration, rapid reaction rate and high capacity of adsorption are determining factors for the application of the waste-based LTA zeolite when scaling up an adsorption process to a pilot or industrial level. In order to estimate

the kinetic parameters and predict the dye sorption rate, pseudo-first order, pseudo-second order, intraparticle diffusion and Elovich kinetic models (Table 4.1) were applied. The fitting results for these kinetics are shown in Figure 4.4.

Table 4.7 – Experimental kinetic results and calculated parameters for the adsorption of the ST dye (C_0 50 mg L^{-1}) onto LTA zeolite (dosage = 21.5 g L^{-1}).

Time (min)	C_e	$q_{t\ exp.}$	PFO			PSO			ID			Elovich		
			$q_{t\ calc}$	q_e	K_1	$q_{t\ calc}$	q_e	K_2	$q_{t\ calc}$	K_{int}	C	$q_{t\ calc}$	α	β
1	1.100 ± 0.000	2.274	2.271	2.27	16.91	2.262	2.27	72.89	1.759	0.08	1.68	2.142	$8.26e^{17}$	20.68
2	1.130 ± 0.070	2.273	2.271			2.268			1.793			2.176		
5	1.205 ± 0.005	2.270	2.271			2.273			1.859			2.220		
10	1.195 ± 0.005	2.270	2.271			2.274			1.934			2.253		
15	1.135 ± 0.005	2.273	2.271			2.274			1.991			2.273		
30	1.150 ± 0.010	2.272	2.271			2.275			2.120			2.306		
60	1.180 ± 0.000	2.271	2.271			2.275			2.303			2.340		
90	1.125 ± 0.045	2.273	2.271			2.275			2.443			2.360		
120	1.290 ± 0.020	2.266	2.271			2.275			2.561			2.373		

C_e (mg L^{-1}) =equilibrium sorbate concentration; q_t (mg g^{-1}) =zeolite sorption capacity at the time (t); q_e (mg g^{-1}) =zeolite sorption capacity at equilibrium; K_1 =rate constant of pseudo-first order sorption kinetics (L min^{-1}); K_2 =equilibrium rate constant of pseudo-second order sorption (g mg^{-1} min^{-1}); K_{int} =intraparticle diffusion rate constant (mg g^{-1} $min^{1/2}$); C =constant indicative of the significant external mass transfer (mg g^{-1}); α =desorption constant and β =initial adsorption rate (mg g^{-1} min^{-1}). Source: created by the author

Figure 4.4 – Kinetic experimental data compared with the kinetic models for ST dye adsorption onto waste-based LTA zeolite.

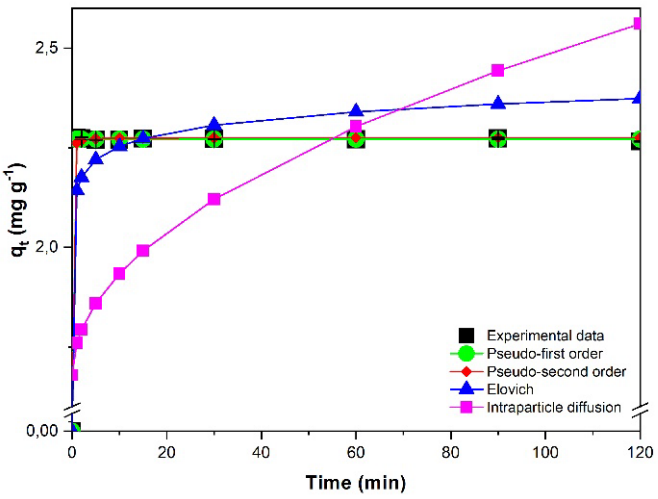

Source: created by the author

The fitting of the obtained experimental data to the kinetic models was determined based on the R^2 (Table 4.2) for the corresponding nonlinear regression equations. Regarding the intraparticle diffusion model, the graphs displayed a relatively low R^2 value, 0.178 (Table 4.8), and the origin of the coordinates was not intercepted

by the straight lines (Figure 4.4). As a result, it was concluded that intraparticle diffusion was not the restricting factor in the adsorption mechanism (LOBO-RECIO et al., 2021). Pseudo-first order, pseudo-second order and Elovich model presented a high R^2 value (>0.98). Various error functions were employed to reduce the distribution of errors between the experimental equilibrium data and those provided by the isotherms. This allowed validation that, among the models used, the PFO is the model that best fits the experimental kinetic data (Table 4.8). This kinetic model was the most suitable for describing the adsorption process due not only to its high coefficient of determination (R^2 = 0.99999) but also to consistently displaying the lowest error values across all evaluated error functions. The interpretations of adsorption mechanisms via kinetic models lack robust theoretical underpinnings and cannot be discerned solely through straightforward curve fitting techniques (HU; PANG; WANG, 2022). However, it can be indicated that the adsorption of the Safranine-T dye by LTA zeolite follows a physical mechanism, which should be corroborated through the corresponding isothermal study. The q_e (2.271 mg g^{-1}) and K_1 (16.913 L min^{-1}) values were consistent with those previously documented for the removal of ST dye using other zeolitic materials (PEREIRA et al., 2018).

Table 4.8 – Parameters of the kinetic models and corresponding error functions values.

Model	**R^2**	**Error Functions**						
		ERRQS	**EABS**	**ARE**	**HYBRID**	**MPSD**	**X^2**	**CND**
PFO	**0.99999**	**0.0001**	**0.0000**	**0.0000**	**0.0003**	**0.0004**	**0.0000**	**0.0000**
PSO	0.99993	0.0003	0.0099	0.0436	0.0016	0.0022	0.0001	0.0001
ID	0.17808	3.8161	0.0000	7.3849	4.8810	6.4457	0.4393	0.8219
Elovich	0.98831	0.0549	0.0018	0.0097	0.2686	0.3547	0.0242	0.0117

Source: created by the author

4.4.4 Sorption Isothermal Results

Isothermal experiments were conducted at room temperature (22 ºC ± 1 ºC), using the dye solution at the pH resulting from its preparation and with 1 minute of contact time (optimal contact time according to the kinetic study). Furthermore, the agitation rate and zeolite dosage were 147 rpm and 21.5 g L^{-1}, respectively,

parameters that were determined through the CCRD. The concentration influence for Safranine-T dye adsorption was studied within the range of 10-100 mg L^{-1} (Table 4.9).

Table 4.9 – Experimental results from the isothermal study for the adsorption of ST dye on LTA zeolite.

C_0 (mg L^{-1})	C_e (mg L^{-1})	Removal (%)	q_e (mg g^{-1})
10	0.665 ± 0.065	93.35 ± 0.65	0.434 ± 0.003
15	0.610 ± 0.020	95.93 ± 0.13	0.669 ± 0.001
20	0.630 ± 0.010	96.85 ± 0.05	0.901 ± 0.000
25	0.710 ± 0.010	97.16 ± 0.04	1.130 ± 0.000
40	0.885 ± 0.045	97.79 ± 0.11	1.819 ± 0.002
50	0.940 ± 0.020	98.12 ± 0.04	2.282 ± 0.001
60	1.445 ± 0.055	97.59 ± 0.09	2.723 ± 0.003
75	2.470 ± 0.070	96.71 ± 0.09	3.373 ± 0.003
80	2.970 ± 0.030	96.29 ± 0.04	3.583 ± 0.001
85	3.675 ± 0.045	95.68 ± 0.05	3.783 ± 0.002
90	5.565 ± 0.005	93.82 ± 0.01	3.927 ± 0.000
100	8.425 ± 0.105	91.58± 0.10	4.259 ± 0.005

Source: created by the author

It was observed that the adsorption capacity (q_e) increased from 0.434 to 4.259 mg g^{-1} when the initial dye concentration was increased from 10 to 100 mg L^{-1}. However, this led to a decrease in the removal efficiency, reducing from 98.12% to 91.58%. According to Yadav et al. (YADAV et al., 2022b), elevated concentrations of dye ions generate a driving force to overcome mass transfer between liquid and solid phases, but at exceedingly high concentrations, binding sites reach saturation, leading to a decline in adsorption efficiency. The waste-based LTA zeolite employed demonstrates high porosity, a significant CEC, and an anionic surface over a broad pH range (LOBO-RECIO et al., 2021). This suggests that the uptake of dye molecules by this material could occur through both adsorption and ion exchange mechanisms (ABUKHADRA; MOHAMED, 2019). Adsorption isotherm models depict the distribution of adsorbed species between the liquid and the adsorbent using graphs constructed based on a set of assumptions. These models are associated with the heterogeneity or homogeneity of the adsorbent, the coverage type, and the potential for interaction among the adsorbate (FOO; HAMEED, 2010). To determine the mechanisms involved in the adsorption process and the maximum adsorption capacity, different isothermal models (Table 4.3) were applied. Figure 4.5 shows the experimental isothermal data compared to the best-fit isothermal models (considering models with R^2 >0.9). The isothermal parameters and corresponding error function values are shown in Table 4.10.

Figure 4.5 – Isothermal experimental data compared with the isothermal models for ST dye adsorption onto waste-based LTA zeolite.

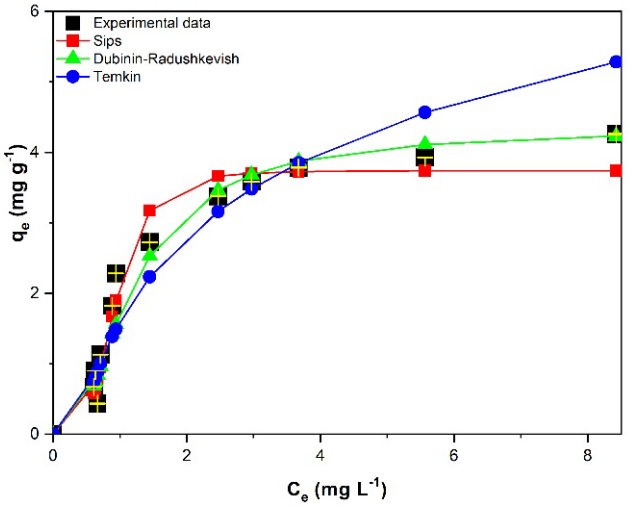

Source: created by the author

Table 4.10 – Parameters of the isothermal models and corresponding error functions values.

Model	Parameters		R^2	Error Functions						
				ERRQS	EABS	ARE	HYBRID	MPSD	X^2	CND
Linear	K_d	0.9963	0.7341	25.5960	0.0000	7.0243	60.7299	74.1543	7.2876	0.2659
Langmuir	q_{max}	7.1344	0.8824	3.4163	2.0163	4.7640	16.8028	71.0435	2.0163	0.1176
	K_L	0.2524								
Freundlich	K_F	1.3311	0.7693	6.3935	4.5733	0.0000	25.2883	85.4151	3.0346	0.2307
	n	1.6975								
Dubinin-Radushkevish	q_{max}	4.3357	0.9658	2.5156	1.2876	0.0001	10.7300	38.6504	3.0346	0.0342
	K_{ads}	0.3239								
Sips	q_{max}	3.7413	**0.9632**	**1.0036**	**0.6312**	**0.4206**	**5.2597**	**23.6249**	**0.6312**	**0.0368**
	K_S	1.3051								
	m	3.9516								
Toth	K_T	56.3653	0.8969	2.8217	1.9066	5.5489	15.6065	71.6528	1.8728	0.1031
	a_T	8.0918								
	t	0.6046								
Redlich-Peterson	K_R	1.4761	0.8600	2.3037	1.5512	3.9906	12.8690	57.2457	2.1278	0.1400
	a_R	0.0272								
	n	2.0393								
Temkin	A_T	2.5170	0.9228	2.8141	0.0000	3.8366	11.2402	41.6778	1.3488	0.0772
	b_T	1.4177								

Source: created by the author

When comparing the R^2 values for all the analyzed isotherms, the fit follows the following sequence: Dubinin-Radushkevich > Sips > Temkin > Toth > Langmuir > Redlich-Peterson > Freundlich > Linear. Hence, the Dubinin-Radushkevish (R^2 = 0.96580) and Sips (R^2 = 0.96320) isotherms were the ones that yielded the most accurate fits. Although the D-R model showed a slightly higher R^2 than the Sips model, it doesn't serve as a suitable means to pinpoint the adsorption mechanism. According to Puccia et al. (PUCCIA; AVENA, 2021), the use of the D-R equation at the the solid-liquid systems has been incorrect, because substituting concentrations in molar units

results in a “chemical” binding, whereas using units in mg L^{-1} leads to a “physical” binding. Moreover, considering the other error functions, it can be seen that with the exception of the *Average Relative Error* (ARE) and the *Coefficient of Nondetermination* (CND) functions, all the others presented lower values for the Sips model. Thus, the Sips model can be considered the isothermal model that best fits the experimental data and best describes the adsorption behavior of the textile dye on the zeolite, concurring with the kinetic studies. The Sips model suggests that, when adsorbate concentrations are low, it adopts the Freundlich form, characterized by the existence of weak physical interactions (van der Waals forces) between the adsorbate and the adsorbent (FOO; HAMEED, 2010). Given that 50 mg L^{-1} can be regarded as a relatively low concentration for textile dyes, the involvement of physisorption processes in the adsorption mechanism can be expected. Physisorption is a reversible adsorption process in which adsorbate molecules adhere to the surface of the adsorbent, forming multiple layers. As the adsorption process unfolds and layers increase, a gradual decrease in interaction between adsorbent and adsorbate molecules is observed, culminating in the completion of the adsorption process (FOO; HAMEED, 2010). This mechanism is confirmed by assessing the values of *n* in the Freundlich model and the adsorption energy (E) in the D-R model. In this context, when n exceeds unity, as in this study where n = 1.07, it is interpreted that the adsorption process is physical, heterogeneous, and multilayered. Furthermore, the value of E, which is 1.24 kJ mol^{-1}, reaffirms that the adsorption mechanism at the active sites of the zeolite is of a physical nature, as E < 8 kJ mol^{-1}, indicating weak and reversible interactions in the adsorption process (HOSSEINI NAMI; MOUSAVI, 2023). The fact that the interactions are attributed to weak intermolecular forces suggests that the ST molecules adsorbed on the surface of the saturated zeolite can be easily desorbed. This would facilitate the reuse of the zeolite and the recovery of the textile dye.

The q_{max} (3.74 mg g^{-1}) obtained by applying the Sips model presented an intermediate value between the values (q_{max} = 1.3 mg g^{-1} and q_{max} = 7.0 mg g^{-1}) reported by Atun et al. (ATUN et al., 2011) and Das et al. (DAS; BARMAN, 2013), respectively, using different zeolitic materials for ST adsorption. Nevertheless, the differences between the corresponding values can be attributable to the dissimilar experimental conditions used for the different authors, i.e, adsorbent dosage, adsorbate concentration, etc. According to Sieren et al. (SIEREN et al., 2020) the

adsorption of the Safranine-T cations is restricted to the outer surface of the zeolites due to the larger size of ST^+ compared to the dimensions of the zeolite channels, which could account for variations in dye removal. Atun et al. (ATUN et al., 2011) attribute the lower q_e values obtained for the adsorption of Safranine-T dye to its larger molecular size compared to the other basic dyes used on the same synthetic zeolite. Ayar et al. (AYAR et al., 2015) found that the removal capacity of the ST dye is related to the pore sizes and cation exchange capacities (CEC) of the adsorbents, using both a natural zeolite and a synthesized one (a mixture of Analcime and Sodalite). With the natural Clinoptilolite zeolite, twice the ST removal was achieved compared to the synthetic zeolite. This difference can be attributed to the lower affinity of Analcime and Sodalite mixture present in the synthetic zeolite towards ST cations, owing to the smaller pore size and reduced cation-exchange capacity (CEC). The waste-based zeolite used in this study has a high CEC (170 meq 100 g^{-1}), but has a very limited pore diameter (3.8 nm) compared to the large size of the ST dye molecules, which may have influenced the adsorption process, corroborating Sieren et al. (SIEREN et al., 2020) who state that adsorption is limited to the zeolite surface area.

4.4.5 Thermodynamic Analysis and Comparison of the Safranine-T Dye Adsorption using Different Zeolite Types

The spontaneity of ST adsorption by the waste-based zeolite was determined by calculating the Standard Gibbs free energy changes (ΔG^0), standard entropy changes (ΔS^0) and standard enthalpy changes (ΔH^0), using Equation 4.4 and Equation 4.5, presented below.

$$\Delta G^0 = -RTln\left(\frac{q_e}{C_e}\right) \quad (4.4)$$

$$\Delta G^0 = \Delta H^0 - T\Delta S^0 \quad (4.5)$$

in which R = universal gas constant (8.314 J mol^{-1} K^{-1}), T = absolute temperature (K), q_e is zeolite sorption capacity at equilibrium (mg g^{-1}) and C_e is equilibrium sorbate concentration (mg L^{-1}). The thermodynamic parameters calculated are presented in Table 4.11.

According to Kaur et al. (KAUR et al., 2015), the negative ΔG^0 suggests that the adsorption of ST onto the LTA zeolite occurs spontaneously and feasibility. The negative ΔH^0 signifies the exothermic character of the adsorption process, indicating a preference for lower temperatures. Additionally, the negative ΔS^0 values indicate substantial disorderliness at the solid-liquid interface, with no notable alteration in the internal zeolite structure and its affinity toward the dye.

Table 4.11 – Thermodynamic parameters for the adsorption of Safranine-T onto waste-based LTA zeolite.

ΔH (kJ mol^{-1})	**ΔS (J mol^{-1} K^{-1})**	**ΔG (kJ mol^{-1})**			
		295K	308K	318K	328K
-13.32	-38.31	-16.55	-14.45	-13.88	-13.82

Source: created by the author

4.4.6 Application of Different Zeolites on the Safranine-T Removal

In addition to the waste-based LTA zeolite, Safranine-T removal was tested using different zeolite types, including a waste-based NaP zeolite, a natural Mordenite zeolite and a commercial LTA zeolite. The results are presented in Table 4.12 and Figure 4.6. It was found a removal efficiency of 94.40 ± 0.16% for the waste-based NaP zeolite, 93.11 ± 0.11% for the natural Mordenite and 82.95 ± 0.17% for the commercial LTA zeolite. These values are lower than the removal efficiency of LTA zeolite used in this study (98.12 ± 0.04%). The final concentration of the textile effluent after the adsorption process varied between 0.94 ± 0.02 mg L^{-1} and 8.53 ± 0.09 mg L^{-1} for the waste-based LTA and commercial LTA zeolites, respectively. The NaP zeolite, also synthesized from aluminum waste (SÁNCHEZ-HERNÁNDEZ et al., 2016), was the second best performer in ST adsorption, in terms of removal efficiency, adsorption capacity and lowest final dye concentration. While the waste-based LTA zeolite showed an adsorption capacity q_e of 2.282 ± 0.001 mg g^{-1}, the waste-based NaP achieved a q_e of 2.195 ± 0.004 mg g^{-1}. These results can be attributed, especially, to structural, textural and cation exchange capacity (CEC) differences between the zeolites (AYAR et al., 2015). Regarding cation exchange capacity (CEC), although the waste-based NaP zeolite has a CEC of 2.73 meq g^{-1}, its performance in adsorbing the ST dye was lower than that of the waste-based LTA (CEC of 1.70 meq g^{-1}). In terms of surface area, the commercial LTA zeolite, which showed the lowest adsorption capacity, was also the one with the lowest S_{BET} (7.37 m^2 g^{-1}) (WANG et al., 2019b),

compared to 19 m^2 g^{-1} for Mordenite (KORKUNA et al., 2006), 14.2 m^2 g^{-1} for waste-based NaP and 19.7 m^2 g^{-1} for the waste-based LTA used in this study. This indicates the important influence of this parameter on the adsorption capacity of the materials tested.

Table 4.12 – Adsorption capacity of the different types of zeolites applied to the removal of ST dye.

Zeolite Type	Ce (mg L^{-1})	Removal (%)	q_e (mg g^{-1})
Waste-based LTA	0.94 ± 0.02	98.12 ± 0.04	2.282 ± 0.001
Waste-based NaP	2.80 ± 0.08	94.40 ± 0.16	2.195 ± 0.004
Natural Mordenite	3.45 ± 0.06	93.11 ± 0.11	2.165 ± 0.003
Commercial LTA	8.53 ± 0.09	82.95 ± 0.17	1.929 ± 0.004

Source: created by the author

Figure 4.6 – Comparison between different zeolites on ST adsorption.

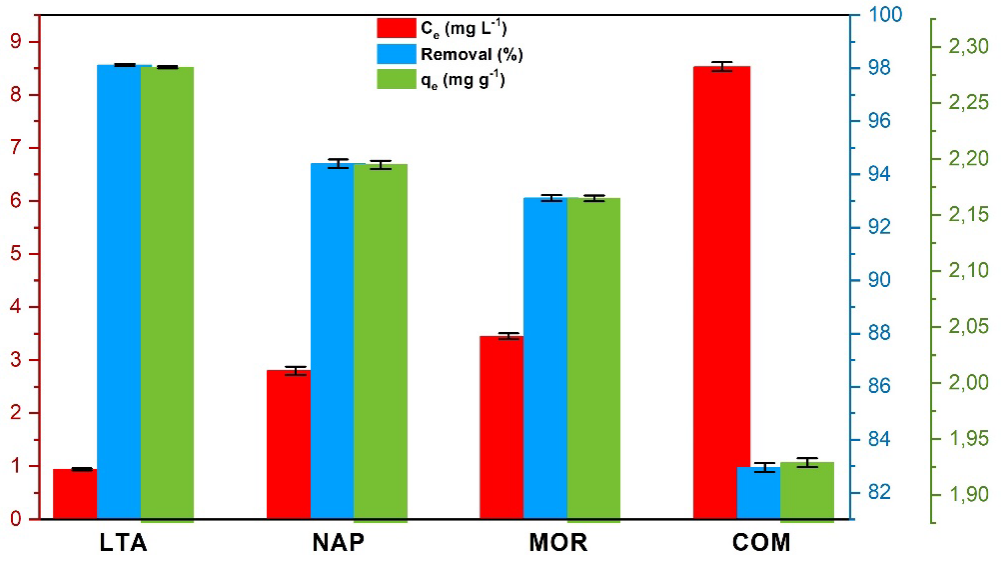

Source: created by the author

4.4.7 Environmental Considerations and Future Challenges

The LTA zeolite, obtained from hazardous waste in the tertiary aluminum industry, has proven to be a highly effective adsorbent for the rapid removal of Safranine-T (utilized as a model for cationic dyes), achieving an efficiency > 98% in synthetic waters within extremely short times (< 1 minute). This methodology not only prevents the discharge of industrial wastewater contaminated with dyes into natural basins but also addresses issues associated with the disposal of hazardous waste in soil, generating a symbiosis between two polluting industries: the tertiary aluminum industry and the textile industry.

The development of this methodology is a significant finding as it overcomes limitations related to the extended durations of conventional adsorption processes (ATUN et al., 2011; AYAR et al., 2015; SHI et al., 2021; SIEREN et al., 2020), making it feasible for the decontamination of waters from the textile industry or other sectors employing dyes.

The promising results, characterized by short times and maximum efficiency, offer the possibility of developing a continuous process for the recovery of contaminated water and spent dye by reusing the zeolite until exhaustion. This continuous process will allow the recovered water to be reused in the same process, ensuring the protection of natural water by reducing industrial water consumption. Furthermore, it will reduce dye consumption by enabling the reuse of the recovered dye, thereby providing environmental and economic benefits to dye-consuming industries.

This industry-promoted approach advocates for greater environmental protection. Additionally, the fully spent zeolite could be reused in other industrial processes, thus establishing a zero-waste process.

Therefore, the removal of dyes from contaminated waters in the textile industry through adsorption on zeolite derived from hazardous waste in the aluminum industry, represents an economical, efficient, and fully sustainable process.

4.5 CONCLUSION

The waste-based LTA zeolite showed an excellent removal efficiency, reaching a remarkable 98.12% for the Safranine-T dye, demonstrating its promising potential as an effective treatment agent for dye-contaminated wastewater. The sorption process was extremely fast and efficient, requiring just 1 min of contact time for virtually complete removal of the dye. The utilization of thermodynamic and adsorption isothermal models revealed that the process of adsorption was spontaneous, displaying an exothermic nature, and occurred via physical mechanism between the Safranine-T molecules and the surface of LTA zeolite.

The optimal experimental conditions, determined statistically, consisted of a zeolite dosage of 21.5 g L^{-1} and agitation at 147 rpm. However, it is noteworthy that the zeolite dosage was the sole variable, expressed in linear and quadratic forms,

exerting a significant influence on ST removal. The obtained R^2 value of 0.9927 indicates a high degree of correlation between experimental and predicted values. Furthermore, the ANOVA demonstrated the model validity at a 95% confidence level without the need for adjustments.

The utilization of different zeolites in the ST adsorption process demonstrated that the waste-based LTA zeolite was the most efficient (98.1%), exhibiting a removal capacity even higher than the commercial LTA zeolite (82.9%). These findings can significantly contribute to sustainability and the circular economy. Furthermore, the application of the LTA zeolite synthesized using hazardous waste from the aluminum industry in the adsorption of textile dyes enables a mutual benefit (symbiosis) between these two industrial sectors, allowing for the co-recycling of aluminum waste while simultaneously treating wastewater with a high pollutant potential.

The results of this research can greatly contribute to sustainability and the circular economy. The highly promising adsorbent properties of the waste-based LTA zeolite applied to the treatment of dye-containing effluents provides a sustainable alternative to the use of materials produced with commercial reagents, thus reducing the consumption of resources, while helping to improve the water quality and mitigating environmental pollution.

5 CHAPTER 5: INFLUENCE OF THE CHEMICAL STRUCTURE OF TEXTILE DYES ON THEIR BIODECOLORIZATION BY *PSEUDOMONAS AERUGINOSA*: INDIGO CARMINE AND SAFRANINE-T AS MODEL DYES IN BIOREMOVAL EXPERIMENTS

ABSTRACT

The proper treatment of dye-contaminated wastewater is a major challenge due to the structural stability, low biodegradability, recalcitrance and toxic characteristics of most dyes. In recent years, research efforts have focused on developing more effective, sustainable and eco-friendly technologies for treating these dye-containing effluents. In the present study, the biological remediation of textile dyes by *Pseudomonas aeruginosa* was carried out, comparing Indigo Carmine (IC) (anionic) and Safranine-T (ST) (cationic). The influence of different initial dye concentrations (50, 100, 150 and 500 mg L^{-1}), agitation rates (static and 125 rpm) and growth medium concentration (25 and 50 g L^{-1}) was also evaluated. It was found that *P. aeruginosa* successfully biodecolorized the IC dye, obtaining removals >96% in agitated media in only 8 h. The biodecolorization rate for IC reached a remarkable 60.27 mg L^{-1} h^{-1}. In contrast, ST only was efficiently biodecolorized (77.2%) in the lowest initial concentration and the highest medium concentration. Second-order kinetic models were determined as the best fitted to the experimental data. The agitation condition positively affected the bioremoval process for both dyes. The better performance obtained for the anionic IC dye can be explained by its probable use as an energy source by bacterial metabolism, while the low removal of ST is attributable to the biosorption mechanism due to its cationic nature. The biodecolorization of textile dyes using microorganisms such as *Pseudomonas aeruginosa* as biological resources can be considered an extremely promising alternative solution to conventional wastewater treatment methods, contributing to environmental preservation and sustainability.

Keywords: biodecolorization, *Pseudomonas aeruginosa*, textile dyes, Safranine-T, Indigo Carmine, wastewater treatment.

5.1 INTRODUCTION

Nowadays, the development of technologies for the decontamination of textile effluents, in order to solve the serious environmental problems arising from their inadequate treatment, is an urgent challenge. A major player on the world economic scene, the textile industry has a production chain known for generating large volumes of wastewaters with a high polluting potential. Dyes, the most common pollutants in textile effluents, have an annual global production of around 1,000,000 tons, 80% of which are consumed in this sector alone (LIN et al., 2023). It is estimated that approximately 280,000 tons of dyes are lost to the environment annually worldwide (DUTTA et al., 2024). Along with other chemicals used in textile production (dispersants, salts, detergents and oxidizers), dyes cause contamination of soil, sediments and surface- and groundwater, which has turned them into a global environmental pollution problem (YASEEN; SCHOLZ, 2019).

Commercial dyes can be classified in various ways. Based on their application and dyeing mechanism, dyes are categorized as reactive, disperse, direct, acid and basic dyes (ISMAIL; SAKAI, 2022). Considering the chemical structure of the chromophore group responsible for conferring the color, they are identified as azo, anthraquinonic, triphenylmethane or heterocyclic dyes (MISHRA; MOHANTY; MAITI, 2019). In addition, dyes are also differentiated based on the charge of the particles after dissolving in an aqueous medium, into anionic, cationic and non-ionic (disperse dyes) (YAGUB et al., 2014).

Anionic dyes are highly soluble in water and correspond to all acid dyes, as well as most reactive and direct dyes, representing the main fraction of dyes in wastewater (HAQUE et al., 2022). With its distinctive blue color, Indigo Carmine (IC) is one of the most important anionic dyes for the textile industry, especially used to dye jeans (VAUTIER; GUILLARD; HERRMANN, 2001). Around 40,000 tons of IC are produced annually (CHOWDHURY et al., 2020). The release of unfixed IC dye during textile processing into the environment is extremely dangerous for human health and can permanently affect the corneas and conjunctiva when in direct contact with the eyes, as well as being very harmful to the respiratory tract and causing severe skin irritation. In addition, its carcinogenic nature can lead to neural, developmental and

reproductive disorders (GUTIÉRREZ-SEGURA; SOLACHE-RÍOS; COLÍN-CRUZ, 2009).

Cationic dyes, on the other hand, due to the nature of their electrostatic interactions and molecular structure, are less soluble in water and decompose easily when in contact with alkaline substances. They have a high color intensity and are very visible even at low concentrations. In addition, they have more harmful effects compared to anionic dyes, due to their stronger and easier interaction with cell membranes (negatively charged), which can cause skin and mucous membrane irritation and allergic dermatitis (SAHA et al., 2021; YAGUB et al., 2014). Safranine-T (ST) is one of the oldest known synthetic cationic dyes, widely used in the dyeing of paper, silk, acrylic fibers, leather and biological analysis procedures (CRINI et al., 2007). It is considered one of the model compounds to represent the dyes that are released into the effluents of these industries (GUPTA et al., 2006). ST is characterized as a nitrogenous heterocyclic dye, which is more difficult to degrade than benzenic compounds, since its degradability is related to properties such as molecular structure, extended aromaticity, particle charge and physicochemical characteristics (JIALIANG et al., 2012). ST dye can cause several acute health problems, affecting the eyes, lips, mouth, throat and stomach (KAMEL et al., 2021).

Both cationic and anionic dyes also have harmful effects on the environment, especially causing pollution of water resources, reducing light penetration and impairing photosynthesis, as well as leading to the formation of teratogenic, mutagenic and carcinogenic by-products (TARA et al., 2020). Even small concentrations of dyes (10-15 mg L^{-1}) in wastewater can significantly affect the transparency, gas solubility and aesthetic value of watercourses (MAQBOOL et al., 2016). Heterocyclic groups (chromophore group), constituents of IC and ST dyes, as well as sulphonic acid (auxochrome group of IC dye) increase solubility and color fastness, but provide greater resistance to microbial attack, making them recalcitrant to oxidative degradation (VALLI NACHIYAR; SUSEELA RAJAKUMAR, 2004). Due to the low biodegradability and structural stability of most dyes, conventional physicochemical and biological methods, such as activated sludge systems, become limited or ineffective (TKACZYK; MITROWSKA; POSYNIAK, 2020). This fact, coupled with the high cost of these conventional treatments, their low versatility, high energy consumption and management of the large volumes of sludge generated

(SRIVASTAVA et al., 2022), means that current trends are towards efficient, cost-effective and eco-friendly remediation technologies, preferably developed from renewable and sustainable energy sources, using biotechnology as a possible solution (RAMYA; SENTHIL KUMAR, 2022). In this sense, biological processes are considered a promising alternative to other existing treatment technologies, as they fulfill all these requirements (KALYANI et al., 2009). Two main mechanisms are involved in the biological decolorization of dyes: biosorption, in which the dyes are adsorbed under the bacterial cell walls, and biodegradation, in which the dyes are metabolized through enzymatic action (SARATALE et al., 2011). Many microorganisms have been tested to decolorize textile dyes, mostly anaerobic bacteria (PANDEY; SINGH; IYENGAR, 2007). However, it has been reported that the anaerobic biodecolorization process can lead to the formation of aromatic amines, which are potentially mutagenic and carcinogenic (VALLI NACHIYAR; SUSEELA RAJAKUMAR, 2004).

Therefore, the use of aerobic bacterial strains should be considered, among which *Pseudomonas aeruginosa* stands out as one of the few capable of degrading dyes aerobically (NACHIYAR; RAJKUMAR, 2003). *P. aeruginosa* is a gram-negative bacterial species known for its ability to survive in both aerobic and anoxic conditions and to compete in complex ecosystems with substrate limitations (BAGCHI; BEHERA, 2021). Its versatile metabolism and applications in waste treatment, as well as in the production of compounds such as antibiotics and enzymes, have awakened considerable interest (JAYAPRIYA; RAMAMURTHY, 2012). In addition, some authors have reported the distinct ability of *P. aeruginosa* to bioremove some dyes (BORAN et al., 2019; JIALIANG et al., 2012; KALYANI et al., 2009; KHAN et al., 2022; MAQBOOL et al., 2016; MISHRA; MAITI, 2018).

Considering this, the present work aims to compare the biodecolorization efficiency of the Indigo Carmine and Safranine-T dyes by *P. aeruginosa*. To the best of our knowledge, studies reporting the biological degradation of these two dyes separately are scarce and no data has been published regarding the biodecolorization process comparing these anionic and cationic dyes. Furthermore, the influence of different dye concentrations, agitation rates and nutritional concentrations in the growth medium on the bioremoval process of textile dyes was studied. The kinetic study for the samples with the best removals of both dyes was also carried out. Understanding

the differences in the decolorization process of anionic and cationic dyes using microorganisms such as *P. aeruginosa* is extremely important for the development and improvement of wastewater treatment technologies. Biological remediation of textile effluents can be considered a cost-effective and environmentally promising alternative, representing a potential solution to the techniques commonly used today.

5.2 MATERIALS AND METHODS

5.2.1 Textile Dyes

IC and ST dyes were purchased from Neon Comercial (Brazil). IC (CI. 73015), also known as Acid Blue 74, was used as a representative of anionic dyes, while ST (CI. 50240) is a cationic dye, also called Basic Red 2. The chemical structure and main properties of these dyes are presented in Figure 5.1 and Table 5.1, respectively.

Figure 5.1 – Chemical structure of (a) Indigo Carmine (IC) and (b) Safranine-T (ST) dyes.

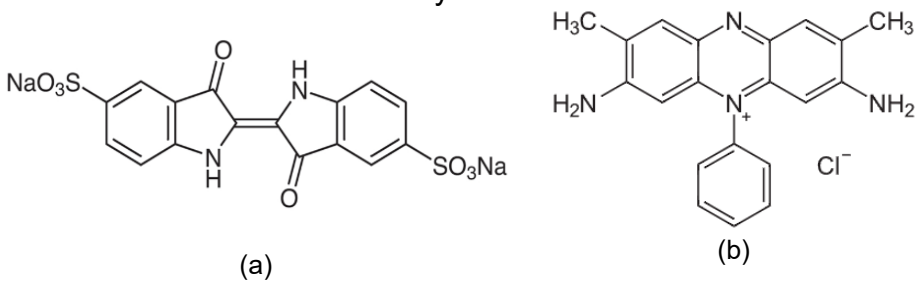

(a) (b)

Source:created by the author

Table 5.1 – Main properties of Indigo Carmine (IC) and Safranine-T (ST) textile dyes.

Dyes	**IC**	**ST**
Chemical form	$C_{16}H_8N_2Na_2O_8S_2$	$C_{20}H_{19}ClN_4$
IUPAC	5,5'-indigodisulfonic acid sodium salt	3,7-dimethyl-10-phenylphenazin-10-ium-2,8-diamine;chloride
CAS number	860-22-0	477-73-6
Molecular weight (g mol^{-1})	466.4	350.8
UV absorption (nm)	610	520

Source: created by the author

The dye solutions were prepared by diluting the stock solution (1 g L^{-1} in distilled water) in Phosphate Buffer Solution (PBS). The PBS has the following composition: 8.0 g L^{-1} sodium chloride (NaCl), 1.44 g L^{-1} disodium phosphate (Na_2HPO_4), 0.24 g L^{-1} monopotassium phosphate (KH_2PO_4) and 0.2 g L^{-1} potassium

chloride (KCl). The aqueous solutions were sterilized by filtration through sterile 0.22 µm pore size filters, following the procedure proposed by Behzat (BEHZAT, 2015).

5.2.2 Strain and Growth Conditions

A pure culture of *Pseudomonas aeruginosa* (strain ATCC 27853) was used as the inoculum in this study. The bacteria were grown overnight on a nutrient agar plate incubated at 37 ± 1 ºC. The inoculum was routinely prepared by dispersing a colony of bacterial cells collected from the agar plate in Luria Bertani broth (LB) (KASVI, Brazil) and incubated at 37 ± 1 °C with constant stirring (125 rpm) until it reached an optical density (O.D.) between 0.6 and 0.8, measured in a HACH DR/3900 UV-Vis spectrophotometer with a selected wavelength of 625 nm. This optical density range corresponds to the logarithmic phase of bacterial growth on the McFarland scale, in which around $1.5x10^8$ cells mL^{-1} are estimated (MCFARLAND, 1907). Subsequently, the required volumes of bacterial suspensions were added to the LB broth in order to obtain an O.D. of 0.1 (MARASSI et al., 2020). The composition of the LB broth was sodium chloride (NaCl, 10 g L^{-1}), tryptone (10 g L^{-1}), yeast extract (5 g L^{-1}). The reaction medium used in the biodecolorization tests was prepared (1:1 volume ratio) with the bacterial suspension in LB broth and dye solutions (in the required concentrations) buffered in PBS. All the glassware and solutions were sterilized in a Luferco model 39211 vertical autoclave at 121 ± 1 ºC for 15 minutes.

5.2.3 Biodecolorization Experiments

Biodecolorization tests were conducted to evaluate the influence of different parameters, including the type and concentration of dyes, agitation rate and concentration of LB culture medium on the removal of IC and ST dyes by *Pseudomonas aeruginosa*.

The assays were carried out in 250 mL Erlenmeyer flasks, with 120 mL of reaction medium, half the volume consisting of bacterial culture in LB broth and the other half of dye solution at the required concentration (buffered in PBS). The experiments were conducted at room temperature using an orbital shaker (Kasvi K40-3020). The pH was monitored throughout the experiments and remained neutral, with

values between 7 and 7.2. All experiments were carried out in duplicate and the results reported as the average value obtained. Controls without microbial culture were also performed.

Different dye types (anionic and cationic) and concentrations (50, 100, 150 and 500 mg L^{-1}) were studied, as well as the effect of the agitation rate (125 rpm and static condition) and the concentration of nutrients in the growth medium (LB broth - KASVI) (25 and 50 g L^{-1}) on the biodecolorization of the textile dyes. Samples were labeled LBA, 2LBA, LBS and 2LBS, where LB refers to the medium with 25 g L^{-1} and 2LB for the doubled concentration of 50 g L^{-1}, under agitation (A) or static (S) condition.

The biodecolorization tests were carried out over 48 hours, with samples collected at time intervals of 0.5, 1, 2, 3, 4, 8, 12, 24 and 48 hours. After treatment, the samples were collected (sterile conditions) and centrifuged at 4000 rpm for 10 minutes. The final concentration of the dyes in the supernatant was determined by colorimetry from calibration curves (concentration range 10 to 125 mg L^{-1}) at wavelengths of 610 and 520 nm for IC an ST, respectively, in a HACH DR/3900 spectrophotometer. The bioremoval efficiency R (%) was calculated using the Equation 5.1, where C_i and C_t are the initial and at the time t (min) dye concentrations (mg L^{-1}), respectively.

$$R(\%) = \frac{(C_i - C_t)}{C_i} . 100 \quad (5.1)$$

The biodecolorization rate (B_R, mg L^{-1} h^{-1}), which refers to the speed with which the dye removal process occurs, was calculated according to Equation 5.2, where C_f is the final dye concentration (mg L^{-1}).

$$B_R = \frac{(C_i - C_f)}{t} \quad (5.2)$$

A kinetics study was conducted for the tests with the highest removals of each dye. The zero, first and second-order linear equations used are shown in Table 5.2.

Table 5.2 – Reaction equations at different orders (n) to determine the decay of the Indigo Carmine (IC) and Safranine-T (ST) dyes.

Order (n)	Linearized equation	Plot	K_n unit
0	$C_t = C_i - K_0 t$	C_t *versus* t	mg L^{-1} h^{-1}
1	$\ln C_t = \ln C_i - K_1 t$	$\ln C_t$ *versus* t	h^{-1}
2	$1/C_t = 1/C_i + K_2 t$	$1/C_t$ *versus* t	L mg^{-1} h^{-1}

Source: adapted from BEHZAT (2015)

5.2.4 Statistical Analysis

STATISTICA® 13.3 software was used to evaluate the effects of the different parameters on the biodecolorization of textile dyes. ANOVA was applied to test for differences between the means of data with normal distribution, followed by Tukey's test. Differences were considered significant when $p < 0.05$.

5.3 RESULTS AND DISCUSSION

5.3.1 Effect of the Initial Dye Concentration, Growth Medium Concentration and Agitation Rate on the Biodecolorization of Textile Dyes

The results of the biodecolorization by *Pseudomonas aeruginosa*, comparing the IC and ST dyes over the 48-hour test are shown in Figure 5.2 and Table 5.3.

From Figure 5.2, it can be seen that, with the exception of the lowest concentration (50 mg L^{-1}) at which ST showed the best results, the bioremoval performance of the IC dye was superior for all the other initial dye concentrations tested. When using 50 mg L^{-1} (Fig. 5.2a), the maximum removal of IC (46.7% - 23.4 mg L^{-1}) occurred in the LBA condition (under agitation). For ST, bioremoval reached 73.6% (36.8 mg L^{-1}) and 77.2% (38.6 mg L^{-1}) for 2LBS and 2LBA, respectively. Applying a concentration of 100 mg L^{-1} (Fig. 5.2b), IC bioremoval was very high, reaching 96.0% efficiency under agitation (LBA and 2LBA). With ST, on the other hand, bioremoval efficiencies did not exceed 45% (2LBA). At this concentration, as with the IC dye, the ST samples with the best removal percentages were those under stirring conditions. The biodecolorization behavior of the dyes was similar to the previous one when an initial dye concentration of 150 mg L^{-1} was used (Fig. 5.2c). Bioremoval of the IC dye reached over 97.0% (> 145 mg L^{-1}) for both, LBA and 2LBA. The best performing sample for ST dye was 2LBA, which achieved approximately 32.0% (48.1 mg L^{-1}) removal efficiency. Finally, a concentration of 500 mg L^{-1} (Fig. 5.2d) was used to assess the ability of *Pseudomonas aeruginosa* to degrade solutions with high dye loads. According to Singh (SINGH, 2015), the concentration of dyes ranges from 10 to

200 mg L^{-1} in textile effluents. For ST, unimpressive results were obtained, 20.1% (2LBA), 18.2% (LBA), 9.9% (2LBS) and 3.6% (LBS). However, the biodecolorization of the IC dye achieved significant removal efficiencies, even at this very high concentration. Both LBA and 2LBA showed over 96.0% (> 480 mg L^{-1}) removal efficiency at the end of the experiment.

Statistical analysis showed that the parameters that significantly influenced (p <0.05) the biodecolorization of the dyes were the dye type and agitation rate. It was found that the concentration of the growth medium (LB or 2LB) had no significant effect on the dye bioremoval process. This was evidenced by the bacterial growth curves with similar colony-forming units for the two nutritional conditions tested (data not shown). The biological removal of dyes can occur through biodegradation or biosorption. In the latter, the molecular structure of the dye and the electrical charges on the surface of the bacterial biomass have a crucial effect (SRINIVASAN; VIRARAGHAVAN, 2010). *Pseudomonas aeruginosa* is classified as a gram-negative bacterium, so when subjected to Gram staining and treated with different reagents, it acquires a reddish color (conferred by the Safranine-T dye applied in this technique), unlike gram-positive bacteria, which turn purple (MINISTÉRIO DA SAÚDE, 1997). Due to the structure and composition of their cell walls and outer membrane, made up predominantly of phospholipids and lipopolysaccharides, their surface electrical charge is negative (BEVERIDGE, 1999). Thus, considering the negatively charged surface of the bacterial biomass and the cationic form of the dye in solution (positive), it can be inferred that the bacterial membrane is capable of attaching the Safranine-T molecules, even though it does not metabolize them, and that the dye removal was therefore due to the biosorption mechanism. In this way, the scarce removal of ST observed in the tests can be attributed to the dye adhering to the bacterial membranes, explaining why the percentage of decolorization decreases when the concentration of Safranine increases since the initial bacterial biomass was similar in all the experiments. The reddish color observed in the pellet formed after centrifuging the samples is an indication that corroborates this statement.

In contrast to ST, the biosorption of negatively charged particles of the anionic dye Indigo Carmine in solution was not favored by the also negative surface charge of *P. aeruginosa*, considering that there was no change in the pH of the reaction medium. Srinivasan et al. (SRINIVASAN; VIRARAGHAVAN, 2010) highlighted the influence of pH on the biosorption process, suggesting that the use of an acid pretreatment could change the surface charges of the bacterial biomass to positive, increasing its attraction to the anionic dye. However, in this study, the pH remained between 7 and 7.2 during all the tests. Meanwhile, Boran et al. (BORAN et al., 2019), tested live and dead pellets of *P. aeruginosa* and showed that the biodecolorization of the IC dye was mainly due to bacterial metabolism and not to the adsorption process. In this sense, it was evident that agitation is a key factor in the biodecolorization of IC and ST dyes, leading to higher removal efficiencies in all evaluated conditions. Ramya et al. (RAMYA; ANUSHA; KALAVATHY, 2008) state that the increase in discoloration in a culture kept under agitation can be attributed to an increase in the activity of microbial enzymes. Agitation is also considered a factor that positively influences the adsorption process, increasing the transfer of external mass (NASCIMENTO et al., 2014). This may explain why, under static conditions, it was not possible to establish a pattern between the amount of ST removed and the increase in the initial concentration of the dye, since the exposed surface of the bacteria in this condition may not have been the same, preventing biosorption from occurring homogeneously as when under agitation. In this regard, dye removal was favored under shaking conditions, regardless of the decolorization mechanism, whether via biosorption for ST or via biodegradation for IC.

Figure 5.2 – Effect of growth medium and agitation on the biodecolorization at different initial dye concentrations: (a) 50 mg L^{-1}, (b) 100 mg L^{-1}, (c) 150 mg L^{-1} and (d) 500 mg L^{-1} of Indigo Carmine and Safranine-T by *Pseudomonas aeruginosa*. Asterisks indicate statistically different means according to Tukey's test (*p*-value <0.05*; <0.005**; <0.0005***).

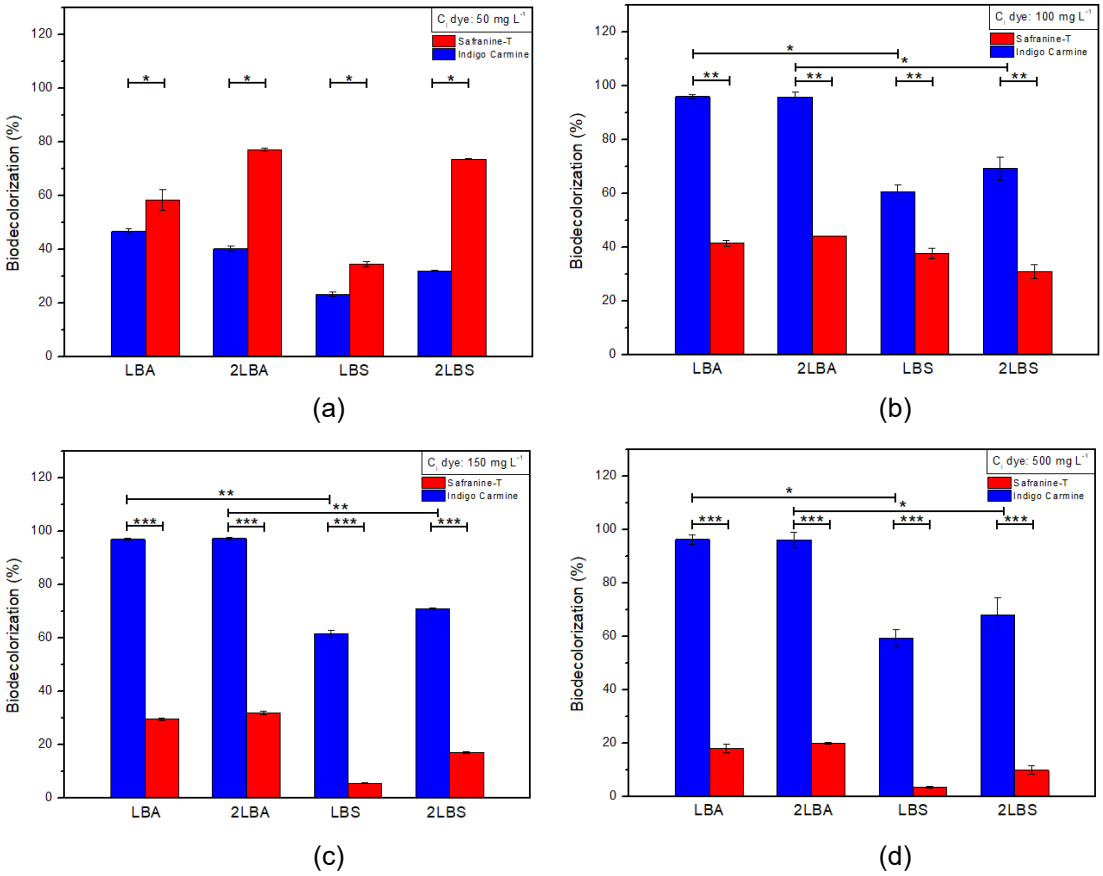

Source: created by the author

Table 5.3 – Quantification and bioremoval efficiencies of Indigo Carmine (IC) and Safranine-T (ST) dyes by *Pseudomonas aeruginosa* under different experimental conditions.

	Indigo Carmine							
Samples	**LBA**		**2LBA**		**LBS**		**2LBS**	
Dye concentration (mg L^{-1})	**R (%)**	**Q (mg L^{-1})**	**R (%)**	**Q (mg L^{-1})**	**R (%)**	**Q (mg L^{-1})**	**R (%)**	**Q (mg L^{-1})**
50	46.7	23.36 ± 0.94	40.3	20.17 ± 0.87	23.4	11.70 ± 0.93	32.0	16.00 ± 0.15
100	96.0	96.03 ± 0.82	96.0	96.00 ± 1.65	60.5	60.54 ± 2.86	69.3	69.31 ± 4.35
150	97.0	145.59 ± 0.43	97.4	146.05 ± 0.53	61.6	92.40 ± 1.20	70.9	106.35 ± 0.30
500	96.4	482.20 ± 1.77	96.3	481.36 ± 2.89	59.5	297.50 ± 3.25	68.2	341.00 ± 6.25
	Safranine-T							
50	58.4	29.19 ± 3.82	77.2	38.61 ± 0.66	34.5	17.24 ± 1.07	73.6	36.80 ± 0.17
100	41.6	41.59 ± 1.07	44.2	44.25 ± 0.13	37.8	37.82 ± 1.94	31.0	31.03 ± 2.53
150	29.7	44.49 ± 0.42	32.0	48.07 ± 0.64	5.6	8.43 ± 0.21	17.1	25.73 ± 0.41
500	18.2	91.15 ± 1.58	20.1	100.55 ± 0.27	3.6	18.20 ± 0.35	9.9	49.65 ± 1.58

R (%): bioremoval efficiency (%); Q: quantitative removal (mg L^{-1}). Source: created by the author

5.3.2 Kinetic Studies on the Biodecolorization of Textile Dyes

The initial concentration of dyes has an important effect on the decolorization process, since high concentrations can negatively affect the efficiency of the biodecolorization due to possible toxicity to microorganisms (SINGH, 2015). The IC and ST biodecolorization tests were conducted using different initial dye concentrations 50, 100, 150 and 500 mg L^{-1}. Figure 5.3 shows the biodecolorization kinetics of the two dyes at these different concentrations as a function of time.

The results obtained with the IC showed that higher removal efficiencies were achieved as the initial concentration of the dye increased (Fig. 5.3). When an initial dye concentration of 50 mg L^{-1} was applied, the bioremoval of the dye by *Pseudomonas aeruginosa* did not exceed 50% in any of the conditions evaluated, but as the concentration increased to 100, 150 and 500 mg L^{-1}, practically quantitative removals (> 96.0%) were obtained for the samples kept under agitation. These findings are superior to those reported by most authors on the biodegradation of this dye using different bacteria (Table 5.4). Oh et al. (OH et al., 2011) using *Citrobacter amalonaticus Y19* obtained a biodecolorization of only 12.5% when applying a low initial concentration of dye (50 mg L^{-1}). *Pseudomonas* strains, Z1, GM3 and Q3, used by Yu et al. (YU, 2001) at 48h incubation time and 100 mg L^{-1} initial dye concentration, did not exceed removal efficiencies of 88%, 69% and 61%, respectively. Boran et al. (BORAN et al., 2019) were able to obtain a high IC removal efficiency of 92% using an initial concentration of 50 mg L^{-1}. However, the stirring rate and temperature used were slightly higher. Furthermore, when they tested a high dye load (500 mg L^{-1}), the bioremoval efficiency was approximately 60% (8 h), considerably lower when compared to the 96.4% obtained in this study for the same period of time.

As shown in Figure 5.3, for a dye concentration of 500 mg L^{-1}, it was observed that the effective removal of IC occurred mainly in the first 8 hours of the test, regardless of the initial concentration used. However, except for the lowest concentration (50 mg L^{-1}), bioremovals of over 90% were achieved within the first 3 hours for the LBA and 2LBA samples. A different behavior was observed when a concentration of 100 mg L^{-1} was used in the static assays (LBS and 2LBS), which required 12 hours to achieve maximum dye biodegradation.

Figure 5.3 – Biodecolorization kinetics at different initial concentrations of (a, c, e, g) Indigo Carmine and (b, d, f, h) Safranine-T dyes by *Pseudomonas aeruginosa*.

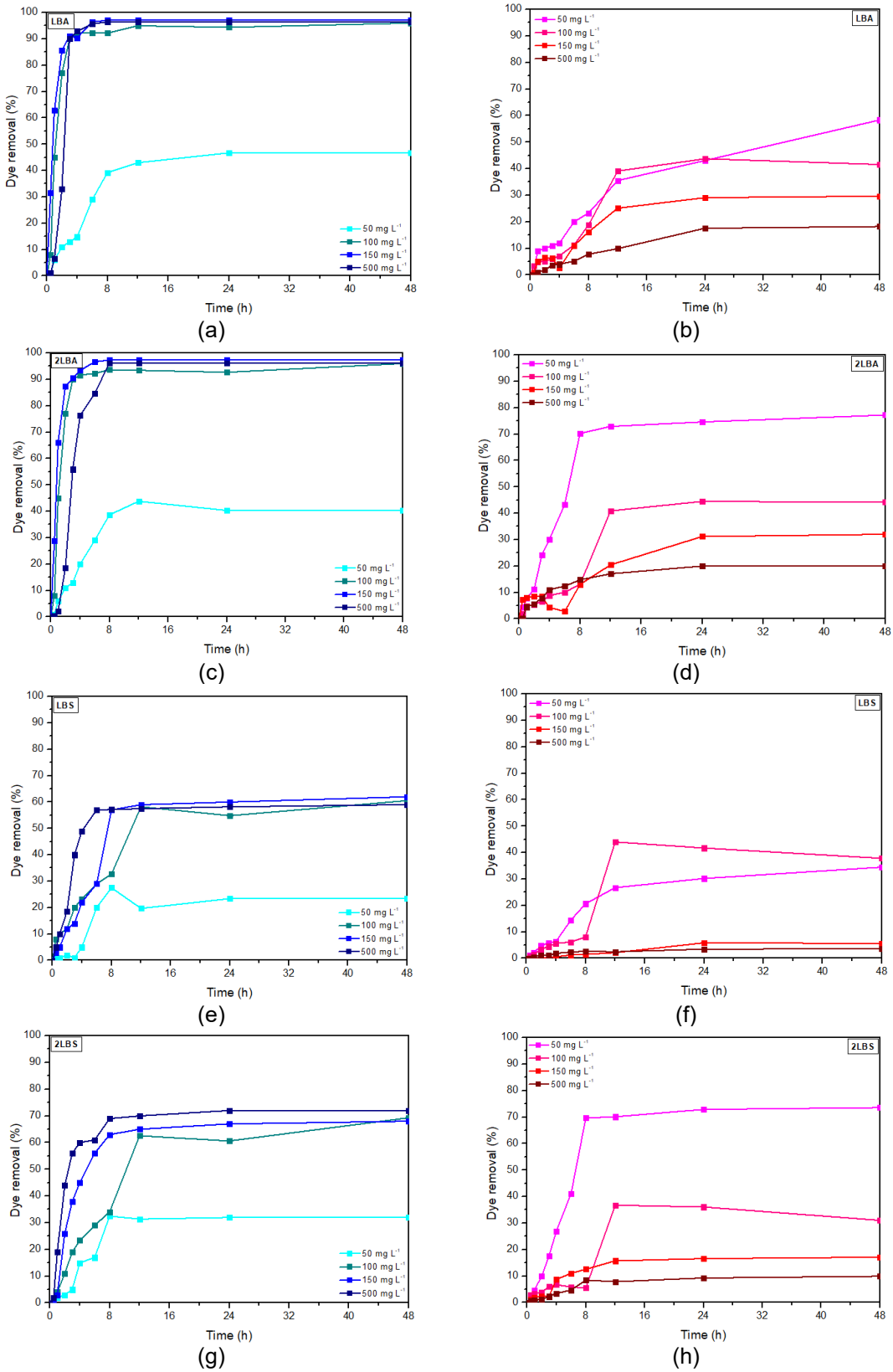

Source: created by the author

Table 5.4 – Indigo Carmine biodecolorization by different bacteria.

Bacteria	C_I (mg L^{-1})	t (h)	T (ºC)	Agitation (rpm)	R (%)	Reference
Citrobacter amalonaticus Y19	50	48	35	100	12.5	(OH et al., 2011)
Bacillus sp.	100	96	37	120	66.6	(JAISWAL; GOMASHE; AGRAWAL, 2014)
Trametes trogii	23.4	24	28	Static	95	(LEVIN; MELIGNANI; RAMOS, 2010)
Trametes villosa					93	
Coriolus versicolor					95	
Paenibacillus larvae	100	8	30	150	100	(RAMYA; ANUSHA; KALAVATHY, 2008)
Bacillus sp. MZS10	100	15	30	Stirred	87.31	(LI et al., 2015)
Bacillus aryabhattai DC100	180	72	37	304.09	98.31	(PAZ et al., 2017)
Aeromonas hydrophila DEC1	100	24	30	Static	60	(CHEN et al., 2003)
Pseudomonas sp. Z1	100	48	35	Static	88	(YU, 2001)
Pseudomonas sp. GM3					69	
Pseudomonas sp. Q3					61	
Pseudomonas aeruginosa ATCC 10145	50	6	30	150	92	(BORAN et al., 2019)
			40		93	
Pseudomonas aeruginosa ATCC 27853	50	8	23	125	39.2	This study
	100				92.2	
	150				97.4	
	500				96.4	
Pseudomonas aeruginosa ATCC 27853	50	48	23	125	46.7	This study
	100				96.0	
	150				97.4	
	500				96.4	
Pseudomonas aeruginosa ATCC 27853	50	48	23	Static	23.4	This study
	100				60.5	
	150				61.6	
	500				59.5	

C_i: initial dye concentration (mg L^{-1}); t: time (h); T: temperature (ºC); R(%): bioremoval efficiency (%).
Source: created by the author

In addition to the high removal efficiencies, high biodecolorization rates were also observed (Table 5.5). For the best conditions (LBA and 2LBA), increasing the IC concentration from 50 to 500 mg L^{-1} led to a faster removal process, ranging from 2.45 to 60.27 mg L^{-1} h^{-1}, respectively. The latter is one of the highest removal rates obtained for IC biodecolorization. Previously mentioned studies have reported decolorization rates ranging from 0.13 to 1.44 mg L^{-1} h^{-1} (OH et al., 2011; YU, 2001) and reaching a maximum of 37.5 mg L^{-1} h^{-1} when high IC dye loads were applied (BORAN et al., 2019).

In the case of ST dye, increasing the initial dye concentration led to a decrease in removal efficiency, although similar amounts (in mg L^{-1}) were biosorbed at concentrations of 50 to 150 mg L^{-1} (Table 5.3). The removal kinetics indicated that the maximum biosorption of ST by *P. aeruginosa* was reached in 24 hours of testing, after

which some of the samples showed a slight decline in removal efficiency, attributed to a possible desorption process of the dye. ST dye also showed lower bioremoval rates than the anionic one, ranging from 1.55 to 4.17 mg L^{-1} h^{-1} (sample 2LBA) at concentrations of 50 and 500 mg L^{-1}, respectively (Table 5.5). Furthermore, for the static samples, the bioremoval rates did not show a linear behavior as occurred with the stirred samples or with the IC dye, since with the increase in the intermediate concentration from 100 to 150 mg L^{-1}, the biodecolorization rates decreased. As previously mentioned, however, this is probably due to differences in the external mass transfer process, the first step in the adsorption mechanism, which is strongly influenced by agitation and the consequent available surface area of the bacterial biomass.

Table 5.6 shows the kinetic constants calculated using linear regression for the samples with the best bioremovals of each dye by *Pseudomonas aeruginosa*. In this sense, for the IC dye, the kinetic study (8 hours) was carried out for the LBA sample at the two highest concentrations. For ST, the kinetic behavior (24 hours) of the 2LBA sample was evaluated, which showed the best removal efficiency at 50 mg L^{-1} (77.2%) and the highest amount removed (100.5 mg L^{-1}) at 500 mg L^{-1}.

Table 5.5 – Biodecolorization rates obtained using different initial concentrations of the dyes Indigo Carmine (8-hour test) and Safranine-T (24-hour test).

Biodecolorization rate (mg L^{-1} h^{-1})								
	Indigo Carmine				**Safranine-T**			
	Dye concentration (mg L^{-1})							
Samples	**50**	**100**	**150**	**500**	**50**	**100**	**150**	**500**
LBA	2.45	11.52	18.20	60.27	0.90	1.82	1.82	3.67
2LBA	2.42	11.71	18.26	60.17	1.55	1.85	1.95	4.17
LBS	1.72	4.08	10.69	35.75	0.63	1.74	0.37	0.73
2LBS	2.03	4.26	12.94	39.38	1.52	1.50	1.04	1.94

Source: created by the author

Table 5.6 – Kinetic rate constants obtained in the best bioremoval conditions for Indigo Carmine (IC) and Safranine-T (ST) dyes.

Dye		**Indigo Carmine**		**Safranine-T**	
Reaction time		**8 hours**		**24 hours**	
Dye concentration (mg L^{-1})		**150**	**500**	**50**	**500**
Order (n)	**Rate constants**	**LBA**	**LBA**	**2LBA**	**2LBA**
0	K_0 (mg L^{-1} h^{-1})	14.682	71.298	1.717	4.075
	R^2	0.5898	0.7625	0.7216	0.7590
1	K_1 (h^{-1})	0.439	0.498	0.066	0.009
	R^2	0.8888	0.8659	0.7667	0.7837
2	K_2 (L mg^{-1} h^{-1})	0.029	0.008	0.003	2E-05
	R^2	0.9523	0.9587	0.7952	0.8076

Source: created by the author

The comparison between the coefficients of determination (R^2) of the different kinetic orders showed that the biodecolorization of IC can be better explained by second-order kinetics at both concentrations. The R^2 were in the range of 0.9523 and 0.9587 for the concentrations of 150 and 500 mg L^{-1}, respectively. This assumes that the decolorization rate increases quadratically as the dye concentration increases, which is in line with the removal behavior observed for this dye. The results obtained for ST also showed a better fit for second-order kinetics, although the coefficients of determination were quite low (R^2 = 0.7952 and 0.8076). Second-order kinetics for the removal of dye (Mordant Yellow 10) by *P. aeruginosa* was also reported by Rethinan et al. (RETHINAM; PALANICHAMY; BRITTO, 2023).

The results found in this study showed that the *Pseudomonas aeruginosa* behaved quite differently when bioremoving the different dyes used. While Indigo Carmine was effectively decolorized in practically all the concentrations tested (100, 150 and 500 mg L^{-1}), Safranine-T dye showed a satisfactory percentual result (77.2%) only when using the lowest dye concentration (50 mg L^{-1}), and its highest quantitative removal (100.5 mg L^{-1}) occurred at 500 mg L^{-1}. In this case, considering that the removal of ST is due to the biosorption process, this behavior can be explained by the driving force generated by the high concentration of dye ions required to overcome the mass transfer between the solid and liquid phases (YADAV et al., 2022a).

Although various bacterial strains have been shown to co-metabolize dyes in the presence of carbon and nitrogen sources, *Pseudomonas* are among the very few that have the ability to use dyes as their sole source of energy (QU et al., 2015). Stolz (STOLZ, 2001) reported that *Pseudomonas* enzymes are capable of reductively cleaving sulphonated structures (present in IC) in addition to the carboxylate groups present in different substrates (glucose, acetate, LB broth).

Furthermore, several studies have shown, through the analysis of metabolites, that the degradation mechanisms can differ completely depending, in addition to the added carbon source, on the bacterial strain and the molecular structure of the dye (LI et al., 2015; PANDEY; SINGH; IYENGAR, 2007). In this sense, the better performance of *P. aeruginosa* in degrading the anionic dye can be attributed to the structure of the IC, containing two sulphonate groups, which could be used by the bacteria as a source of energy and metabolized through the action of enzymes. The cationic nature of ST,

in turn, had an important effect on the uptake of the dye by *P. aeruginosa* due to its affinity with bacterial cell structures.

Although reasonably explained on the basis of the data obtained and the available literature, further studies would be necessary to confirm the mechanisms of dye bioremoval with certainty. To this end, continued research into the removal of these dyes using bioelectrochemical technologies will be carried out.

5.4 CONCLUSION

Pseudomonas aeruginosa was used with different success in the biodecolorization of different textile dyes. A bioremoval of 77.2% was achieved for Safranine-T (50 mg L^{-1}) and remarkable removal efficiencies (>96.0%) for Indigo Carmine (100, 150 and 500 mg L^{-1}). The IC bioremoval process was efficient and considerably fast. Its effective decolorization occurred within 8 hours, with 90% of the removal achieved in the first 3 hours. Increasing the initial dye concentration led to a higher efficiency and biodecolorization rate for IC, reaching an impressive 60.27 mg L^{-1} h^{-1}. For ST, the effect was the opposite, % bioremoval decreased with the increase of initial dye concentration, although similar quantitative removals were obtained at concentrations of 50 to 150 mg L^{-1}. The kinetic study revealed that the second-order kinetic model was the best fitted to the experimental data obtained for the dyes, with higher coefficients of determination (R^2 >0.95) for the anionic IC dye. In addition, this study showed that the bioremoval of both dyes was significantly influenced by agitation. The most likely assumption is that IC biodecoloration occurs via biodegradation, favored by the presence of sulfonate groups in its structure, since *P. aeruginosa* is capable of cleaving C-S bonds. Biodecoloration of IC through bioadsorption was not benefited due to its anionic character, not being attracted to the negative bacterial surface. In contrast, the presence of a precipitate of strongly colored cells and practically no effect on decolorization when incubated in different nutritional inputs or different oxygen availability (static vs. aerated) suggest that the removal mechanism of the ST cationic dye was via bioadsorption. ST biodegradation does not seem to be favored due to the absence of sulfonate or carboxylate groups in its structure. Based on the results presented, it can be concluded that the knowledge of

the structure and surface charge of the dyes is fundamental for predicting effective bacterial bioremediation of textile wastewater.

This study demonstrates the ability of *Pseudomonas aeruginosa* to biodecolorize anionic sulphonated textile dyes, requiring moderate conditions of time, temperature, pH and agitation to achieve effective removals, which is advantageous for its practical application. Thus, bioremediation using bacteria represents an attractive, promising and sustainable alternative strategy to conventional methods, providing a low-cost and eco-friendly solution in the treatment of textile wastewaters.

6 CHAPTER 6: ECO-FRIENDLY DECOLORIZATION OF INDIGO CARMINE AND SAFRANINE-T DYES WITH SIMULTANEOUS BIOENERGY GENERATION USING AN AIR-CATHODE SINGLE-CHAMBER MICROBIAL FUEL CELL

ABSTRACT

Developing sustainable technologies for the treatment of dye-contaminated wastewater is an urgent requirement to reduce the pollution of water resources and also a major challenge due to the toxic and recalcitrant characteristics of most dyes. In this context, the present study investigated the effect of the concentration of different model dyes, the anionic Indigo Carmine (IC) and the cationic Safranine-T (ST), on decolorization, chemical oxygen demand (COD) removal and bioelectricity generation using a single-chamber microbial fuel cell (MFC) equipped with a membrane electrode assembly (MEA) and inoculated with anaerobic sludge. It was found that the best MFC biodecolorization performance occurred for the ST cationic dye, achieving remarkable efficiency (>93%) when removing high concentrations of dye (500 mg L^{-1}). On the other hand, the anionic IC dye showed the best COD removal (189.81 mg L^{-1}, 36.82%), Coulombic efficiency (17.05%), and bioenergy generation. The maximum output voltage, power and current densities of 300 mV, 34.54 mW m^{-2} and 210.58 mA m^{-2}, respectively, were achieved when applying the highest concentration of IC dye. Phytotoxic effects were reduced after treatment in the MFC system under all the conditions evaluated. The differences observed between dyes suggested that all the parameters tested were strongly affected by their molecular structures. Analysis of the richness and diversity of the microbial community revealed that the most predominant genera in the MFC were *Rhodopseudomonas* (46%) and unidentified genera from the families *Comamonadaceae* (18%) and *Geobacteraceae* (12%), all belonging to the dominant phylum *Proteobacteria* (62%), indicating the development of dominant dye-degrading and electroactive microbial profiles adapted to the anodic environment of the MEA-MFC. The findings of this study support that the improvement of promising MFC technology paves the way for a more sustainable future, using renewable sources to provide clean energy while decontaminating environmentally harmful effluents.

Keywords: Microbial Fuel Cell (MFC), textile dyes, Indigo Carmine, Safranine-T, bioelectrochemical technology, wastewater treatment.

6.1 INTRODUCTION

Continuous population growth and accelerated industrial development have led to increased energy demand and the growing generation of wastes and effluents, triggering an unprecedented energy and climate crisis. It is estimated that by 2050, energy and fresh water demand will increase by almost 30% (SINGH; DAHIYA; MISHRA, 2021). In this context, the development of sustainable treatment technologies using renewable sources has been identified as one of the alternatives for mitigating energy requirements and reducing pollution of water resources.

In recent years, many research efforts have focused on improving microbial fuel cells (MFCs) due to their potential to generate energy in an eco-friendly way (GUL *et al*., 2021). MFCs are bioreactors capable of directly converting the chemical energy contained in the bonds of organic and inorganic compounds into electricity (LOGAN; REGAN, 2006). One of the most promising applications of MFCs is in wastewater treatment, using pollutants as substrates for the metabolism of electroactive microorganisms, thus coupling these bioremediation systems with bioenergy production (KARDI *et al*., 2017; RATHOUR *et al*., 2019). Among these effluents, dye-contaminated wastewaters have shown a high potential for remediation by MFCs.

The textile industry is known as a major water polluter, discharging huge volumes of hazardous effluents into the environment every year (N LOTHA et al., 2024). In fact, approximately 20% of global water pollution is due to the activities of the textile sector, ranking second among the most water-polluting industries, only behind the petrochemicals (PERIYASAMY, 2024; UNEP, 2018). In the different textile manufacturing processes, around 150 L of water are used for each kg of fabric, resulting in approximately 200 billion liters of dye-contaminated wastewaters every year worldwide (ISMAIL; SAKAI, 2022; TKACZYK; MITROWSKA; POSYNIAK, 2020). In low- and middle-income countries, it is estimated that 80% of textile effluents are still discharged without proper treatment or used directly for irrigation, contaminating soil, groundwater and surface water (LIN et al., 2023).

Dyes are the main pollutants contained in textile wastewaters, one of the most complex industrial effluents (DEKA et al., 2022). The result of the metabolization of dyes via conventional biological treatment is the formation of by-products, such as aromatic amines, benzidines and other intermediates, known for their harmful characteristics even in low concentrations, such as reproductive disorders, alterations in the immune system and central nervous system, kidney, lung, liver and brain damages, and their carcinogenic and mutagenic effects (DES LIGNERIS; DUMÉE; KONG, 2018; SUKRITI *et al*., 2017; TARA *et al*., 2020). In addition to dyes, textile effluents generally have a high biochemical oxygen demand (BOD) and chemical oxygen demand (COD), affecting light penetration and gas solubility in water bodies, thus interfering with photosynthetic activity (DUTTA et al., 2024). High water solubility, stability and complex chemical structure are obstacles to the degradation of dyes (SINGH; DAHIYA; MISHRA, 2021). The physicochemical methods commonly used to treat textile effluents (coagulation/flocculation, electrocoagulation, Fenton, ozonation, UV-H_2O_2) have several limitations, including their low efficiency and versatility, high cost, waste management and secondary pollutants produced (SRIVASTAVA et al., 2022; TACAS et al., 2021). The high cost is especially related to the energy-intensive requirements (YADAV et al., 2022).

In this sense, MFCs have numerous advantages over conventional wastewater treatment technologies, offering a combination of biological and electrochemical processes, better treatment performances and minimal sludge generation, as well as being self-sustaining systems (RATHOUR et al., 2019). However, some limitations still challenge their scale-up (UDUMA et al., 2023). With regard to configuration, single-chamber air-cathode devices are considered the most effective for use in the treatment of textile effluents. In this arrangement, the cathode does not require active aeration during dye degradation, as oxygen from the air can passively diffuse through the cathode and result in the oxygen reduction reaction (GUL et al., 2021).

In addition to the more economical design, exposing the cathode to air significantly improves power generation, since there is less internal resistance due to the higher conductivity than in an aqueous medium (FATIMA et al., 2021; KARUPPIAH et al., 2018). An interesting alternative to overcome the shortcomings related to low energy production is to use a membrane electrode assembly (MEA). This structure

reduces the space between the electrodes and lowers the internal resistance, thus leading to an increase in energy production potential (HUBENOVA et al., 2022).

Furthermore, electroactive bacteria play a key role in the remediation of dyes, due to their inherent capacity for redox degradation of organic matter (TACAS et al., 2021). Several microorganisms have been tested in MFCs for the bioremediation of textile dyes, including *Pseudomonas aeruginosa*, *Escherichia coli*, *Geobacter sp*., *Shewanella putrefaciens*, *Aeromonas hydrophila*, *Bacillus sp*., among others (ARKATKAR; MUNGRAY; SHARMA, 2021; RAMYA; SENTHIL KUMAR, 2022; RITTER et al., 2024 (submitted to ACS Omega)). However, strict operating conditions and selective substrates are required for pure bacterial cultures, while mixed consortia are more suitable for the treatment of complex substrates, such as colored textile effluents (CAO et al., 2019). MFCs based on mixed microbial cultures have attracted increasing attention due to their tendency to produce higher current densities, as well as their greater robustness, adaptability, stability and resistance to stress compared to those inoculated with pure cultures (SOLANKI; SUBRAMANIAN; BASU, 2013; ZHOU et al., 2022).

From this perspective, this work aimed to treat dye-containing synthetic solutions using a single-chamber MEA-MFC populated with a mixed culture of anaerobic sludge. The degradation of two different dyes, Indigo Carmine (IC) and Safranine-T (ST), was tested. The two selected dyes represent the model compounds of different types of dyes present in textile effluents, anionic (IC) and cationic (ST) dyes (CHOWDHURY et al., 2020; GUPTA et al., 2006). The effects of the type and different initial concentrations of dyes were investigated with regard to color removal efficiency, COD removal and bioenergy production. In addition, bioassays were carried out to determine the phytotoxicity of dye-contaminated synthetic solutions, before and after bioelectrochemical treatment, using *Lactuca sativa* seeds as test-organisms. 16S rRNA sequencing of the bacterial consortium used as inoculum and of the biofilm formed in the anodic compartment of the MFC at the end of the entire experiment was also performed.

The present study reports for the first time, to the best of our knowledge, the treatment performance of an MFC system in the bioremediation of Indigo Carmine and Safranine-T dyes. The application of innovative MFC technology represents a lasting green alternative for improving wastewater treatment, contributing to the energy supply

from a clean, renewable and sustainable source and helping to preserve natural resources, meeting the United Nations Sustainable Development Goals (UN, 2015) with regard to Clean Water and Sanitation, Affordable and Clean Energy and Responsible Consumption and Production (Goals 6, 7 and 12, respectively), thus forming part of the water-energy nexus.

6.2 MATERIALS AND METHODS

6.2.1 Textile Dyes

The textile dyes Indigo Carmine (IC) (CI. 73015) and Safranine-T (ST) (CI. 50240) (Neon Comercial, Brazil) were used in this study. ST, also known as Basic Red 2, was used as a model for the cationic dyes. The IC or Acid Blue 74, represented the anionic dyes. The molecular structure and main properties of these dyes are shown in Table 6.1. Stock solutions (1.0 g L^{-1}) were prepared by completely diluting and homogenizing the required amount of each dye in distilled water.

Table 6.1 – Main characteristics of the textile dyes Indigo Carmine (IC) and Safranine-T (ST).

Dye	Molecular structure	Chemical formula	Molecular weight (g mol^{-1})	λ_{max} (nm)
Indigo Carmine	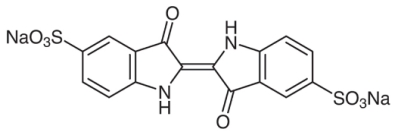	$C_{16}H_8N_2Na_2O_8S_2$	466.4	610
Safranine-T	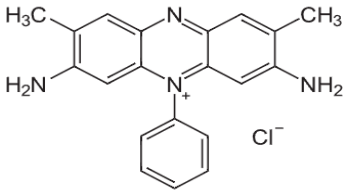	$C_{20}H_{19}ClN_4$	350.8	520

Source: created by the author

6.2.2 MFC Configuration

The single-chamber air-cathode microbial fuel cell (MFC) was made of acrylic, with a prismatic shape, a square base (13.0 cm x 13.0 cm) and a total volume of 1L. The membrane electrode assembly (MEA) consisted of a carbon paper anode (gas diffusion electrode - GDE) and a carbon cloth cathode (gas diffusion layer - GDL)

covered with a microporous layer of carbon nanoparticles and PTFE polymer (Teflon®), interposed with a Nafion™ 212 proton separator membrane (Novocell, Americana-Brazil). A catalyst load of 0.4 mg Pt cm^{-2} was applied to the cathode (nominal area 141.6 cm^2). Stainless steel plates served as current collectors and the electrical connections were made using copper wires.

A digital multimeter equipped with a datalogger was used to measure the voltage and record the information at 1-minute time intervals. The MFC was placed on a magnetic stirrer to ensure complete homogenization inside the acrylic chamber and the temperature was controlled (37 ºC ± 2 ºC). An external resistor of 1000 Ω was used. The MFC setup is shown in Figure 6.1.

Figure 6.1 – (a) MFC pilot set for dye-containing solution treatment and (b) detail view of the single-chamber MEA-MFC.

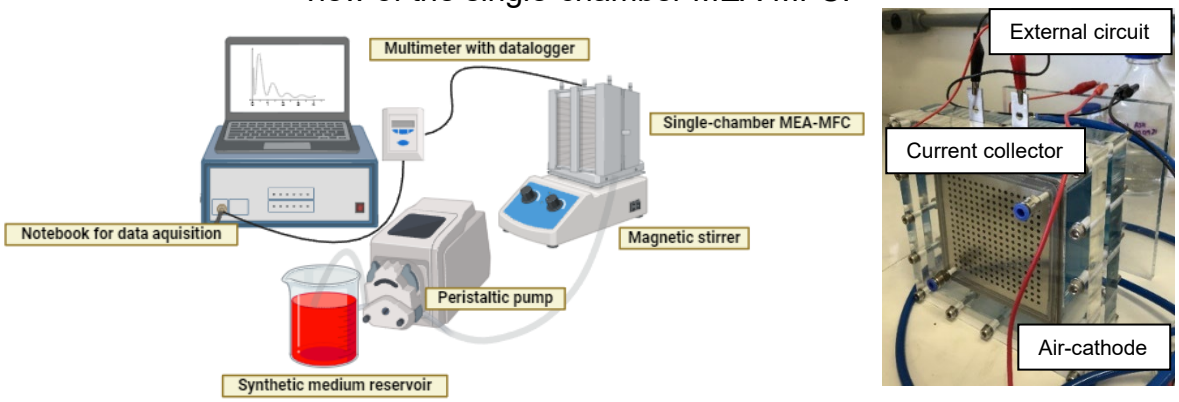

(a) (b)

Source: created by the author using Biorender®

6.2.3 Inoculation, Acclimatization and Operating Conditions

Anaerobic sludge collected from a municipal wastewater treatment plant (CASAN, Florianópolis/Brazil) was used as inoculum source. The MFC was inoculated with a mixture of anaerobic sludge and synthetic medium in a 1:1 volume ratio. Since single-chamber MFCs can easily acidify due to microbial action, it is common to use buffer solutions to control this condition (SINGH et al., 2019). Thus, the synthetic medium consisted of phosphate buffer solution (PBS) (pH 7.5), nutrients and carbon sources with the following composition: disodium phosphate (Na_2HPO_4, 4.58 g L^{-1}), monosodium phosphate (NaH_2PO_4, 2.45 g L^{-1}), ammonium chloride (NH_4Cl, 0.31 g L^{-1}), potassium chloride (KCl, 0.13 g L^{-1}), and solid sodium acetate (CH_3COONa, 0.5 g

L^{-1}). A mineral solution (12.5 mL L^{-1}) and vitamin solution (12.5 mL L^{-1}) prepared according to the methodology proposed by Lovley et al. (LOVLEY; PHILLIPS, 1988) were also added to the synthetic medium in the anode compartment.

During acclimatization, half the volume (500 mL) of the MFC was replenished with fresh medium/sludge mixture every 24 hours using a peristaltic pump. At the end of the 22-day period required for biofilm formation and voltage generation, the air-cathode MFC was operated in fed-batch mode, receiving increasing concentrations (50, 100, 150 and 500 mg L^{-1}) of the dyes IC and then ST, introduced into the synthetic medium, while the anaerobic sludge was no longer added. The hydraulic retention time (HRT) was 24 hours, i.e. every 24 hours the MFC was completely emptied, and the synthetic medium was added, testing a higher dye concentration.

6.2.4 Analytical Procedures and Measurements

The performance of the MFC was evaluated in terms of the decrease in dye concentration, COD removal and bioelectricity generation. The decolorization of the samples, collected from the anode compartment, was determined by colorimetry in a UV-Vis spectrophotometer (HACH DR/3900) at λ 610 and 520 nm for the experiments with IC and ST, respectively. The samples were previously centrifuged at 4500 rpm for 5 min to remove the suspended biomass from the liquid portion.

COD removal was determined by the closed reflux method using the HACH Kit (APHA, 2012). The COD removal efficiency, as well as the decolorization of the dyes, were calculated using Equation 6.1. The measurements were replicated and the results expressed as the average of the values obtained.

$$E = \frac{(C_0 - C_f)}{C_0}.100 \quad (6.1)$$

where E is the removal efficiency (%), C_0 and Cf are the initial and final concentrations (mg L^{-1}), respectively.

The current (I, mA) (Equation 6.2) was calculated according to Ohm's Law, where V corresponds to the voltage (mV) and R_{ext} is the external electrical resistance (Ω). Power (P, mW) was quantified using Equation 6.3.

$$I = \frac{V}{R_{ext}} \quad (6.2)$$

$$P = I.V \quad (6.3)$$

The conversion of the substrate into electrical energy was calculated using the Coulombic efficiency (CE, %) (Equation 6.4).

$$CE = \frac{M.I}{F.b.V.\Delta COD} \quad (6.4)$$

where I is the average current (mA), M is the molar weight of oxygen (32 g mol^{-1}), F is the Faraday constant (96.485 C mol^{-1}), b is the number of moles of electrons produced per mole of substrate (4 mol e^- mol^{-1} O_2), V is the volumetric flow rate (L s^{-1}) and ΔCOD is the removed COD (g L^{-1}) (LOGAN et al., 2006).

The polarization curves were used to determine the maximum current density and power density, which were normalized in relation to the cathode area and anode volume (LOGAN et al., 2006). These data were obtained by first running the MFC in open circuit for about 30 minutes and then varying the external resistances between 1000 and 10 Ω every 10 minutes and monitoring the current generation after stabilization. Polarization curves were recorded for the MFC after its acclimatization and for the strategies using the IC and ST dyes at concentrations of 100 and 500 mg L^{-1}.

6.2.5 Phytotoxicity Analysis

Using higher plants to determine phytotoxicity is one of the most economical, simple and sensitive methods, and *Lactuca sativa* (lettuce) is considered a model species for use in bioassays due to its high sensitivity to toxic compounds and rapid germination (LYU et al., 2018). The phytotoxicity tests were conducted according to the methodology proposed by Sobrero et al. (SOBRERO; RONCO, 2004). The tests consisted of exposing *L. sativa* seeds to the anodic solution containing the textile dyes (before and after treatment) at a controlled temperature (22 ºC ± 1 ºC) and sheltered from light for 120 hours. Petri dishes covered with filter paper received 10 seeds (each) and were soaked with 2 mL of effluent in different dilutions (0, 25, 50 and 75%). The tests were carried out in duplicate. Mineral water was used as positive control. Phytotoxicity was assessed by seed germination and root elongation, which have been

widely used to determine the toxicity of complex effluents (LYU et al., 2018). The seed germination (SG, %) and relative root growth (RRG, %) (LUO et al., 2018) were calculated according to Equations 6.5 and 6.6, respectively.

$$SG = \frac{number\ of\ germinated\ seeds}{number\ of\ total\ seeds}.100 \quad (6.5)$$

$$RRG = \frac{total\ root\ length\ of\ the\ germinated\ seeds\ (sample)}{total\ root\ length\ of\ the\ germinated\ seeds\ (control)}.100 \quad (6.6)$$

6.2.6 Microbial Community Analysis

Diversity and structure analysis of the microbial community developed on the anode was carried out using 16S rRNA NextSeq 1000 Illumina sequencing (Illumina INC., USA) by the company Neoprospecta (Florianópolis, Brazil). Once all the experiments had been completed, and after the disruption of the MFC, the anodic biofilm sample was collected. An initial sample of anaerobic sludge, used as inoculum, was also tested. Both samples were stored at −20 °C until analyzed.

The V3-V4 variable regions were amplified using the universal primers 341F 5′ CCTACGGGRSGCAGCAG-3′ and 806R 5′-GGACTACHVGGGTWTCTAAT-3′. Sequencing data analysis was performed using QIIME 2, version 2 (2021.11) (BOLYEN et al., 2019), on VirtualBox (version 7.1). DADA2 (CALLAHAN et al., 2016) was used for quality control and sequences were classified according to taxonomy using the SILVA database (QUAST et al., 2012), with features related to mitochondria and chloroplasts removed. The percentage of readings in each sample corresponding to the 15 phyla and the 30 most abundant genera was plotted and compared between the samples. Alpha diversity analysis using the Shannon index (QIIME 2) was performed to assess the complexity of the microbial community of the two samples, which reflects the diversity of the bacterial community and the microbial richness (OTU) corresponding to the number of unique species in a sample (SILVEIRA et al., 2022).

6.3 RESULTS AND DISCUSSION

6.3.1 MFC Acclimatization

The start-up phase of the MFC is essential for the development of an electrically active microbial biofilm. The biofilm plays a central role in energy production, since the increased density of bacterial cells enables greater electron transfer (RAMÍREZ-VARGAS et al., 2018). In this study, using a 1000 Ω resistor, a stable voltage generation of around 350 mV in the MFC was achieved after 22 days (Fig. 6.2a). Voltage generation increased gradually from the first day after MFC inoculation, in which it reached 190 mV to the maximum output voltage of 364 mV. This result is within the range of values reported by other authors using similar configurations. Thung et al. (THUNG et al., 2015), using a single-chamber membrane-less MFC (0.11L volume) inoculated with anaerobic sludge, reported a voltage of approximately 175 mV during the 30-day acclimatization phase. Sun et al. (SUN et al., 2009), also using a single-chamber air-cathode MFC with the same volume used in this study (1L), achieved a voltage of around 550 mV in the start-up phase, but with a 500 Ω resistor. Applying lower external resistors usually leads to higher output voltages, but in this study, a 1000 Ω resistance was selected because it provides greater stability of the biofilm and microbial metabolism (ZHANG et al., 2011). A similar output voltage (around 325 mV) was obtained using a double chamber MFC (0.4 L anodic volume) also inoculated with anaerobic sludge by Sun et al. (SUN et al., 2016).

On the 22nd day, considering the acclimatized MFC, polarization tests were carried out to assess its bioelectrical performance. From the top of the parabola (Fig. 6.2b), a maximum current density of 303.03 mA m^{-2} and a maximum power density of 71.52 mW m^{-2} were determined (R_{ext} = 55Ω). Similar values were reported by Min et al. (MIN; ROMÁN; ANGELIDAKI, 2008) and Wang et al. (WANG et al., 2019) when acetate was used as an electron donor during the microbial acclimatization phase.

Figure 6.2 – (a) Voltage generation and (b) polarization curves during the MFC acclimatization phase.

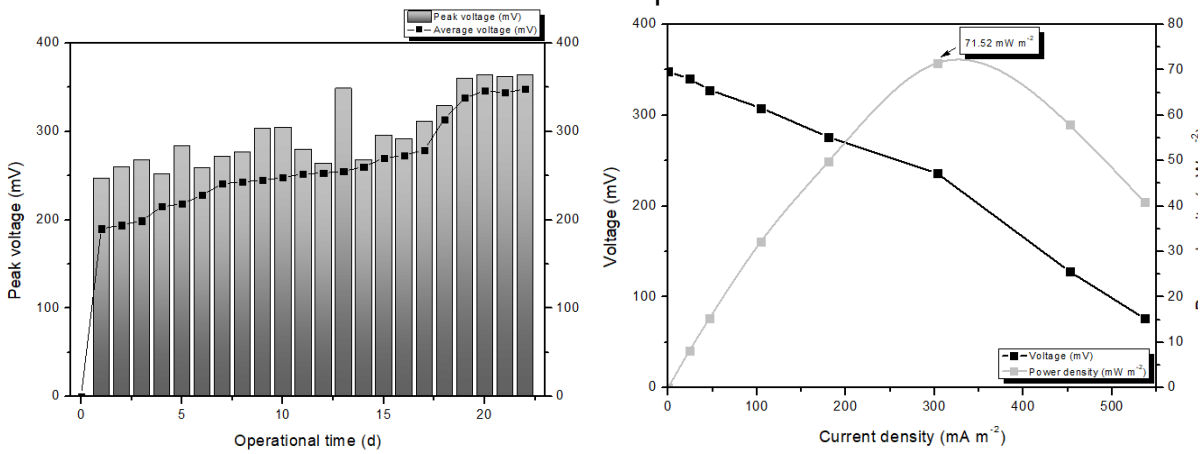

(a) (b)

Source: created by the author

6.3.2 Decolorization and COD Removal of Dye-containing Solutions

After the start-up period required for biofilm formation on the MFC, the acclimatized bacteria were subjected to increasing concentrations of dyes added to the synthetic medium, which contained acetate (0.5 g L^{-1}) as a co-substrate. The performance of the single-chamber air-cathode MFC and the effect of different concentrations (50, 100, 150 and 500 mg L^{-1}) of Indigo Carmine and Safranine-T dyes were tested with regard to decolorization efficiency and COD removal, as shown in Table 6.2.

Table 6.2 – Quantification and efficiency removal of COD and decolorization of textile Indigo Carmine and Safranine-T dyes (HRT = 24 hours).

Dye	C_0 dye (mg L^{-1})	Removed dye (mg L^{-1})	Dye removal (%)	Decolorization rate (mg L^{-1} h^{-1})	COD_0 (mg L^{-1})	Removed COD (mg L^{-1})	COD removal (%)
Indigo Carmine	50	18.17 ± 0.06	36.34 ± 0.13	0.76 ± 0.00	515.50	189.81 ± 6.19	36.82 ± 1.20
	100	34.20 ± 0.17	34.20 ± 0.17	1.43 ± 0.01	549.50	185.07 ± 4.73	33.68 ± 0.86
	150	41.43 ± 0.75	27.62 ± 0.50	1.73 ± 0.03	577.00	150.14 ± 8.89	26.02 ± 1.54
	500	119.00 ± 12.5	23.80 ± 2.50	4.96 ± 0.52	581.00	126.48 ± 0.70	21.77 ± 0.12
Safranine-T	50	32.38 ± 0.12	64.75 ± 0.24	1.35 ± 0.00	531.50	176.09 ± 3.72	33.13 ± 0.70
	100	75.27 ± 0.04	75.27 ± 0.04	3.14 ± 0.00	556.50	176.47 ± 4.01	31.71 ± 0.72
	150	120.39 ± 0.08	80.26 ± 0.05	5.02 ± 0.00	577.50	128.38 ± 6.64	22.23 ± 1.15
	500	469.20 ± 2.75	93.84 ± 0.55	19.55 ± 0.11	581.50	114.79 ± 3.78	19.74 ± 0.65

C_0 dye: initial dye concentration (mg L^{-1}). Source: created by the author

For ST, it was observed that both the amount of dye removed (in mg L^{-1}) and the removal rate increased with dye concentration, reaching the best removal performance of 93.84% (469.20 mg L^{-1}) by applying the highest dye initial concentration. In contrast, the IC removal (%) decreased with the increase of the dye concentration, despite showing an increasing trend in the decolorization rate, although

much less than in the ST case. Decolorization rates ranged from 0.76 to 4.96 mg L^{-1} h^{-1} for IC and from 1.35 to 19.55 mg L^{-1} h^{-1} for ST. It is worth highlighting the very high removal rate of ST with 500 mg L^{-1} initial concentration. Similar behaviors has been reported by other authors. Tan et al. (TAN et al., 2021) obtained increasing removal rates from 0.77 to 1.49 mg L^{-1} h^{-1} for Methyl Orange and from 0.78 to 1.97 mg L^{-1} h^{-1} for Reactive Black 5, by varying the initial concentration of the dyes from 50 to 75 mg L^{-1}. Removal rates of 2.36 to 9.49 mg L^{-1} h^{-1} were obtained by Dai et al. (DAI et al., 2020) for concentrations of 100 and 500 mg L^{-1} of Congo Red, respectively.

The concentration of dyes is a crucial factor in the decolorization process, since high concentrations can be toxic to microorganisms (SINGH, 2015). According to Solanki et al. (SOLANKI; SUBRAMANIAN; BASU, 2013), the behavior demonstrated by the IC dye is the most common; in general, the decolorization efficiency decreases with increasing dye concentration. This is due to co-substrate limitations causing an electron deficiency at the anode, so the dye molecules cannot be effectively reduced as the dye concentration increases (TAN et al., 2021). However, in addition to concentration, the type of dye has a major influence on MFC performance, and chemical structures can significantly affect the ability of bacteria to decolorize dyes. Dyes with a simpler structure and low molecular weight, such as ST, commonly show higher decolorization rates than dyes with high molecular weight and electron-withdrawing groups. Furthermore, the presence of sulphonated groups makes dyes such as IC recalcitrant, due to their difficulty in crossing the bacterial cell membrane (UDUMA et al., 2023). Thus, the higher decolorization efficiency of the ST dye could be explained by both its lower molecular weight and structural simplicity, which require a lower number of electrons for its anaerobic decolorization compared to IC.

On the other hand, biological decolorization of dyes can take place by (*i*) biodegradation, with their metabolization through the action of enzymes; (*ii*) bioaccumulation, with active uptakes by growing cells that accumulate the dyes in their cytoplasm; or (*iii*) biosorption, in which the dyes are adsorbed onto bacterial cell walls (SINGH, 2015; TACAS et al., 2021). In the latter, the electrical charges on the surface of the bacterial biomass and the molecular structure of the dyes play a key role (SRINIVASAN; VIRARAGHAVAN, 2010). In microbial consortia, such as the anaerobic sludge used in this study, there is usually a predominance of gram-negative bacteria,

with a high ability to degrade a wide range of complex compounds (SRINIVASAN; VIRARAGHAVAN, 2010). In this sense, although the removal of the negatively charged particles of the anionic dye IC is not favored by this mechanism, the decolorization of the Safranine-T dye via biosorption cannot be ruled out, since the negatively charged surface of the bacterial consortium is capable of fixing the dye molecules due to its cationic (positively charged) nature. According to Tacas et al. (TACAS et al., 2021), decolorization via a metabolism-dependent mechanism can be reduced and color removal can occur mainly by biosorption when the dyes used or their high concentrations are toxic to the bacteria. However, biosorption decolorization prevents the electron transfer mechanism, hindering the generation of bioenergy in the MFC (TACAS et al., 2021). In this regard, in the following Section 6.6.3, it will be shown that bioelectricity generation performance was strongly affected in the case of ST (500 mg L^{-1}), presenting the lowest power density among the conditions evaluated, possibly due to decolorization through the biosorption mechanism. Other authors have also attributed the removal of dyes in MFC systems to bioadsorption (SENTHILKUMAR et al., 2020).

In order to better elucidate the dye removal mechanisms, the UV-Visible absorption spectra of the dye-containing solutions were recorded (Fig. 6.3).

Figure 6.3 – UV-Vis absorption spectra of (a) Indigo Carmine (IC) and (b) Safranine-T (ST) at different initial dye concentrations before and after treatment in the MFC.

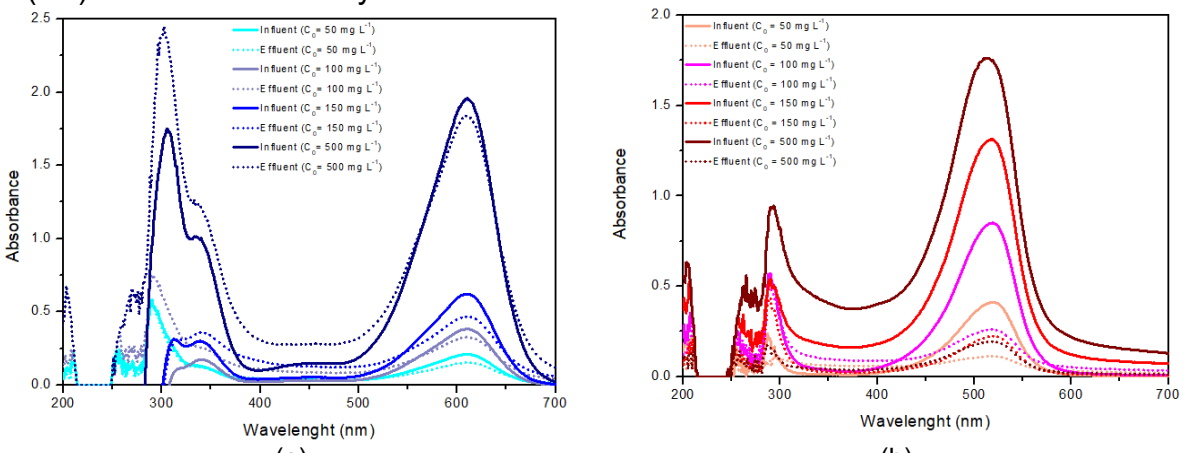

(a) (b)

Source: created by the author

From the input influent to the output effluent, at the different concentrations tested, the UV-Vis absorption spectrum data shows a reduction in absorbance in the visible region, at λ_{max} 610 and 520 nm, for the IC and ST dyes, respectively, which is

consistent with the decolorization efficiency results previously presented. However, the absorbance in the UV region, 200-300 nm, showed an increase at the end of the 24 hours of operation for the IC dye, which is possibly related to the formation of intermediates from its metabolization (SUN et al., 2009). Several authors have indicated that the degradation pathway of the IC dye results in the formation of different intermediates, such as 2-amino-5(sodium benzenesulfonate)-benzoic acid, anthranilic acid, benzoic acid and aniline (TERRES et al., 2014); isatin sulfonic acid and anthranilic acid (RAMYA; ANUSHA; KALAVATHY, 2008); and isatin, isatin sulfonic acid and indoline sulfonic acid (LI et al., 2015); whose maximum absorbance wavelengths occur around 200 and 300 nm. Thus, the detection of these intense absorption bands in the spectra of the outgoing effluent samples (Fig. 6.3a) suggests that a longer treatment time would be required to completely degrade these compounds. From Figure 6.3b, the decrease in intensity of the bands located between 200 and 280 nm suggests the adsorption of ST on the bacterial biofilm and/or the breaking of some benzene rings consisting of the ST chromophore groups (SYDORCHUK et al., 2023).

COD removal was higher for the IC dye than for ST one at every concentration tested (Table 6.2). The maximum COD removal of approximately 37% (189.81 mg L^{-1}) was obtained for an IC concentration of 50 mg L^{-1} in 24 hours. In addition, the removal efficiency and the amounts of COD removed decreased as the concentration of both dyes increased. It was noticed that the influent COD was higher as the concentration of IC and ST dyes increased, and this was due to the presence of dyes contributing a fraction of the COD. According to Sun et al. (SUN et al., 2009), the reduction in COD removal efficiency with higher dye concentrations occurred because in addition to the higher initial COD, as the dye molecules were degraded, there was also an increase in the amount of intermediate compounds in the anodic medium, further increasing the COD content. The low COD removal values mean low mineralization of the organic matter initially present in the samples, thus confirming the deductions from UV-Vis spectra.

6.3.3 Bioenergy Generation

MFC technology has been increasingly highlighted for its ability to produce bioenergy by converting the polluting compounds in wastewater into electricity. Table 6.3 shows the results of the MFC's performance in producing bioelectricity considering that the voltage generation was conducted using a 1000 Ω resistor and the data recorded every one minute on a datalogger.

Before adding the dyes, the maximum output voltage reached by the MFC was 364 mV. In Table 6.3, it can be seen that from the introduction of 50 mg L^{-1} of the IC dye, there was a reduction of approximately 32% in the output voltage to 248 mV. However, despite not restoring the initial level before the addition of the dyes, as the IC concentration increased, there was also an increase in the output voltage, reaching 300 mV at 500 mg L^{-1}. A similar behavior was noticed for concentrations of 50 to 150 mg L^{-1} of ST cationic dye, with output voltages increasing between 264 and 304 mV, with the exception of the highest load applied (500 mg L^{-1}) which reduced the voltage to 165 mV. These results differ from those reported by other authors (KHAN et al., 2021; THUNG et al., 2015), who indicated a downward trend in voltage generation with increasing dye concentrations. They attribute the deterioration in voltage generation to the insufficiency of electrons to act simultaneously in the degradation of high dye loads and electricity generation. According to Sun et al. (SUN et al., 2011), dyes can act as electron acceptors competing with the anode, and as a result, more electrons are used for decolorization instead of generating bioelectricity. However, when using an air-exposed cathode MFC, as in this study, oxygen will inevitably play this role, since it is a more thermodynamically favorable electron acceptor than any dye (CHEN et al., 2010).

The findings of this study agree with the results of Tan et al. (TAN et al., 2021), who also revealed an upward trend in the output voltage when using higher concentrations of the Reactive Blue 5 dye. They attributed this increase to the intermediate compounds generated by the degradation of the dyes and to the dye itself acting as a redox mediator and improving the performance of bioelectricity generation. Both IC and ST used in the present work have proven abilities as redox mediators. For the IC dye, its ability to enhance ionic conductivity and specific capacitance has been demonstrated with its application in polymer gel electrolytes for supercapacitors (MA et al., 2015), while Sund et al. (SUND et al., 2007) reported that the Safranine-T dye

(28 mg L^{-1}) was used precisely as an artificial redox mediator to increase electron transfer in an MFC inoculated with *Clostridium cellulolyticum* for cellulose digestion.

The decrease in the output voltage shown for ST at 500 mg L^{-1}, in turn, may be related to the toxicity of the intermediate compounds formed from its degradation at the highest concentration, inhibiting microbial action, which will be discussed in Section 3.4 below, or, as already mentioned, due to the removal mechanism, via biosorption, preventing the transfer of electrons and, consequently, the energy production (TACAS et al., 2021; TAN et al., 2021).

Coulombic efficiency (CE) was calculated based on the output voltage and COD removal at each fed batch cycle and is related to the acceptance of electrons accelerating the electrochemical reaction in the MFC. According to Logan et al. (LOGAN et al., 2006), CE corresponds to the Coulombs effectively transferred from the substrate to the anode in relation to the maximum transfer if the entire substrate was transformed into energy. In this study, CE ranging from 9.33 to 17.05% were obtained, which means that the system had the capacity to transform between 9.33 and 17.05% of the substrate used directly into electricity. Although the Coulombic efficiencies resulting from this study cannot be considered high, they are higher than those reported by other authors using similar configurations and operating conditions. Thung et al. (THUNG et al., 2015) obtained CE of 6.68 and 6.49% when applying concentrations of 50 and 75 mg L^{-1} of the anionic dye Acid Orange 7, respectively. The results published by Khan et al. (KHAN et al., 2021), also reported that increasing the concentration of another anionic dye, Acid Blue 29, from 100 to 200 mg L^{-1}, led to a decrease in CE from 3.18 to 3.00%.

However, the findings of this study agree with those reported by Mu et al. (MU et al., 2009), who supported that the increase in CE may be attributable to greater electron uptake with higher dye concentrations. With regard to the relatively low CE obtained, it indicated that most of the electrons generated from the degradation of the co-substrate by the bacteria were not directed towards electricity generation. This may be related to the geometry of the MFC, the low surface area of the electrode and also to the synergism of the mixed bacterial culture used, since not all the bacteria present in the reactor are electroactive and capable of contributing to increased bioelectricity generation (TAN et al., 2021).

Table 6.3 – Quantification of electrochemical parameters during the decolorization of Indigo Carmine and Safranine-T dyes (HRT = 24 hours and R_{ext} = 1000 Ω).

Dye	C_0 dye (mg L^{-1})	Voltage (mV)	Current density (mA m^{-2})	Power density (mW m^{-2})	Volume power density (mW m^{-3})	CE (%)
Indigo Carmine	50	248	17.51	4.34	61.50	9.33
	100	296	20.90	6.19	87.62	11.42
	150	300	21.19	6.36	90.00	14.16
	500	300	21.19	6.36	90.00	17.05
Safranine-T	50	264	18.64	4.92	69.70	10.70
	100	282	19.92	5.62	79.52	11.41
	150	304	21.47	6.53	92.42	16.78
	500	165	11.65	1.92	27.23	10.33

Source: created by the author

The polarization curves (Fig. 6.4) performed at two different concentrations (100 and 500 mg L^{-1}) of the IC and ST dyes were also used to evaluate the performance of the single-chamber MEA-MFC, by varying the external resistances between 1000 and 10 Ω. The linear behavior of the polarization curves (Fig. 6.4a) obtained in this study indicated a similarity between the internal resistances and the external resistances applied, which is typically observed in microbial fuel cells (LOGAN et al., 2006). From Figure 6.4b, it can be seen that the power density increases as the external resistance decreases and, after reaching the maximum peak, at 55 Ω for all the conditions evaluated, it decreases continuously, also demonstrating a common behavior of MFCs (SENTHILKUMAR et al., 2020).

The bioelectricity generation performance was in agreement with the decolorization rate for the IC dye, for which maximum power densities of 31.25 and 34.54 mW m^{-2} were obtained at 100 and 500 mg L^{-1}, respectively. In contrast, for the ST dye, the maximum power density was 23.06 mW m^{-2} at 100 mg L^{-1}, and increasing the concentration to 500 mg L^{-1} reduced this value to 9.94 mW m^{-2}. Similar values were found by other authors using similar systems to treat different dyes, reporting maximum power densities of 7.07 to 39.98 mW m^{-2} (OON et al., 2017; TAN et al., 2021; THUNG et al., 2015).

According to Oon et al. (OON et al., 2017), the power density produced is closely related to the chemical structure of the dyes. The presence of sulfonic groups, which are strong electron-withdrawing groups, as well as the higher redox potential of Indigo Carmine favor its electrochemical reduction, allowing a greater transfer of electrons to the anode compared to ST (ÇEKIÇ et al., 2010; LOGAN, 2008). In the case of ST, the deterioration in power density with increasing dye concentration was

probably related to the mechanism of dye removal by biosorption, interfering with the electron transfer process and thus reducing electricity generation.

Figure 6.4 – (a) Polarization and (b) power density curves of the MFC at different concentrations of Indigo Carmine (IC) and Safranine-T (ST) textile dyes.

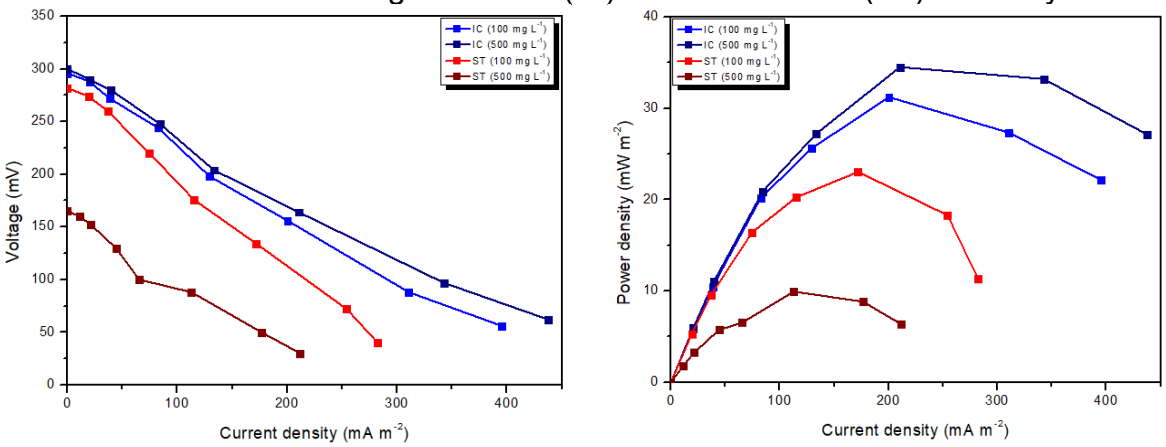

(a) (b)

Source: created by the author

6.3.4 Phytotoxicity Assessment

Synthetic solutions containing the IC and ST dyes at different concentrations (100 and 500 mg L^{-1}), before and after treatment in the MEA-MFC, were used to investigate the germination rate (Fig. 6.5) and root elongation (Fig. 6.6) of *Lactuca sativa* seeds under controlled laboratory conditions.

The seed germination bioassay is one of the simplest and most widely used methods for assessing phytotoxicity, since it is during germination that the first material exchange between the developing plant and the environment takes place (LYU et al., 2018). According to Luo et al. (LUO et al., 2018), SG ≥70% indicates that the compound tested has no toxic effects on seed germination. The results of the lethal effects (inhibition of germination) (Fig. 6.5) showed that the germination rate of the lettuce seeds in the control was 100% and, after the seeds were exposed to the untreated effluent samples, there was an inhibition of germination (SG ≤70%), except for the IC dye at 100 mg L^{-1} which showed an SG of 80%. The SG index showed lower values when 500 mg L^{-1} of IC and ST dyes were applied, indicating that higher concentrations had a greater phytotoxic effect on the development of the bioindicator (*L. sativa*). After treatment, the dye-containing samples showed an increase in the average germination percentage, which reached between 80-90%. Consequently, no

toxic effects were observed, since the seed germination index remained above 70%. However, the sample containing the ST dye at 500 mg L^{-1}, despite improving the germination rate, continued to exert an inhibitory effect on seed germination. The lower germination rate shown by the seeds when exposed to high concentrations of Safranine-T is probably related to the nature of the electrostatic interactions and the molecular structure of the cationic dye, to which more harmful effects are attributed due to easier and stronger interactions with cell membranes (negatively charged) compared to anionic ones (SAHA et al., 2021; YAGUB et al., 2014). Overall, these findings indicated that the treatment carried out in the MFC system was able to detoxify the colored effluents and, furthermore, that the intermediate compounds resulting from bacterial degradation were less toxic than the original dyes. The results obtained showed advantages compared to other treatment technologies often used for dye remediation, such as advanced oxidative processes, which, although efficient in removing color, frequently lead to an increase in the toxicity of the treated wastewater (SANTOS KLIENCHEN DALARI et al., 2022).

Figure 6.5 – Phytotoxic effect of synthetic solutions containing different concentrations of Indigo Carmine (IC) and Safranine-T (ST) dyes on *L. sativa* germination rate before and after treatment in MFC.

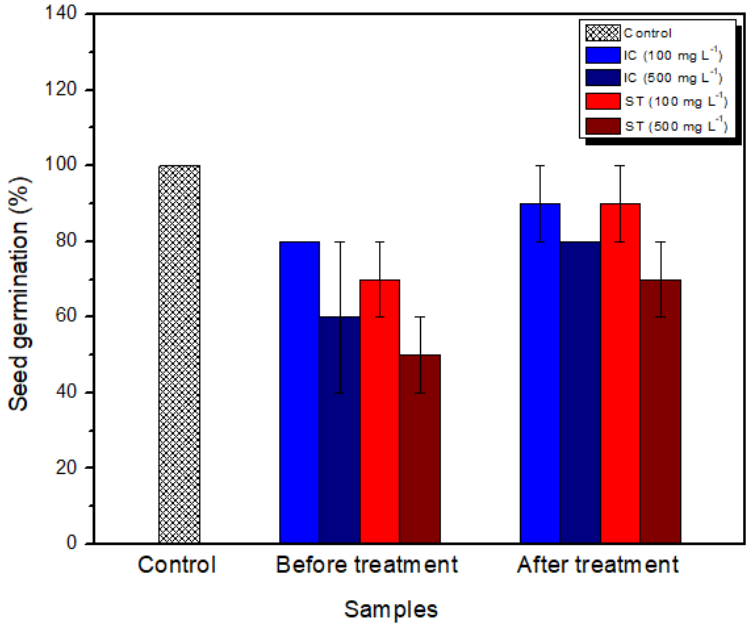

Source: created by the author

According to Priac et al. (PRIAC; BADOT; CRINI, 2017), although seed germination (lethal effect) is the most commonly used endpoint, root length (sublethal effect) has been shown to be a more sensitive parameter. In this sense, phytotoxicity

was assessed based on the relative root growth (RRG) index, which considers that RRG ≥50% does not cause inhibitory effects on root elongation (LUO et al., 2018).

Figure 6.6 depicts the relative root growth (in relation to the positive control, using mineral water) of the bioindicator *L. sativa* when exposed to effluent samples containing the IC and ST dyes in different dilutions, before (t=0 h) and after (t=24 h) treatment in MFC. Before treatment (Fig. 6.6a), the undiluted samples had RRG ≤50%, indicating the toxic effect of dye-containing effluents on the elongation of lettuce seed roots. The results showed that, in general, the anionic IC dye had better indices compared to the ST dye, and that the samples containing lower concentrations (100 mg L^{-1}) exerted less toxic effects than when higher concentrations were applied (500 mg L^{-1}). In addition, there was an increase in the RRG index as the samples were more diluted. After treatment (Fig. 6.6b), all the samples showed a slight increase in relative root growth and, consequently, a slight reduction in phytotoxicity. Considering the undiluted effluent samples, RRG ≥ 50% was obtained for the IC dye at 100 mg L^{-1}, suggesting that the toxicity of the intermediates during IC degradation was successfully reduced by the microorganisms in the MFC for the given conditions.

Additionally, the effect of dye toxicity on bioelectricity generation was also assessed. In this respect, the electrochemical parameters (Table 6.3 and Fig. 6.4) showed that the anionic IC dye performed better than the cationic ST dye, but unlike the phytotoxicity bioassays, the best results were obtained at the highest IC concentration. According to Tacas et al. (TACAS et al., 2021), when dyes are toxic to bacterial cells, there is a decrease in the number of viable cells, reducing the ability to generate higher power densities. Regarding this statement, the results of this study showed that, although the most sensitive phytotoxic sublethal index was not surpassed by all the samples, the high power densities achieved suggest that the intermediate compounds resulting from dye degradation did not exert a toxic effect capable of rendering the bacterial cells. However, it is worth commenting that for the ST dye at 500 mg L^{-1} a significant reduction in power density had been reported (Table 6.3). This decrease may be related to the phytotoxic effect of the high dye concentration, but also to the removal mechanism via biosorption, so the decrease in bioelectricity generation cannot be attributed undoubtedly or exclusively to one factor, and most likely both contribute to this scenario.

Figure 6.6 – Phytotoxic effect of synthetic solutions containing different concentrations of Indigo Carmine (IC) and Safranine-T (ST) dyes on *L. sativa* root elongation (a) before and (b) after treatment in MFC.

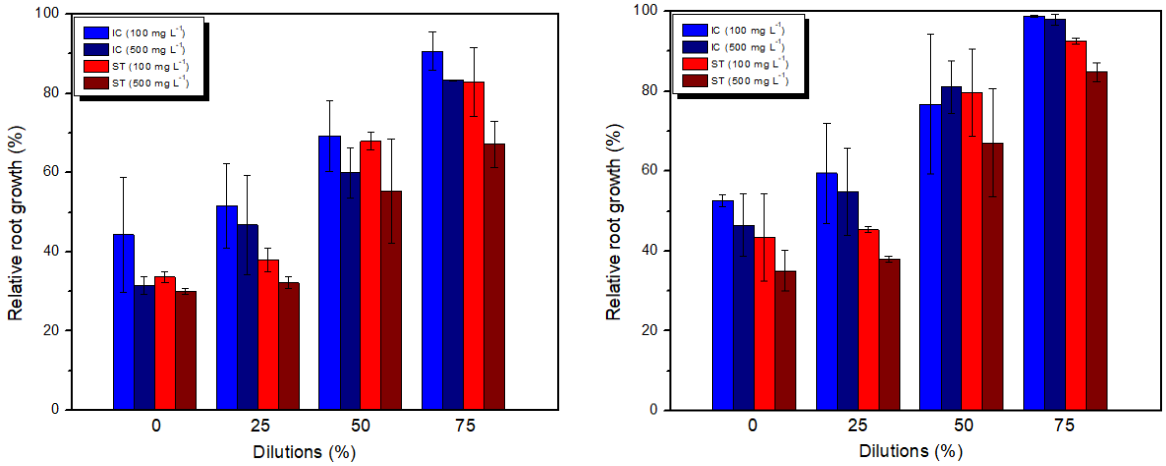

(a) (b)

Source: created by the author

6.3.5 Microbial Community Analysis

Analysis of the microbial community acclimatized in the MFC is a key point in unraveling the performance of the proposed treatment system, since bacteria are the biocatalysts responsible for both dye degradation and energy production. The microorganisms present in the anaerobic sludge used as inoculum and those actually forming the microbial biofilm after the entire experiment were analyzed by 16S rRNA gene sequencing and categorized at phylum and genus levels.

Alpha diversity indices indicated the presence of a highly diverse and rich microbial community in the samples evaluated in this study. The Shannon index showed that the microbial community in the inoculum (8.00) was more diverse than in the biofilm (5.55), and was also richer, since the number of OTUs in the inoculum (376) was higher than in the biofilm (70), which suggests microbial adaptive profiles depending on the environment in the MFC. This change in the alpha diversity of the anodic biofilm compared to the inoculum was noticed at both phylum and genus (Fig. 6.7) levels. *Proteobacteria* (36%), *Bacteroidota* (15%), *Chloroflexi* (13%), *Actinobacteriota* (10%) and *Firmicutes* (7%) were the dominant phyla (Fig. 6.7a) in the inoculum. After acclimatization, the *Proteobacteria* phylum became even richer (62%), while the other phyla mentioned above showed a reduction and together reached 23% relative abundance. Cao et al. (CAO et al., 2019) state that most electrogenic microorganisms belong to the *Proteobacteria* and *Firmicutes* phyla. The presence of

Proteobacteria, *Bacteroidota* and *Firmicutes* in the anodic compartment of different MFC systems has been also reported by other authors (LONG et al., 2019; NGUYEN; PHAM; PHAM, 2021). Several electrochemically active bacteria belonging to the most abundant phyla detected in this study have been reported enriching the anode compartment of MFCs applied to the treatment of synthetic wastewater (RATHOUR et al., 2019).

Figure 6.7b depicts in detail the diversity and structure of the microbial community in the inoculum and MFC biofilm at the genus level. As with the phylum, relative genus abundance was depleted in the anode biofilm, indicating that, after acclimatization, the richness of the microbial community was reduced while enriching the dominant microorganisms (WANG et al., 2019). These results are consistent with other studies using anaerobic sludge as inoculum in MFCs applied to the treatment of dye-containing effluents (DAI et al., 2020; KHAN et al., 2021). It is interesting to note that among the most prevalent genera in the inoculum were unidentified genera from the *Anaerolineaceae* (15%), *Saprospiraceae* (8%) and *Comamonadaceae* (5%) families. The genera *Saccharimonadales*, *Bdellovibrio* and *Candidatus Competibacter* had relative abundances of 6, 5 and 5%, respectively. Meanwhile, 22% of the total composition was not classified at genus level, which reflects the diversity and complexity of the microbial communities present in the inoculated sludge. The microbial genera acclimatized in the MFC were mainly composed of *Rhodopseudomonas* (46%) and unclassified genera from the *Comamonadaceae* (18%) and *Geobacteraceae* (12%) families. The genus *Rhodopseudomonas* was also predominant in the anodic biofilm of two MFC systems studied by Nguyen et al (NGUYEN; PHAM; PHAM, 2021). According to these authors, the presence of *Pseudomonas* contributes to the generation of bioelectricity in MFCs due to self-produced redox mediators for electron transport. Logan et al. (LOGAN, 2009) indicated that *Rhodopseudomonas palustris* strains are capable of producing the *p*-coumaroyl-HSl quorum signal, while *Pseudomonas aeruginosa* produces pyocyanin, which also functions as an electron shuttle, allowing the generation of electric current in MFCs. In addition, *Pseudomonas* are also recognized for their ability to degrade dyes and other aromatic compounds (KHAN et al., 2021). *Comamonas*, a genus belonging to the

family identified among the most abundant in the anode of the MFC, express important metabolic abilities, such as the degradation of polyaromatic and aliphatic compounds (LONG et al., 2019). In turn, gram-negative anaerobic bacteria, such as *Geobacter*, are able to improve bioelectricity generation performance in MFCs through direct extracellular electron transfer using nanowires or soluble redox mediators (DAI et al., 2020). Such observed results indicated that the acclimatization of the anaerobic sludge in the anodic compartment of the MEA-MFC and the presence of IC and ST dyes provided a supportive environment to enrich the dominant dye-degrading microorganisms while simultaneously producing electricity.

Figure 6.7 – Relative abundance of bacterial taxa observed in the inoculum and biofilm of the MFC at (a) phylum and (b) genus level.

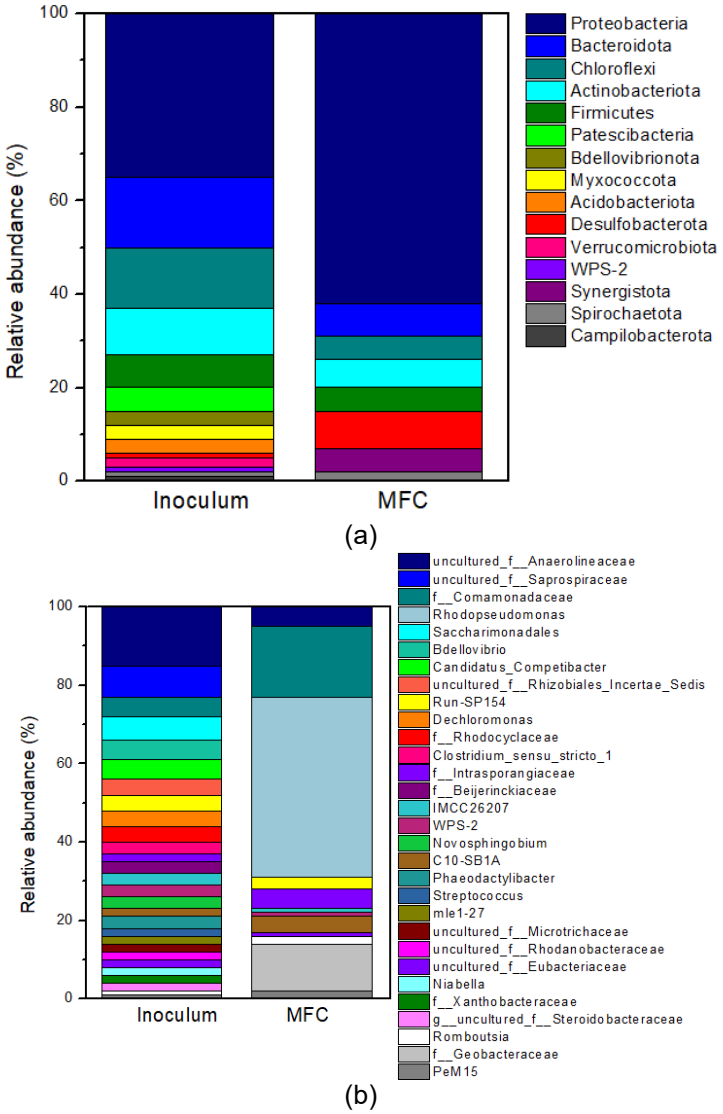

Source: created by the author

6.4 CONCLUSION

The results of this study demonstrated the excellent ability of single-chamber MEA-MFC to decolorize high concentrations of the cationic ST dye, exceeding 93% removal efficiency. In contrast, the best bioenergy production performance was achieved at the highest concentration of the anionic IC dye.

The dissimilarities observed between IC and ST in response to the treatment of dyes suggested that the MFC system's ability to decolorize and generate bioelectricity was strongly influenced by the different chemical structures of the dyes. The presence of sulphonic groups (strong electron withdrawing groups) and the higher redox potential of the anionic IC dye acted to favor its electrochemical oxidation and allowed a greater transfer of electrons to the anode, promoting the generation of bioelectricity in the MFC, while the affinity between the positively charged surface of the ST cationic dye and the negatively charged surface of the microbial biomass allowed its remarkable removal via biosorption, but at the same time prevented the electron transfer mechanism, thus reducing energy densities.

The phytotoxicity results showed that although ST is more toxic than IC, the treatment carried out on the MFC was able to reduce the lethal and sub-lethal effects under all the conditions tested. Furthermore, microbial community analysis contributed to this study, indicating that the anodic compartment of the MEA-MFC and the presence of the IC and ST dyes provided a favorable environment for the development of dominant exoelectrogenic and dye-degrading microorganisms, which significantly supported the decolorization performance and bioelectricity generation of the system.

The improvement of this innovative and eco-friendly technology represents an important milestone for the circular economy and sustainable development, ensuring an alternative electricity supply from clean and renewable sources and simultaneously contributing to the preservation of the environment by eliminating highly contaminating dyes.

7 CHAPTER 7: CONCLUDING REMARKS

In the initial stage of this research, different types of highly crystalline zeolites (NaP, LTA and SOD) were synthesized under optimal experimental conditions using hydrothermal or sol-gel methods, employing a novel co-recycling approach that combines a hazardous waste from the aluminum industry (salt slag) and an agro-industrial waste, rice husk ash (RHA), as precursor sources of aluminum and silicon, respectively.

NaP-type zeolite synthesis:

- Obtained from hydrolyzed aluminum salt slag and silicate solution from calcined RHA via hydrothermal process at 105 ºC for 20 hours.
- Produced a zeolite with 73.4% crystallinity and over 90% zeolitic content, featuring excellent adsorption characteristics, including a surface area of 21.11 $m^2\ g^{-1}$ and a CEC of 3.67 meq g^{-1}.

LTA and SOD zeolite synthesis:

- Achieved via the sol-gel process using aluminate and silicate solutions derived from wastes.
- SOD was obtained at 70 ºC with a reaction time of 6 hours and LTA was synthesized at the same temperature after 24 hours.
- The experimental conditions (T, t and $[Na^+]$) were crucial in the development of each specific zeolite phase; that is, increasing $[Na^+]$ promoted SOD formation, whereas LTA was obtained at higher temperatures and extended ageing times;
- The LTA zeolite synthesized from wastes exhibited a mineralogical profile comparable to that of commercial zeolite obtained from pure reagents and a high CEC of 3.40 meq g^{-1}.

This co-recycling process of industrial waste offers an alternative and sustainable management route, contributing to the conservation of natural resources, environmental protection, and the advancement of the circular economy through symbiosis between different industrial sectors.

Application of waste-based LTA zeolite as a dye adsorbent:

- A high removal efficiency of 98.12% was achieved for the cationic dye Safranine-T (ST) (50 mg L^{-1}) with an LTA dosage of 21.5 g L^{-1} and a stirring rate of 147 rpm in just 1 min of contact time.
- The synthesized LTA zeolite exhibited superior performance compared to a commercial zeolite, for which the ST removal efficiency did not exceed 82.9%.
- LTA zeolite did not remove the anionic dye Indigo Carmine (IC).

The influence of the dye charge on the adsorption process by the LTA zeolite, with a negative surface charge (at pH levels above 5.6) was demonstrated. The excellent adsorbent properties of the synthesized LTA, when applied to the treatment of wastewaters containing cationic dyes, offer a sustainable alternative to the use of commercial adsorbent produced from pure reagents, as it reduces resource consumption, improves water quality, and contributes to mitigating environmental pollution.

The second stage of this research provided important information on the degradation of the molecular structures of the different types of dyes through biological and bioelectrochemical processes.

Bioremediation using *Pseudomonas aeruginosa*:

- The anionic dye IC achieved a removal efficiency of over 96% primarily through biodegradation, in which the enzymatic activity breaks the C-S bonds of the sulfonated groups. Bioadsorption was limited due to the anionic character of the dye, which inhibited electrostatic interactions with the negatively charged bacterial biomass.
- The cationic dye ST reached a removal efficiency of 77.2% mainly via the bioadsorption mechanism, where the positively charged dye was attracted to the negative charges of the bacterial biomass, as evidenced by the reddish precipitate after centrifugation.
- Agitation enhanced bioremoval efficiency for both dye types.
- Dye structure is a crucial factor for effective bioremediation of wastewater contaminated by dyes.

The bacterium *P. aeruginosa* exhibited excellent properties for decolorizing sulfonated anionic dyes, requiring moderate conditions of time, pH, temperature, and

agitation rate to achieve effective removals, which is quite advantageous for its practical application. In this way, treatment strategies based on bioremediation using bacteria as renewable biological resources represent an attractive, promising and sustainable alternative to conventional methods, providing a low-cost and eco-friendly solution for the treatment of textile wastewater.

Performance evaluation of the bioelectrochemical technology using the single-chamber Microbial Fuel Cell (MFC) inoculated with a mixed culture of anaerobic sludge:

- Different molecular structures of dyes affected the treatment capacity in Microbial Fuel Cells (MFCs).
- Cationic dye ST achieved excellent decolorization through biosorption, with a remarkable removal rate of 93.84% in 24 hours. However, it exhibited lower electron transfer efficiency, resulting in reduced current and power densities.
- Anionic dye IC resulted in lower decolorization (36.34%), but higher COD removal and less phytotoxicity effects on the bioindicator (*Lactuca sativa* seeds). In addition, the higher redox potential and the presence of sulfonated groups improved electrochemical oxidation and increased current generation.
- *Rhodopseudomonas* (46%) from the *Proteobacteria* (62%) phylum was the predominant genus in the anodic compartment;
- Lower microbial diversity and richness were observed in the acclimatized biofilm compared to the inoculum, indicating that the MFC environment supported the growth of exoelectrogenic and dye-degrading microorganisms.

This research demonstrated that both adsorption technology and bioelectrochemical treatment using single-chamber MEA-MFC achieved the most successful decolorization of the cationic dye, while the best performance in removing the anionic dye was obtained through biological decolorization using a pure culture of *P. aeruginosa*. These findings highlight the importance of understanding the structural characteristics and surface charges of the dyes to select the most appropriate treatment technology. The proposed treatment solutions are based on renewable, sustainable and environmentally friendly principles, offering promising alternatives to

conventional technologies for treating dye-containing wastewater, thus contributing to the preservation of water resources and the environment.

Finally, it should be noted that all the objectives of this research were attainted and the hypotheses confirmed, with exception of IV, which was only partially verified.

7.1 RECOMMENDATIONS

With a view to improving the proposed treatment solutions and achieving the environmental benefits that the future application of these technologies will provide, the following are recommendations for further research:

- Considering the aluminum-rich composition of the synthesized waste-based zeolites, tailoring their surfaces with surfactants to enable the removal of anionic dyes;
- Finding ways to study the removal of dyes in continuous flow mode, since the adsorption process is very fast and must be scaled up;
- Explore other types of anionic and cationic dyes, with different molecular structures, to better elucidate the decolorization mechanisms;
- Apply these technologies to real textile effluents;
- Conduct long-term studies on MFC, applying higher hydraulic detention times to obtain better removal efficiencies, especially for anionic dyes;
- In addition, different operational strategies can be tested in MFC, such as alternating aerated and non-aerated cycles and bioaugmentation of the inoculum with pure electroactive microbial cultures;
- Carry out an economic feasibility study of the two technologies to assess their cost-effectiveness compared to conventional methods.

As a final recommendation, it is worth mentioning that a combination of technologies is often necessary to achieve the desired treatment quality standards and meet environmental requirements. Adsorption technology using zeolites seems most promising when applied as a final polishing, while bioelectrochemical technology using MFCs could be used at an early stage to degrade the dyes and generate bioenergy. Further studies involving the treatment of different dyes through the combined use of these two attractive, innovative and environmentally friendly technologies could be a suggestion for future research in this field of knowledge.

REFERENCES

ABDEL HAMEED, R. et al. Exploitation of industrial solid wastes for preparing zeolite as a value-added product and its kinetics as adsorbent for heavy metal ions. **Physicochemical Problems of Mineral Processing**, v. 57, n. 1, p. 87–99, 2020.

ABDELRAHMAN, E. A. et al. Utilization of rice husk and waste aluminum cans for the synthesis of some nanosized zeolite, zeolite/zeolite, and geopolymer/zeolite products for the efficient removal of Co(II), Cu(II), and Zn(II) ions from aqueous media. **Journal of Hazardous Materials**, v. 401, p. 123813, 2021.

ABDELRAHMAN, E. A.; HEGAZEY, R. M. Utilization of waste aluminum cans in the fabrication of hydroxysodalite nanoparticles and their chitosan biopolymer composites for the removal of Ni(II) and Pb(II) ions from aqueous solutions: Kinetic, equilibrium, and reusability studies. **Microchemical Journal**, v. 145, p. 18–25, 2019.

ABUKHADRA, M. R.; MOHAMED, A. S. Adsorption Removal of Safranin Dye Contaminants from Water Using Various Types of Natural Zeolite. **Silicon**, v. 11, n. 3, p. 1635–1647, 2019.

ALABA, P. A. et al. Synthesis of hierarchical nanoporous HY zeolites from activated kaolin, a central composite design optimization study. **Advanced Powder Technology**, v. 28, n. 5, p. 1399–1410, 2017.

AL-DAHRI, T.; ABDULRAZAK, A. A.; ROHANI, S. Preparation and characterization of Linde-type A zeolite (LTA) from coal fly ash by microwave-assisted synthesis method: its application as adsorbent for removal of anionic dyes. **International Journal of Coal Preparation and Utilization**, v. 42, n. 7, p. 2064–2077, 2022.

AL-TOHAMY, R. et al. A critical review on the treatment of dye-containing wastewater: Ecotoxicological and health concerns of textile dyes and possible remediation approaches for environmental safety. **Ecotoxicology and Environmental Safety**, v. 231, p. 113160, 2022.

ANDRADES, R. C. et al. Influence of Alkalinity on the Synthesis of Zeolite A and Hydroxysodalite from Metakaolin. **Journal of Nano Research**, v. 61, p. 51–60, 2020.

ANUWATTANA, R.; KHUMMONGKOL, P. Conventional hydrothermal synthesis of Na-A zeolite from cupola slag and aluminum sludge. **Journal of Hazardous Materials**, v. 166, n. 1, p. 227–232, 2009.

APHA. American Public Health Association. **Standard Methods for the Examination of Water and Wastewater.** 22nd edn. American Water Works Association, Water Environment Federation, Washington, 2012.

ARKATKAR, A.; MUNGRAY, A. K.; SHARMA, P. Study of electrochemical activity zone of *Pseudomonas aeruginosa* in microbial fuel cell. **Process Biochemistry**, v. 101, p. 213–217, 2021.

ASEFA, M. T.; FEYISA, G. B. Comparative Investigation on Two Synthesizing Methods of Zeolites for Removal of Methylene Blue from Aqueous Solution. **International Journal of Chemical Engineering**, v. 2022, p. 1–12, 2022.

ASHRAFIVALA, M. et al. Investigation of H_2O_2/UV advanced oxidation process on the removal rate of coliforms from the industrial effluent: A pilot-scale study. **International Journal of Hydrogen Energy**, v. 47, n. 78, p. 33530–33540, 2022.

ATTIA, N.; HASSAN, K. M.; HASSAN, M. I. Environmental Impacts of Aluminum Dross After Metal Extraction. Em: MARTIN, O. (Ed.). **Light Metals**. The Minerals, Metals & Materials Series. Cham: Springer International Publishing, p. 1155–1161, 2018.

ATUN, G. et al. A comparison of basic dye adsorption onto zeolitic materials synthesized from fly ash. **Journal of Hazardous Materials**, v. 187, n. 1–3, p. 562–573, 2011.

AYAR, N. et al. Cationic dye adsorption onto natural and synthetic zeolites in the presence of Cs^{+} and Sr^{2+} ions. **Toxicological & Environmental Chemistry**, v. 97, n. 1, p. 11–21, 2015.

AYAWEI, N.; EBELEGI, A. N.; WANKASI, D. Modelling and Interpretation of Adsorption Isotherms. **Journal of Chemistry**, v. 2017, p. 1–11, 2017.

AYELE, L. et al. Synthesis of zeolite A from Ethiopian kaolin. **Microporous and Mesoporous Materials**, v. 215, p. 29–36, 2015.

BAGCHI, S.; BEHERA, M. Bioaugmentation using *Pseudomonas aeruginosa* with an approach of intermittent aeration for enhanced power generation in ceramic MFC. **Sustainable Energy Technologies and Assessments**, v. 45, p. 101138, 2021.

BANDURA, L. et al. Synthetic zeolites from fly ash as effective mineral sorbents for land-based petroleum spills cleanup. **Fuel**, v. 147, p. 100–107, 2015.

BEHIN, J. et al. Using Coal Fly Ash and Wastewater for Microwave Synthesis of LTA Zeolite. **Chemical Engineering & Technology**, v. 37, n. 9, p. 1532–1540, 2014.

BEHZAT, B. Decolorization of Reactive Black 39 and Acid Red 360 by *Pseudomonas aeruginosa*. **Water Science and Technology**, v. 72, n. 8, p. 1266–1273, 2015.

BELVISO, C. et al. The crystallisation of zeolite (X- and A-type) from fly ash at 25°C in artificial sea water. **Microporous and Mesoporous Materials**, v. 162, p. 115–121, 2012.

BEVERIDGE, T. J. Structures of Gram-Negative Cell Walls and Their Derived Membrane Vesicles. **Journal of Bacteriology**, v. 181, n. 16, p. 4725–4733, 1999.

BOHRA, S.; KUNDU, D.; NASKAR, M. K. One-pot synthesis of NaA and NaP zeolite powders using agro-waste material and other low cost organic-free precursors. **Ceramics International**, v. 40, n. 1, p. 1229–1234, 2014.

BOLYEN, E. et al. Reproducible, interactive, scalable and extensible microbiome data science using QIIME 2. **Nature Biotechnology**, v. 37, n. 8, p. 852–857, 2019.

BORAN, F. et al. Comparison of indigo carmine decolorization by *Pseudomonas aeruginosa* and crude laccase enzyme from *Funalia trogii*. **Turkish Journal of Biology**, v. 43, n. 1, p. 37–46, 2019.

BOX, G.; HUNTER, W.; HUNTER, S. **Statistics for experimenters: An introduction to design, data analysis, and model building**. John Wiley & Sons Inc, New Jersey, p. 374–418.1978.

BRAR, T.; FRANCE, P.; SMIRNIOTIS, P. G. Control of Crystal Size and Distribution of Zeolite A. **Industrial & Engineering Chemistry Research**, v. 40, n. 4, p. 1133–1139, 2001.

CALLAHAN, B. J. et al. DADA2: High-resolution sample inference from Illumina amplicon data. **Nature Methods**, v. 13, n. 7, p. 581–583, 2016.

CAO, J.; WANG, P.; SUN, Q. Green Synthesis of Magnetic Zeolite LTA using NaOH Activated Fly Ash. **Journal of Inorganic and General Chemistry**, v. 646, n. 20, p. 1666–1670, 2020.

CAO, Y. et al. Electricigens in the anode of microbial fuel cells: pure cultures versus mixed communities. **Microbial Cell Factories**, v. 18, n. 1, p. 39, 2019.

CARDOSO, A. M. et al. Integrated synthesis of zeolites 4A and Na–P1 using coal fly ash for application in the formulation of detergents and swine wastewater treatment. **Journal of Hazardous Materials**, v. 287, p. 69–77, 2015.

ÇEKIÇ, S. Z. et al. Mediated electron transfer with P450cin. **Electrochemistry Communications**, v. 12, n. 11, p. 1547–1550, 2010.

CHEN, B.-Y. et al. Feasibility study of simultaneous bioelectricity generation and dye decolorization using naturally occurring decolorizers. **Journal of the Taiwan Institute of Chemical Engineers**, v. 41, n. 6, p. 682–688, 2010.

CHEN, K.-C. et al. Decolorization of the textile dyes by newly isolated bacterial strains. **Journal of Biotechnology**, v. 101, n. 1, p. 57–68, 2003.

CHOSTAK, C. L. **Remoção de íons metálicos de meios aquosos impactados pela drenagem ácida de mina via técnicas de sorção com a Zeólita Linde Tipo-A imobilizada em gel de agarose.** Universidade Federal de Santa Catarina. Programa de Pós-Graduação em Engenharia Ambiental. p. 156, 2023.

CHOSTAK, C. L. et al. Use of a Waste-Derived Linde Type-A Immobilized in Agarose for the Remediation of Water Impacted by Coal Acid Mine Drainage at Pilot Scale. **Materials**, v. 16, n. 11, p. 4038, 2023a.

CHOSTAK, C. L. et al. Agarose-Immobilized LTA Zeolite: a Novel Material to Use in an Improved Treatment Process of Mine-Impacted Water. **Water, Air, & Soil Pollution**, v. 234, n. 6, p. 365, 2023b.

CHOWDHURY, M. F. et al. Current treatment technologies and mechanisms for removal of indigo carmine dyes from wastewater: A review. **Journal of Molecular Liquids**, v. 318, p. 114061, 2020.

COLLINS, F. et al. A critical review of waste resources, synthesis, and applications for Zeolite LTA. **Microporous and Mesoporous Materials**, v. 291, p. 109667, 2020.

CRINI, G. et al. Removal of C.I. Basic Green 4 (Malachite Green) from aqueous solutions by adsorption using cyclodextrin-based adsorbent: Kinetic and equilibrium studies. **Separation and Purification Technology**, v. 53, n. 1, p. 97–110, 2007.

DAI, Q. et al. Sulfide-mediated azo dye degradation and microbial community analysis in a single-chamber air cathode microbial fuel cell. **Bioelectrochemistry**, v. 131, p. 107349, 2020.

DALARI, B. L. **Aplicação de líquido iônico à base de fosfônio para remoção de corantes reativos.** Universidade Federal de Santa Catarina. Programa de Pós-Graduação em Engenharia Ambiental. p. 142, 2022.

DALBOSCO, V. **Remoção de azo-corante em reator anaeróbio seguido de eletro-biorreator à membrana híbrido.** Universidade Federal de Santa Catarina. Programa de Pós-Graduação em Engenharia Ambiental. p. 147, 2021.

DAS, S.; BARMAN, S. Studies on removal of Safranine-T and Methyl Orange dyes from aqueous solution using NaX zeolite synthesized from fly ash. **Journal of Environmental Science and Engineering**, v. 2, n. 4, p. 735–747, 2013.

DEKA, R. et al. A techno-economic approach for eliminating dye pollutants from industrial effluent employing microalgae through microbial fuel cells: Barriers and perspectives. **Environmental Research**, v. 212, p. 113454, 2022.

DES LIGNERIS, E.; DUMÉE, L.; KONG, L. Nanofiber-Based Materials for Persistent Organic Pollutants in Water Remediation by Adsorption. **Applied Sciences**, v. 8, n. 2, p. 166, 2018.

DIMITRIJEVIC, R. et al. Structural characterization of pure Na-nephelines synthesized by zeolite conversion route. **Journal of Physics and Chemistry of Solids**, v. 65, n. 10, p. 1623–1633, 2004.

DUBININ, M.M.; RADUSHKEVICH, L.V. The equation of the characteristic curve of the activated charcoal. **Proceedings Union Soviet Socialist Republics Academy of Sciences**, v 55, p. 331–337, 1947.

DUTTA, S. et al. Contamination of textile dyes in aquatic environment: Adverse impacts on aquatic ecosystem and human health, and its management using bioremediation. **Journal of Environmental Management**, v. 353, p. 120103, 2024.

EL BOJADDAYNI, I. et al. A review on synthesis of zeolites from natural clay resources and waste ash: Recent approaches and progress. **Minerals Engineering**, v. 198, p. 108086, 2023.

ELOVICH, S.Y.; LARINOV, O.G. Theory of adsorption from solutions of non-electrolytes on solid (I) equation adsorption from solutions and the analysis of its simplest form, (II) verification of the equation of adsorption isotherm from solutions, **Izvestiya Akademii Nauk SSSR**, Otdelenie Khimicheskikh Nauk, v. 2, p. 209–216, 1962.

ESPEJEL-AYALA, F. et al. Use of drinking water sludge in the production process of zeolites. **Research on Chemical Intermediates**, v. 40, n. 8, p. 2919–2928, 2014.

EWC. **European Waste Catalogue and Hazardous Waste List**, Published by Environmental Protection Agency. Ireland. 2001. Avaiable online: https://archive.org/details/ewccodebook/mode/2up. Accessed on: 02 nov. 2023.

FALLAH, Z. et al. Toxicity and remediation of pharmaceuticals and pesticides using metal oxides and carbon nanomaterials. **Chemosphere**, v. 275, p. 130055, 2021.

FAO. **Food and Agriculture Organization of the United Nations**, 2022. Available online: https://openknowledge.fao.org/handle/20.500.14283/cd1158en. Accessed on: 4 aug. 2023.

FAO. **Food Outlook – Biannual report on global food markets**, 2024. Available online: https://openknowledge.fao.org/handle/20.500.14283/cd1158en. Accessed on: 30 may 2024.

FATIMA, M. et al. Low-Cost Single Chamber MFC Integrated With Novel Lignin-Based Carbon Fiber Felt Bioanode for Treatment of Recalcitrant Azo Dye. **Frontiers in Energy Research**, v. 9, p. 672817, 21 jun. 2021.

FERNÁNDEZ, A. S. **Microbial fuel cells running on high strength animal wastewater - Nitrogen removal strategies and microbial community characterization**. Barcelona: Universidad Politècnica de Catalunya, 2015.

FLANIGEN, E. M.; SAND, L. B. (EDS.). **Molecular Sieve Zeolites**. American Chemical Society: Washington, D. C., v. 101, p. 201–229, 1974.

FOLETTO, E. L. et al. Conversion of rice husk ash into zeolitic materials. **Latin American Applied Research**, v. 39, p. 75–78, 2009.

FOO, K. Y.; HAMEED, B. H. Insights into the modeling of adsorption isotherm systems. **Chemical Engineering Journal**, v. 156, n. 1, p. 2–10, 2010.

FRANKS, A. E.; NEVIN, K. P. Microbial Fuel Cells, A Current Review. **Energies**, v. 3, n. 5, p. 899–919, 2010.

FREUNDLICH, H.M.F. Over the adsorption in solution, **The Journal of Physical Chemistry**, v, 57, p. 385–471, 1906.

GHOLAMI, A. et al. Highly efficient treatment of petrochemical spent caustic effluent via electro-Fenton process for COD and TOC removal: optimization and experimental. **Biomass Conversion and Biorefinery**, v. 14, p. 17481–17497, 2023.

GHOSH, I. et al. Adsorptive removal of Safranin-O dye from aqueous medium using coconut coir and its acid-treated forms: Adsorption study, scale-up design, MPR and GA-ANN modeling. **Sustainable Chemistry and Pharmacy**, v. 19, p. 100374, 2021.

GUL, H. et al. Progress in microbial fuel cell technology for wastewater treatment and energy harvesting. **Chemosphere**, v. 281, p. 130828, 2021.

GÜNTHER, C. et al. Synthesis and characterization of a sulfur containing hydroxy sodalite without sulfur radicals. **Microporous and Mesoporous Materials**, v. 214, p. 1–7, 2015.

GUPTA, V. K. et al. Adsorption of Safranin-T from wastewater using waste materials—activated carbon and activated rice husks. **Journal of Colloid and Interface Science**, v. 303, n. 1, p. 80–86, 2006.

GUTIÉRREZ-SEGURA, E.; SOLACHE-RÍOS, M.; COLÍN-CRUZ, A. Sorption of indigo carmine by a Fe-zeolitic tuff and carbonaceous material from pyrolyzed sewage sludge. **Journal of Hazardous Materials**, v. 170, n. 2–3, p. 1227–1235, 2009.

HANSEN, S. et al. On the crystal chemistry of NaP zeolites. **Zeolites**, v. 13, n. 4, p. 276–280, 1993.

HAQUE, A. N. M. A. et al. Sustainable Adsorbents from Plant-Derived Agricultural Wastes for Anionic Dye Removal: A Review. **Sustainability**, v. 14, n. 17, p. 11098, 2022.

HASSAN, I.; GRUNDY, H. D. Structure of basic sodalite, $Na_8Al_6Si_6O_{24}(OH)_2.2H_2O$. **Acta Crystallographica Section C Crystal Structure Communications**, v. 39, n. 1, p. 3–5, 1983.

HO, Y. S.; MCKAY, G. Pseudo-second order model for sorption processes. **Process Biochemistry**, v. 34, n. 5, p. 451–465, 1999.

HOLKAR, C. R. et al. A critical review on textile wastewater treatments: Possible approaches. **Journal of Environmental Management**, v. 182, p. 351–366, 2016.

HOSSEINI NAMI, S.; MOUSAVI, S. B. Nitrate Removal Performance of Different Granular Adsorbents Using a Novel Fe-Exchanged Nanoporous Clinoptilolite. **Industrial & Engineering Chemistry Research**, v. 62, n. 8, p. 3659–3671, 2023.

HU, Q.; PANG, S.; WANG, D. In-depth Insights into Mathematical Characteristics, Selection Criteria and Common Mistakes of Adsorption Kinetic Models: A Critical Review. **Separation & Purification Reviews**, v. 51, n. 3, p. 281–299, 2022.

HUANG, X.-L. et al. Characterization of salt cake from secondary aluminum production. **Journal of Hazardous Materials**, v. 273, p. 192–199, 2014.

HUBENOVA, Y. et al. Gram-positive bacteria covered bioanode in a membrane-electrode assembly for use in bioelectrochemical systems. **Bioelectrochemistry**, v. 144, p. 108011, 2022.

ISLAM, T. et al. Synthesis of chemically modified carbon embedded silica and zeolite from rice husk to adsorb Crystal Violet dye from aqueous solution. **Applied Ecology and Environmental Research**, v. 16, n. 4, p. 3955–3967, 2018.

ISMAIL, G. A.; SAKAI, H. Review on effect of different type of dyes on advanced oxidation processes (AOPs) for textile color removal. **Chemosphere**, v. 291, p. 132906, 2022.

JAISWAL, S.; GOMASHE, A. V.; AGRAWAL, S. Original Research Article Decolorization potential of *Bacillus sp*. for removal of synthetic textile dyes. **International Jornal of Current Microbiology and Applied Sciences**, v. 3, p. 83–88, 2014.

JAYAPRIYA, J.; RAMAMURTHY, V. Use of non-native phenazines to improve the performance of *Pseudomonas aeruginosa* MTCC 2474 catalysed fuel cells. **Bioresource Technology**, v. 124, p. 23–28, 2012.

JIALIANG, R. et al. Biodegradation of Safranine T by an isolated bacterium *Pseudomonas aeruginosa* WZS-A. **World Automation Congress 2012**, Puerto Vallarta, Mexico, p. 1–4, 2012.

JIMÉNEZ, A. et al. Synthesis of pollucite and analcime zeolites by recovering aluminum from a saline slag. **Journal of Cleaner Production**, v. 297, p. 126667, 2021.

JOHNSON, E. B. G.; ARSHAD, S. E. Hydrothermally synthesized zeolites based on kaolinite: A review. **Applied Clay Science**, v. 97–98, p. 215–221, 2014.

KAFSHGARI, L. A. et al. Modeling and optimization of Direct Red 16 adsorption from aqueous solutions using nanocomposite of $MnFe_2O_4$/MWCNTs: RSM-CCRD model. **Journal of Molecular Liquids**, v. 233, p. 370–377, 2017.

KALYANI, D. C. et al. Ecofriendly biodegradation and detoxification of Reactive Red 2 textile dye by newly isolated *Pseudomonas sp.* SUK1. **Journal of Hazardous Materials**, v. 163, n. 2–3, p. 735–742, 2009.

KAMEL, M. M. et al. A glassy polyvinyl alcohol/silica gel hybrid composite for safranin removal: Adsorption, kinetic and thermodynamic studies. **Research on Chemical Intermediates**, v. 47, n. 3, p. 925–944, 2021.

KARDI, S. N. et al. Dye removal of AR27 with enhanced degradation and power generation in a microbial fuel cell using bioanode of treated clinoptilolite-modified graphite felt. **Environmental Science and Pollution Research**, v. 24, n. 23, p. 19444–19457, 2017.

KARUPPIAH, T. et al. Deriving electricity from dye processing wastewater using single chamber microbial fuel cell with carbon brush anode and platinum nano coated air cathode. **3 Biotech**, v. 8, n. 10, p. 437, 2018.

KAUR, S. et al. Synthesis and adsorption properties of mesoporous material for the removal of dye safranin: Kinetics, equilibrium, and thermodynamics. **Journal of Industrial and Engineering Chemistry**, v. 22, p. 19–27, 2015.

KHAN, A. U. et al. Biological Mineralization of Methyl Orange by *Pseudomonas aeruginosa*. **Water**, v. 14, n. 10, p. 1551, 2022.

KHAN, M. D. et al. Integrated air cathode microbial fuel cell-aerobic bioreactor set-up for enhanced bioelectrodegradation of azo dye Acid Blue 29. **Science of The Total Environment**, v. 756, p. 143752, 2021.

KIM, J. K.; LEE, H. D. Effects of step change of heating source on synthesis of zeolite 4A from coal fly ash. **Journal of Industrial and Engineering Chemistry**, v. 15, n. 5, p. 736–742, 2009.

KIM, J.-C. et al. Synthesis of uniform-sized zeolite from windshield waste. **Materials Chemistry and Physics**, v. 166, p. 20–25, 2015.

KORKUNA, O. et al. Structural and physicochemical properties of natural zeolites: clinoptilolite and mordenite. **Microporous and Mesoporous Materials**, v. 87, n. 3, p. 243–254, 2006.

KUROKI, S. et al. Selective synthesis of zeolites A and X from two industrial wastes: Crushed stone powder and aluminum ash. **Journal of Environmental Management**, v. 231, p. 749–756, 2019.

LACH, C. E. **Avaliação do processo de tratamento integrado utilizando célula a combustível microbiana (CCM) e eletro-Fenton (EF) na degradação de azo-corante têxtil.** Universidade Federal de Santa Catarina. Programa de Pós-Graduação em Engenharia Ambiental. p. 194, 2023.

LAGERGREN, S. About the theory of so-called adsorption of soluble substances. **Kungliga Svenska Vetenskapsakademiens Handlingar**, v. 24, p. 1–39, 1898.

LANGMUIR, I. The constitution and fundamental properties of solids and liquids. Part I. Solids. **Journal of the American Chemical Society**, v. 38, n. 11, p. 2221–2295, 1916.

LEE, W.-H.; LIN, Y.-W.; LIN, K.-L. Parameter optimization, characterization, and crystallization mechanisms underlying the synthesis of zeolite A using liquid crystal display waste glass and sandblasting waste as alternative raw materials. **Journal of Environmental Chemical Engineering**, v. 10, n. 5, p. 108506, 2022.

LEVIN, L.; MELIGNANI, E.; RAMOS, A. M. Effect of nitrogen sources and vitamins on ligninolytic enzyme production by some white-rot fungi. Dye decolorization by selected culture filtrates. **Bioresource Technology**, v. 101, n. 12, p. 4554–4563, 2010.

LI, H.-X. et al. Reductive decolorization of indigo carmine dye with *Bacillus sp.* MZS10. **International Biodeterioration & Biodegradation**, v. 103, p. 30–37, 2015.

LI, W. et al. Studies on the adsorption of dyes, Methylene blue, Safranin T, and Malachite green onto Polystyrene foam. **Separation and Purification Technology**, v. 276, p. 119435, 2021.

LIN, J. et al. Environmental impacts and remediation of dye-containing wastewater. **Nature Reviews Earth & Environment**, v. 4, n. 11, p. 785–803, 2023.

LIN, S. et al. Zeolite greenly synthesized from fly ash and its resource utilization: A review. **Science of The Total Environment**, v. 851, p. 158182, 2022.

LIU, G. et al. Preparation of NaA zeolite molecular sieve based on solid waste fly ash by high-speed dispersion homogenization-assisted alkali fusion-hydrothermal method and its performance of ammonia-nitrogen adsorption. **Journal of Science: Advanced Materials and Devices**, v. 9, n. 1, p. 100673, 2024.

LIU, Y. et al. Synthesis of zeolite P1 from fly ash under solvent-free conditions for ammonium removal from water. **Journal of Cleaner Production**, v. 202, p. 11–22, 2018.

LOBO-RECIO, M. Á. et al. Highly efficient removal of aluminum, iron, and manganese ions using Linde type-A zeolite obtained from hazardous waste. **Chemosphere**, v. 267, p. 128919, 2021.

LOGAN, B. E. et al. Microbial Fuel Cells: Methodology and Technology. **Environmental Science & Technology**, v. 40, n. 17, p. 5181–5192, 2006.

LOGAN, B. E. **Microbial fuel cells**. Hoboken, N.J: Wiley-Interscience, 2008.

LOGAN, B. E. Exoelectrogenic bacteria that power microbial fuel cells. **Nature Reviews Microbiology**, v. 7, n. 5, p. 375–381, 2009.

LOGAN, B. E.; REGAN, J. M. Electricity-producing bacterial communities in microbial fuel cells. **Trends in Microbiology**, v. 14, n. 12, p. 512–518, 2006.

LONG, X. et al. The Azo Dye Degradation and Differences Between the Two Anodes on the Microbial Community in a Double-Anode Microbial Fuel Cell. **Water, Air, & Soil Pollution**, v. 230, n. 11, p. 265, 2019.

LÓPEZ-DELGADO, A. et al. Zero-waste process for the transformation of a hazardous aluminum waste into a raw material to obtain zeolites. **Journal of Cleaner Production**, v. 255, p. 120178, 2020.

LOVLEY, D. R.; PHILLIPS, E. J. P. Novel Mode of Microbial Energy Metabolism: Organic Carbon Oxidation Coupled to Dissimilatory Reduction of Iron or Manganese. **Applied and Environmental Microbiology**, v. 54, n. 6, p. 1472–1480, 1988.

LUO, Y. et al. Seed germination test for toxicity evaluation of compost: Its roles, problems and prospects. **Waste Management**, v. 71, p. 109–114, 2018.

LYU, J. et al. Testing the toxicity of metals, phenol, effluents, and receiving waters by root elongation in Lactuca sativa L. **Ecotoxicology and Environmental Safety**, v. 149, p. 225–232, 2018.

MA, G. et al. A redox mediator doped gel polymer as an electrolyte and separator for a high performance solid state supercapacitor. **Journal of Materials Chemistry A**, v. 3, n. 7, p. 4035–4041, 2015.

MALLAPUR, V. P.; OUBAGARANADIN, J. U. K. A Brief Review on the Synthesis of Zeolites from Hazardous Wastes. **Transactions of the Indian Ceramic Society**, v. 76, n. 1, p. 1–13, 2017.

MAQBOOL, Z. et al. Use of RSM modeling for optimizing decolorization of simulated textile wastewater by *Pseudomonas aeruginosa* strain ZM130 capable of simultaneous removal of reactive dyes and hexavalent chromium. **Environmental Science and Pollution Research**, v. 23, n. 11, p. 11224–11239, 2016.

MARASSI, R. J. et al. Long-term performance and acute toxicity assessment of scaled-up air–cathode microbial fuel cell fed by dairy wastewater. **Bioprocess and Biosystems Engineering**, v. 43, n. 9, p. 1561–1571, 2020.

MARKETS AND MARKETS. **Zeolites Market by Type (Natural, Synthetic), Function (Ion-Exchange, Catalyst, Molecular Sieve), Synthetic Zeolite Application (Detergents, Adsorbent, Catalysts), Natural Zeolite Application, and Region – Global Forecast to 2026**. Available online: https://www.marketsandmarkets.com/Market-Reports/zeolites-market-76442083.html. Accessed on: 5 oct. 2023.

MCFARLAND, J. The nephelometer: Na instrument for estimatinf the number of bacteria in suspensios used for calculating the opsonic index and for vaccines. **JAMA: The Journal of the American Medical Association**, v. XLIX, n. 14, p. 1176, 1907.

MELO, C. R. et al. Production of Zeolite from Rice Husk Ash. **Materials Science Forum**, v. 798–799, p. 617–621, 2014.

MILTON, R. M. Molecular Sieve Adsorbents. **Molecular Sieve Adsorbents**, United State Patent Office 2,882,243. 1953.

MIN, B.; ROMÁN, Ó. B.; ANGELIDAKI, I. Importance of temperature and anodic medium composition on microbial fuel cell (MFC) performance. **Biotechnology Letters**, v. 30, n. 7, p. 1213–1218, 2008.

MINISTÉRIO DA SAÚDE. **Técnica de Coloração de Gram**, 1997. Available online: http://bvsms.saude.gov.br/bvs/publicacoes/115_03gram.pdf. Accessed on: 15 apr. 2024.

MISHRA, S.; MAITI, A. The efficacy of bacterial species to decolourise reactive azo, anthroquinone and triphenylmethane dyes from wastewater: a review. **Environmental Science and Pollution Research**, v. 25, n. 9, p. 8286–8314, 2018.

MISHRA, S.; MOHANTY, P.; MAITI, A. Bacterial mediated bio-decolourization of wastewater containing mixed reactive dyes using jack-fruit seed as co-substrate: Process optimization. **Journal of Cleaner Production**, v. 235, p. 21–33, 2019.

MOHAMED, R. M.; MKHALID, I. A.; BARAKAT, M. A. Rice husk ash as a renewable source for the production of zeolite NaY and its characterization. **Arabian Journal of Chemistry**, v. 8, n. 1, p. 48–53, 2015.

MOUNA, S.; HAJJI, S.; TOUNSI, H. Waste to health: Green synthesis of Zn loaded LTA zeolite prepared from waste glass and aluminum scrap with high antioxidant and antimicrobial activities. **Journal of Cleaner Production**, v. 434, p. 139946, 2024.

MU, Y. et al. Decolorization of Azo Dyes in Bioelectrochemical Systems. **Environmental Science & Technology**, v. 43, n. 13, p. 5137–5143, 2009.

MUSYOKA, N. M. et al. Optimization of hydrothermal synthesis of pure phase zeolite Na-P1 from South African coal fly ashes. **Journal of Environmental Science and Health, Part A**, v. 47, n. 3, p. 337–350, 2012.

MUSYOKA, N. M. et al. Thermal stability studies of zeolites A and X synthesized from South African coal fly ash. **Research on Chemical Intermediates**, v. 41, n. 2, p. 575–582, 2015.

N LOTHA, T. et al. Advancement in Sustainable Wastewater Treatment: A Multifaceted Approach to Textile Dye Removal through Physical, Biological and Chemical Techniques. **Chemistry Select**, v. 9, n. 11, p. e202304093, 2024.

NACHIYAR, C. V.; RAJKUMAR, G. S. Degradation of a tannery and textile dye, Navitan Fast Blue S5R by *Pseudomonas aeruginosa*. **World Journal of Microbiology & Biotechnology**, v. 19, p. 609–614, 2003.

NARAYANASAMY, S.; JAYAPRAKASH, J. Improved performance of *Pseudomonas aeruginosa* catalyzed MFCs with graphite/polyester composite electrodes doped with metal ions for azo dye degradation. **Chemical Engineering Journal**, v. 343, p. 258–269, 2018.

NASCIMENTO, R. F. et al. **Adsorção aspectos teóricos e aplicações ambientais**. Fortaleza: Imprensa Universitária, Brazil, p. 1–258, 2014.

NC 626. Natural zeolites - **Determination of exchange capacity total cationic - Ammonium chloride method**. 2008. Available online: https://ftp.isdi.co.cu/Biblioteca/BIBLIOTECA%20UNIVERSITARIA%20DEL%20ISDI/COLECCION%20DIGITAL%20DE%20NORMAS%20CUBANAS/2014/NC%20626%20a2014%206p%20lco.pdf. Accessed on: 20 aug. 2024.

NGUYEN, D. A.; PHAM, N.; PHAM, H. T. Wastewater treatment performance and microbial community of anode electrodes of membrane and membrane-less MFCs under effect of sunlight. **Journal of Water Process Engineering**, v. 42, p. 102159, 2021.

NÚÑEZ-GÓMEZ, D. et al. Optimization of acid mine drainage remediation with central composite rotatable design model. **Energy Procedia**, v. 136, p. 233–238, out. 2017.

NÚÑEZ-GÓMEZ, D. **Valorização da casca de camarão para tratamento da drenagem ácida mineral do carvão visando a obtenção de água de reuso.** Universidade Federal de Santa Catarina. Programa de Pós-Graduação em Engenharia Ambiental. p. 217, 2018.

OH, Y.-K. et al. Decolorization of synthetic dyes by *Citrobacter amalonaticus* Y19. **Journal of the Taiwan Institute of Chemical Engineers**, v. 42, n. 3, p. 492–497, 2011.

OON, Y.-S. et al. Microbial fuel cell operation using monoazo and diazo dyes as terminal electron acceptor for simultaneous decolourisation and bioelectricity generation. **Journal of Hazardous Materials**, v. 325, p. 170–177, 2017.

PADILLA, I. et al. Sustainable Management of Salt Slag. **Sustainability**, v. 14, n. 9, p. 4887, 2022.

PANDEY, A.; SINGH, P.; IYENGAR, L. Bacterial decolorization and degradation of azo dyes. **International Biodeterioration & Biodegradation**, v. 59, n. 2, p. 73–84, 2007.

PANGAN, N. et al. Hydrothermal Synthesis and Characterization of Zeolite A from Corn (Zea Mays) Stover Ash. **Materials**, v. 14, n. 17, p. 4915, 2021.

PAZ, A. et al. Biological treatment of model dyes and textile wastewaters. **Chemosphere**, v. 181, p. 168–177, 2017.

PEREIRA, P. et al. Synthesis of Zeolite A from Metakaolin and Its Application in the Adsorption of Cationic Dyes. **Applied Sciences**, v. 8, n. 4, p. 608, 2018.

PERIYASAMY, A. P. Recent Advances in the Remediation of Textile-Dye-Containing Wastewater: Prioritizing Human Health and Sustainable Wastewater Treatment. **Sustainability**, v. 16, n. 2, p. 495, 2024.

PODE, R. Potential applications of rice husk ash waste from rice husk biomass power plant. **Renewable and Sustainable Energy Reviews**, v. 53, p. 1468–1485, 2016.

PRIAC, A.; BADOT, P.-M.; CRINI, G. Treated wastewater phytotoxicity assessment using *Lactuca sativa*: Focus on germination and root elongation test parameters. **Comptes Rendus Biologies**, v. 340, n. 3, p. 188–194, 2017.

PROKOF'EV, V. YU.; GORDINA, N. E. Preparation of granulated LTA and SOD zeolites from mechanically activated mixtures of metakaolin and sodium hydroxide. **Applied Clay Science**, v. 101, p. 44–51, 2014.

PUCCIA, V.; AVENA, M. J. On the use of the Dubinin-Radushkevich equation to distinguish between physical and chemical adsorption at the solid-water interface. **Colloid and Interface Science Communications**, v. 41, p. 100376, 2021.

QU, Y. et al. Biodegradation of indole by a newly isolated *Cupriavidus sp. SHE*. **Journal of Environmental Sciences**, v. 34, p. 126–132, 2015.

QUAST, C. et al. The SILVA ribosomal RNA gene database project: improved data processing and web-based tools. **Nucleic Acids Research**, v. 41, n. D1, p. D590–D596, 2012.

QUEROL, X. et al. Synthesis of zeolites from coal fly ash: an overview. **International Journal of Coal Geology**, v. 50, n. 1–4, p. 413–423, 2002.

RAMÍREZ-VARGAS, C. et al. Microbial Electrochemical Technologies for Wastewater Treatment: Principles and Evolution from Microbial Fuel Cells to Bioelectrochemical-Based Constructed Wetlands. **Water**, v. 10, n. 9, p. 1128, 2018.

RAMYA, M.; ANUSHA, B.; KALAVATHY, S. Decolorization and biodegradation of Indigo carmine by a textile soil isolate Paenibacillus larvae. **Biodegradation**, v. 19, n. 2, p. 283–291, 2008.

RAMYA, M.; SENTHIL KUMAR, P. A review on recent advancements in bioenergy production using microbial fuel cells. **Chemosphere**, v. 288, p. 132512, 2022.

RATHOUR, R. et al. Treatment of Various Types of Wastewaters Using Microbial Fuel Cell Systems. **Microbial Electrochemical Technology**, p. 665–692, 2019.

RAVADELLI, M. **Aplicação de eletrocoagulação em um biorreator a membrana precedido de tanque anóxico para o tratamento de efluente têxtil.** Universidade

Federal de Santa Catarina. Programa de Pós-Graduação em Engenharia Ambiental. p. 129, 2021.

REDLICH, O.; PETERSON, D.L. A useful adsorption isotherm. **The Journal of Physical Chemistry**, v. 63, p. 1024–1026, 1959.

RETHINAM, B.; PALANICHAMY, R.; BRITTO, J. D. J. Analysis of Batch Kinetic Data of Biodecolorization Reaction: Theoretical Approach for the Design of Packed Bed Reactor. **Journal of Environmental Engineering**, v. 149, n. 10, p. 7269, 2023.

RITTER, M. T. et al. Salt slag and rice husk ash as raw materials in zeolite synthesis: Process optimization using central composite rotational design. **Sustainable Chemistry and Pharmacy**, v. 39, p. 101599, 2024a.

RITTER, M. T. et al. Adsorption of Safranine-T dye using a waste-based zeolite: Optimization, kinetic and isothermal study. **Journal of Industrial and Engineering Chemistry**, v. 136, p. 177–187, 2024b.

RITTER, M. T. et al. **Waste Symbiosis through the Synthesis of Highly Crystalline LTA and SOD Zeolites**, 2024c. Available online: https://www.preprints.org/manuscript/202408.0742/v1. Accessed on: 30 aug. 2024.

ROZHKOVSKAYA, A.; RAJAPAKSE, J.; MILLAR, G. J. Synthesis of high-quality zeolite LTA from alum sludge generated in drinking water treatment plants. **Journal of Environmental Chemical Engineering**, v. 9, n. 2, p. 104751, 2021.

SAHA, S. et al. Production and purification of bioflocculants from newly isolated bacterial species: a comparative decolourization study of cationic and anionic textile dyes. **Environmental Technology**, v. 42, n. 23, p. 3663–3674, 2021.

SALLEH, M. A. M. et al. Cationic and anionic dye adsorption by agricultural solid wastes: A comprehensive review. **Desalination**, v. 280, n. 1–3, p. 1–13, 2011.

SÁNCHEZ-HERNÁNDEZ, R. et al. One-step synthesis of NaP1, SOD and ANA from a hazardous aluminum solid waste. **Microporous and Mesoporous Materials**, v. 226, p. 267–277, 2016.

SANTOS KLIENCHEN DALARI, B. L. et al. Application of a phosphonium-based ionic liquid for reactive textile dye removal: Extraction study and toxicological evaluation. **Journal of Environmental Management**, v. 304, p. 114322, 2022.

SARATALE, R. G. et al. Bacterial decolorization and degradation of azo dyes: A review. **Journal of the Taiwan Institute of Chemical Engineers**, v. 42, n. 1, p. 138–157, 2011.

SARWAR, B. et al. Comparative study of ZIF-8-materials for removal of hazardous compounds using physio-chemical remediation techniques. **Environmental Research**, v. 220, p. 115168, 2023.

SAYEHI, M. et al. Synthesis of high value-added Na–P1 and Na-FAU zeolites using waste glass from fluorescent tubes and aluminum scraps. **Materials Chemistry and Physics**, v. 248, p. 122903, 2020.

SCHALLEMBERGER, J. B. **Remoção de corantes têxteis utilizando o substrato residual da produção de cogumelo *Pleurotus ostratus*: Degradação enzimática e adsorção.** Universidade Federal de Santa Catarina. Programa de Pós-Graduação em Engenharia Ambiental. p. 139, 2021.

SCHERRER, P. **Estimation of the size and internal structure of colloidal particles by means of röntgen**. Nachrichten von der Gesellschaft der Wissenschaften zu Göttingen. v. 2, p. 96–100, 1918.

SELIM, M. M. et al. Preparation and characterization of Na-A zeolite from aluminum scrub and commercial sodium silicate for the removal of Cd^{2+} from water. **Journal of the Association of Arab Universities for Basic and Applied Sciences**, v. 24, n. 1, p. 19–25, 2017.

SELVARAJ, K. Transformation of chemically fine tuned zeolite A precursor into dense lithium aluminosilicates – A comprehensive phase evolution and sintering study. **Microporous and Mesoporous Materials**, v. 135, n. 1–3, p. 82–89, 2010.

SENTHILKUMAR, K. et al. Simultaneous power generation and Congo red dye degradation in double chamber microbial fuel cell using spent carbon electrodes. **Energy Sources, Part A: Recovery, Utilization, and Environmental Effects**, p. 1–17, 2020.

SHABANI, J. M. et al. Fusion-Assisted Hydrothermal Synthesis and Post-Synthesis Modification of Mesoporous Hydroxy Sodalite Zeolite Prepared from Waste Coal Fly Ash for Biodiesel Production. **Catalysts**, v. 12, n. 12, p. 1652, 2022.

SHARAFINIA, S.; FARROKHNIA, A.; LEMRASKI, E. G. The adsorption of cationic dye onto ACPMG@ZIF-8 core-shell, optimization using central composite response surface methodology (CCRSM). **Colloids and Surfaces A: Physicochemical and Engineering Aspects**, v. 634, p. 128039, 2022.

SHARMA, P. et al. GIS-NaP1 zeolite microspheres as potential water adsorption material: Influence of initial silica concentration on adsorptive and physical/topological properties. **Scientific Reports**, v. 6, n. 1, p. 22734, 2016.

SHEN, H.-B. et al. Enhanced bioelectricity generation by improving pyocyanin production and membrane permeability through sophorolipid addition in *Pseudomonas aeruginosa*-inoculated microbial fuel cells. **Bioresource Technology**, v. 167, p. 490–494, 2014.

SHI, Y. et al. Removal of Toluidine Blue and Safranin O from Single and Binary Solutions Using Zeolite. **Crystals**, v. 11, n. 10, p. 1181, 2021.

SHINOHARA, Y.; KOHYAMA, N. Quantitative Analysis of Tridymite and Cristobalite Crystallized in Rice Husk Ash by Heating. **Industrial Health**, v. 42, n. 2, p. 277–285, 2004.

SHOUMKOVA, A.; STOYANOVA, V. Zeolites formation by hydrothermal alkali activation of coal fly ash from thermal power station “Maritsa 3”, Bulgaria. **Fuel**, v. 103, p. 533–541, 2013.

SHU, R. et al. Controlled design of Na–P1 zeolite/ porous carbon composites from coal gasification fine slag for high-performance adsorbent. **Environmental Research**, v. 217, p. 114912, 2023.

SIEREN, B. et al. Sorptive Removal of Color Dye Safranin O by Fibrous Clay Minerals and Zeolites. **Advances in Materials Science and Engineering**, v. 2020, p. 1–12, 2020.

SILVEIRA, D. D. et al. Structural and functional spatial dynamics of microbial communities in aerated and non-aerated horizontal flow treatment wetlands. **Science of The Total Environment**, v. 838, p. 156600, 2022.

SIMANJUNTAK, W. et al. The effect of crystallization time on structure, microstructure, and catalytic activity of zeolite-A synthesized from rice husk silica and food-grade aluminum foil. **Biomass and Bioenergy**, v. 148, p. 106050, 2021.

SINGH, A.; DAHIYA, S.; MISHRA, B. K. Microbial fuel cell coupled hybrid systems for the treatment of dye wastewater: A review on synergistic mechanism and performance. **Journal of Environmental Chemical Engineering**, v. 9, n. 6, p. 106765, 2021.

SINGH, H. M. et al. Microbial fuel cells: a sustainable solution for bioelectricity generation and wastewater treatment. **Biofuels**, v. 10, n. 1, p. 11–31, 2019.

SINGH, S. N. (ED.). **Microbial Degradation of Synthetic Dyes in Wastewaters**. Environmental Science and Engineering. Cham: Springer International Publishing, 2015.

SIPS, R. On the Structure of a Catalyst Surface. **The Journal of Chemical Physics**, v. 16, n. 5, p. 490–495, 1948.

SIVALINGAM, S.; SEN, S. Rapid ultrasound assisted hydrothermal synthesis of highly pure nanozeolite X from fly ash for efficient treatment of industrial effluent. **Chemosphere**, v. 210, p. 816–823, 2018.

SOBRERO, M. C.; RONCO, A. **Ensayo de toxicidad aguda con semillas de lechuga *Lactuca sativa*.** Ensayos toxicológicos y métodos evaluación Calidad aguas. Estandarización, intercalibración, Resultados y Aplicación. p. 55–67, 2004.

SOLANKI, K.; SUBRAMANIAN, S.; BASU, S. Microbial fuel cells for azo dye treatment with electricity generation: A review. **Bioresource Technology**, v. 131, p. 564–571, 2013.

SORGATO, A. C. **Célula a Combustível Microbiana: Operação em diferentes tempos de detenção hidráulica e extração de energia ativa.** Universidade Federal de Santa Catarina. Programa de Pós-Graduação em Engenharia Ambiental. p. 129, 2022.

SRINIVASAN, A.; VIRARAGHAVAN, T. Decolorization of dye wastewaters by biosorbents: A review. **Journal of Environmental Management**, v. 91, n. 10, p. 1915–1929, 2010.

SRIVASTAVA, A. et al. Emerging bioremediation technologies for the treatment of textile wastewater containing synthetic dyes: a comprehensive review. **Journal of Chemical Technology & Biotechnology**, v. 97, n. 1, p. 26–41, 2022.

SRIVASTAVA, A.; MESHRAM, A. On trending technologies of aluminium dross recycling: A review. **Process Safety and Environmental Protection**, v. 171, p. 38–54, 2023.

STATISTA. **Market volume of secondary aluminum worldwide in 2020, with a forecast for 2027**, 2023. Available online: https://www.statista.com/statistics/1306589/global-market-volume-of-secondary-aluminum. Accessed on: 5 sep. 2023.

STOLZ, A. Basic and applied aspects in the microbial degradation of azo dyes. **Applied Microbiology and Biotechnology**, v. 56, n. 1–2, p. 69–80, 2001.

SUKRITI et al. Sequestration of dyes from artificially prepared textile effluent using RSM-CCD optimized hybrid backbone based adsorbent-kinetic and equilibrium studies. **Journal of Environmental Management**, v. 190, p. 176–187, 2017.

SULEMAN, M. et al. Castor Leaves-Based Biochar for Adsorption of Safranin from Textile Wastewater. **Sustainability**, v. 13, n. 12, p. 6926, 2021.

SUN, J. et al. Simultaneous decolorization of azo dye and bioelectricity generation using a microfiltration membrane air-cathode single-chamber microbial fuel cell. **Bioresource Technology**, v. 100, n. 13, p. 3185–3192, 2009.

SUN, J. et al. Further treatment of decolorization liquid of azo dye coupled with increased power production using microbial fuel cell equipped with an aerobic biocathode. **Water Research**, v. 45, n. 1, p. 283–291, 2011.

SUN, J. et al. Regulation of biocathode microbial fuel cell performance with respect to azo dye degradation and electricity generation via the selection of anodic inoculum. **International Journal of Hydrogen Energy**, v. 41, n. 9, p. 5141–5150, 2016.

SUND, C. J. et al. Effect of electron mediators on current generation and fermentation in a microbial fuel cell. **Applied Microbiology and Biotechnology**, v. 76, n. 3, p. 561–568, 2007.

SYDORCHUK, V. et al. Mechanochemical transformation of Pb_2MoO_5 single crystal into nano-dispersed state. **Applied Nanoscience**, v. 13, n. 10, p. 7069–7075, 2023.

TACAS, A. C. J. et al. Degradation and biotoxicity of azo dyes using indigenous bacteria-acclimated microbial fuel cells (MFCs). **Process Biochemistry**, v. 102, p. 59–71, 2021.

TAN, S.-M. et al. Biotreatment of sulfonated dyestuffs with energy recovery in microbial fuel cell: Influencing parameters, kinetics, degradation pathways, mechanisms, and phytotoxicity assessment. **Journal of Environmental Chemical Engineering**, v. 9, n. 4, p. 105525, 2021.

TAN, W.-C. et al. Synthesis and characterization of zeolites NaA and NaY from rice husk ash. **Adsorption**, v. 17, n. 5, p. 863–868, 2011.

TARA, N. et al. Nano-engineered Adsorbent for the Removal of Dyes from Water: A Review. **Current Analytical Chemistry**, v. 16, n. 1, p. 14–40, 2020.

TEMKIN, M.I.; PYZHEV, V. Kinetics of ammonia synthesis on promoted iron catalyst. **Acta Physicochimica USSR**, v. 12, p. 327–356, 1940.

TERRES, J. et al. Decolorization and degradation of Indigo Carmine dye from aqueous solution catalyzed by horseradish peroxidase. **Biocatalysis and Biotransformation**, v. 32, n. 1, p. 64–73, 2014.

TERZANO, R. et al. Facile Zeolite Synthesis from Municipal Glass and Aluminum Solid Wastes. **Clean – Soil, Air, Water**, v. 43, n. 1, p. 133–140, 2015.

THUNG, W.-E. et al. A highly efficient single chambered up-flow membrane-less microbial fuel cell for treatment of azo dye Acid Orange 7-containing wastewater. **Bioresource Technology**, v. 197, p. 284–288, 2015.

TKACZYK, A.; MITROWSKA, K.; POSYNIAK, A. Synthetic organic dyes as contaminants of the aquatic environment and their implications for ecosystems: A review. **Science of The Total Environment**, v. 717, p. 137222, 2020.

TOMASSONI, F. **Remoção de cor de efluente têxtil sintético por processos de eletrocoagulação e adsorção com carvões ativados produzidos a partir de folhas de *Persea americana Mill* e de *Cassia fistula L*.** Universidade Federal de Santa Catarina. Programa de Pós-Graduação em Engenharia Ambiental. p. 177, 2019.

TOTH, J. State equations of the solid gas interface layer. **Acta Chimica Academiae Scientiarum Hungaricae**, v. 69, p. 311–317, 1971.

TOUNSI, H.; MSEDDI, S.; DJEMEL, S. Preparation and characterization of Na-LTA zeolite from Tunisian sand and aluminum scrap. **Physics Procedia**, v. 2, n. 3, p. 1065–1074, 2009.

TRAN-NGUYEN, P. L. et al. Facile synthesis of zeolite NaX using rice husk ash without pretreatment. **Journal of the Taiwan Institute of Chemical Engineers**, v. 123, p. 338–345, 2021.

TSAKIRIDIS, P. E. Aluminium salt slag characterization and utilization – A review. **Journal of Hazardous Materials**, v. 217–218, p. 1–10, 2012.

TURP, S. M. et al. Enhanced adsorption of methylene blue from textile wastewater by using natural and artificial zeolite. **Water Science and Technology**, p. 2020358, 2020.

UDUMA, R. C. et al. Bioelectrochemical technologies for simultaneous treatment of dye wastewater and electricity generation: a review. **International Journal of Environmental Science and Technology**, v. 20, n. 9, p. 10415–10434, 2023.

UN. **Millennium Development Goals Report, New York: United Nations**, 2015. Available online: http://www.

un.org/millenniumgoals/2015_MDG_Report/pdf/MDG%202015%20rev%20(July%201).pdf. Accessed on: 3 apr. 2024.

UNEP. **UN Environment Programme. Annual Report**, 2018. Available online: https://www.unep.org/resources/unenvironment-2018-annual-report. Accessed on: 6 may 2024.

VALLI NACHIYAR, C.; SUSEELA RAJAKUMAR, G. Mechanism of Navitan Fast Blue S5R degradation by *Pseudomonas aeruginosa*. **Chemosphere**, v. 57, n. 3, p. 165–169, out. 2004.

VAN DEN BERG, H. H. J. L. et al. How current risk assessment and risk management methods for drinking water in The Netherlands cover the WHO water safety plan approach. **International Journal of Hygiene and Environmental Health**, v. 222, n. 7, p. 1030–1037, 2019.

VASCONCELOS, A. A. et al. Zeolites: A Theoretical and Practical Approach with Uses in (Bio)Chemical Processes. **Applied Sciences**, v. 13, n. 3, p. 1897, 2023.

VAUTIER, M.; GUILLARD, C.; HERRMANN, J.-M. Photocatalytic Degradation of Dyes in Water: Case Study of Indigo and of Indigo Carmine. **Journal of Catalysis**, v. 201, n. 1, p. 46–59, 2001.

VEGERE, K. et al. Comparative study of hydrothermal synthesis routes of zeolite A. **Materials Today: Proceedings**, v. 33, p. 1984–1987, 2020.

WAJIMA, T. et al. Synthesis of Zeolite-A Using Silica from Rice Husk Ash. **Journal of Chemical Engineering of Japan**, v. 42, n. Supplement., p. S61–S66, 2009.

WANG, C. et al. Evaluation of zeolites synthesized from fly ash as potential adsorbents for wastewater containing heavy metals. **Journal of Environmental Sciences**, v. 21, n. 1, p. 127–136, 2009.

WANG, H. et al. Bioelectricity generation from the decolorization of reactive blue 19 by using microbial fuel cell. **Journal of Environmental Management**, v. 248, p. 109310, 2019a.

WANG, J.; GUO, X. Adsorption kinetic models: Physical meanings, applications, and solving methods. **Journal of Hazardous Materials**, v. 390, p. 122156, 2020.

WANG, P. et al. Synthesis of Zeolite 4A from Kaolin and Its Adsorption Equilibrium of Carbon Dioxide. **Materials**, v. 12, n. 9, p. 1536, 2019b.

WANG, Y. et al. Synthesis, characterization and CO2 adsorption of NaA, NaX and NaZSM-5 from rice husk ash. **Solid State Sciences**, v. 86, p. 24–33, 2018.

WEBER, W.J.; MORRIS, J.C. Kinetics of adsorption on carbon from solution. **Journal of the Sanitary Engineering Division**, v. 89, p. 31–59, 1963.

WONGWICHIEN, J. Synthesis and Use of Zeolite Na-A from Waste Sludge of Water Treatment Plant for Ammonium Removal. **Chiang Mai Journal of Science**, v. 41, p. 1262–1273, 2014.

XU, H. et al. Adsorption of acid fuchsin onto LTA-type zeolite derived from fly ash. **Science China Technological Sciences**, v. 57, n. 6, p. 1127–1134, 2014.

XU, R. et al. **Chemistry of Zeolites and Related Porous Materials: Synthesis and Structure**. John Wiley & Sons, 2007.

YADAV, A. et al. Microbial fuel cells for mineralization and decolorization of azo dyes: Recent advances in design and materials. **Science of The Total Environment**, v. 826, p. 154038, 2022a.

YADAV, S. et al. Novel composites of Pennisetum glaucum with CNT: preparation, characterization and application for the removal of safranine O and methylene blue dyes from single and binary systems. **Biomass Conversion and Biorefinery**, p. 1–18, 2022b.

YAGUB, M. T. et al. Dye and its removal from aqueous solution by adsorption: A review. **Advances in Colloid and Interface Science**, v. 209, p. 172–184, 2014.

YASEEN, D. A.; SCHOLZ, M. Textile dye wastewater characteristics and constituents of synthetic effluents: a critical review. **International Journal of Environmental Science and Technology**, v. 16, n. 2, p. 1193–1226, 2019.

YI, S. et al. Application of response surface methodology and central composite rotatable design in optimizing the preparation conditions of vinyltriethoxysilane modified silicalite/polydimethylsiloxane hybrid pervaporation membranes. **Separation and Purification Technology**, v. 71, n. 2, p. 252–262, 2010.

YONG, X.-Y. et al. An integrated aerobic-anaerobic strategy for performance enhancement of *Pseudomonas aeruginosa*-inoculated microbial fuel cell. **Bioresource Technology**, v. 241, p. 1191–1196, 2017.

YU, J. Optimal Decolorization and Kinetic Modeling of Synthetic Dyes by *Pseudomonas* Strains. **Water Research**, v. 35, n. 15, p. 3579–3586, 2001.

ZHANG, L. et al. Biofilm formation and electricity generation of a microbial fuel cell started up under different external resistances. **Journal of Power Sources**, v. 196, n. 15, p. 6029–6035, 2011.

ZHOU, L. et al. Recent development in microbial electrochemical technologies: Biofilm formation, regulation, and application in water pollution prevention and control. **Journal of Water Process Engineering**, v. 49, p. 103135, 2022.

ZHOU, Q. et al. Synthesis of high-quality Na P1 zeolite from municipal solid waste incineration fly ash by microwave-assisted hydrothermal method and its adsorption capacity. **Science of The Total Environment**, v. 855, p. 158741, 2023.

ZIEJEWSKA, C. et al. Eco-friendly zeolites for innovative purification of water from cationic dye and heavy metal ions. **Journal of Cleaner Production**, v. 406, p. 136947, 2023.

APPENDIX A – SALT SLAG AND RICE HUSK ASH AS RAW MATERIALS IN ZEOLITE SYNTHESIS: PROCESS OPTIMIZATION USING CENTRAL COMPOSITE ROTATIONAL DESIGN

Sustainable Chemistry and Pharmacy 39 (2024) 101599

Contents lists available at ScienceDirect

Sustainable Chemistry and Pharmacy

journal homepage: www.elsevier.com/locate/scp

Salt slag and rice husk ash as raw materials in zeolite synthesis: Process optimization using central composite rotational design

Magali Teresinha Ritter[a, b], María Ángeles Lobo-Recio[b, c], Isabel Padilla[a, *], Maximina Romero[a], Aurora López-Delgado[a]

[a] Department of Materials, Eduardo Torroja Institute for Construction Sciences (IETcc-CSIC), Serrano Galvache Street, 4, 28033, Madrid, Spain
[b] Department of Sanitary and Environmental Engineering, Federal University of Santa Catarina (UFSC), Campus Reitor João David Ferreira Lima, 88040-900, Florianópolis, SC, Brazil
[c] Department of Energy and Sustainability, Federal University of Santa Catarina (UFSC), Campus Araranguá, Rod. Gov. Jorge Lacerda, 3201, Jardim das Avenidas, 88.906-072, Araranguá, SC, Brazil

ARTICLE INFO

Handling Editor: Fabio Aricò

Keywords:
Waste-based zeolites
NaP zeolite
Hazardous waste
Salt slag
Rice husk ash
Central composite rotational design

ABSTRACT

The growing demand of zeolites for many industrial applications has led to a search for eco-friendly alternatives for their production, in an attempt to reduce costs, save natural resources and alleviate the associated environmental impacts. In the present study, hazardous aluminum salt slag (aluminum source) and rice husk ash (silicon source) were used as secondary raw materials to synthesize sustainable NaP-type zeolites through a hydrothermal process. A central composite rotational experimental design was applied to evaluate the effect of the reaction time and hydrothermal temperature on the obtained zeolites crystallinity. Using the proposed experimental design, temperatures between 85 and 115 °C and different reaction times (2–28 h) were tested. It was found that the interaction between the variables (time and temperature) and both variables, independently, exerted a significant influence on the crystallinity of the zeolites. The optimal experimental conditions (105 °C and 20 h), statistically determined, enabled a high degree of crystallinity (>73%) to be achieved. Thus, the use of hazardous aluminum and agri-food wastes as unconventional precursors for the production of zeolites represents a sustainable alternative to manage these wastes, by transforming them into secondary raw materials.

1. Introduction

Zeolites are crystalline materials with a three-dimensional structure composed of AlO_4 and SiO_4 tetrahedra. Due to their unique properties, they have been extensively used in many industrial applications as adsorbents, catalysts, membrane materials, ion exchangers, and chemical sensors, among others (Abdel-Hameed et al., 2020). Zeolites represent the most important group of microporous materials (Xu et al., 2007), and their global demand is increasing, especially stimulated by the detergent industry, where synthetic zeolites are employed as an alternative to replace contaminating phosphate agents, following more restrictive regulations implemented in several countries (, 2023Markets and Markets). Zeolites can be obtained from natural deposits or synthesized from a wide variety of aluminum and silicon sources (Xu et al., 2007). According to a recent report by (2023)Markets and Markets, the global zeolite market was 4872 metric tons (12.1 billion dollars) in 2021 and an estimated 5453 metric tons (14.1 billion dollars) in 2026, of which 5.9 billion dollars correspond to synthetic zeolites.

* Corresponding author. Department of Materials, Eduardo Torroja Institute for Construction Sciences, IETcc-CSIC, Serrano Galvache Street, 4, 28033, Madrid, Spain.
E-mail address: isabel.padilla@ietcc.csic.es (I. Padilla).

https://doi.org/10.1016/j.scp.2024.101599
Received 27 February 2024; Received in revised form 18 April 2024; Accepted 28 April 2024
Available online 8 May 2024

Concerning synthetic zeolites, research efforts have recently focused on the production of zeolites using different wastes as unconventional raw materials. Converting waste into functional value-added products is of great importance for sustainability and environmental protection (Shu et al., 2023). A variety of wastes have been used in the zeolite synthesis, including coal fly ash, waste glass, alum sludge, rice husk, bauxite residue, etc. (Collins et al., 2020).

Among aluminum waste, salt slag is the main solid waste, generated in large quantities by the secondary aluminum industry (~0.5 tons of salt slag per ton of recycled aluminum produced) (Padilla et al., 2022). By 2027, it is estimated that more than 26 million metric tons of salt slag recycled aluminum will be generated worldwide (Statista, 2023), representing approximately 13 million metric tons of slat slag. The management of this waste is considered a major problem. The European Catalogue of Hazardous Waste (2001) classifies salt slag as a toxic and hazardous waste (code 10 03 08), and considered highly irritant, harmful, leachable and flammable (EWC, 2001). Salt slag contains a significant amount of harmful leachable salts and its disposal has negative effects on both the environment and human health, polluting soil and groundwater (Srivastava and Meshram, 2023). In addition, it is highly reactive in contact with water or even moisture in the air, leading to the formation of toxic gases, such as CH_4, NH_3, H_2, H_2S and PH_3, whose emissions into the atmosphere cause serious environmental damage (Tsakiridis, 2012). However, its aluminum-rich composition makes salt slag a potential candidate for zeolite synthesis. In this sense, in a preliminary study (Padilla et al., 2022), a NaP-type zeolite was synthesized using salt slag and a commercial sodium silicate as silicon source. The synthesis process was performed at 100 °C for 24 h. The as-obtained zeolite exhibited a specific surface area of 17 $m^2\ g^{-1}$, a cation exchange capacity (CEC) of 2.12 meq g^{-1} and a predominant pore size of 3.8 nm.

Regarding to silicon waste, rice husk ash (RHA) is a silicon-rich material and is considered one of the most abundant agri-food wastes. It results from the thermal transformation of rice husks, a readily available and inexpensive material. The Organization of the United Nations for Food and Agriculture (FAO, 2022) estimated that more than 31 million tons of rice husk ash would be generated in the world by the end of 2023. Although RHA is not considered a hazardous waste, its landfill disposal and slow biodegradation cause several environmental impacts. Thus, zeolite synthesis from RHA opens a new route for the use of this waste, which is presented as an alternative and low-cost substitute for commercial silica (Mallapur and Oubagaranadin, 2017; Mohamed et al., 2015; Tan et al., 2011; Tran-Nguyen et al., 2021; Vasconcelos et al., 2023). In this way, Mohamed et al. (2015) reported the synthesis of NaY zeolite, using RHA and commercial aluminate. The process involved extracting silica from the RHA through acid washing and alkali activation (NaOH) followed by a two-step synthesis in which a feedstock solution and a seed gel were prepared, kept at room temperature for 24 h and then mixed and stirred at 110 °C for the same period of time. In a similar way to the aforementioned authors, Tan et al. (2011) obtained NaY and NaA zeolites using RHA and commercial aluminate. The process consisted of preparing the seed and feedstock solution by adding the required amounts of reactants, stirring vigorously until completely mixed and then aging at room temperature for 24 h. The mixture of both solutions forms a gel that was kept at room temperature for 24 h and finally, using a Teflon bottle, heated to 100 °C for a further 5 h. The difference in the zeolitic material obtained was related to the silica extraction process; alkaline activation using NaOH pellets led to the formation of NaY-type zeolite, while with NaOH (1 M) solution, NaA zeolite was formed. Tran-Nguyen et al. (2021) obtained a NaX zeolite using RHA and commercial aluminum powder. The silicate solution was prepared by treating RHA with a 5 M NaOH solution at 90 °C for 3 h, and the aluminate solution was also produced by alkaline dissolution of the aluminum powder. The synthesis was carried out by mixing the two solutions under vigorous stirring (at 50 °C for 2 h) and heating the obtained gel at 90 °C for 4 h.

With regard to the methodologies used in zeolite synthesis, most studies report the use of processes involving several steps, as mentioned above. Furthermore, in most cases, zeolitic materials are synthesized from a single waste as a source of silicon or aluminum, supplementing the necessary content of the other precursor with chemical reagents. In this work, both hazardous salt slag and rice husk ash have been used as exclusive aluminum and silicon sources, respectively, and the hydrothermal synthesis of waste-based zeolites, more specifically NaP zeolite, was carried out in a single-step under mild conditions. To our knowledge, the combination of these two wastes has not been reported in the literature. Indeed, the process developed can be considered as a co-recycling of two different wastes. In order to determine the effect of the main synthesis parameters (time and temperature) on the crystallization of zeolites, a central composite rotational design (CCRD) was applied (Alaba et al., 2017). The use of experimental design is underexploited by researchers but represents an important optimization strategy for determining the optimal synthesis parameters, allowing the simultaneous analysis of factors at different levels and reducing the number of required experiments. Optimizing the experimental conditions is a crucial point in the synthesis of crystalline zeolites. The convencional orthogonal method, although extensively employed for optimizing operational parameters in Various processes, is not capable of generating a clear functional relationship between factors and response values, posing challenges in identifying the ideal parameter combination (Yi et al., 2010). In the present investigation, the CCRD was used to determine the optimal synthesis conditions and overcome these disadvantages of the traditional orthogonal method. The use of hazardous aluminum and agri-food wastes as less-common precursors for the production of zeolites is presented as a sustainable alternative to the waste management, generating value-added materials with promising applications, and greatly contributing to environmental preservation, circular economy, and industrial symbiosis.

2. Materials and methods

2.1. Characterization techniques

A wavelength dispersive X-ray fluorescence (XRF) spectrometer (Bruker, S8 Tiger) was used to determine the chemical composition of the raw materials. The composition of the silicate solution extracted from the RHA was analyzed by an inductively coupled plasma optical emission spectrometer (ICP-OES) (Spectro Arcos). Mineralogical characterization of the wastes and obtained zeolites

was performed by X-ray diffraction (XRD) using a Bruker D8 Advance Diffractometer with CuKα radiation, with 2θ from 5° to 60°, at a scan rate 2θ of 0.02°, 5 s per step. The crystallite sizes were calculated using the Scherrer equation (**Equation (1)**) (Scherrer, 1918):

$$D_{hkl} = {}^{K.\lambda}/_{FWHM.cos\ \theta} \quad (1)$$

where K is the constant of Scherrer (0.9), λ is the x-ray wavelength (0.154 nm), FWHM is the Full Width at Half Maximum (in rad) and θ corresponds to the diffraction angle (in rad) of the most intense reflection centered around 28.1° (2θ), corresponding to the hkl [301]. The FWHM was determined by non-linear fit to the Gauss function, using OriginPro 8.5 software. The degree of crystallinity and semiquantification of the crystalline phases of the zeolites was performed using Diffrac.Suite EVA software. The thermal behavior of rice husk ash was studied using thermogravimetric analysis and differential thermal analysis (TG/DTA) on a Thermoanalyzer model SDT-Q600 (TA Instruments), with a heating rate of 10 °C min^{-1} under an air flow of 100 mL min^{-1}. The morphology of the zeolites was examined by Scanning Electron Microscopy (SEM), using a Hitachi S4800 microscope equipped with an energy dispersive X-ray spectroscopy detector (EDS). The textural characterization of the zeolite was performed by determination of nitrogen adsorption/desorption isotherms at −196 °C in an ASAP 2010 Micromeritics system. The sample was previously outgassed at 250 °C in vacuum for 24 h. The specific surface area (S_{BET}) and pore size distribution was determined through multi-point measurements using the Brunauer-Emmett-Teller (BET) method and the Barrett-Joyner-Halenda (BJH) method, respectively. The external area (S_{Ext}) was calculated by the t-plot method from the slope of the linear fit in the thickness range (t) of 0.35–0.5 nm according to the Harkins-Jura equation. The NH_4^+ ion exchange method using a 1 M NH_4Cl solution (pH ~ 7) was applied to determine the cation exchange capacity (CEC) of the zeolites, with tests conducted in duplicate (NC 626, 2008).

2.2. Raw materials

Aluminum salt slag (ASS) and rice husk ash (RHA) were used as aluminum and silicon source, respectively, for the synthesis of zeolite type P ($Na_6Al_6Si_{10}O_{32}{\cdot}12H_2O$).

The as-received ASS (Alusigma S.A, Gijón, Spain) consisted of a dark-grayish granular solid (Fig. 1a), with a particle size distribution ranging from very fine powder (< 0.5 mm) to granules larger than 5.7 mm, and the major fraction (53%) composed of coarse grain sizes (1–4 mm). Due to its granulometric and compositional heterogeneity, salt slag was subjected to a grinding process in order to standardize the particle size (< 0.25 mm) and enable a better reaction in the synthesis stage. A sample of around 3 kg of ASS was divided into eight representative aliquots using a Laborette 27 Rotary Cone Sample Divider, with one of these aliquots used in the experiments. This procedure aimed to guarantee the reproducibility and accuracy of the results.

Due to its high NaCl content, ASS was subjected to a hydrolysis process (see Section **2.3**) before being used as a raw material in the synthesis of zeolites.

The as-received rice husk ash (RHA) (Herba Ricemills, Seville, Spain) consisted of a homogeneous dark powdery solid with some white fibers and a predominant particle size of 0.1–0.5 mm (Fig. 1c).

2.3. Pretreatment of waste materials

The salt slag was hydrolyzed in order to eliminate *(i)* excess salt that could interfere with the process of transforming the slag into zeolites and *(ii)* cause the reaction of the aluminum compounds, transforming them into oxides and thus releasing the corresponding gases (such as ammonia, hydrogen and hydrogen sulfide).

The hydrolysis of the aluminum salt slag was carried out by placing 300 g of sample in a volumetric flask and dripping distilled water using a peristaltic pump. After adding the corresponding volume of water, the suspension was maintained at a temperature of 90 °C under continuous stirring for 2 h. After filtering under pressure, the cake (hydrolyzed slag, HS) was dried for 24 h at 100 °C. HS (Fig. 1b) was the only source of aluminum used in the zeolite synthesis.

A silicate solution was prepared from calcined rice husk ash (Fig. 1d) in order to provide the silicon required for formation of zeolite. The extraction of silicon from CRHA was carried out by mixing 48 g of RHA with a 3 M NaOH solution in a Teflon-lined autoclave reactor (Parr, 1 L volume) and kept under constant stirring for a reaction time of 3 h at 120 °C. After the reaction, the products were filtered to separate the sodium silicate solution. The composition of the silicate solution was analyzed by inductively coupled plasma optical emission spectrometer (ICP-OES).

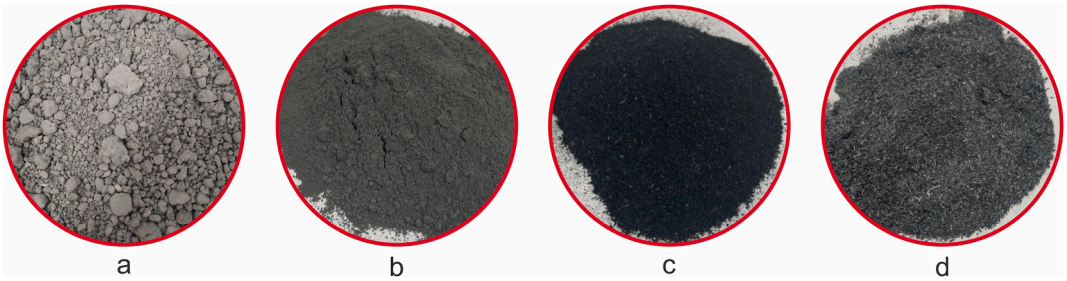

Fig. 1. Macroscopic appearance of the (a) aluminum salt slag (ASS), (b) hydrolyzed slag (HS), (c) rice husk ash (RHA) and (d) calcined rice husk ash (CRHA).

2.4. Synthesis of zeolites

The waste-based zeolites were produced following the procedure shown in Fig. 2. Synthesis was carried out in the $Na_2O–Al_2O_3–SiO_2–H_2O$ system by the conventional hydrothermal method. The reactants, solid aluminum hydrolyzed slag, and the silicate solution extracted from the CRHA, were mixed in appropriate proportions to provide the stoichiometric Si/Al ratio fot NaP-type zeolite ($Na_6Al_6Si_{10}O_{32}{\cdot}12H_2O$), and they were placed, along with the corresponding volumes of 1 M NaOH solution and distilled water, in the autoclave reactor. For the objective of synthesizing NaP type-zeolite, all the experiments were performed with continuous stirring and under autogenous pressure. Different temperatures (85–115 °C) and reaction times (2–28 h) were tested according to the experimental design (Table 1) presented in Section **2.5**. After the synthesis, the solid products were separated by filtration, rinsed with distilled water, and subjected to driying at 100 °C for 24 h.

2.5. Experimental design

Design of experiments is an important tool for modeling, developing, improving, and optimizing processes, determining the effects of factors on a response at different levels. Furthermore, this method minimizes the number of required experiments and allows the determination of the optimal factors values influencing the process (Kafshgari et al., 2017). In order to determine the optimal conditions for the hydrothermal synthesis of the zeolite, a central composite rotational design (CCRD) with two factors and two levels (2^2) was developed. Hydrothermal temperature and reaction time were considered as the independent variables influencing zeolite synthesis, and the degree of crystallinity of the obtained zeolites was chosen as the response (dependent variable). The CCRD was developed using the STATISTICA® 13.3 software. Eleven tests were carried out, using the factor scores (−1 and +1), which indicate the minimum and maximum level of each variable; 3 central points (0) and the axial portions (−1.414 and + 1.414), calculated by **Equation (2)**.

$$\alpha = (2^n)^{1/4} \tag{2}$$

where α is the axial distance from the central point and n is the number of independent variables ($n = 2$). Factor values at the central point (100 °C and 15 h) were determined based on preliminary tests. The variable levels used in this study are shown in Table 1. The statistical analysis of the experimental results were analyzed using the p-value, where values of 0.05 being statistically significant at the 95% confidence level. The optimal experimental conditions were determined based on the median of the statistical critical points.

3. Results and discussion

3.1. Characterization of raw and processed materials

The chemical composition of salt slag mainly consists of about 35 wt.% aluminum (expressed as Al_2O_3) and 18 wt.% Na_2O, along with chloride, according to the X-ray fluorescence (XRF) analysis presented in Table 2. The X-ray diffraction (XRD) pattern of the aluminum slag (Fig. 3), consistent with its chemical composition, shows the aluminum content distributed in different phases: corundum (Al_2O_3), aluminum nitride (AlN), metallic aluminum (Al) and spinel (Al_2MgO_4); and quartz (SiO_2). Salt slag exhibits pronounced

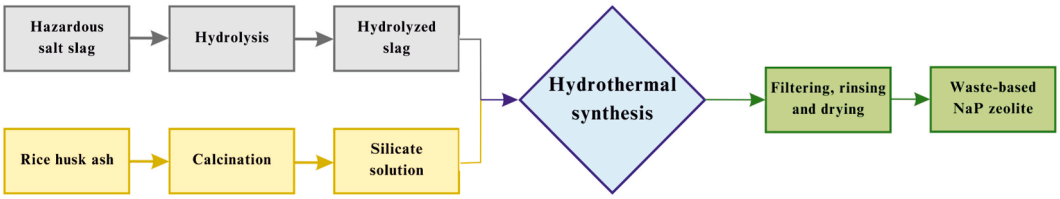

Fig. 2. Schematic procedure for the synthesis of waste-based zeolite.

Table 1
Levels of variables used for CCRD.

Variable	(-1.414)	(-1)	(0)	(+1)	(+1.414)
Hydrothermal temperature (°C)	85	90	100	110	115
Reaction time (h)	2	6	15	24	28

Table 2
Chemical composition (XRF, expressed as wt.% oxide) and loss of ignition (LOI) (%) of the aluminum salt slag (ASS), hydrolyzed slag (HS), as-received rice husk ash (RHA) and calcined rice husk ash (CRHA).

	Al_2O_3	SiO_2	Na_2O	Cl	MgO	CaO	Fe_2O_3	K_2O	ZnO	P_2O_5	TiO_2	CuO	LOI
ASS	35.5	6.4	18.3	16.7	5.1	3.9	1.7	0.5	0.4	<0.1	0.4	0.4	9.8
HS	63.5	7.7	1.6	1.5	7.9	4.5	3.0	0.2	0.8	<0.1	0.7	0.8	6.2
RHA	0.2	73.5	0.4	0.7	1.1	1.3	0.8	3.9	<0.1	1.4	–	<0.1	15.7
CRHA	0.3	89.7	0.4	<0.1	0.8	1.3	0.2	3.6	<0.1	1.7	–	–	0.2

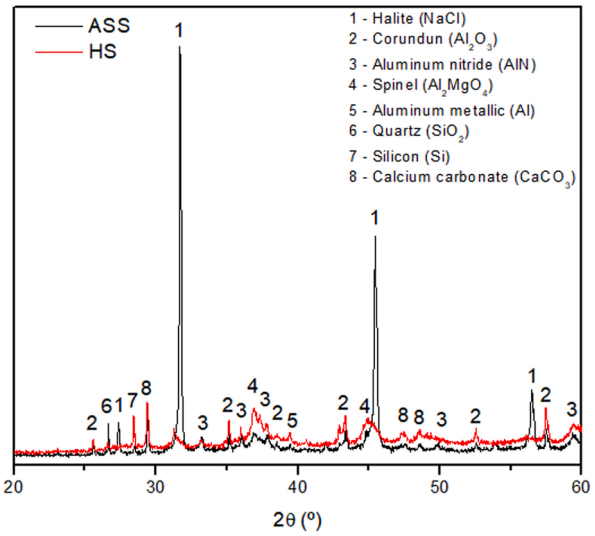

Fig. 3. XRD pattern of the aluminium salt slag (ASS) and hydrolyzed slag (HS).

peaks related to halite (NaCl), derived from the high amounts of salt used in the aluminum scrap melting process. The high background of the XRD pattern also suggest the existence of non-crystalline or amorphous phases, which may include metallic oxides such as iron oxide, among others. This presence may vary depending on the type of scrap used in the production of secondary aluminum.

Due to its high salt content, the salt slag was hydrolyzed before being used as a raw material. The main component of the hydrolyzed slag was aluminum oxide (Al_2O_3), and its content in relation to the initial composition of salt slag (Table 2) increased significantly, from 35.5% to 63.5%. This increased can be attributed to the effectiveness of the hydrolysis process, which resulted in a reduction of more than 90% in NaCl content, along with the newly formed aluminum oxides from the reaction of metallic aluminum, aluminum nitride and other aluminum compounds with water.

The chemical composition of the RHA (Table 2), shows that its main component is SiO_2 (73.5 wt.%), followed by small amounts of potassium, phosphorus, calcium, and magnesium. The XRD pattern (Fig. 4a) indicates that RHA is composed of silica in its crystalline form, cristobalite, due to the predominant presence of peak located at $2\theta = 21.8^{\circ}$ (Shinohara and Kohyama, 2004). The amorphous, crystalline or combined forms of silica are related to the ash production method and its calcination temperature. The silica contained in the ash is predominantly crystalline when high temperatures are used to calcine the rice husk (Foletto et al., 2009; Melo et al., 2014).

Due to the high LOI value (Table 2), RHA was thermally treated to eliminate the carbonaceous material. Previously, a thermal analysis was carried out to determine the optimal calcination temperature. Fig. 4b shows the TG/DTA curves. Three stages are clearly observed in TG curve. The first one, at temperature below 100 °C, corresponds to the loss of water due to humidity (2.72 wt.%). Between 200 and 600 °C, the greatest loss of mass takes place, with a value of 12.84 wt.%, which can be attributed to the combustion of carbonous material, as it is accompanied by a exothermic peak, centered around 450 °C (associated energy of 15.46 μV min mg^{-1}). Finally, a small mass loss of 1.23 wt.% can be observed between 800 and 1000 °C. This loss can be attributed to the decomposition of chlorinated compounds and/or the formation of gases containing chlorine, which occurs at high temperatures, since there is a decrease in the presence of this component, from 0.7 to <0.1 (Table 2). The total loss of mass was 16.79 % obtained by thermal analysis is quite similar to the loss of ignition (LOI) of 15.69 %. In this way, knowing the temperature required to remove the carbon content,

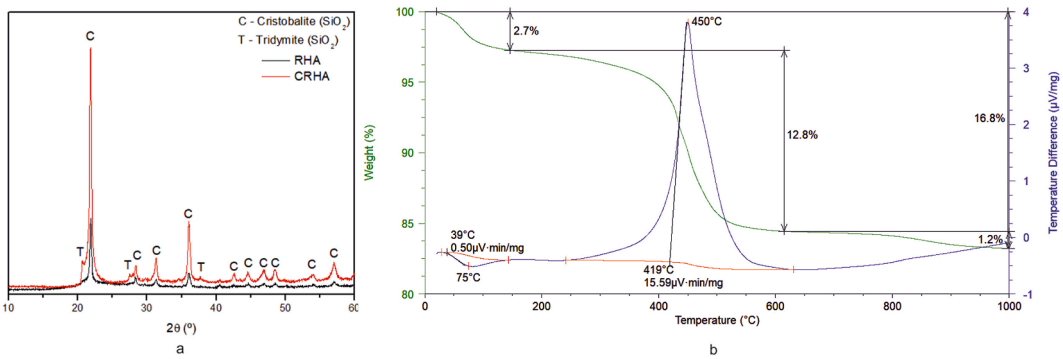

Fig. 4. (a) XRD pattern of the rice husk ash (RHA) and calcined rice husk ash (CRHA), and (b) TG/DTA curves.

the initial RHA was calcined at 800 °C for 8 h in a Thermo Concept furnace. The appearance of calcined RHA is shown in Fig. 1d and its XRD pattern (Fig. 4a) indicates that cristobalite remains the predominant component of the CRHA, but it has increased in crystallinity and other SiO_2 phase, tridymite, has developed. The LOI reduction from 15.7 to 0.2 % (Table 2) confirms the effectiveness of the calcination of the RHA.

To achieve the stoichiometric ratio of silicon for the synthesis of NaP zeolite, a silicate solution was produced from CRHA, since it is composed of high crystalline cristobalite (Fig. 4a), which is a very stable form of SiO_2, and accordingly makes it difficult to react properly (especially at lower temperatures), with aluminate ions. The silicate solution consisted mainly of Na (69.7 g L^{-1}) and Si (58.3 g L^{-1}), with minor participation of other elements (Table 3).

3.2. Statistical analysis of the waste-based zeolite synthesis

The synthesis of the waste-based zeolites was carried out using hydrolyzed slag and silicate solution from calcined rice husk ash as aluminum and silicon sources, respectively. The effect of the synthesis parameters on the zeolites crystallization was explored using a CCRD (Table 1). According to the experimental design proposed, hydrothermal temperatures between 85 and 115 °C were tested using different reaction times (2–28 h). The 2^2-CCRD data matrix with the sample names, factor values and responses is presented in Table 4.

Most of the conditions tested showed a degree of crystallization of over 70% for the waste-based NaP zeolites, with the exception of runs 1 and 7, in which lower reaction times were used. In run 3, although a low reaction time (6 h) was also used, the hydrothermal temperature was higher (110 °C), resulting in a sample with 72% crystallinity. Using a high hydrothermal temperature (110 °C) for the longest reaction time (24 h), run 4 resulted in the highest crystallinity, 73.9%. The estimated effects, presented in Table 5, were based on the p-value. At a significance level of 95%, the planning determined that, in the implemented model, the interaction ($Q_1 vs Q_2$) between the variables (time and temperature) had a significant influence ($p < 0.05$) on the crystallization of synthetic zeolites. In addition, the independent variables temperature (Q_1) in linear form, and time (Q_2) in both linear and quadratic form, were also significant ($p < 0.05$) and influenced the crystallization process. The crystallinity of the waste-based zeolites is linearly dependent on the hydrothermal temperature and reaction time, and their effects are positive (3.2941 and 4.1572, respectively), i.e., when increasing temperature and time there is also an increase in the degree of crystallization of the zeolite. Coefficient of determination (R^2) provides the measure of the proportion of variation explained by the regression equation in relation to the variation in responses. For the zeolite crystallization, an $R^2 = 0.8367$ was obtained, indicating that the model is able to explain approximately 83.7% of the

Table 3
Quantitative chemical composition of silicate solution from CRHA (ICP–OES, in g L^{-1}).

Na	Si	K	S	Al	Ca	Fe	Mg
69.7	58.3	4.1	0.27	0.14	0.007	0.006	<0.001

Table 4
Factorial design (2^2) results for waste-based zeolite synthesis using HS and CRHA.

Run n°	Factors				Sample	Responses
	Hydrothermal Temperature		Reaction Time			
	Factor Level	Temperature (°C)	Factor Level	Time (h)		Crystallinity (%)
1	−1	90	−1	6	Z90-6	63.2
2	−1	90	1	24	Z90-24	71.4
3	1	110	−1	6	Z110-6	72.0
4	1	110	1	24	Z110-24	73.9
5	−1.414	85	0	15	Z85-15	70.3
6	1.414	115	0	15	Z115-15	72.1
7	0	100	−1.414	2	Z100-2	68.5
8	0	100	1.414	28	Z100-28	72.7
9	0	100	0	15	Z_A100-15	72.0
10	0	100	0	15	Z_B100-15	71.4
11	0	100	0	15	Z_C100-15	71.5

Table 5
Estimated effects for the crystallization of the waste-based zeolites.

	Coefficient	Effect	Standard error	t(2)	p-value
Temperature (L)	Q_1	*3.2941*	*0.2205*	*14.9382*	*0.0045*
Temperature (Q)	Q_{12}	−0.6844	0.2461	−2.7808	0.1086
Time (L)	Q_2	*4.1572*	*0.2301*	*18.0673*	*0.0030*
Time (Q)	Q_{22}	*−1.6467*	*0.2797*	*−5.8873*	*0.0277*
Temperature vs Time	$Q_1 vs Q_2$	*−3.1500*	*0.3214*	*−9.7992*	*0.0103*

L: Linear; Q: Quadratic; p-value significant at $p < 0.05$.

variations in the crystallization of the obtained zeolites. The variance analysis (ANOVA) was performed, and it was found that for the crystallization of the zeolites, $F_{calculated} > F_{tabulated}$ (Table 6), confirming the statistical representativeness of the sample distribution. Therefore, the ANOVA regarding the crystallization of the obtained zeolites demonstrated the validity of the model within the 95% confidence interval, indicating no need for adjustments within the examined range. This outcome indicates an excellent reproduction of the experimental samples.

According to (Núñez-Gómez et al., 2017), the linear and quadratic coefficients, along with their interations, are part of the template employed to construct the surface that define the optimal conditions for maximizing the response. Response surface and contour curve graphics (Fig. 5) allow visualization of the optimal (or near optimal) values, in which the combination of variables led to these better responses. The results indicate that zeolite crystallization was maximum (>74%) when the synthesis was performed at high temperatures (>115 °C), even with shorter reaction times of up to 18 h (Fig. 5). In other conditions, the interaction between these two variables determines the degree of crystallization of the obtained zeolites. Using longer reaction times, high crystallinity can be obtained even at lower temperatures. At temperatures of up to 100 °C, synthesis times of over 24 h are required to obtain crystallinity of up to 74%. The same occurs at shorter times using higher hydrothermal temperatures. A synthesis conducted for 6 h can result in a zeolite with a degree of crystallinity of up to 72% when using a temperature of 110 °C.

This indicates that there was variation in the crystallization process of the synthetic zeolites related to the hydrothermal temperature and reaction time, in agreement with the corresponding p-value discussed above (Table 5). The critical values statistically determined using the STATISTICA® 13.3 software, were a hydrothermal temperature of 105 °C and a reaction time of 20 h. An experiment with these determined factor values was conducted to assess the validity of the results, as other experimental factors were not taken into account in the statistical analysis. In this sample (named Z_{oc}105-20), a high degree of crystallinity was observed (73.4%), even though an intermediate temperature and reaction time were used. This value was only slightly below than that of run 4, which resulted in a crystallinity of 73.9%. However, in this case, the synthesis was carried out at a higher temperature (110 °C) and using a longer reaction time (24 h). The observed difference in terms of crystallinity of the obtained zeolites is very small considering the energy and time savings between the two processes, so the results demonstrate the suitability of CCRD planning to determine the optimum synthesis conditions.

Equation (3) represents the model describing the degree of crystallization (%). A quadratic regression of the functional variable for the crystallinity response is proposed, where 't' represents the reaction time and 'T' denotes the hydrothermal temperature.

$$\text{Crystallinity (\%)} = 23.172 + 0.427\ T + 2.240\ t + 0.009\ t^2 - 0.0175\ t\ T \quad (3)$$

Table 6
Analysis of variance for the waste-based zeolite crystallization for the 2^2 factorial design.

Variation source	SS	df	MS	F		*p*
				Calc.	Tab.[a]	
Regression	68.0548	3	22.6849	11.153	4.347	<0.05
Sediments	14.2416	7	2.0345			
Total	82.2963	10				

SS: sum of square; df: degree of freedom; MS: mean of square; F: Fisher's ratio; p: probability.
[a] Tabulated values (Box et al., 1978).

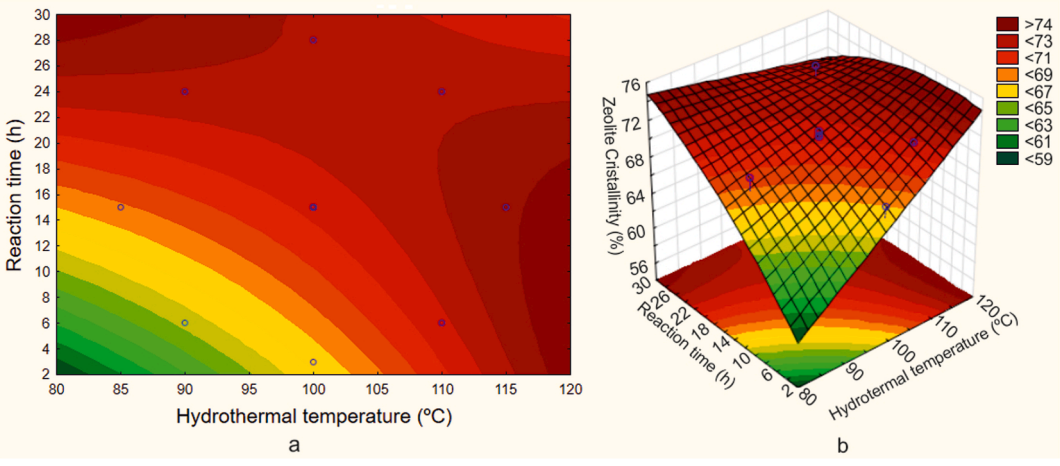

Fig. 5. (a) Response surface and (b) contour curve for waste-based zeolite crystallization.

3.3. Characterization of the synthesized waste-based zeolites

The XRD spectra of the waste-based zeolites synthesized under different conditions (Runs 1 to 11, Table 4) are shown in Fig. 6.

All samples presented a profile characteristic of tetragonal type P zeolite (NaP, $Na_6Al_6Si_{10}O_{32}{\cdot}12H_2O$). According to Hansen et al. (1993), the different symmetries (cubic, tetragonal or orthorhombic) depend on the synthesis conditions. In this regard, Sánchez-Hernández et al. (2016) also obtained a NaP zeolite with tetragonal symmetry, using different aluminum waste (sleeve filter fine dust from slag milling) and commercial waterglass by hydrothermal synthesis at 120 °C for 6 h. Padilla et al. (2022) synthesized a NaP-type zeolite with cubic symmetry from salt slag and commercial silicate at 100 °C for 24 h. This corroborates the influence of the experimental synthesis conditions, but also indicates that the starting reagents used affect the symmetry of the zeolite crystals.

The XRD pattern of the obtained zeolites exhibits narrow, well-defined peaks, with the most intense reflection centered around 28.1° (2θ), corresponding to the hkl [301]. The difference in the intensity and FWHM of this peak with the synthesis conditions can be seen in Fig. 7.

Table 7 shows the intensity, diffraction angle (2θ) and Full Width at Half Maximum (FWHM) of the most intense diffraction peak [301] for each waste-based zeolite synthesized, as well as the crystallite size (D_{hkl}) determined using the Scherrer equation (**Equation (1)**) (presented in Section 2.1). The obtained zeolites showed the most intense peak (3042–5063 counts) centered between 28.07° and 28.14° (2θ), and the crystallite sizes ranged from 21 to 28 nm. For the samples corresponding to the central points of the CCRD (Z_A100-15, Z_B100-15 and Z_C100-15), determined to assess the repeatability of the results, the average values of the peak parameters were calculated. A maximum intensity of 4490 ± 331 counts was observed, centered on the diffraction angle 28.08° ± 0.01°, with a FWHM of 0.33° ± 0.03° and a crystallite size of 25 nm ± 2 nm.

In addition to the peak parameters and crystallite sizes, the semi-quantification of the most crystalline phases for the Z90-24, Z110-6, Z110-24 and Z_{OC}105-20 waste-based zeolites (obtained using the Diffrac.Suite EVA software) and the yield of the synthesis reaction are shown in Table 8.

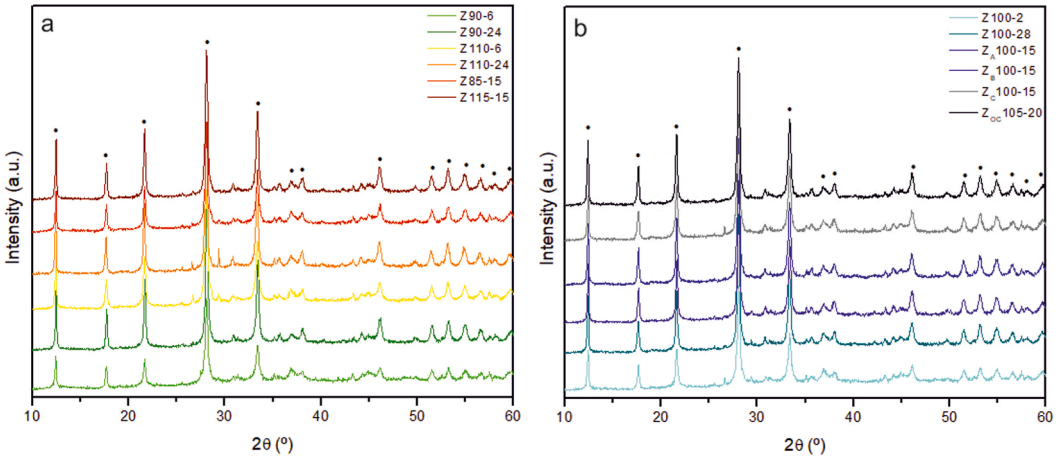

Fig. 6. XRD spectra of zeolite materials synthesized under various parameter settings: (a) Run 1-Run 6 and (b) Run 7-Run 11 and Z_{OC}105-20 (• = NaP zeolite, reference file ICDD PDF = 39–0219).

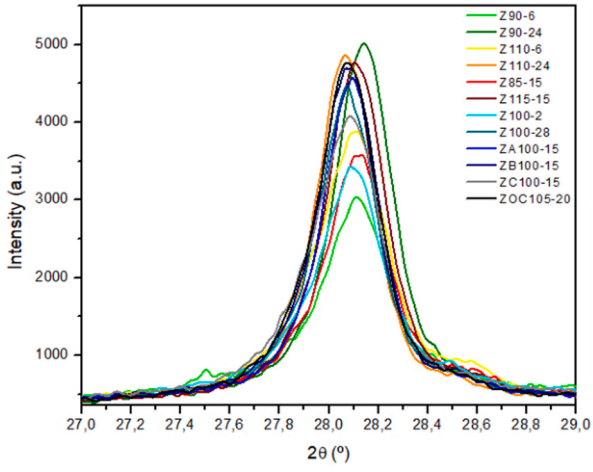

Fig. 7. Most intense reflection of the synthesized waste-based zeolites.

Table 7
Peak parameters (intensity, 2θ and FWHM) and crystallite sizes (D_{hkl}) of the synthesized waste-based zeolites.

Sample	Intensity (counts)	2θ (°)	FWHM (°)	D_{hkl} (nm)
Z90-6	3042	28.11	0.3950	21
Z90-24	5063	28.14	0.3117	26
Z110-6	3910	28.09	0.3901	21
Z110-24	4892	28.07	0.2968	28
Z85-15	3270	28.11	0.3513	23
Z115-15	4821	28.11	0.3183	26
Z100-2	3456	28.09	0.3706	22
Z100-28	4509	28.07	0.3165	26
Z_A100-15	4619	28.09	0.3064	27
Z_B100-15	4738	28.07	0.3158	26
Z_C100-15	4114	28.07	0.3614	23
Z_{OC}105-20	4778	28.07	0.3280	25

Table 8
Semi-quantification of the NaP zeolite (reference file ICDD PDF = 39–0219) and yield of the synthesis reaction.

Sample	NaP (%)	Yield (Kg zeolite/Kg HS)
Z90-24	89.1	1.70
Z110-6	82.6	1.69
Z110-24	83.6	1.75
ZOC105-20	90.8	1.77

The semi-quantitative analysis of the samples shows that the waste-based zeolite synthesis resulted in the formation of materials with high NaP zeolite content, ranging from 82.6% (Z110-6) to 90.8% (Z_{OC}105-20). No other type of zeolite was observed. However, small amounts of compounds from salt slag that did not react completely could be tentatively identified in these samples, including corundum and spinel. Furthermore, for each kg of hydrolyzed slag used in the synthesis process, between 1.69 and 1.77 kg of zeolites can be produced. The zeolite synthesized at 110 °C for 24 h (Z110-24) showed a slightly higher yield (1.75) and percentage of NaP zeolite (83.6%) compared to the synthesis carried out for 6 h (Z110-6), which were 1.69 and 82.6%, respectively. Also, the longer reaction time increased the crystallinity of this sample (73.9%) compared to the previous one (72.0%) (Table 4). Despite the lower yield (1.70) and crystallinity (71.4%) compared to Z110-24, sample Z90-24 has significantly higher amount of NaP zeolite, 89.1% compared to 83.6%. Comparing samples Z90-24 and Z110-6, it can be observed that a longer reaction time has a greater impact than temperature on crystallinity, resulting in a higher content of NaP zeolite in the synthesized material. Although the Z_{OC}105-20 sample presents a slightly lower degree of crystallinity (73.4%) than that obtained for Z110-24 (73.9%), it was the one that obtained the highest yield (1.77) and the highest content of NaP zeolite (90.8%). This confirms that the optimal experimental conditions for hydrothermal synthesis, obtained through CCRD, are a moderate temperature of 105 °C and a reaction time of 20 h.

The textural properties of the selected zeolites Z90-24, Z110-6, Z110-24 and Z_{OC}105-20, including specific surface area (S_{BET}), external surface area (S_{Ext}) and pore size, determined from adsorption isotherms/N_2 desorption (Fig. 8a), as well as their cation exchange capacity (CEC) are presented in Table 9.

The nitrogen adsorption/desorption isotherms of the zeolites showed the same type IV behavior typical of mesoporous materials (2–50 nm). The mesoporous characteristic of NaP zeolite possibly results from the assembly of nanometric crystallites that form its

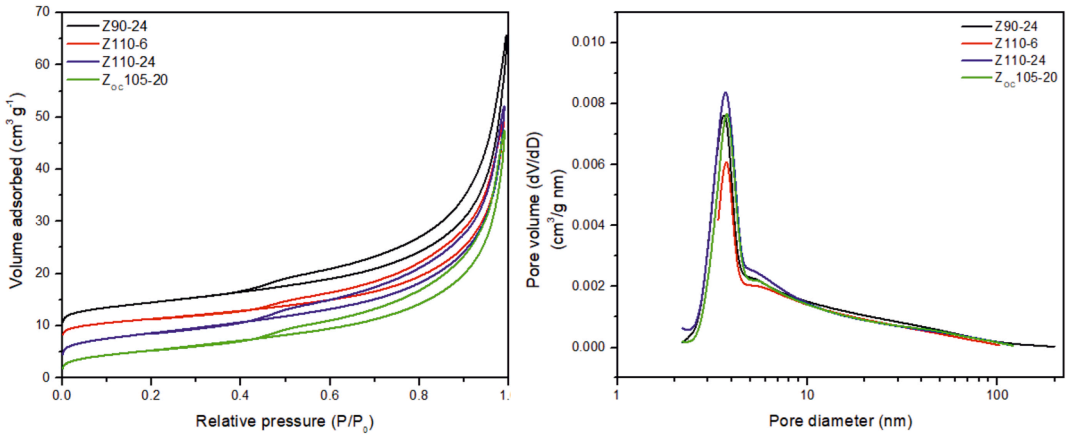

Fig. 8. (a) Nitrogen adsorption/desorption isotherms and (b) distribution of pore diameter of the waste-based NaP zeolites.

Table 9
Textural properties and CEC of the synthesized waste-based zeolites.

	S_{BET} ($m^2\ g^{-1}$)	S_{Ext} ($m^2\ g^{-1}$)	Micropore volume ($x10^{-4}\ cm^3\ g^{-1}$)	Pore size (nm)	CEC (meq g^{-1})
Z90–24	22.45	22.11	1.86	3.80	3.55 ± 0.002
Z110–6	18.49	17.53	4.82	3.79	2.86 ± 0.054
Z110–24	23.18	23.57	Not determined	3.80	3.23 ± 0.035
Z_{OC}105–20	21.11	20.77	1.89	3.80	3.67 ± 0.039

aggregates (Sayehi et al., 2020). In all cases, the hysteresis loop (H3 type – according to the IUPAC classification) was observed at P/P_0 range between 0.45 and 0.98 (maximum pressure) indicating the presence of many nanometer-sized pores and characterizing solid materials with slit-shaped pores of non-uniform sizes or shapes (Bandura et al., 2015). The pore size distribution curve, acquired by the BJH method (Fig. 8b) shows a mesoporous distribution with a predominant pore size of 3.8 nm observed in all samples. The smaller peaks located at 5.4 nm (Z90-24, Z110-6 and Z110-24) and 5.6 nm (Z_{OC}105-20) could indicate a secondary pore size.

In terms of S_{BET} (Table 9), values between 18.49 and 23.18 $m^2\ g^{-1}$ were obtained. The observation of tabulated values suggests that the difference in surface area of the obtained zeolites was influenced to a greater extent by the reaction time than by the synthesis temperature. The Z_{OC}105-20 zeolite, synthesized under optimal experimental conditions, showed a S_{BET} of 21.11 $m^2\ g^{-1}$ and S_{ext} = 20.77 $m^2\ g^{-1}$. This small difference indicates the low micropore volume (1.89 × 10^{-4} $cm^3\ g^{-1}$) of the zeolite. The small micropore volume observed in the samples is probably due to the shape (bottleneck) of the micropores, which interferes with the entry of the gas and, consequently, its determination (Sharma et al., 2016). S_{BET} values were higher when compared to those obtained for NaP-type zeolites using other aluminum waste (14.2 $m^2\ g^{-1}$) (Sánchez-Hernández et al., 2016), salt slag (17.0 $m^2\ g^{-1}$) (Padilla et al., 2022) and fly ash (18.5 $m^2\ g^{-1}$) (Liu et al., 2018). Although differences in the degasification conditions may affect these values of S_{BET}, the results obtained in this work indicate that the waste-based NaP zeolite owing potential characteristic to be used as an adsorbent material.

The CEC values for NH_4Cl ranged from 2.86 to 3.67 meq g^{-1} for the synthesized NaP zeolites. The highest CEC (3.67 meq g^{-1}) was obtained for the zeolite Z_{OC}105-20. This value is higher than those reported for waste-based NaP-type zeolites. Using aluminum waste, as already mentioned, Padilla et al. (2022) and Sánchez-Hernández et al. (2016), obtained a CEC of 2.12 and 2.73 meq g^{-1}, respectively. From coal fly ash, Cardoso et al. (2015) obtained CEC of 2.6 meq g^{-1} through hydrothermal synthesis with 3 M NaOH at 100 °C for 24 h. Musyoka et al. (2012) achieved a CEC of 2.98 meq g^{-1} in a two-step synthesis at 100 °C for 48 h. Additionally, Zhou et al. (2023) reported a CEC of 2.58 meq g^{-1} for zeolite synthesized in a two-step process with a microwave reaction at 180 °C for 2 h after 12 h of stirring. This characteristic also enables zeolite to be used as an adsorbent.

The morphology of the Z90-24, Z110-6, and Z110-24 zeolites at different magnifications is shown in Fig. 9. All the samples exhibited a homogeneous 'cauliflower-like' morphology, characteristic of NaP-type structures (Sánchez-Hernández et al., 2016). In the figure, it can be observed that the units constituting the aggregates are particles measuring between 420 and 990 nm, while the joining of these units forms conglomerates measuring between 2 and 5 μm.

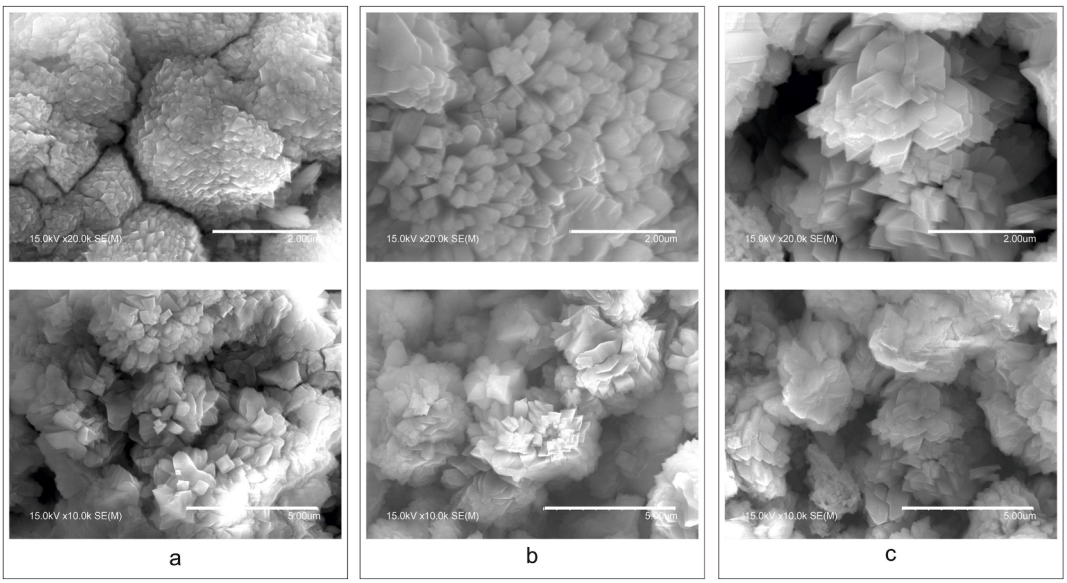

Fig. 9. SEM images of the waste-based zeolites (a) Z90-24, (b) Z110-6 and (c) Z110-24, at different magnifications.

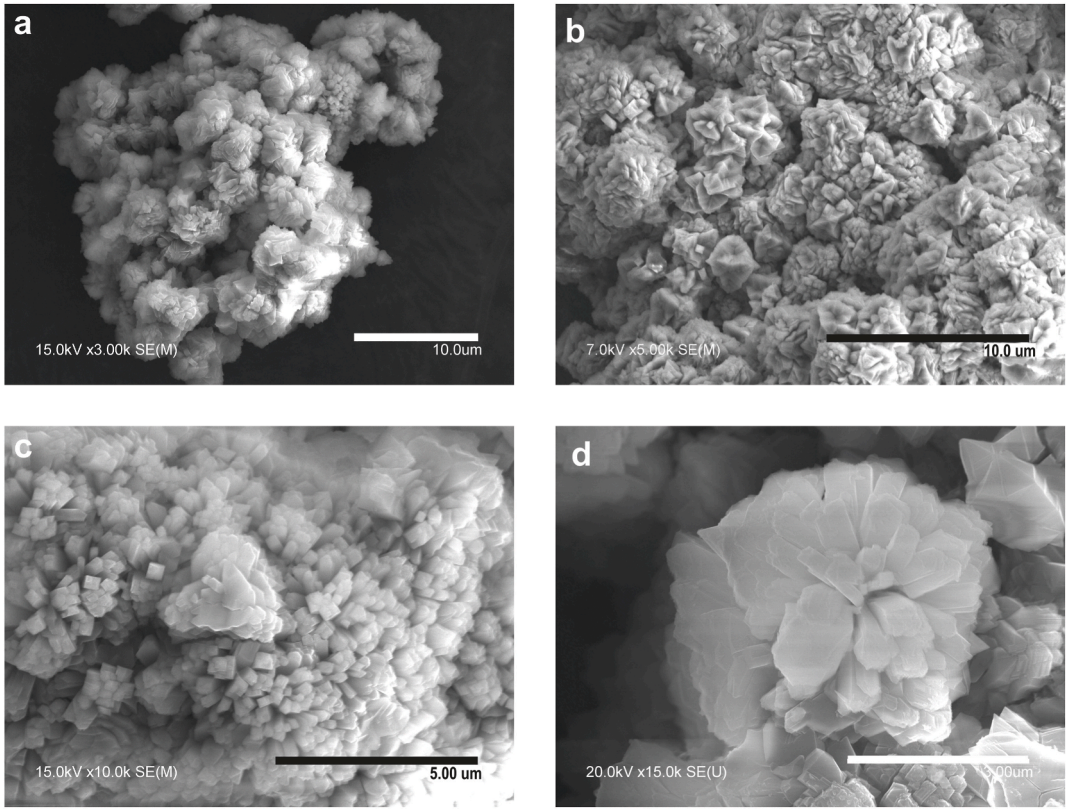

Fig. 10. SEM images of the waste-based zeolite synthesized under the optimal conditions at different magnifications.

Fig. 10 shows the SEM images at different magnifications of the Z_{OC}105-20 zeolite. This NaP zeolite exhibited a morphology composed by agglomerates of around 10–50 μm (Fig. 10a and **b**). As can be seen at high magnification (Fig. 10c and **d**), these clusters were formed by smaller secondary aggregates with defined contours growing in different directions.

4. Conclusion

In this study, hazardous salt slag (aluminum source) and rice husk ash (silicon source) were valorized through their use as uncommon raw materials for the production of zeolites with excellent sorbent characteristics and promising applications. Almost all the tested synthesis conditions showed a degree of crystallization greater than 70% for the waste-based NaP zeolites. It was found that the variables of time and temperature, separately and the interaction between them, exerted a significant influence on the crystallization of the zeolites. The optimal experimental conditions (105 °C and 20 h), statistically determined, resulted in a zeolite with a high degree of crystallinity (73.4%) and containing more than 90% zeolitic material. ANOVA analysis regarding the crystallization of the obtained zeolites indicated that the valitiy of the model within the 95% confidence interval, and no adjustment were required within the evaluated range. This led to an outstanding reproducibility of experimental samples. Both S_{BET} (21.11 $m^2\ g^{-1}$) and CEC (3.67 meq g^{-1}) showed higher values than those reported by other authors for the synthesis of NaP-type zeolites using different wastes, suggesting adequate properties of the waste-based NaP-zeolite for effluent treatments via adsorption and ion exchange mechanisms. The co-recycling of both hazardous aluminum and agri-food wastes into zeolites promotes an industrial symbiosis and can be considered a sustainable alternative in waste management, generating value-added materials and greatly contributing to environmental preservation.

CRediT authorship contribution statement

Magali Teresinha Ritter: Writing – original draft, Investigation, Formal analysis, Data curation. **María Ángeles Lobo-Recio:** Writing – review & editing. **Isabel Padilla:** Writing – review & editing, Supervision, Methodology. **Maximina Romero:** Writing – review & editing. **Aurora López-Delgado:** Writing – review & editing, Supervision, Conceptualization.

Declaration of competing interest

The authors declare that they have no known competing financial interests or personal relationships that could have appeared to influence the work reported in this paper.

Data availability

No data was used for the research described in the article.

Acknowledgements

This research was financed by the LIFE Project 101114027 — LIFE22-ENV-ES-Z-ONA4LIFE, and Eduardo Torroja Institute for Construction Sciences (IETcc-CSIC), Spain. This work was supported by the Brazilian National Council of Scientific and Technologic Development (CNPq), Brazil and Coordination for the Improvement of the Higher-Level Personnel (CAPES), Brazil-finance code 001. The authors thank Herba Ricemills S.L.U (Spain) for providing the rice husk ash sample and Alusigma S.A (Spain) for supplying the salt slag sample.

References

Abdel-Hameed, R., Farghaly, E.E., Abdel-Aal, E.A., Ibrahim, I.A., Ahmed, M.A., Abdel-Messih, M.F., Abdel Khalek, M.A., 2020. Exploitation of industrial solid wastes for preparing zeolite as a value-added product and its kinetics as adsorbent for heavy metal ions. Physicochem. Probl. Miner. Process. 57 (1), 87–99. https://doi.org/10.37190/ppmp/128744.

Alaba, P.A., Sani, Y.M., Mohammed, I.Y., Abakr, Y.A., Daud, W.M.A.W., 2017. Synthesis of hierarchical nanoporous HY zeolites from activated kaolin, a central composite design optimization study. Adv. Powder Technol. 28 (5), 1399–1410. https://doi.org/10.1016/j.apt.2017.03.008.

Bandura, L., Franus, M., Józefaciuk, G., Franus, W., 2015. Synthetic zeolites from fly ash as effective mineral sorbents for land-based petroleum spills cleanup. Fuel 147, 100–107. https://doi.org/10.1016/j.fuel.2015.01.067.

Box, G.E.P., Hunter, W.G., Hunter, J.S., 1978. Fractional factorial design at two levels, Statistics for Experimenters: an Introduction to Design, Data Analysis, and Model Building. John Wiley & Sons, Inc, New Jersey, pp. 374–418.

Cardoso, A.M., Horn, M.B., Ferret, L.S., Azevedo, C.M.N., 2015. Integrated synthesis of zeolites 4A and Na–P1 using coal fly ash for application in the formulation of detergents and swine wastewater treatment. J. Hazard Mater. 287, 69–77. https://doi.org/10.1016/j.jhazmat.2015.01.042.

Collins, F., Rozhkovskaya, A., Outram, J.G., Millar, G.J., 2020. A critical review of waste resources, synthesis, and applications for Zeolite LTA. Microporous Mesoporous Mater. 291, 109667. https://doi.org/10.1016/j.micromeso.2019.109667.

EWC, 2001. European Waste Catalogue and Hazardous Waste List, Published by Environmental Protection Agency. Ireland. https://ec.europa.eu/eurostat/documents/342366/351806/Guidance-on-EWCStat-categories-2010.pdf/0e7cd3fc-c05c-47a7-818f-1c2421e55604 (Accessed 10 February 2024).

FAO, 2022. Food Agricult. Organizat. United Nat. 2022. Avaiable online: https://www.fao.org/home/en. (Accessed 24 January 2024).

Foletto, E.L., Castoldi, M.M., Oliveira, L.H., Hoffmann, R., Jahn, S.L., 2009. Conversion of rice husk ash into zeolitic materials. Lat. Am. Appl. Res. 39, 75–78.

Hansen, S., Hakansson, U., Landa-Canovas, A.R., Falth, L., 1993. On the crystal chemistry of NaP zeolites. Zeolites 13 (4), 276–280.

Kafshgari, L.A., Ghorbani, M., Azizi, A., Agarwal, S., Gupta, V.K., 2017. Modeling and optimization of Direct Red 16 adsorption from aqueous solutions using nanocomposite of $MnFe_2O_4$/MWCNTs: RSM-CCRD model. J. Mol. Liq. 233, 370–377. https://doi.org/10.1016/j.molliq.2017.03.047.

Liu, Y., Yan, C., Zhao, J., Zhang, Z., Wang, H., Zhou, S., Wu, L., 2018. Synthesis of zeolite P1 from fly ash under solvent-free conditions for ammonium removal from water. J. Clean. Prod. 202, 11–22. https://doi.org/10.1016/j.jclepro.2018.08.128.

Mallapur, V.P., Oubagaranadin, J.U.K., 2017. A brief review on the synthesis of zeolites from hazardous wastes. Trans. Indian Ceram. Soc. 76 (1), 1–13. https://doi.org/10.1080/0371750X.2016.1231086.

Markets and Markets. Zeolites Market by Type (Natural, Synthetic), Function (Ion-Exchange, Catalyst, Molecular Sieve), Synthetic Zeolite Application (Detergents, Adsorbent, Catalysts), Natural Zeolite Application, and Region – Global Forecast to 2026. Avaiable online: https://www.marketsandmarkets.com/Market-Reports/zeolites-market-76442083.html. Accessed on: 5 October. 2023.

Melo, C.R., Francisco, A.C., Kuhnen, N.C., Rocha, M.R., Melo, A.R., Riella, H.G., Angioletto, E., 2014. Production of zeolite from rice husk ash. Mater. Sci. Forum 798–799, 617–621. https://doi.org/10.4028/www.scientific.net/MSF.798-799.617.

Mohamed, R.M., Mkhalid, I.A., Barakat, M.A., 2015. Rice husk ash as a renewable source for the production of zeolite NaY and its characterization. Arab. J. Chem. 8 (1), 48–53. https://doi.org/10.1016/j.arabjc.2012.12.013.

Musyoka, N.M., Petrik, L.F., Gitari, W.M., Balfour, G., Hums, E., 2012. Optimization of hydrothermal synthesis of pure phase zeolite Na-P1 from South African coal fly ashes. J. Environ. Sci. Health, Part A 47 (3), 337–350. https://doi.org/10.1080/10934529.2012.645779.

NC 626, 2008. Natural Zeolites - Determination of Exchange Capacity Total Cationic - Ammonium Chloride Method.

Núñez-Gómez, D., Lapolli, F.R., Nagel-Hassemer, M.E., Lobo-Recio, M.Á., 2017. Optimization of acid mine drainage remediation with central composite rotatable design model. Energy Proc. 136, 233–238. https://doi.org/10.1016/j.egypro.2017.10.248.

Padilla, I., Romero, M., López-Andrés, S., López-Delgado, A., 2022. Sustainable management of salt slag. Sustainability 14 (9), 4887. https://doi.org/10.3390/su14094887.

Sánchez-Hernández, R., López-Delgado, A., Padilla, I., Galindo, R., López-Andrés, S., 2016. One-step synthesis of NaP1, SOD and ANA from a hazardous aluminum solid waste. Microporous Mesoporous Mater. 226, 267–277. https://doi.org/10.1016/j.micromeso.2016.01.037.

Sayehi, M., Garbarino, G., Delahay, G., Busca, G., Tounsi, H., 2020. Synthesis of high value-added Na–P1 and Na-FAU zeolites using waste glass from fluorescent tubes and aluminum scraps. Mater. Chem. Phys. 248, 122903. https://doi.org/10.1016/j.matchemphys.2020.122903.

Scherrer, P., 1918. Estimation of the size and internal structure of colloidal particles by means of röntgen, Nachrichten von der Gesellschaft der Wissenschaften zu Göttingen. 2, 96–100.

Sharma, P., Song, J.S., Han, M.H., Cho, C.H., 2016. GIS-NaP1 zeolite microspheres as potential water adsorption material: influence of initial silica concentration on adsorptive and physical/topological properties. Sci. Rep. 6 (1), 22734. https://doi.org/10.1038/srep22734.

Shinohara, Y., Kohyama, N., 2004. Quantitative analysis of tridymite and cristobalite crystallized in rice husk ash by heating. Ind. Health 42 (2), 277–285.

Shu, R., Qiao, Q., Guo, F., Dong, K., Liu, S., Xu, L., Bai, Y., Zhou, N., 2023. Controlled design of Na–P1 zeolite/porous carbon composites from coal gasification fine slag for high-performance adsorbent. Environ. Res. 217, 114912. https://doi.org/10.1016/j.envres.2022.114912.

Srivastava, A., Meshram, A., 2023. On trending technologies of aluminium dross recycling: a review. Process Saf. Environ. Protect. 171, 38–54. https://doi.org/10.1016/j.psep.2023.01.010.

Statista, 2023. Market volume of secondary aluminum worldwide in 2020, with a forecast for 2027. Avaiable online: https://www.statista.com/statistics/1306589/global-market-volume-of-secondary-aluminum. (Accessed 5 September 2023).

Tan, W.-C., Yap, S.-Y., Matsumoto, A., Othman, R., Yeoh, F.-Y., 2011. Synthesis and characterization of zeolites NaA and NaY from rice husk ash. Adsorption 17 (5), 863–868. https://doi.org/10.1007/s10450-011-9350-6.

Tran-Nguyen, P.L., Lyb, K.-P., Thanhb, L.H.V., Angkawijayac, A.E., Santosod, S.P., Trane, N.-P.-D., Tsaie, M.-L., Juc, Y.-H., 2021. Facile synthesis of zeolite NaX using rice husk ash without pretreatment. J. Taiwan Inst. Chem. Eng. 123, 338–345. https://doi.org/10.1016/j.jtice.2021.05.009.

Tsakiridis, P.E., 2012. Aluminium salt slag characterization and utilization – a review. J. Hazard Mater. 217–218, 1–10. https://doi.org/10.1016/j.jhazmat.2012.03.052.

Vasconcelos, A.A., Len, T., Oliveira, A.N., da Costa, A.A.F., Souza, A.R.S., da Costa, C.E.F., Luque, R., Filho, G.N.R., Noronha, R.C.R., do Nascimento, L.A.S., 2023. Zeolites: a theoretical and practical approach with uses in (Bio)Chemical processes. Appl. Sci. 13 (3), 1897. https://doi.org/10.3390/app13031897.

Xu, R., Pang, W., Yu, J., Huo, Q., Chen, J., 2007. Chemistry of Zeolites and Related Porous Materials: Synthesis and Structure [s.l.]. John Wiley & Sons.

Yi, S., Su, Y., Qi, B., Su, Z., Wan, Y., 2010. Application of response surface methodology and central composite rotatable design in optimizing the preparation conditions of vinyltriethoxysilane modified silicalite/polydimethylsiloxane hybrid pervaporation membranes. Sep. Purif. Technol. 71 (2), 252–262. https://doi.org/10.1016/

j.seppur.2009.12.005.
Zhou, Q., Jiang, X., Qiu, Q., Zhao, Y., Long, L., 2023. Synthesis of high-quality Na P1 zeolite from municipal solid waste incineration fly ash by microwave-assisted hydrothermal method and its adsorption capacity. Sci. Total Environ. 855, 158741. https://doi.org/10.1016/j.scitotenv.2022.158741.

APPENDIX B – WASTE SYMBIOSIS THROUGH THE SYNTHESIS OF HIGHLY CRYSTALLINE LTA AND SOD ZEOLITES

materials

MDPI

Article

Waste Symbiosis through the Synthesis of Highly Crystalline LTA and SOD Zeolites

Magali Teresinha Ritter [1,2], Isabel Padilla [1], María Ángeles Lobo-Recio [2,3], Maximina Romero [1] and Aurora López-Delgado [1,*]

[1] Department of Materials, Eduardo Torroja Institute for Construction Sciences (IETcc-CSIC), Serrano Galvache Street, 4, 28033 Madrid, Spain; magali.ritter@posgrad.ufsc.br (M.T.R.); isabel.padilla@ietcc.csic.es (I.P.); mromero@ietcc.csic.es (M.R.)
[2] Department of Environmental Engineering, Federal University of Santa Catarina (UFSC), Campus Reitor João David Ferreira Lima, Florianópolis 88040-900, SC, Brazil; maria.lobo@ufsc.br
[3] Department of Energy and Sustainability, Federal University of Santa Catarina (UFSC), Campus Araranguá, Rodovia Governador Jorge Lacerda, 3201, Jardim das Avenidas, Araranguá 88906-072, SC, Brazil
* Correspondence: alopezdelgado@ietcc.csic.es

Abstract: In recent years, the demand for natural and synthetic zeolites has surged due to their distinctive properties and myriad industrial applications. This research aims to synthesise crystalline zeolites by co-recycling two industrial wastes: salt slag (SS) and rice husk ash (RHA). Salt slag, a problematic by-product of secondary aluminium smelting, is classified as hazardous waste due to its reactive and leachable nature, though it is rich in aluminium. Conversely, RHA, an abundant and cost-effective by-product of the agro-food sector, boasts a high silicon content. These wastes were utilised as aluminium and silicon sources for synthesising various zeolites. This study examined the effects of temperature, ageing time, and sodium concentration on the formation of different zeolite phases and their crystallinity. Results indicated that increased Na^+ concentration favoured sodalite (SOD) zeolite formation, whereas Linde type–A (LTA) zeolite formation was promoted at higher temperatures and extended ageing times. The formation range of the different zeolites was defined and supported by crystallographic, microstructural, and morphological analyses. Additionally, the thermal behaviour of the zeolites was investigated. This work underscores the potential to transform industrial waste, including hazardous materials like salt slag, into sustainable, high-value materials, fostering efficient waste co-recycling and promoting clean, sustainable industrial production through cross-sectoral industrial symbiosis.

Keywords: sol–gel synthesis; waste-based zeolites; LTA and SOD zeolites; hazardous waste; salt slag; rice husk ash

Citation: Ritter, M.T.; Padilla, I.; Lobo-Recio, M.Á.; Romero, M.; López-Delgado, A. Waste Symbiosis through the Synthesis of Highly Crystalline LTA and SOD Zeolites. *Materials* **2024**, *17*, 4310. https://doi.org/10.3390/ma17174310

Academic Editor: Bruno de Gennaro

Received: 8 August 2024
Revised: 26 August 2024
Accepted: 27 August 2024
Published: 30 August 2024

1. Introduction

Demand for zeolites has grown considerably in recent years, driven mainly by the detergent industry, where synthetic zeolites have been used to replace phosphate-based agents, which are highly polluting to the environment. In addition to detergents, zeolites have been widely applied in several other areas, including petrochemicals, biotechnology, fertilisers, construction, gas separation, environmental remediation, and even biodiesel production [1].

A recent analysis by Markets and Markets [2] predicts a 3.1% Compound Annual Growth Rate (CAGR) in the global zeolite market from 2021 to 2026, expanding from 4872 metric tonnes to 5453 metric tonnes, with synthetic zeolites comprising approximately 42% of the total. Despite the availability of natural zeolites, they are generally contaminated to varying degrees by other minerals, metals, or other zeolites, making them unsuitable for commercial and industrial applications that require high purity and uniformity [3]. Consequently, there is growing interest in the synthesis of zeolites, which allows the

production of zeolitic structures with high purity, more uniform sizes, better ion exchange capacity, high selectivity, and higher thermal resistance [4].

With regard to synthetic zeolites, the LTA type–A (LTA) zeolite is one of the most widely used, especially due to its three-dimensional structural arrangement, which provides high adsorption and ion exchange capacity. This makes it suitable for use as molecular sieves and adsorbents in cooling, cleansing, and water softening systems [1,4]. The LTA zeolite ($Na_{12}Al_{12}Si_{12}O_{48}{\cdot}27H_2O$) framework is formed by the so-called β-cages or sodalite cages (24 T atoms [T = Si^{4+} or Al^{3+}]), in which the primary units are SiO_4 and AlO_4 tetrahedra (Figure 1). These units are connected to the six nearest neighbouring β-cages by double T4 rings [D4Rs]. When connected to neighbouring β-cages via single T4 rings [S4Rs], the sodalite zeolite structure is formed, which is the simplest structure among zeolites [5]. The cubic framework of the sodalite (SOD) zeolite ($Na_8Al_6Si_6O_{24}(OH)_2{\cdot}2H_2O$) has small pore sizes and thus a low application potential for ion exchange and molecular sieving. However, it is considered a promising material as a membrane separator for small molecules of liquids and gases, including H_2 and He [6].

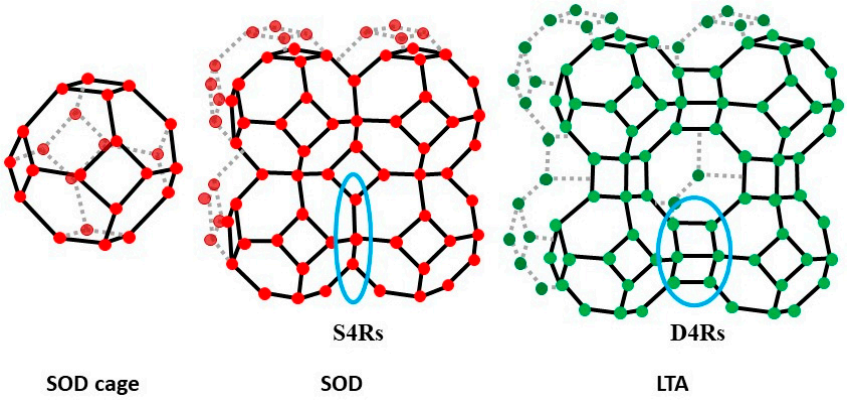

Figure 1. LTA- and SOD–type frameworks. The double D4R and single S4R bonds are in blue.

The formation of LTA or SOD zeolites is defined by the ideal synthesis condition, as the development of the desired zeolite phase depends on a specific temperature range, reaction time, and the molar ratio of the initial gel composition, which directly affect the nucleation and crystal growth processes [7].

In recent years, the synthesis of zeolites using secondary raw materials has attracted increasing attention in order to reduce production costs and mitigate the associated environmental impacts. In this sense, a great variety of wastes have been tested to produce LTA and SOD zeolites, including waste glass [8–10], rice husks [11–15], fly ash [16–26], alum sludge [27–30], and aluminium waste [6,31–36]. The synthesis methods applied often involve several steps and high temperature or long reaction time. Melo et al. [12] reported the synthesis of LTA through a hydrothermal process, employing a commercial sodium aluminate solution and a sodium silicate derived from RHA treated at 1200 °C for 2 h. Abdelharam et al. [32] employed a sol–gel process involving RHA and aluminium can waste at 150 °C for 12 h. RHA was also used by Simanjuntak et al. [13] together with food-grade aluminium foil in a process that entailed the alkaline dissolution of both wastes, followed by the ageing of the solution mixture for 24 h at room temperature and a crystallisation stage at 100 °C for 72 h; the resulting product was then subjected to a calcination process at 550 °C for 8 h to form zeolite A.

Among aluminium waste, salt slag is the main waste produced by the secondary aluminium industry, generating approximately 0.5 tons of salt slag for every ton of recycled aluminium produced [37]. Based on data published by Statista (2023) [38], it is estimated that more than 13 million metric tons of salt slag will be generated worldwide by 2027. This figure has almost tripled in 20 years and is on an upward trend due to the increased use and recycling of aluminium [39]. In addition to the large volumes, the management and disposal

of this waste is a major concern due to its potential for environmental contamination. Salt slag is considered toxic and hazardous waste, highly harmful, flammable, irritating, and leachable, according to the European Catalogue of Hazardous Waste [40] code 10 03 08. Its irritant properties pose a threat to human health and can cause damage through contact with the skin or mucous membranes, ingestion, and inhalation. Disposal in landfills is an environmental catastrophe due to the leachable salts, which can cause irreversible impacts on groundwater and soil [41]. Furthermore, the high reactivity of salt slag in contact with water leads to the formation of toxic gases (NH_3, CH_4, H_2S, H_2, and PH_3), which also pollute the atmosphere [37]. Nevertheless, its aluminium-rich composition makes salt slag a potential candidate for producing zeolites.

Although, as mentioned above, some authors have used different aluminium wastes as precursor materials in the synthesis of zeolites, few studies have been conducted with salt slag [37,42]. In addition, commercial silicate solutions were used as the source of silicon in these works.

Concerning silicon waste, rice husk ash (RHA) has been identified as a promising low-cost alternative to commercial silica [43]. It is a silicon-rich material resulting from the thermal transformation of rice husks and is considered to be one of the most abundant agro-food waste products. According to the Food and Agriculture Organization of the United Nations [44], more than 31 million tons of RHA were generated worldwide in 2023. Although rice husk ash is not hazardous waste as salt slag is, its high production, slow biodegradation, small particle size, and need to be disposed of in landfills cause several environmental problems.

In a previous paper, the authors studied the synthesis of NaP-type zeolite from salt slag and RHA by a hydrothermal method. Moreover, a central composite rotational design (CCRD) was applied to determine the best experimental conditions required to obtain NaP zeolite [45]. This work reports for the first time the synthesis of LTA and SOD zeolites from two unconventional raw materials, such as hazardous aluminium salt slag and rice husk ash. The aim of this study was to promote the co-recycling of these two wastes via the sol–gel process as a way of minimising the environmental impacts associated with their management. The evolution in terms of crystallinity, microstructure, and morphology of zeolitic materials synthesised under different experimental conditions was evaluated, assessing the influence of reaction time, temperature, and alkalinity. In addition, the thermal behaviour of the zeolites and their cation exchange capacity were also studied. The novelty and applicability of this work fall under the development of a synthesis method under mild conditions that makes it possible to produce highly crystalline LTA- and SOD-type zeolites from the combination of two industrial wastes.

2. Materials and Methods

2.1. Raw Materials

For the synthesis of zeolites, two different industrial wastes were employed: a hazardous waste from the secondary aluminium industry named salt slag (SS) and a waste from the agro-food industry, specifically rice husk ash (RHA). The wastes were selected for their respective contents of alumina (SS) and silicon (RHA), the two main components of zeolite composition. SS was supplied by Alusigma S.A. (Gijón, Spain), and its chemical composition mainly consists of Al_2O_3 (63.5 wt.%) and smaller amounts of MgO (7.9 wt.%), SiO_2 (7.7 wt.%), CaO (4.5 wt.%), and Fe_2O_3 (3.0 wt.%). Rice husk ash (RHA) was used to provide the necessary amount of silicon for zeolite synthesis. The RHA sample was supplied by Herba Ricemills S.L.U. (Seville, Spain). The main component of RHA is SiO_2 (89.7 wt.%), followed by minor amounts of K_2O (3.6 wt.%), P_2O_5 (1.7 wt.%), and CaO (1.3 wt.%).

The complete characterisation of both wastes (SS and RHA) was reported in a previous work [45]. Furthermore, a commercial sample of LTA zeolite, used for comparative purposes, was supplied by Industrias Químicas del Ebro, S.A. (Zaragoza, Spain).

2.2. Zeolite Synthesis

The waste-based zeolites were synthesised using a sol–gel process followed by an ageing step. Firstly, aluminate and silicate solutions were prepared by treating the initial SS and RHA in an alkaline medium (NaOH solution). Preliminary studies were conducted at different times (1–24 h), temperatures (room temperature—120 °C), and alkalinities (1–5 M) in order to determine the best conditions for obtaining aluminate and silicate solutions with the highest aluminium and silicon contents, respectively. The highest Al concentration, 19.88 g/L, was achieved by treating 0.15 g/mL of SS with a 5 M NaOH solution for 1 h at 100 °C. Similarly, the highest silicon content (58.34 g/L) of the silicate solution prepared from RHA was achieved by treating 0.16 g/mL of RHA with a 3 M NaOH solution for 3 h at 120 °C. The Na concentrations in the aluminate and silicate solutions were 105.3 and 69.66 g/L, respectively.

The sol–gel synthesis was performed by adding the silicate solution, in the required amounts to obtain a Si/Al ratio = 1, to the aluminate solution at room temperature with constant stirring. The resulting gel was kept under constant stirring under different ageing conditions (Table 1). Due to the high sodium content of the aluminate and silicate solutions, only distilled water in the appropriate volumes was added to the synthesis, and no additional NaOH solution was required. The different Na^+ concentrations used focused on obtaining the LTA zeolite phase, while the temperatures and ageing times tested aimed to increase the crystallinity of the resulting samples [5,46]. Nine experiments were carried out under different ageing conditions to evaluate their effect on the type and properties of the zeolites obtained. The samples obtained were labelled Z1–Z9 (Table 1).

Table 1. Experimental ageing conditions of the synthesised waste-based materials and Na^+ concentration in the solution.

Samples	T (°C)	t (h)	[Na^+] (mol/L)
Z1	RT	24	1.27
Z2	RT	240	1.27
Z3	RT	240	2.36
Z4	70	15	1.27
Z5	70	24	1.27
Z6	RT	240	4.12
Z7	50	24	1.27
Z8	70	6	1.27
Z9	RT	120	2.36

RT: room temperature.

After the tests, the resulting solid products were filtered, washed with distilled water, and dried at 100 °C for 24 h. The samples were then characterised by XRD, SEM, and FTIR according to the procedures described in the following Section 2.3. In addition, their cation exchange capacity (CEC) and thermal behaviour (TG/DTA) were also determined.

2.3. Characterisation Techniques

The composition of the aluminate and silicate solutions extracted from salt slag and RHA, respectively, was analysed using an inductively coupled plasma optical emission spectrometer, ICP-OES (Varian 725-ES, Agilent Technology, Santa Clara, CA, USA). The mineralogical characterisation of the zeolites was carried out by X-ray diffraction (XRD) using a Bruker D8 Advance diffractometer (Bruker, Champs–sur–Marne, France) with CuKα radiation, 2θ from 5° to 60°, and a scan rate of 2θ of 0.02°, 5 s per step. Diffrac.Suite EVA Plus 13.0 software (Bruker, AXS GmbH, Karlsruhe, Germany) was used to semi-quantify the crystalline phases of the zeolitic materials obtained. A crystallographic study of the zeolites was performed, which included the determination of interplanar spacing and network parameters. The interplanar spacing d (Å) was calculated by applying Bragg's

law (Equation (1)), where n is a natural number other than zero (n = 1), λ is the wavelength of the incident radiation (0.154 nm), and θ is the diffraction angle.

$$d = n\lambda/2\sin\theta \quad (1)$$

The lattice parameter a was calculated according to the crystalline system (cubic) using Equation (2), where d corresponds to the interplanar spacing and hkl to the Müller indices relative to the diffraction planes.

$$a = d\sqrt{\left(h^2 + k^2 + l^2\right)} \quad (2)$$

Thermogravimetric and differential thermal analysis (TG-DTA) was carried out on a Thermoanalyzer model SDT-Q600 (TA Instruments, New Castle, DE, USA), under an air flow of 100 mL/min and a heating rate of 10 °C/min. The Fourier transform infrared (FTIR) spectra (Nicolet Nexus 670–870, Nexus, Singapur, Malasia) were recorded on KBr discs in the 400–4000 cm^{-1} range. The cation exchange capacity (CEC) of the zeolites was determined by the ammonium ion exchange method using an NH_4Cl solution (1 M), as described in the Standard number NC 626 [47].

3. Results and Discussion

3.1. Effect of Ageing Time, Temperature, and Alkali Concentration

The XRD patterns of the nine samples of the zeolites synthesised using aluminate and silicate solutions from SS and RHA are shown in Figure 2a (samples Z1 to Z5) and Figure 2b (samples Z6 to Z9), based on the predominant zeolitic material obtained, for better viewing. The crystallographic parameters, including the intensity, diffraction angle (2θ), and Full Width at Half Maximum (FWHM) of the most intense reflections, are shown in Table 2. In addition, the semi-quantification of the most crystalline phases identified using Diffrac.Suite EVA software is presented, as is the crystallite size (D) determined from the most intense peak of the zeolite phase using the Scherrer equation: D = (0.9·λ)/(FWHM·cos θ), where λ is the X-ray wavelength (0.154 nm) and θ is the diffraction angle (in rad).

Table 2. Crystallographic parameters (intensity, 2θ, and FWHM), semi-quantification of the zeolite phases, and crystallite sizes (D) of the synthesised waste-based materials.

Samples	Phase	Zeolite (%)	Intensity (Counts)	2θ (°)	FWHM (°)	D (nm)
Z1	Amorphous phase	-	-	-	-	-
Z2	LTA + amorphous phase	47.4	1162	29.92	0.3743	22
Z3	LTA	100	4101	29.88	0.1848	45
Z4	LTA SOD	95.6 4.4	4423	29.96	0.1496	55
Z5	LTA	100	5864	29.96	0.1564	53
Z6	SOD	24.6	1464	24.49	0.1808	45
Z7	SOD	30.0	1783	24.48	0.7829	10
Z8	SOD	81.3	4955	24.48	0.2703	30
Z9	SOD	81.8	6723	24.47	0.1992	41

FWHM: Full Width at Half Maximum; D: crystallite size, determined from the most intense reflection.

From Figure 2 and Table 2, it can be observed that, with the exception of sample Z1, in which no crystalline phase could be identified, and sample Z2, with an incipient appearance of peaks, all the other samples resulted in the formation of crystalline zeolites. By increasing the ageing time from 24 h (Z1) to 240 h (Z2), the XRD pattern shows the development of small peaks with a profile characteristic of the cubic zeolite LTA, with a crystallite size of 22 nm. Increasing the Na^+ concentration from 1.27 mol/L (Z2) to 2.36 mol/L (Z3) at 240 h and room temperature resulted in the development of narrow, very intense, and

well-defined peaks (>4000 counts), which fit well with those of the XRD pattern of the LTA zeolite from the International Centre for Diffraction Data (ICDD), reference file PDF 73-2340. A crystallite size of 45 nm was calculated for this sample. This result highlights that a higher concentration of Na^+ promotes the formation of LTA when the ageing time is extended. Both samples Z4 and Z5, synthesised with a NaOH concentration of 1.27 mol/L at 70 °C, resulted in 100% zeolitic material. However, for the sample synthesised over 15 h (Z4), several peaks corresponding to the SOD–type zeolite were observed along with corresponding ones to LTA, the latter with a crystallite size of 55 nm. By increasing the ageing time to 24 h (Z5), a single LTA zeolite phase was obtained with very intense and well-defined peaks (>5800 counts) and a crystallite size of 53 nm. This indicates that a longer ageing time favours the formation of LTA zeolite.

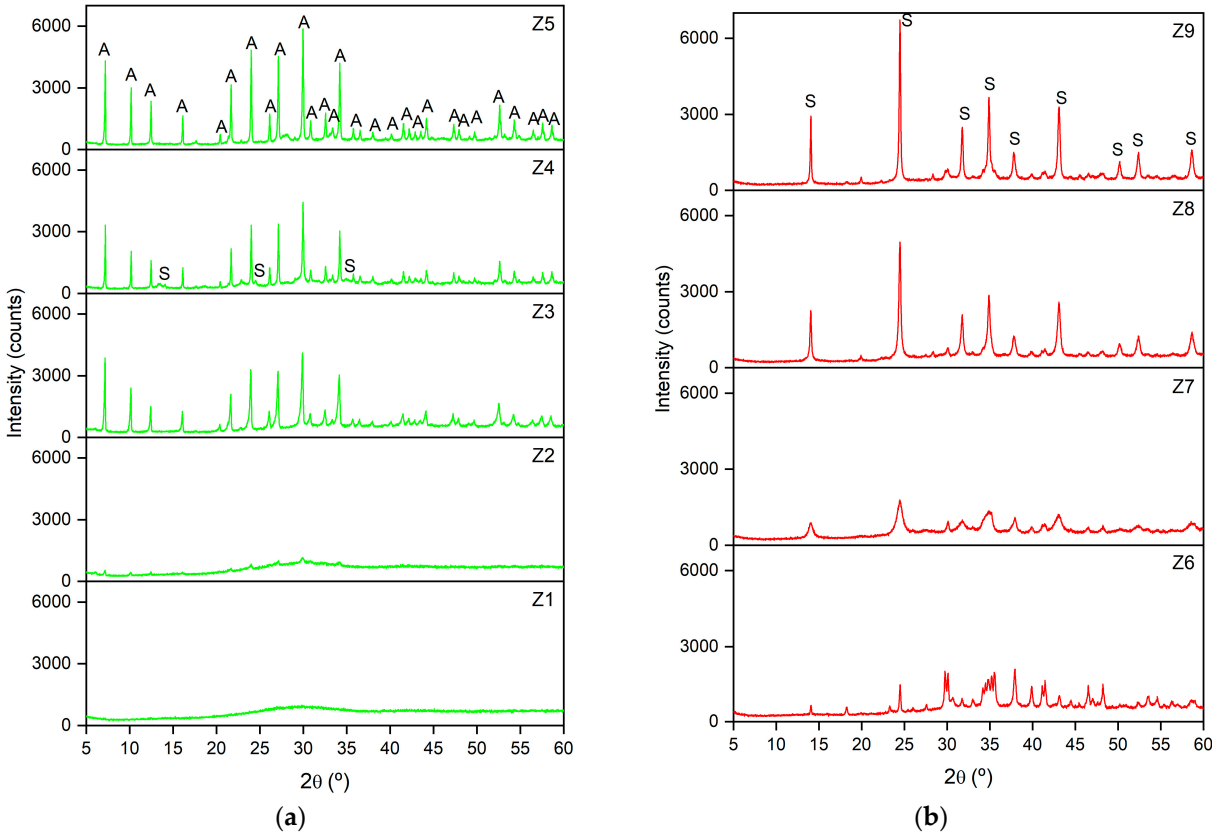

Figure 2. XRD patterns of the waste-based materials (**a**) Z1 to Z5 (green) and (**b**) Z6 to Z9 (red), synthesised under different experimental conditions [A = LTA zeolite (PDF 73–2340) and S = SOD zeolite (PDF 76–1639)].

Regarding samples Z6, Z7, Z8, and Z9, the XRD patterns (Figure 2b) principally showed peaks corresponding to the SOD–type zeolite (ICDD PDF 76-1639). A certain amorphous phase content, decreasing from Z6 (close to 40%) to Z9 (around 25%), is also consistent with the background of the patterns. At room temperature, 240 h, and 4.12 mol/L of Na^+ (Z6), SOD showed a peak intensity >1400 counts and a crystallite size of 45 nm. Increasing the temperature to 50 °C for 24 h while maintaining a Na^+ concentration of 1.27 mol/L (Z7) resulted in SOD with a peak intensity >1700 counts and a crystallite size of 10 nm. At 70 °C for 6 h (Z8), the percentage of crystalline SOD in the sample reached 81.3%, with a maximum peak intensity around 5000 counts and a crystallite size of 30 nm. Finally, sample Z9, synthesised at room temperature for 120 h with 2.36 mol/L of Na^+, resulted in the highest percentage of crystalline SOD and the highest peak intensity (>6700 counts), with a crystallite size of 41 nm.

The crystallite sizes of the different zeolite phases synthesised as a function of the experimental conditions applied (ageing time, temperature, and Na^+ concentration) are shown in Figure 3.

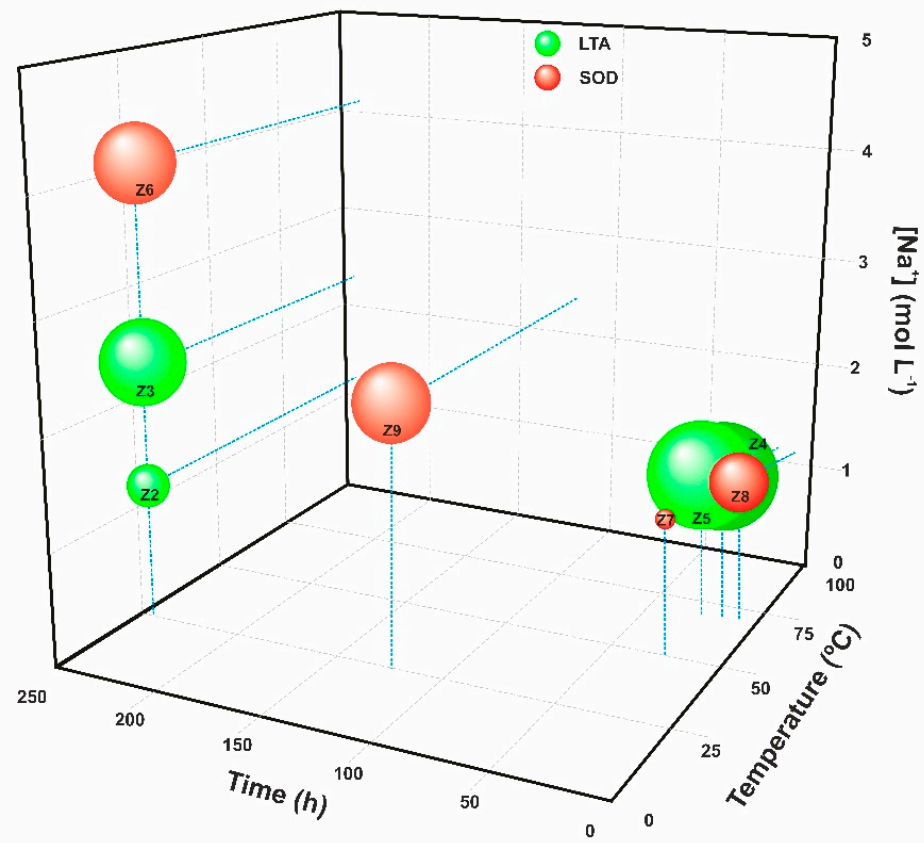

Figure 3. Zeolite phase and corresponding crystallite size obtained according to different experimental conditions (LTA in green and SOD in red).

Several factors, including temperature, ageing, pressure, reagent sources, Si/Al ratio, and water content [46], influence not only the development of specific zeolite phases and their crystallinity but also the size of the crystals formed. Thus, increasing the ageing time from 24 to 240 h at room temperature resulted in the evolution from a geopolymer (Z1) to the incipient formation of LTA zeolite (Z2). However, this trend was not observed at a higher temperature; in the synthesis conducted at 70 °C, extending the reaction time from 15 to 24 h resulted in similar crystallite sizes (samples Z4 and Z5). Sodium concentration had the most significant effect on crystallite size. Increasing the Na^+ concentration from 1.27 mol/L to 2.36 mol/L caused the crystallite size of the LTA zeolites to increase from 22 nm (Z2) to 45 nm (Z3). Nevertheless, obtaining a specific zeolite phase is defined by the alkali concentration in the mixing reaction and the crystallisation kinetics [36,48]. Comparing samples Z2, Z3, and Z6, synthesised under the same conditions of time (240 h) and temperature (RT), revealed that increasing the sodium content resulted in the development of the SOD phase, known for its higher Na_2O/Al_2O_3 ratio (close to 1.33 for the stoichiometric phase) compared to the LTA zeolite (Na_2O/Al_2O_3 = 1). This conclusion is supported by the fact that a high concentration of NaOH solution (>3.5 M) destabilises the structure of the LTA zeolite, causing the destruction of double T4 rings [D4Rs] and leading to the binding of β-cages via single T4 rings [S4Rs] and the consequent formation of sodalite [5,46].

According to the results, longer ageing times and higher temperatures led to the formation of LTA–type zeolites. This behaviour was observed by comparing Z7 and Z5, when the temperature was increased from 50 to 70 °C to a fixed Na^+ concentration of

1.27 mol/L, and with samples Z9 and Z3, which transitioned from an SOD zeolite to an LTA zeolite by doubling the ageing time (120 to 240 h). Shorter ageing times disproved this outcome when comparing samples Z8, Z4, and Z5, which transitioned from an SOD zeolite (6 h) to a mixture of LTA–SOD (15 h) and a pure LTA (24 h). This suggests that sodalite could serve as an intermediate phase that evolves into an LTA zeolite as the ageing time increases, as indicated by the mixture of zeolitic phases identified for an intermediate ageing time (Z4). Similar results were reported by other authors. Simanjuntak et al. [13], who synthesised zeolites using RHA and aluminium foil as raw materials, corroborate the findings, also reporting that an SOD zeolite was obtained with a shorter reaction time (48 h) compared to a longer time (72 h) which resulted in an LTA–type zeolite. This result suggests that an increase in reaction temperature enhances the partial dissolution of silica and alumina components from the gel into the aqueous phase and subsequently promotes the formation of crystal nuclei within the gel matrix [36]. It can be inferred that different heating rates lead to the formation of slightly different initial gels and consequently to the development of different zeolite phases. Thus, the interplay between temperature and ageing time is key for obtaining highly crystalline single-phase LTA zeolites.

In regard to the crystallite size, the values obtained are quite similar to those reported by other authors who have synthesised LTA– and SOD– type zeolites from wastes. Al-Dahri et al. [16] obtained LTA zeolite with a crystallite size of 45 nm from coal fly ash using a microwave-assisted method. The sol–gel synthesis performed by Asefa & Feyisa [49] from aluminium foil waste and sugarcane bagasse ash resulted in LTA zeolite with a crystallite size of 49 nm. Meanwhile, the SOD zeolite produced by this same method had crystallites ranging from 46 to 64 nm when aluminium can waste was used [50].

The reported differences in crystallinity and structure were also observed in the morphology of the waste-based zeolites obtained under different ageing conditions (Figure 4). Corroborating the XRD analysis, the SEM micrograph of sample Z1 (Figure 4Z1) shows agglomerates of tiny, rounded particles (<0.1 μm) characteristic of geopolymeric materials, whereas in the case of sample Z2 (Figure 4Z2), larger particles (1–1.6 μm) have begun to develop which, although predominantly amorphous, present an incipient cubic morphology (1–1.6 μm) but without well-defined edges and boundaries. The micrograph of sample Z3 (Figure 4Z3) shows a stacking of particles with a cubic tendency and edges with a higher degree of definition than those observed in Z2, with sizes varying between 0.1 and 0.9 μm, indicating the formation of a more crystalline LTA zeolite. The lack of definition on the edges of the cubes is due to the low temperature during the ageing stage. The synthesis temperature affects the morphology of the zeolites, with low temperatures leading to the formation of rounder crystals and higher temperatures leading to more cubic shapes [1,51]. This is corroborated by the predominant presence of well-defined cubic crystals in the SEM images of samples Z4 (Figure 4Z4) and Z5 (Figure 4Z5), characteristics of crystalline LTA zeolite. In the first sample, the largest cubes ranged in size from 2.5 to 5 μm and the smallest from 0.2 to 1.5 μm. As for sample Z5, the cubic crystals exhibit perfectly defined and slightly chamfered edges. In this sample, some cubic twinned crystals are also observed, along with very small cubes (500 to 900 nm) developed on top of the larger ones.

The morphology of the Z6–Z9 samples (Figure 4Z6–Z9) confirms the XRD analysis by presenting structures consistent with sodalite–type zeolites, similar to those reported by other authors [50,52]. SEM images of samples Z6 and Z9 show clusters (30–100 μm) of slightly rounded "flower-like" particles with average diameters of 2–10 μm, which are characteristic of the SOD–type structure [22].

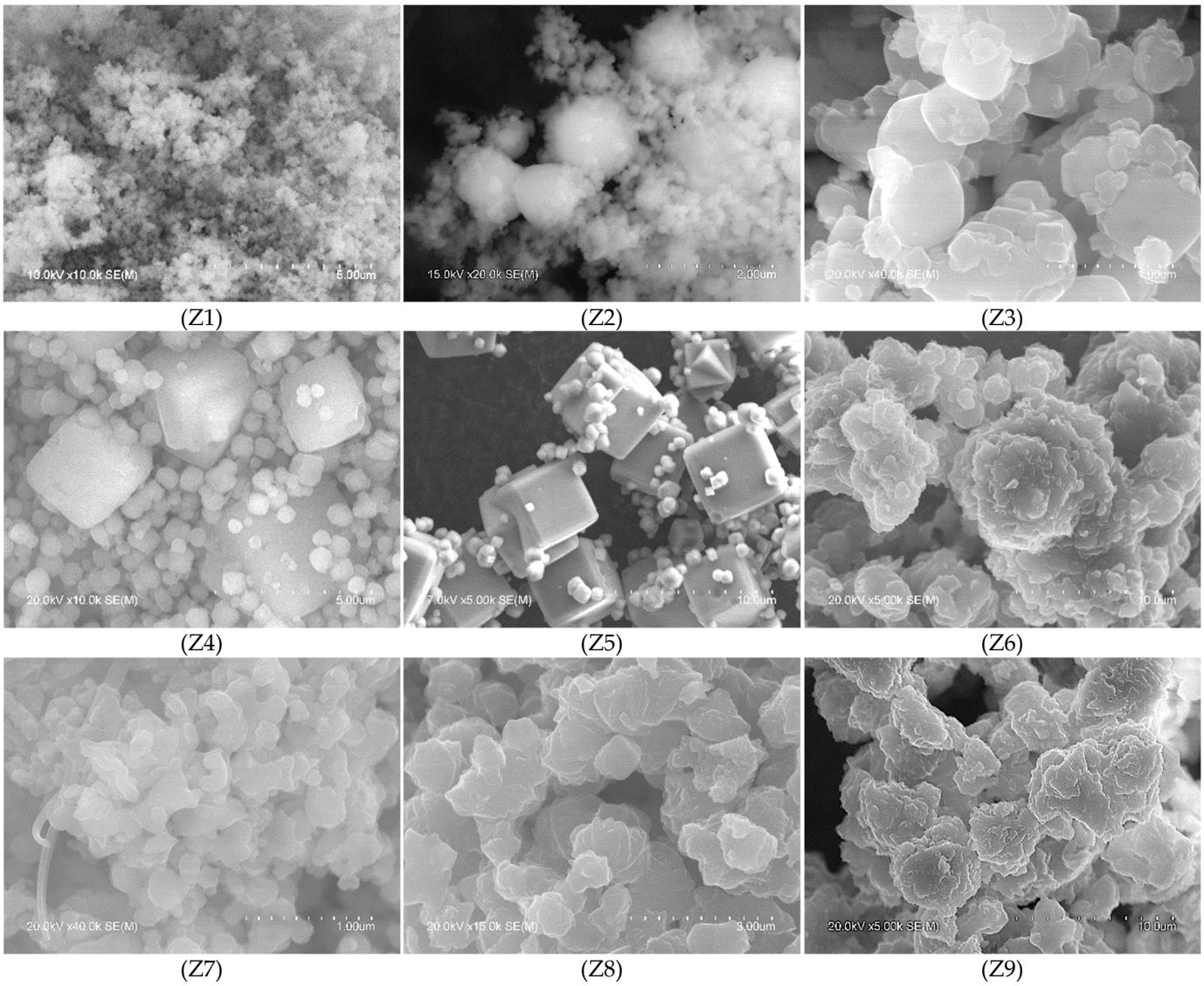

Figure 4. SEM images of the waste–based synthesised materials Z1–Z9.

3.2. Study of LTA and SOD Zeolites

As mentioned above, samples Z5 and Z9 correspond to well-defined LTA– and SOD–type zeolites, respectively, so both samples were subjected to more in-depth analysis.

Due to the high crystallinity and well-defined peaks of LTA zeolite obtained from Z5, its XRD pattern and crystallographic parameters were compared with those of a commercial LTA zeolite (ZCOM) (Figure 5, Table 3).

The LTA zeolite synthesised from SS and RHA showed an XRD profile quite similar to that of the commercial zeolite, with well-developed peaks and slightly higher intensities (Figure 5). The most significant peaks of the Z5 sample compared to the commercial LTA zeolite; the reference file PDF 73–2340 showed the similarity of the interplanar spacing values obtained as well as the relative intensities (I/I_0) [53]. The most intense reflection of the synthesised LTA zeolite, centred at 29.96 ° (2θ), corresponds to the diffraction hkl index [6 4 4], according to PDF 73–2340. In addition, the lattice parameter a, calculated according to Equation (2), which considers the cubic crystal system of the LTA zeolite, was 12.29 Å, very similar to the 12.32 Å reported in the reference ICDD files.

In the case of the SOD zeolite, the most significant peaks of the Z9 sample coincide completely with the reference file PDF 76–1639 [54] (Table 4). The interplanar spacing and the relative intensities of the most intense reflections show practically identical values. The

most intense reflection corresponding to the SOD phase was centred at 24.47° (2θ), which corresponds to the hkl index [2 1 1].

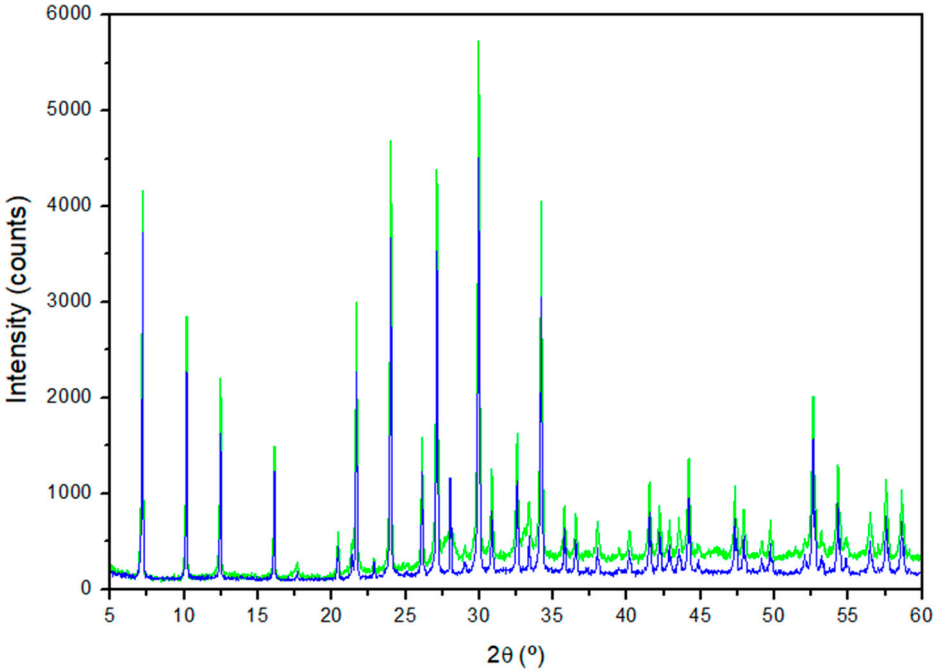

Figure 5. XRD patterns of the waste-based LTA zeolite (Z5) in green and commercial LTA zeolite (ZCOM) in blue.

Table 3. Crystallographic parameters of waste-based LTA zeolite, commercial LTA zeolite, and reference ICDD files.

Z5 (LTA)			ZCOM			PDF 73-2340			
d (Å)	**2θ (°)**	**I/I_0**	**d (Å)**	**2θ (°)**	**I/I_0**	**d (Å)**	**2θ (°)**	**I/I_0**	**hkl**
12.27	7.20	73	12.27	7.20	64	12.31	7.18	69	[2 0 0]
8.69	10.17	51	8.69	10.17	39	8.70	10.16	46	[2 2 0]
7.09	12.47	40	7.09	12.47	28	7.10	12.45	51	[2 2 2]
4.10	21.68	54	4.10	21.68	39	4.10	21.65	39	[6 0 0]
3.71	24.00	82	3.71	24.00	63	3.71	23.97	54	[6 2 2]
3.41	26.12	29	3.41	26.12	21	3.41	26.09	8	[6 4 0]
3.29	27.13	77	3.29	27.13	60	3.29	27.09	67	[6 4 2]
2.98	29.96	100	2.98	29.96	100	2.98	29.92	100	[6 4 4]
2.75	32.56	30	2.75	32.56	19	2.75	32.52	22	[8 4 0]
2.62	34.20	72	2.62	34.18	52	2.62	34.15	50	[6 6 4]

Table 4. Crystallographic parameters of waste-based SOD zeolite.

Z9 (SOD)			PDF 76–1639			
d (Å)	**2θ (°)**	**I/I_0**	**d (Å)**	**2θ (°)**	**I/I_0**	**hkl**
6.30	14.05	44	6.29	14.08	44	[1 1 0]
3.64	24.47	100	3.63	24.51	100	[2 1 1]
2.81	31.79	37	2.81	31.81	40	[3 1 0]
2.57	34.88	55	2.57	34.93	48	[2 2 2]
2.10	43.10	49	2.10	43.14	56	[4 1 1]

The calculated lattice parameter, which, as for the LTA zeolite, also considers the cubic-type crystal system of the SOD zeolite, was 8.90 Å, compared to 8.89 Å assigned by the reference file.

The FTIR spectra of samples Z5 (LTA) and Z9 (SOD) (Figure 6) were recorded in the mid-infrared wavenumber region (1200 to 400 cm^{-1}), where the fundamental vibrations of the framework (Si, Al)O_4 tetrahedra are located [55]. The spectrum of sample Z5 shows the four absorption bands characteristic of LTA zeolite. The bands at 995 and 664 cm^{-1} are due to asymmetrical and symmetrical internal stretching vibrations, respectively. The band at 461 cm^{-1} corresponds to the Si-O-Al bending mode, and the medium-intensity vibration at 552 cm^{-1} is attributed to the vibration of the secondary structural units [D4Rs] [36]. Similar FTIR values were reported by López-Delgado et al. [31], who also prepared LTA zeolite from an aluminium waste, as well as the those reported by Vegere et al. [56] for zeolite 4A prepared from commercial raw materials. Thispoints the high purity of the synthesised waste-based LTA zeolite. Sample Z9 showed the typical triplet of SOD zeolite, with bands at 735, 709 and 665 cm^{-1} corresponding to the symmetrical stretching mode. The two bands at 464 and 434 cm^{-1} represent the octahedral bending mode. In addition, two low-intensity bands are observed at 881 and 867 cm^{-1}, attributable to the symmetrical external stretching of T-O-T (T = Si and/or Al) [32]. These results are corroborated by Sánchez-Hernández et al. [6] for SOD zeolite produced from an aluminium waste and commercial sodium silicate.

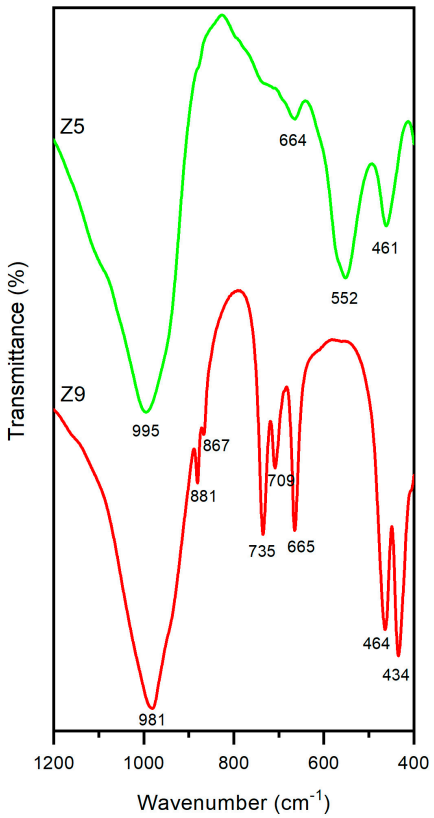

Figure 6. FTIR spectra of LTA (Z5) in green and SOD (Z9) in red.

The TG-DTA curves of samples Z5 (LTA) and Z9 (SOD) are shown in Figure 7. Both samples exhibit endothermic effects below 250 °C. The structured profile of these bands indicates that the dehydration of both zeolites occurs in several overlapped steps and is due to different types of water (absorbed, zeolitic, etc.). Concerning LTA, a second mass loss takes place below 400 °C and is associated with the loss of water due to a dehydroxylation process. The total mass loss for sample Z5, according to the TG curve, was 21.7%, similar to the loss observed for a commercial zeolite [57]. This value corresponds to a loss of

approximately 26 water molecules, which is quite similar to the corresponding one for the stoichiometric theoretical LTA zeolite ($Na_{12}Al_{12}Si_{12}O_{48}{\cdot}27H_2O$). After that, no mass loss is observed in the TG curve, but the DTA curve exhibits two exothermic peaks centred at 913 and 969 °C. These peaks are attributed to the topotactic transformation of the cubic framework of LTA zeolite into the hexagonal framework of nepheline ($NaAlSiO_4$). Several authors reported that this transformation occurs at temperatures higher than 700 °C [58]. A temperature of 890 °C has also been reported for LTA zeolite obtained at pilot scale from an aluminium waste and commercial water glass [31]. Selvaraj et al. [59] also observed two exothermic peaks between 800 and 900 °C in the DTA curve of a commercial LTA zeolite due to the transformation and recrystallisation of nepheline.

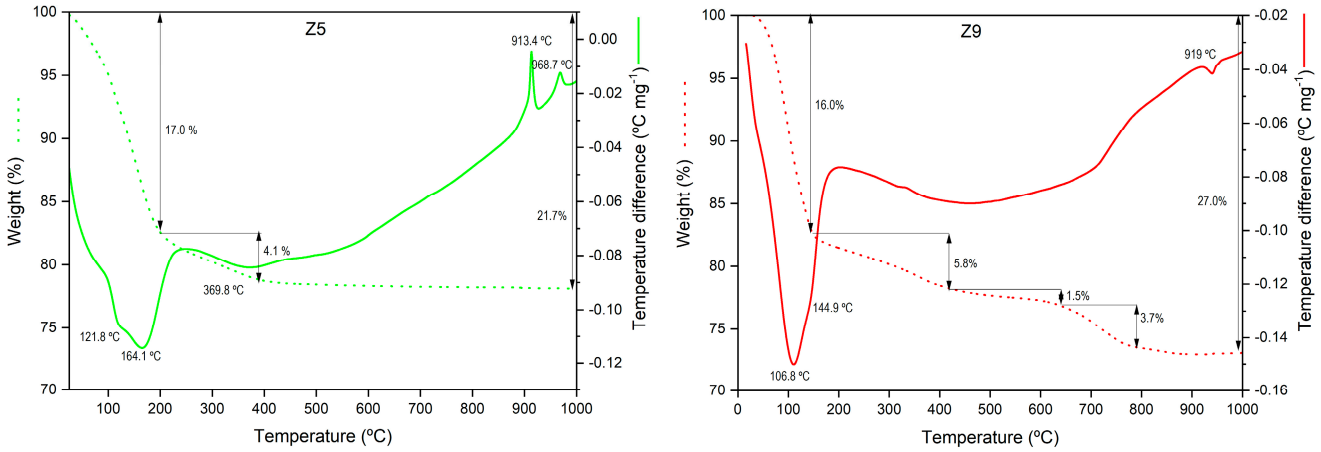

Figure 7. TG (dot line) and DTA (solid line) for the selected waste-based zeolites LTA (Z5) and SOD (Z9).

In the case of sample Z9 (SOD), a total mass loss of 27% took place from room temperature up to 800 °C, corresponding to the release of 22 water molecules. Between 400 and 800 °C, the mass loss of 5.2% can be attributed to the crystallisation and structural water, which fit well to the theoretical value for a sodalite stoichiometry of $Na_8Al_6Si_6O_{24}(OH)_2{\cdot}2H_2O$ [60]. Above 790 °C, the DTA curve shows an inflection point without any corresponding mass loss. This observation suggests the onset of a gradual transformation from sodalite to nepheline, although the transformation remains incomplete at the test temperature.

Overall, the zeolites studied exhibit the ability to retain their structure and only lose water during thermal treatment at temperatures below 800 °C for both Z5 and Z9. This characteristic makes these zeolites useful in processes requiring high temperatures or those needing high-temperature treatment for regeneration [57].

Concerning the cation exchange capacity (CEC), the value for Z5 was 3.40 meq/g, higher than that of Z9 (1.82 meq/g). The CEC is one of the main requirements for the use of zeolites, especially in detergent formulation and water decontamination [61,62]. The CEC results found in this study are remarkable when compared to the values reported by other authors who synthesised A-type zeolites using different wastes [17,30,31,48,63]. Pangan et al. [48] reported a CEC value of 2.44 meq/g for an LTA zeolite synthesised from corn straw ash by a hydrothermal method at 90 °C for 9 h, while other authors reported values of CEC lower than 2 meq/g for zeolites obtained from aluminium slag milling waste [31], fly ash by a microwave-assisted hydrothermal process [17], or alum sludge by hydrothermal synthesis at 90 °C for 9 h [30]. The high CEC value of the LTA zeolite synthesised in this study suggests its promising application in processes such as the treatment of metal-contaminated wastewaters. The CEC of SOD zeolite, although lower than that of LTA, was higher than that reported by other authors [6].

4. Conclusions

The co-recycling of hazardous aluminium salt slag and rice husk ash through a synthesis process under mild conditions resulted in highly crystalline LTA and SOD zeolites. A highly crystalline LTA zeolite was obtained at a temperature of 70 °C for 24 h, while under the same conditions, the SOD zeolite was synthesised in only 6 h. The results showed the great influence of the experimental conditions on the development of a specific zeolite phase. The increase in sodium concentration favours the formation of SOD zeolite. The effect of temperature on the crystallinity of the zeolites is much more significant than the effect of ageing time. A high value of cation exchange capacity of 3.40 meq/g was obtained for the LTA. This indicates that the LTA-type zeolite prepared from wastes could have potential applications in the same way as commercial zeolites. The synthesis of zeolites can be considered as a new alternative route to conventional waste management methods, especially for hazardous wastes such as salt slag, leading to the production of value-added materials, which are in increasing demand worldwide and have significant applications in several fields. The valorisation of these wastes through their conversion into advanced materials, such as LTA- and SOD-type zeolites, contributes above all to saving natural resources and preserving the environment. Finally, yet importantly, this approach favours the circular economy, creating a symbiosis between the different industrial segments, given that many industries that generate aluminium and agro-food waste use zeolites in their industrial gas and effluent treatment systems.

Author Contributions: Conceptualisation, A.L.-D.; methodology, I.P.; software, M.T.R.; formal analysis, M.T.R.; investigation, M.T.R.; data curation, M.T.R., I.P., and A.L.-D.; writing—original draft preparation, M.T.R.; writing—review and editing, M.Á.L.-R., I.P., M.R., and A.L.-D.; supervision, A.L.-D., I.P., M.R., and M.Á.L.-R.; funding acquisition, A.L.-D. and M.R. All authors have read and agreed to the published version of the manuscript.

Funding: This research was funded by EU LIFE Programme (Project 101114027-LIFE22-ENV-ES-Z-ONA4LIFE). The scholarship to support the stay of M.T. Ritter at the Eduardo Torroja Institute for Construction Sciences (IETcc-CSIC) was financed by the Coordination for the improvement of Higher Education Personnel (CAPES), under the CAPES-PrInt Proggrame no. 88887.310573/2018/-00).

Institutional Review Board Statement: Not applicable.

Informed Consent Statement: Not applicable.

Data Availability Statement: The raw data supporting the conclusions of this article will be made available by the authors on request.

Acknowledgments: The authors would like to thank CINEA for the LIFE Project 101114027 and the Eduardo Torroja Institute for Construction Sciences (IETcc-CSIC), Spain, and the Federal University of Santa Catarina (UFSC) for the technical and academic support provided. The authors also thank Alusigma S.A. (Spain) for providing the salt slag sample, Herba Ricemills S.L.U. (Spain) for providing the rice husk ash sample, and Industrias Químicas del Ebro, S.A. (Spain) for providing a commercial LTA zeolite sample used as a reference sample.

Conflicts of Interest: The authors declare no conflicts of interest.

References

1. Collins, F.; Rozhkovskaya, A.; Outram, J.G.; Millar, G.J. A Critical Review of Waste Resources, Synthesis, and Applications for Zeolite LTA. *Microporous Mesoporous Mater.* **2020**, *291*, 109667. [CrossRef]
2. Markets and Markets. Zeolites Market by Type (Natural, Synthetic), Function (Ion-Exchange, Catalyst, Molecular Sieve), Synthetic Zeolite Application (Detergents, Adsorbent, Catalysts), Natural Zeolite Application, and Region—Global Forecast to 2026. 2023. Available online: https://www.marketsandmarkets.com/Market-Reports/zeolites-market-76442083.html (accessed on 5 July 2024).
3. Mallapur, V.P.; Oubagaranadin, J.U.K. A Brief Review on the Synthesis of Zeolites from Hazardous Wastes. *Trans. Indian Ceram. Soc.* **2017**, *76*, 1–13. [CrossRef]
4. El Bojaddayni, I.; Emin Küçük, M.; El Ouardi, Y.; Jilal, I.; El Barkany, S.; Moradi, K.; Repo, E.; Laatikainen, K.; Ouammou, A. A Review on Synthesis of Zeolites from Natural Clay Resources and Waste Ash: Recent Approaches and Progress. *Miner. Eng.* **2023**, *198*, 108086. [CrossRef]

5. Prokof'ev, V.Y.; Gordina, N.E. Preparation of Granulated LTA and SOD Zeolites from Mechanically Activated Mixtures of Metakaolin and Sodium Hydroxide. *Appl. Clay Sci.* **2014**, *101*, 44–51. [CrossRef]
6. Sánchez-Hernández, R.; López-Delgado, A.; Padilla, I.; Galindo, R.; López-Andrés, S. One-Step Synthesis of NaP1, SOD and ANA from a Hazardous Aluminum Solid Waste. *Microporous Mesoporous Mater.* **2016**, *226*, 267–277. [CrossRef]
7. Wang, C.; Li, J.; Wang, L.; Sun, X.; Huang, J. Adsorption of Dye from Wastewater by Zeolites Synthesized from Fly Ash: Kinetic and Equilibrium Studies. *Chin. J. Chem. Eng.* **2009**, *17*, 513–521. [CrossRef]
8. Mouna, S.; Hajji, S.; Tounsi, H. Waste to Health: Green Synthesis of Zn Loaded LTA Zeolite Prepared from Waste Glass and Aluminum Scrap with High Antioxidant and Antimicrobial Activities. *J. Clean. Prod.* **2024**, *434*, 139946. [CrossRef]
9. Kim, J.-C.; Choi, M.; Song, H.J.; Park, J.E.; Yoon, J.-H.; Park, K.-S.; Lee, C.G.; Kim, D.-W. Synthesis of Uniform-Sized Zeolite from Windshield Waste. *Mater. Chem. Phys.* **2015**, *166*, 20–25. [CrossRef]
10. Lee, W.-H.; Lin, Y.-W.; Lin, K.-L. Parameter Optimization, Characterization, and Crystallization Mechanisms Underlying the Synthesis of Zeolite A Using Liquid Crystal Display Waste Glass and Sandblasting Waste as Alternative Raw Materials. *J. Environ. Chem. Eng.* **2022**, *10*, 108506. [CrossRef]
11. Bohra, S.; Kundu, D.; Naskar, M.K. One-Pot Synthesis of NaA and NaP Zeolite Powders Using Agro-Waste Material and Other Low Cost Organic-Free Precursors. *Ceram. Int.* **2014**, *40*, 1229–1234. [CrossRef]
12. Melo, C.R.; Francisco, A.C.; Kuhnen, N.C.; da Rocha, M.R.; Melo, A.R.; Riella, H.G.; Angioletto, E. Production of Zeolite from Rice Husk Ash. *Mater. Sci. Forum* **2014**, *798–799*, 617–621. [CrossRef]
13. Simanjuntak, W.; Pandiangan, K.D.; Sembiring, Z.; Simanjuntak, A.; Hadi, S. The Effect of Crystallization Time on Structure, Microstructure, and Catalytic Activity of Zeolite-A Synthesized from Rice Husk Silica and Food-Grade Aluminum Foil. *Biomass Bioenergy* **2021**, *148*, 106050. [CrossRef]
14. Wajima, T.; Kiguchi, O.; Sugawara, K.; Sugawara, T. Synthesis of Zeolite-A Using Silica from Rice Husk Ash. *J. Chem. Eng. Jpn.* **2009**, *42* (Suppl. 1), S61–S66. [CrossRef]
15. Wang, Y.; Du, T.; Jia, H.; Qiu, Z.; Song, Y. Synthesis, Characterization and CO_2 Adsorption of NaA, NaX and NaZSM-5 from Rice Husk Ash. *Solid State Sci.* **2018**, *86*, 24–33. [CrossRef]
16. Al-dahri, T.; AbdulRazak, A.A.; Rohani, S. Preparation and Characterization of Linde-Type A Zeolite (LTA) from Coal Fly Ash by Microwave-Assisted Synthesis Method: Its Application as Adsorbent for Removal of Anionic Dyes. *Int. J. Coal Prep. Util.* **2022**, *42*, 2064–2077. [CrossRef]
17. Behin, J.; Bukhari, S.S.; Dehnavi, V.; Kazemian, H.; Rohani, S. Using Coal Fly Ash and Wastewater for Microwave Synthesis of LTA Zeolite. *Chem. Eng. Technol.* **2014**, *37*, 1532–1540. [CrossRef]
18. Belviso, C.; Cavalcante, F.; Javier Huertas, F.; Lettino, A.; Ragone, P.; Fiore, S. The Crystallisation of Zeolite (X- and A-Type) from Fly Ash at 25 °C in Artificial Sea Water. *Microporous Mesoporous Mater.* **2012**, *162*, 115–121. [CrossRef]
19. Cao, J.; Wang, P.; Sun, Q. Green Synthesis of Magnetic Zeolite LTA Using NaOH Activated Fly Ash. *J. Inorg. Gen. Chem.* **2020**, *646*, 1666–1670. [CrossRef]
20. Cardoso, A.M.; Horn, M.B.; Ferret, L.S.; Azevedo, C.M.N.; Pires, M. Integrated Synthesis of Zeolites 4A and Na–P1 Using Coal Fly Ash for Application in the Formulation of Detergents and Swine Wastewater Treatment. *J. Hazard. Mater.* **2015**, *287*, 69–77. [CrossRef]
21. Kim, J.K.; Lee, H.D. Effects of Step Change of Heating Source on Synthesis of Zeolite 4A from Coal Fly Ash. *J. Ind. Eng. Chem.* **2009**, *15*, 736–742. [CrossRef]
22. Shoumkova, A.; Stoyanova, V. Zeolites Formation by Hydrothermal Alkali Activation of Coal Fly Ash from Thermal Power Station "Maritsa 3", Bulgaria. *Fuel* **2013**, *103*, 533–541. [CrossRef]
23. Xu, H.; Wu, L.; Shi, T.; Liu, W.; Qi, S. Adsorption of Acid Fuchsin onto LTA-Type Zeolite Derived from Fly Ash. *Sci. China Technol. Sci.* **2014**, *57*, 1127–1134. [CrossRef]
24. Ziejewska, C.; Grela, A.; Łach, M.; Marczyk, J.; Hordyńska, N.; Szechyńska-Hebda, M.; Hebda, M. Eco-Friendly Zeolites for Innovative Purification of Water from Cationic Dye and Heavy Metal Ions. *J. Clean. Prod.* **2023**, *406*, 136947. [CrossRef]
25. Liu, G.; Lin, Y.; Zhang, L.; Zhang, M.; Gu, C.; Li, J.; Zheng, T.; Chai, J. Preparation of NaA Zeolite Molecular Sieve Based on Solid Waste Fly Ash by High-Speed Dispersion Homogenization-Assisted Alkali Fusion-Hydrothermal Method and Its Performance of Ammonia-Nitrogen Adsorption. *J. Sci. Adv. Mater. Devices* **2024**, *9*, 100673. [CrossRef]
26. Shabani, J.M.; Ameh, A.E.; Oyekola, O.; Babajide, O.O.; Petrik, L. Fusion-Assisted Hydrothermal Synthesis and Post-Synthesis Modification of Mesoporous Hydroxy Sodalite Zeolite Prepared from Waste Coal Fly Ash for Biodiesel Production. *Catalysts* **2022**, *12*, 1652. [CrossRef]
27. Anuwattana, R.; Khummongkol, P. Conventional Hydrothermal Synthesis of Na-A Zeolite from Cupola Slag and Aluminum Sludge. *J. Hazard. Mater.* **2009**, *166*, 227–232. [CrossRef]
28. Espejel-Ayala, F.; Schouwenaars, R.; Durán-Moreno, A.; Ramírez-Zamora, R.M. Use of Drinking Water Sludge in the Production Process of Zeolites. *Res. Chem. Intermed.* **2014**, *40*, 2919–2928. [CrossRef]
29. Rozhkovskaya, A.; Rajapakse, J.; Millar, G.J. Synthesis of High-Quality Zeolite LTA from Alum Sludge Generated in Drinking Water Treatment Plants. *J. Environ. Chem. Eng.* **2021**, *9*, 104751. [CrossRef]
30. Wongwichien, J. Synthesis and Use of Zeolite Na-A from Waste Sludge of Water Treatment Plant for Ammonium Removal. *Chiang Mai J. Sci.* **2014**, *41*, 1262–1273.

31. López-Delgado, A.; Robla, J.I.; Padilla, I.; López-Andrés, S.; Romero, M. Zero-Waste Process for the Transformation of a Hazardous Aluminum Waste into a Raw Material to Obtain Zeolites. *J. Clean. Prod.* **2020**, *255*, 120178. [CrossRef]
32. Abdelrahman, E.A.; Abou El-Reash, Y.G.; Youssef, H.M.; Kotp, Y.H.; Hegazey, R.M. Utilization of Rice Husk and Waste Aluminum Cans for the Synthesis of Some Nanosized Zeolite, Zeolite/Zeolite, and Geopolymer/Zeolite Products for the Efficient Removal of Co(II), Cu(II), and Zn(II) Ions from Aqueous Media. *J. Hazard. Mater.* **2021**, *401*, 123813. [CrossRef] [PubMed]
33. Kuroki, S.; Hashishin, T.; Morikawa, T.; Yamashita, K.; Matsuda, M. Selective Synthesis of Zeolites A and X from Two Industrial Wastes: Crushed Stone Powder and Aluminum Ash. *J. Environ. Manag.* **2019**, *231*, 749–756. [CrossRef]
34. Selim, M.M.; EL-Mekkawi, D.M.; Aboelenin, R.M.M.; Sayed Ahmed, S.A.; Mohamed, G.M. Preparation and Characterization of Na-A Zeolite from Aluminum Scrub and Commercial Sodium Silicate for the Removal of Cd^{2+} from Water. *J. Assoc. Arab Univ. Basic Appl. Sci.* **2017**, *24*, 19–25. [CrossRef]
35. Terzano, R.; D'Alessandro, C.; Spagnuolo, M.; Romagnoli, M.; Medici, L. Facile Zeolite Synthesis from Municipal Glass and Aluminum Solid Wastes. *CLEAN Soil Air Water* **2015**, *43*, 133–140. [CrossRef]
36. Tounsi, H.; Mseddi, S.; Djemel, S. Preparation and Characterization of Na-LTA Zeolite from Tunisian Sand and Aluminum Scrap. *Phys. Procedia* **2009**, *2*, 1065–1074. [CrossRef]
37. Padilla, I.; Romero, M.; López-Andrés, S.; López-Delgado, A. Sustainable Management of Salt Slag. *Sustainability* **2022**, *14*, 4887. [CrossRef]
38. Statista. Market Volume of Secondary Aluminum Worldwide in 2020, with a Forecast for 2027. 2023. Available online: https://www.statista.com/statistics/1306589/global-market-volume-of-secondary-aluminum (accessed on 5 July 2024).
39. Huang, X.-L.; Badawy, A.E.; Arambewela, M.; Ford, R.; Barlaz, M.; Tolaymat, T. Characterization of Salt Cake from Secondary Aluminum Production. *J. Hazard. Mater.* **2014**, *273*, 192–199. [CrossRef] [PubMed]
40. EWC. *European Waste Catalogue and Hazardous Waste List, Published by Environmental Protection Agency. Ireland*. 2001. Available online: https://archive.org/details/ewccodebook/mode/2up (accessed on 2 June 2024).
41. Attia, N.; Hassan, K.M.; Hassan, M.I. Environmental Impacts of Aluminum Dross After Metal Extraction. In *Light Met*; Martin, O., Ed.; The Minerals, Metals & Materials Series; Springer International Publishing: Cham, Switzerland, 2018; pp. 1155–1161. [CrossRef]
42. Jiménez, A.; Misol, A.; Morato, Á.; Rives, V.; Vicente, M.A.; Gil, A. Synthesis of Pollucite and Analcime Zeolites by Recovering Aluminum from a Saline Slag. *J. Clean. Prod.* **2021**, *297*, 126667. [CrossRef]
43. Pode, R. Potential Applications of Rice Husk Ash Waste from Rice Husk Biomass Power Plant. *Renew. Sustain. Energy Rev.* **2016**, *53*, 1468–1485. [CrossRef]
44. FAO. *Food Outlook—Biannual Report on Global Food Markets*. 2024. Available online: https://openknowledge.fao.org/handle/20.500.14283/cd1158en (accessed on 30 May 2024).
45. Ritter, M.T.; Lobo-Recio, M.Á.; Padilla, I.; Romero, M.; López-Delgado, A. Salt Slag and Rice Husk Ash as Raw Materials in Zeolite Synthesis: Process Optimization Using Central Composite Rotational Design. *Sustain. Chem. Pharm.* **2024**, *39*, 101599. [CrossRef]
46. Johnson, E.B.G.; Arshad, S.E. Hydrothermally Synthesized Zeolites Based on Kaolinite: A Review. *Appl. Clay Sci.* **2014**, *97–98*, 215–221. [CrossRef]
47. *NC 626:2014*; Nat. Zeolites—Determ. Exch. Capacit. Total Cationic—Ammonium Chloride Method. Cuban National Bureau of Standards: Havana, Cuba, 2014. Available online: https://ftp.isdi.co.cu/Biblioteca/BIBLIOTECA%20UNIVERSITARIA%20DEL%20ISDI/COLECCION%20DIGITAL%20DE%20NORMAS%20CUBANAS/2014/NC%20626%20a2014%206p%20lco.pdf (accessed on 20 August 2024).
48. Pangan, N.; Gallardo, S.; Gaspillo, P.; Kurniawan, W.; Hinode, H.; Promentilla, M. Hydrothermal Synthesis and Characterization of Zeolite A from Corn (Zea Mays) Stover Ash. *Materials* **2021**, *14*, 4915. [CrossRef]
49. Asefa, M.T.; Feyisa, G.B. Comparative Investigation on Two Synthesizing Methods of Zeolites for Removal of Methylene Blue from Aqueous Solution. *Int. J. Chem. Eng.* **2022**, *2022*, 1–12. [CrossRef]
50. Abdelrahman, E.A.; Hegazey, R.M. Utilization of Waste Aluminum Cans in the Fabrication of Hydroxysodalite Nanoparticles and Their Chitosan Biopolymer Composites for the Removal of Ni(II) and Pb(II) Ions from Aqueous Solutions: Kinetic, Equilibrium, and Reusability Studies. *Microchem. J.* **2019**, *145*, 18–25. [CrossRef]
51. Brar, T.; France, P.; Smirniotis, P.G. Control of Crystal Size and Distribution of Zeolite A. *Ind. Eng. Chem. Res.* **2001**, *40*, 1133–1139. [CrossRef]
52. Andrades, R.C.; Neves, R.F.; Díaz, F.R.V.; Júnior, A.H.M. Influence of Alkalinity on the Synthesis of Zeolite A and Hydroxysodalite from Metakaolin. *J. Nano Res.* **2020**, *61*, 51–60. [CrossRef]
53. Milton, R.M. Molecular Sieve Adsorbents. United State Pat. Off. 2882243, 1–12. Available online: https://patents.google.com/patent/US2882243A/en (accessed on 20 August 2024).
54. Hassan, I.; Grundy, H.D. Structure of Basic Sodalite, $Na_8Al_6Si_6O_{24}(OH)_2.2H_2O$. *Acta Crystallogr. Sect. C Struct. Chem.* **1983**, *39*, 3–5. [CrossRef]
55. Flanigen, E.M.; Sand, L.B. *Molecular Sieve Zeolites*; American Chemical Society: Washington, DC, USA, 1974; Volume 101, pp. 201–229. [CrossRef]
56. Vegere, K.; Kravcevica, R.; Krauklis, A.E.; Juhna, T. Comparative Study of Hydrothermal Synthesis Routes of Zeolite A. *Mater. Today Proc.* **2020**, *33*, 1984–1987. [CrossRef]

57. Musyoka, N.M.; Petrik, L.F.; Hums, E.; Kuhnt, A.; Schwieger, W. Thermal Stability Studies of Zeolites A and X Synthesized from South African Coal Fly Ash. *Res. Chem. Intermed.* **2015**, *41*, 575–582. [CrossRef]
58. Dimitrijevic, R.; Dondur, V.; Vulic, P.; Markovic, S.; Macura, S. Structural Characterization of Pure Na-Nephelines Synthesized by Zeolite Conversion Route. *J. Phys. Chem. Solids* **2004**, *65*, 1623–1633. [CrossRef]
59. Selvaraj, K. Transformation of Chemically Fine Tuned Zeolite A Precursor into Dense Lithium Aluminosilicates—A Comprehensive Phase Evolution and Sintering Study. *Microporous Mesoporous Mater.* **2010**, *135*, 82–89. [CrossRef]
60. Günther, C.; Richter, H.; Voigt, I.; Michaelis, A.; Tzscheutschler, H.; Krause-Rehberg, R.; Serra, J.M. Synthesis and Characterization of a Sulfur Containing Hydroxy Sodalite without Sulfur Radicals. *Microporous Mesoporous Mater.* **2015**, *214*, 1–7. [CrossRef]
61. Ayele, L.; Pérez-Pariente, J.; Chebude, Y.; Díaz, I. Synthesis of Zeolite A from Ethiopian Kaolin. *Microporous Mesoporous Mater.* **2015**, *215*, 29–36. [CrossRef]
62. Querol, X.; Moreno, N.; Umaña, J.C.; Alastuey, A.; Hernández, E.; López-Soler, A.; Plana, F. Synthesis of Zeolites from Coal Fly Ash: An Overview. *Int. J. Coal Geol.* **2002**, *50*, 413–423. [CrossRef]
63. Lobo-Recio, M.Á.; Rodrigues, C.; Custódio Jeremias, T.; Lapolli, F.R.; Padilla, I.; López-Delgado, A. Highly Efficient Removal of Aluminum, Iron, and Manganese Ions Using Linde Type-A Zeolite Obtained from Hazardous Waste. *Chemosphere* **2021**, *267*, 128919. [CrossRef]

APPENDIX C – ADSORPTION OF SAFRANINE-T DYE USING A WASTE-BASED ZEOLITE: OPTIMIZATION, KINETIC AND ISOTHERMAL STUDY

Journal of Industrial and Engineering Chemistry 136 (2024) 177–187

Contents lists available at ScienceDirect

Journal of Industrial and Engineering Chemistry

journal homepage: www.elsevier.com/locate/jiec

Adsorption of Safranine-T dye using a waste-based zeolite: Optimization, kinetic and isothermal study

Magali Teresinha Ritter [a,b], María Ángeles Lobo-Recio [b,c], Isabel Padilla [a,*], Maria Eliza Nagel-Hassemer [b], Maximina Romero [a], Aurora López-Delgado [a]

[a] Department of Materials, Eduardo Torroja Institute for Construction Sciences (IETcc)-CSIC, Serrano Galvache, 4, 28033 Madrid, Spain
[b] Departament of Environmental Engineering, Federal University of Santa Catarina (UFSC), Campus Reitor João David Ferreira Lima, 88040-900 Florianópolis, SC, Brazil
[c] Department of Energy and Sustainability, Federal University of Santa Catarina (UFSC), Campus Araranguá, Rod. Gov. Jorge Lacerda, 3201, Jardim das Avenidas, 88.906-072 Araranguá, SC, Brazil

ARTICLE INFO

Keywords:
Adsorption
Cationic dye
Safranine-T
LTA zeolite
Aluminum waste
Central composite rotational design

ABSTRACT

The global issue of water resource pollution due to wastewater containing dyes is a significant environmental concern. The proper treatment of these harmful wastewaters is a great challenge due to their characteristic structural complexity and low biodegradability. The present work reports the application of a Linde Type-A (LTA) zeolite synthesized from a hazardous aluminum waste as an adsorbent to remediate Safranine-T dye from aqueous solutions. The optimal experimental conditions (agitation rate and zeolite dosage of 147 rpm and 21.5 g/L, respectively) were determined through a central composite rotational design (CCRD), and enabled a removal efficiency of 98.12 % of the textile dye. The model that showed the best fit to the experimental data and better explained the adsorption mechanism, according to the isothermal studies, was the Sips model. The kinetics followed the pseudo-first order model and revealed that Safranine-T dye removal was achieved in a contact time of just one minute. The waste-based LTA zeolite exhibited highly promising adsorbent properties with an efficient and extremely fast adsorption capacity. Its use as a treatment agent for dye-contaminated wastewater can significantly contribute to sustainability and the circular economy.

Introduction

Contamination of water resources is a major environmental problem in the world today [1]. Industrial development has led to an increasing generation of wastes and effluents containing various harmful and damaging components, which adversely affect water quality and human health when discharged into the environment without proper treatment [2]. Dyes are one of the most commonly found pollutants in wastewater due to their large-scale production and widespread use in many areas, including the food, textile, cosmetic, paper and plastic industries [3–4].

The textile industry is a highly polluting industry for the aquatic resources due to the use of dyes. Throughout the different stages of the dyeing process, and depending on the type of fabric and dye used, dye losses can range between 5 % and 50 %, generating nearly 200 billion liters of dye-containing effluents every year [5]. Annually, around 280,000 tons of dyes are lost within the textile industry, ending up in aquatic ecosystems [6].

In terms of environmental impacts, the textile industry requires a significant amount of freshwater to process its textile products, resulting in the discharge of highly contaminated effluents [7–8]. Thus, textile industry ranks second among the most water-polluting industries, trailing behind the petroleum industry [9].

Textile dyes discharged into aquatic ecosystems, even in small amounts, result in the deterioration of water quality, affecting its odor and color. Additionally, they reduce light penetration thereby impacting the efficiency of photosynthetic function and decreasing oxygen levels, leading to negative consequences for aquatic life [10]. Recent research has revealed that these toxic dyes can cause gene mutations and even trigger the development of cancer [11].

Safranine-T (ST) (Fig. 1) is a synthetic cationic dye available as a powder or reddish crystals with the molecular formula $C_{20}H_{19}ClN_4$ (3,7–dimethyl–10–phenylphenazin–10–ium–2,8–diaminechloride).

This dye is extensively used in dyeing cotton, silk, tannin, wool, leather, bast fibers and paper, and is considered a model compound

* Corresponding author.
E-mail address: isabel.padilla@ietcc.csic.es (I. Padilla).

https://doi.org/10.1016/j.jiec.2024.02.005
Received 14 December 2023; Received in revised form 27 January 2024; Accepted 1 February 2024
Available online 4 February 2024

representing the dyes released into the effluents of the textile industry [13]. Due to their easy and strong interaction with negatively charged cell membranes, cationic dyes pose a higher risk compared to anionic dyes and can cause allergies and respiratory difficulties [14]. Contamination with dyes, especially with Safranine-T, can cause stomach discomfort, irritation of the respiratory tract, throat discomfort, as well as irritation and redness of the eyes and skin [3]. Hence, environmental protection agencies and relevant legislation demand compliance with the established permissible limits for dye discharge in wastewater, necessitating their elimination before being discharged into mainstreams [15].

ST is also classified as a nitrogenous heterocyclic dye, which is more difficult to degrade compared to the aromatic ones [16]. In this regard, the structural complexity and stability of these dyes significantly affect the decolorization process, making them difficult to treat by the methods normally utilized in wastewater plants [17–18]. Physicochemical methods commonly used in wastewater treatment, such as membrane separation, coagulation-flocculation and advanced oxidation processes have several limitations related to their high cost, low versatility, limited efficiency, generation of secondary pollutants and waste management [19–20]. Thus, recently, a great deal of research has been focused on improving water treatment processes and expanding technologies to increase the quality of treated effluents, with the aim of eliminating these toxic and biologically harmful components [21].

Among these technologies, adsorption stands out as the most extensively utilized technique for eliminating dyes from wastewater [22]. In recent years, this method has garnered increased attention due to its ease of use and efficiency, particularly with the development of low-cost alternative adsorbents [23]. A wide range of new adsorbent materials has been studied, with especial emphasis on zeolitic materials. Zeolites are aluminosilicates structured in a three-dimensional network formed by AlO_4 and SiO_4 tetrahedra interconnected through oxygen atoms, creating intracrystalline channels of atomic size [24]. Zeolites have been employed in various industrial applications due to their regular porous structure and unique properties, encompassing areas such as gas purification, water remediation, and catalysis, among other industrial uses [25].

Zeolites occur naturally or can be synthesized from various sources or silicon and aluminum. Currently, the authors have focused their research on producing zeolites from waste materials rich in silica and alumina, as an alternative to the use of pure chemical products and to preserve mineral resources. This approach leads to a reduction in process costs and environmental impact [26]. According to López-Delgado et al. [27], the utilization of hazardous waste from aluminum industry is an uncommon choice for zeolite synthesis, offering an altenative while also reducing the generation and management of such waste.

In recent years, the adsorption of Safranine-T using zeolites has been widely investigated [4,12,28–33]. In relation to the synthetized zeolite, Atun et al. [29] conducted the synthesis of various zeolites using fly ash, varying the parameters of time and temperature. The zeolite that exhibited the most favorable adsorption results for ST was obtained at a temperature of 90 °C after 7 days. Throughout this process, the formation of a mixture of NaP, X, Y, Analcime, and Sodalite zeolites was achieved. The adsorption capacity at equilibrium, considering a equilibrium time of 60 min, reached 7.02 mg/g. Ayar et al. [30] also investigated the adsorption of ST using a zeolite synthesized from fly ash at a temperature of up to 150 °C for 1 day, resulting in a mixture of Analcime and Sodalite. The adsorption capacity was determined after 40 days, reaching a q_e of 15.72 mg/g. Furthermore, Das et al. [31] conducted the synthesis of NaX and NaA zeolites from fly ash through alkali fusion at 650 °C for 1 h, followed by a hydrothermal treatment at 90 °C for 6 h, aimed at removing Safranin-T from water. The adsorption capacity at equilibrium was determined after 24 h, reaching a value of 1.27 mg/g, and, finally, Pereira et al. [32] synthesized LTA zeolite from metakaolin through a hydrothermal process at 80 °C for 24 h. The obtained zeolite was utilized for the adsorption of Safranin-T, achieving a q_e of 9.4 mg/g after 5 min. However, as far as is known, there are no studies on the adsorption of dyes, including Safranine-T, using zeolites synthesized from aluminum waste.

In this context, this work was envisaged as an opportunity to create a symbiosis between two industrial sectors: on one hand, the aluminum industry produces a hazardous waste, which is transformed by a simple process into LTA zeolite. On the other hand, this waste-based zeolite is applied for the remediation of wastewater from the dyeing industry. After selecting the optimal temperature and pH for studying the adsorption of ST on LTA zeolite, a factorial planning based on central composite rotatable design (CCRD) was employed to model, assess, and enhance treatment efficiency, as well as to identify optimal parameters in the remediation process. Moreover, kinetic and isothermal studies were performed to investigate the zeolite sorption kinetics, and its adsorption capacity and mechanism. In addition, under the best experimental conditions, a comparison of ST dye adsorption using different zeolite types was also evaluated.

Materials and methods

Adsorbent material

In this research, LTA zeolite obtained on a pilot scale through a moderate-temperature hydrothermal process, using hazardous

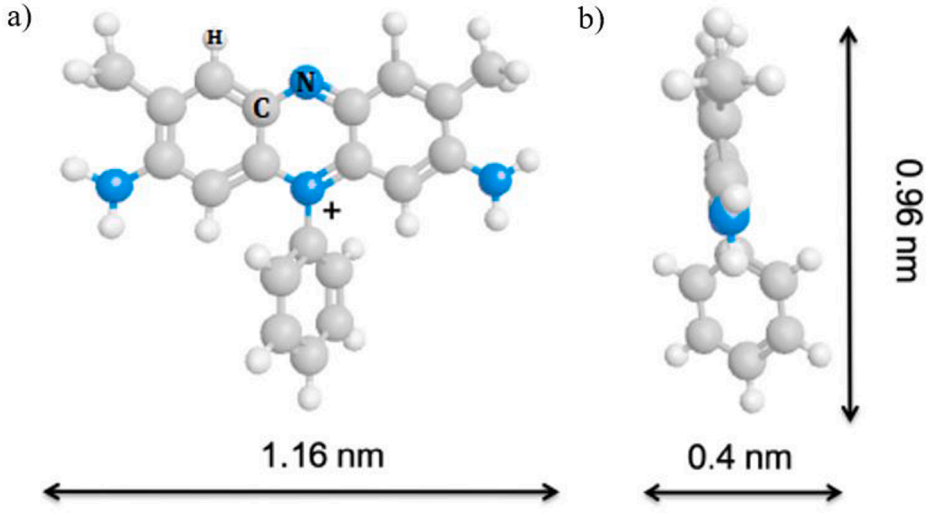

Fig. 1. Molecular 3D structure of Safranine-T dye a) Front view; b) Side view [12].

aluminum waste as raw material, was employed [27]. The aluminum waste used originates from the terciary aluminum industry and consists of the finest power fraction captured in sleeve filters during the aluminum slag process. The chemical composition consists of about 77 wt% Al_2O_3 and 4 wt% SiO_2, while mineralogical composition is primarily distributed among metallic aluminum, aluminum nitride, corundum, spinel and alkaline salts [27].

LTA zeolite [$Na_{12}Al_{12}Si_{12}O_{48}(H_2O)_{27}$] consists of a homogeneous fine-grain solid with a particle size < 100 μm. The textural characterization of the zeolite was carried out by determining the nitrogen adsorption/desorption isotherms at 77 K (ASAP 2010 Micromeritics) with the sample previously degassed (250 °C in vacuum for 24 h). The specific surface area (S_{BET}) of 19.7 m^2/g was determined through multipoint measurements using the Brunauer-Emmett-Teller (BET) method and the pore size distribution using the Barrett-Joyner-Halenda (BJH) method. The external area (S_{ext}) (7.7 m^2/g) was calculated by the t-plot method from the slope of the linear fit in the thickness range (t) of 0.35–0.5 nm according to the Harkins-Jura equation. This zeolite presents a relatively high micropore area of 12 m^2/g, a micropore volume of 0.006 cm^3/g and a predominant pore diameter of 3.8 nm [26]. The cation exchange capacity (CEC), determined by the NH_4^+ ion exchange method using a 1 M NH_4Cl solution, was 170 meq/100 g; and zeta potential (Pz), determined using a doppler laser electrophoresis analyzer (Zetasizer Nano, Malvern) shows that the zeolite exhibits a negatively charged surface at a pH higher than > 5.6 [23,26 22]. All these characteristics suggest that the waste-based LTA zeolite employed in this research possesses favorable adsorption properties for cationic dye removal. Preliminary studies carried out to assess the stability of the adsorbent material in response to pH variations showed that the zeolite was stable at pH > 4.

Adsorbate

The Safranine-T (Neon Commercial, Brazil), herein named ST, is a basic dye, also known as Basic Red 2 (CAS n° 477–73-6). A ST stock solution (1.0 g/L) was prepared in distilled water and the pH values adjusted by using either 0.1 M HCl or NaOH solutions in a multiMeter (Crison MM41). The aqueous ST solutions for adsorption tests were prepared to the required concentrations by diluting the stock solution in distilled water. As with the adsorbent material, the pH stability of the adsorbate was also determined. Preliminary tests were conducted at pH 4 to 11. The stability of the ST was demonstrated, since there were no variations in the absorbance of the dye over the pH range evaluated.

Sorption experiments

Batch adsorption experiments were performed using 100 mL conical flasks in which 50 mL of dye solution at the required concentration and the corresponding amount of zeolite were added. The pH of the dye solution was kept as obtained, approximately 7.5 (before mixing with the zeolite). All the experiments were carried out at room laboratory temperature, using a rotational shaker (Rotabit/SELECTA), reaching a maximum agitation speed of 230 rpm. The tests were conducted in duplicate and the results were expressed as the average of these values. Blank control trials were also performed. After treatment, the suspensions were centrifuged at a speed of 5300 rpm during 5 min (OrtoAlresa Digicen 21 Centrifuge), recovering the supernatant solution for measurement. The measurements of dye concentration were carried out in duplicate within the concentration range of 0.1 to 20.0 mg/L, using a HACH DR/3900 VIS spectrophotometer with a selected wavelength of 520 nm. The dye removal efficiency E (%) was calculated using Equation 1.

$$E\,(\%) = \left(\frac{C_0 - C_t}{C_0}\right).100 \tag{1}$$

where C_0 and C_t represent, respectively, the initial concentration and the concentration at the time t (min) of ST in (mg/L).

Adsorption essays were performed at different pH values (5, 7, 9 and 11) and temperatures (22, 35, 45 and 55 °C ± 1 °C). Moreover, three different types of zeolite, namely a waste-based NaP zeolite [32], a natural Mordenite type zeolite and a commercial LTA zeolite were also tested in the optimal experimental conditions determined, in order to verify their effectiveness on the adsorption process and complement the performed study.

Statistical determination of the optimal treatment conditions

In adsorption experiments, the sorbent adsorption capacity is dependent on various parameters, such as the nature of the adsorbate and the adsorbent, and the operational conditions [34]. In this context, statistical analysis serves as a valuable tool for comprehending the interactions among factors and for ascertaining the optimal conditions for dye removal, which, if required, can be extrapolated with fewer experiments compared to the traditional univariate method [35].

Thus, to determine the best treatment conditions and optimize the dye removal efficiency, a CCRD involving two factors, each composed of two levels (2^2), was developed. It was considered that the agitation rate and zeolite dosage were the independent variables and exerted influence on the treatment efficiency, and the percentage of ST removal was chosen as the response (dependent variable). Factorial scores (−1 and +1), indicating the minimum and maximum level for each variable, axial portions (−1.414 and +1.414) (calculated by Equation (2), and 4 central (0) points were used in the experiment, totaling 12 assays.

$$\alpha = (2^n)^{1/4} \tag{2}$$

where n is the number of independent variable ($n = 2$) and α is the axial distance from the central point.

Experiments were conducted using 50 mL of dye solution (C_0 50 mg/L), under optimal pH and temperature conditions. The contact time was 10 min. The values of the factors at the central point, which were 15 g/L of zeolite and 150 rpm, were established after conducting some preliminary tests. The experimental outcomes underwent statistical scrutiny using the STATISTICA® 13.3 software. This involved employing analysis of variance (ANOVA) in order to assess statistical parameters and appraise the predictive capabilities of the mathematical model.

Sorption kinetics

The kinetic studies seek to ascertain the required contact time for treatment and the adsorption process rate. The rate was determined through nine assays (1, 2, 5, 10, 15, 30, 60, 90 and 120 min), using 50 mL of 50 mg/L ST solution, in the optimal pH and temperature conditions, and employing a zeolite dosage and agitation rate based on the data determined by the CCRD, (following the procedure described in Section 2.3). The adsorption kinetic process was assessed using the pseudo-first order (PFO), pseudo-second order (PSO), intraparticle diffusion (ID) and Elovich kinetic models. These models, presented in Table 1, were utilized to achieve a clearer understanding of the adsorption process, including aspects such as the type and rate of adsorption, saturation time and controlling steps [22].

Usually for determining the best fit of experimental data with the proposed assessment models, the linear regression method is employed, especially due to its simplicity. However, the process of linearization alters the variables considered independent or dependent, potentially leading to error propagation and inaccurate parameter estimations [40]. Hence, to ensure consistent and accurate estimations for fitting the experimental data to the studied kinetic models, the non-linear regression method utilizing the Excel Solver add-in was utilized. Finally, several error functions (Table 2) were applied to determine the model with the best fit to the experimental data. However, since the adoption

Table 1
Equations for the models employed in the study of kinetics.

Model	Equation	Reference
Pseudo-first order	$q_t = q_e(1 - e^{(-K_1 t)})$	[36]
Pseudo-second order	$q_t = \frac{K_2 {q_e}^2 t}{1 + K_2 q_e t}$	[37]
Intraparticle diffusion	$q_t = K_{int} t^{\frac{1}{2}} + C$	[38]
Elovich	$q_t = \frac{1}{\beta}\ln(1 + \alpha\beta t)$	[39]

q_t = dye amount sorbed at time t (mg/g); q_e = dye amount sorbed at equilibrium (mg/g); K_1 = rate constant of pseudo-first order sorption kinetics (L/min); K_2 = equilibrium rate constant of pseudo-second order sorption (g/(mg min)); K_{int} = intraparticle diffusion rate constant (mg/g $min^{1/2}$); C = constant indicative of the significant external mass transfer (mg/g); α = desorption constant; β = initial adsorption rate (mg/(g min)) and t = time.

of different error criteria leads to obtaining different sets of parameters, the standard normalizing procedure (known as *Sum of Normalized Errors* – SNE) was applied following the proposed by Foo and Hameed [41]. This process entails the following steps: (i) selecting the model and error function, identifying the parameters that can be adjusted to reduce the error function; (ii) identifying the remaining error functions based on the parameter set; (iii) computing the parameters and their respective error function values (restarting the process upon minimizing the error function); (iv) selecting the most significant parameters contributing to the highest error; and (v) summing the parameters contributing to the least error.

Sorption isotherms

Adsorption equilibrium is an essential requirement in the analysis of an adsorption separation process. Isothermal studies were conducted to determine how much sorbate (ST dye) is sorbed per gram of adsorbent material (zeolite) after reaching equilibrium (q_e), and also the process mechanism. To obtain the adsorption isotherms, different dye solution concentrations (10–100 mg/L) were treated under optimal pH and temperature conditions, using the agitation rate and zeolite dosage obtained from the CCRD. As described in section 2.3, the experimental method was carried out, and through the execution of kinetic tests, the optimal contact time was determined. Equation (3) was used to calculate the adsorption capacity q_e (mg/g).

$$q_e = \frac{(C_0 - C_e)V}{m} \quad (3)$$

in which q_e = sorbent adsorption capacity ($mg_{sorbate}/g_{adsorbent}$) at the equilibrium; C_0 is the initial sorbate concentration (mg/L); $_{Ce}$ is the equilibrium sorbate concentration (mg/L); V is the ST solution volume (L); and m is the quantity of adsorbent applied (g).

In order to determine the mechanisms governing the adsorption process, several mathematical models were applied, such as Linear, Langmuir, Freundlich, Dubinin-Radushkevish (D-R), Sips, Toth, Redlich-

Table 3
Equations for the models employed in the study of isothermal.

Model	Equation	Reference
Linear	$q_e = K_d C_e$	[43]
Langmuir	$q_e = \frac{q_{max} K_L C_e}{1 + K_L C_e}$	[44]
Freundlich	$q_e = K_F {C_e}^{1/n}$	[43]
Dubinin-Radushkevish	$q_e = q_{max}\exp(-K_{ads}\varepsilon^2)$ $\varepsilon = RTln\left(1 + \left(\frac{1}{C_e}\right)\right)$ $E = \frac{1}{\sqrt{2K_{ads}}}$	[45]
Sips	$q_e = \frac{q_{max} K_S C e^m}{1 + K_S C e^m}$	[46]
Toth	$q_e = \frac{K_T C_e}{\frac{1}{(a_T + C_e)^t}}$	[47]
Redlich-Peterson	$q_e = \frac{K_R C_e}{1 + a_R {C_e}^n}$	[48]
Temkin	$q_e = \frac{RT}{b_T} ln(A_T C_e)$	[49]

q_{max} = maximum adsorption capacity (mg/g); K_d = sorbent distribution constant (L/g); K_L = Langmuir adsorption equilibrium constant (L/mg); K_F = Freundlich adsorption [(mg/g) $(mg/L)^{-1/n}$]; 1/n = empirical coefficient; K_S = Sips isotherm constant (L/g); m = Sips isotherm exponent; K_T = Tóth isotherm constant (mg/g); t = exponent inverse of the Tóth model; a_T = constant (L/mg); K_R = Redlich-Peterson isotherm constant (L/g); a_R = Redlich-Peterson constant (L/mg); n = exponent of Redlich-Peterson model; K_{ads} = Dubinin-Radushkevich isotherm constant (mol^2/kJ^2); ε = mean adsorption energy (kJ/mol); R = gas constant (0.008314 kJ/mol K); T = temperature (K); b_T = Temkin heat of adsorption constant and A_T = equilibrium biding constant (L/mg).

Table 2
Error functions used in the isothermal and kinetic analysis (Adaptation of Ayawei et al. [42].

Error function	Equation
Sum Square of Errors (ERRSQ)	$ERRSQ = \sum_{i=1}^{n}\left(q_{ecalc} - q_{eexp}\right)^2$
Hybrid Fractional Error Function (HYBRID)	$HYBRID = \frac{100}{n-p}\sum_{i=1}^{n}\left[\frac{\left(q_{eexp} - q_{ecalc}\right)^2}{q_{eexp}}\right]$
Average Relative Error (ARE)	$ARE = \frac{100}{n}\sum_{i=1}^{n}\left[\frac{q_{ecalc} - q_{eexp}}{q_{eexp}}\right]$
Marquardt's Percent Standard Deviation (MPSD)	$MPSD = \sqrt{\frac{1}{n-p}\sum_{i=1}^{n}\left(\frac{\left(q_{eexp} - q_{ecalc}\right)}{q_{eexp}}\right)^2}$
Sum of Absolute Errors (EABS)	$EABS = \sum_{i=1}^{n}\left[q_{eexp} - q_{ecalc}\right]$
Coefficient of Determination (R^2)	$R^2 = \frac{\sum\left(q_{ecalc} - q_{mexp}\right)^2}{\sum\left[\left(q_{ecalc} - q_{mexp}\right)^2 + \left(q_{ecalc} - q_{eexp}\right)^2\right]}$
Nonlinear Chi-Square Test (X^2)	$X^2 = \sum_{i=1}^{n}\frac{\left(q_{ecalc} - q_{eexp}\right)^2}{q_{eexp}}$
Coefficient of Nondetermination (CND)	$CND = 1 - R^2$

$q_{e\ calc}$ = dye amount sorbed at equilibrium (mg/g) (calculated/theoretical); $q_{e\ exp}$ = dye amount sorbed at equilibrium (mg/g) (experimentally determined); $q_{m\ exp}$ = average amount of dye sorbed at equilibrium (mg/g) (experimentally determined); n = number of the data points; p = number of the parameters and R^2 = coefficient of determination.

Table 4
Data matrix and responses of CCRD design (C_0 50 mg/L).

Run n°	Factors				Responses
	Agitation Rate		Zeolite Dosage		
	Factor Level	Agitation Rate (rpm)	Factor Level	Zeolite Dosage (g/L)	Cf (mg L^{-1}) [Removal (%)]
1	−1	100	−1	5	29.45 ± 0.05 [41.10]
2	−1	100	1	25	1.25 ± 0.04 [97.51]
3	1	200	−1	5	27.40 ± 0.00 [45.20]
4	1	200	1	25	1.26 ± 0.02 [97.48]
5	−1.414	80	0	15	2.12 ± 0.05 [95.77]
6	1.414	220	0	15	2.09 ± 0.04 [95.83]
7	0	150	−1.414	0.85	46.54 ± 0.46 [6.92]
8	0	150	1.414	29.15	1.22 ± 0.09 [97.57]
9	0	150	0	15	2.00 ± 0.09 [96.01]
10	0	150	0	15	2.04 ± 0.06 [95.93]
11	0	150	0	15	2.09 ± 0.10 [95.82]
12	0	150	0	15	2.01 ± 0.01 [95.98]

Peterson (R-P) and Temkin. Their corresponding equations are presented in Table 3. As in the kinetic studies, nonlinear regression and the error functions (Table 2), with minimizing the error distributions through a standard normalization procedure was applied to evaluate the isothermal models.

Results and discussion

Effect of the pH and temperature

The influence of initial pH and temperature was studied in the adsorption process of ST dye. The pH of the mixed solution (adsorbent + adsorbate) is a critical parameter that influences the removal of the adsorbate, affecting the structural stability of the adsorbent, the state of functional groups on the adsorbent surface, and the ionization of the sorbate within the solution [22]. In this research, the effect of pH was investigated at room temperature, with a contact time of 1 min at different pH values [5,7]. This pH range was selected based on the fact that at pH values below 4, zeolites lose its stability, while at pH values above 11, Safranine-T evolves into its anionic structure, interfering with the colorimetric determination. It was found that more basic pH leads to a greater ability of the zeolite to remove the dye. The maximum removal was reported at pH 11, reaching 98.12 % of removal. At pH 9, ST removal was 84.62 %; at pH 7, 82.68 % and, at pH 5, 78.71 %. This is advantageous, since textile wastewaters are usually basic. The behavior of the zeolite in the adsorption process at different dye solution pH can be clarified by considering the relationship between the zeta potential (Pz) of LTA zeolite and the dissociated state of Safranine-T molecules.

Table 6
Analysis of variance for Safranine-T removal for the 2^2 factorial design.

Variation source	SS	df	MS	F		*p*
				Calc.	Tab.[a]	
Regression	10172.477	1	10172.477	1326.489	4.965	<0.05
Sediments	76.687	10	7.669			
Total	10249.164	11				

SS: sum of square; df: degree of freedom; MS: mean of square; F: Fisher's ratio; p: probability.
[a] Tabulated values [35].

The Pz of the LTA zeolite was found to be negative when the pH values exceeded 5.6, indicating a negatively charged zeolite surface at these pH values, which facilitates the electrostatic interaction between the LTA zeolite and the cationic molecules of ST dye. Consequently, this leads to an increased percentage of removal [28]. On the contrary, there was reduced dye adsorption at acidic pH, likely due to a higher concentration of free protons competing for the avaiable adsorption sites on the zeolite with the cationic groups on the dye for available [50].

Temperature is another important factor in adsorption processes, especially when the system involves a solid adsorbent and a liquid or gaseous adsorbate. Temperature variations affect the kinetic energy of molecules, the adsorbate-adsorbent molecular affinity, adsorption capacity and changes in the adsorbate stability. The effect of the temperature was analyzed at 22, 35, 45 and 55 ± 1 °C. This temperature range was selected because 22 °C represents the average ambient laboratory temperature, while temperature of 55 °C was chosen as a possible

Table 5
Estimated effects for Safranine-T removal variables.

	Coefficient	Effect	Standard error	t(6)	p-value
Agitation (*L*)	Q_1	1.0490	2.540712	0.4129	0.694048
Agitation (*Q*)	Q_{12}	−2.0753	2.869380	−0.7233	0.496737
Zeolite dosage (L)	***Q_2***	***59.2070***	***2.527274***	***23.4272***	***0.000000***
Zeolite dosage (Q)	***Q_{22}***	***−45.4985***	***2.821168***	***−16.1275***	***0.000004***
Agitation *vs* Zeolite dosage	$Q_1 vs Q_2$	−2.0650	3.575099	−0.5776	0.584538

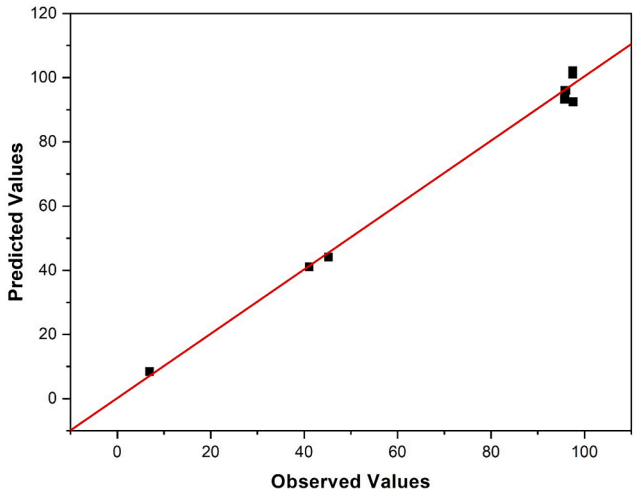

Fig. 2. Residual distribution for ST dye removal (R^2 = 0.9927) (observed values and values predicted by the model).

extreme environmental condition. The result obtained showed a slight decrease in dye removal from 98.12 % to 94.50 %, as the temperature increase within the mentioned range. As a result, the optimal parameters selected for conducting the adsorption process include a pH equal to that of the adsorbate/adsorbent mixture (~11), at room laboratory temperature (22 °C ± 1 °C).

Statistical analysis for ST removal

In Table 4, the 2^2-CCRD data matrix is presented, which included the levels of the factors, the corresponding values, and the obtained responses. The utilization of LTA zeolite for adsorbing dye-containing solutions proved to be highly efficient, as evidenced by the high levels of dye removal, higher than 95 % in almost all the conditions evaluated, with the exception of runs 1, 3 and 7, in which small doses of zeolite were used.

The estimated effects were based on the p-value (Table 5). At a 95 % confidence level, the only variable that significantly influenced ($p < 0.05$) the dye removal efficiency was the dosage of zeolite, in both its linear (Q2) and quadratic (Q22) forms. ST removal is linearly dependent on the zeolite dosage and its effect is positive (59.0026), i.e., when increasing the zeolite dosage, the dye removal also increased. Agitation rate (linear (Q_1) and quadratic (Q_{12})) did not significantly ($p > 0.05$) influence dye removal. Determination coefficient (R^2) quantifies the extent to which the regression equation accounts for the variability in responses compared to the overall variation. For the ST dye removal, a R^2 = 0.9927 was obtained. This values suggests a strong interrelentionship between the values obtained through experimentation and those predicted by the model, both for the independent variables and for the responses. That is, the model is able to explain approximately 99.27 % of the variations in the final concentration of the dye.

The analysis of variance (ANOVA) showed that, for the removal efficiency of the ST dye, the $F_{calculated} > F_{tabulated}$ (Table 6), which confirms that the sample distribution is statistically representative. Thus, the ANOVA for ST removal indicated that the model is valid within the 95 % confidence interval, and that no adjustment was required within this interval, resulting in an excellent reproduction of the experimental samples. Furthermore, to reinforce the model's validity, a residual distribution graph (Fig. 2) was employed, which compares the percentage removal predicted by the model with the values obtained in the experimental tests. In these graph (Fig. 2), it is observed that the experimental values (represented by dots) are close to the line (predicted values), showing proportional negative and positive deviations. This may indicate a strong correlation and indicates the quality of fit between the predicted and the experimental values.

Fig. 3 displays response surface plots and contour curves, enabling visualization of the optimal values where the combination of variables led to an improved response [51]. The results reveals that the highest removal of ST was achieved when an agitation rate within the range of 90–200 rpm and a zeolite dosage of 19–24 g/L were employed (Fig. 3). This indicates that there was no variation in the removal efficiency related to the agitation rate, in agreement with the corresponding p-value above discussed (Table 5). The critical values, determined through statistical analysis using Statistica® 13.3 software, were established at 21.5 g of zeolite per liter and an agitation rate of 147 rpm. An experiment was conducted using the established factor values to assess the appropriateness of the results, as not all experimental factors could be considered in the statistical analysis. Due to the high removal of ST dye (97.61 %), the suitability of the planning carried out by the CCRD for establishing the optimal treatment conditions is demonstrated.

Sorption kinetic results

The kinetic study is a crucial point to evaluate the adsorption, allowing the determination of the appropriate contact time to control the process and assisting in identifying the predominant adsorption mechanism. Adsorption kinetics were conducted at 22 ± 1 °C, using a

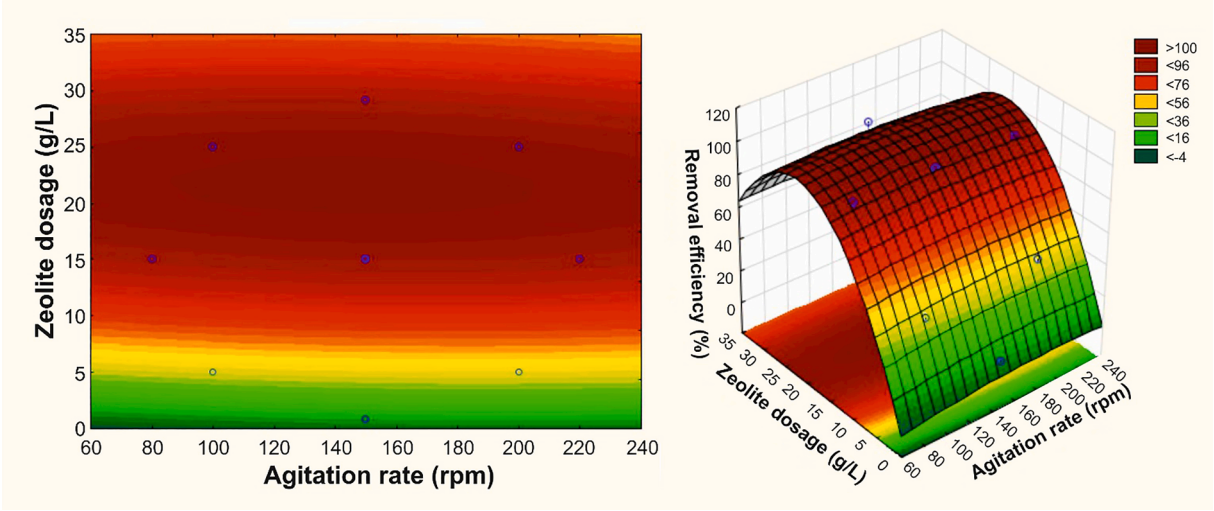

Fig. 3. Response surface (left) and contour curve (right) for ST removal (%).

Table 7
Experimental kinetic results and calculated parameters for the adsorption of the ST dye (C_0 50 mg/L) onto LTA zeolite (dosage = 21.5 g/L).

Time (min)	C_e	q_t exp.	PFO			PSO			ID			Elovich		
			q_t calc	q_e	K_1	q_t calc	q_e	K_2	q_t calc	K_{int}	C	q_t calc	α	β
1	1.100 ± 0.000	2.274	2.271	2.271	16.91	2.262	2.275	72.89	1.759	0.08	1.68	2.142	$8.26E^{17}$	20.68
2	1.130 ± 0.070	2.273	2.271			2.268			1.793			2.176		
5	1.205 ± 0.005	2.270	2.271			2.273			1.859			2.220		
10	1.195 ± 0.005	2.270	2.271			2.274			1.934			2.253		
15	1.135 ± 0.005	2.273	2.271			2.274			1.991			2.273		
30	1.150 ± 0.010	2.272	2.271			2.275			2.120			2.306		
60	1.180 ± 0.000	2.271	2.271			2.275			2.303			2.340		
90	1.125 ± 0.045	2.273	2.271			2.275			2.443			2.360		
120	1.290 ± 0.020	2.266	2.271			2.275			2.561			2.373		

C_e (mg/L): equilibrium sorbate concentration; q_t (mg/g): zeolite sorption capacity at the time (t); q_e (mg/g): zeolite sorption capacity at equilibrium. K_1 = rate constant of pseudo-first order sorption kinetics (L/min); K_2 = equilibrium rate constant of pseudo-second order sorption (g/(mg min)); K_{int} = intraparticle diffusion rate constant (mg/(g $min^{1/2}$)); C = constant indicative of the significant external mass transfer (mg/g); α = desorption constant and β = initial adsorption rate (mg/(g min)).

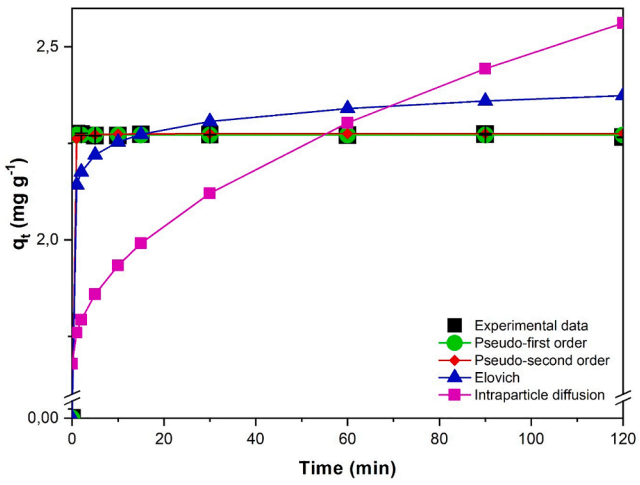

Fig. 4. Kinetic experimental data compared with the kinetic models for ST dye adsorption onto waste-based LTA zeolite.

dye concentration of 50 mg/L, and operating with the optimal values of pH, zeolite dosage, and agitation rate. Different contact times (1-120 min) between the zeolite and textile dye solutions were tested. The experimental kinetic data and the calculated parameters are presented in Table 7. Dye removal efficiency reached 97.80 % (C_e = 1.100 ± 0.000 mg/L) in the first minute of the test, and remained in this range for all tested contact times, indicating an extremely fast adsorption kinetics. This brief contact duration, rapid reaction rate and high capacity of adsorption are determining factors for the application of the waste-based LTA zeolite when scaling up an adsorption process to a pilot or industrial level. In order to estimate the kinetic parameters and predict the dye sorption rate, pseudo-first order, pseudo-second order, intra-particle diffusion and Elovich kinetic models (Table 1) were applied. The fitting results for these kinetics are shown in Fig. 4.

The fitting of the obtained experimental data to the kinetic models was determined based on the R^2 (Table 2) for the corresponding nonlinear regression equations. Regarding the intraparticle diffusion model, the graphs displayed a relatively low R^2 value, 0.178 (Table 8), and the origin of the coordinates was not intercepted by the straight lines (Fig. 4). As a result, it was concluded that intraparticle diffusion was not the restricting factor in the adsorption mechanism [23]. Pseudo-first order, pseudo-second order and Elovich model presented a high R^2 value (>0.98). Various error functions were employed to reduce the distribution of errors between the experimental equilibrium data and those provided by the isotherms. This allowed validation that, among the models used, the PFO is the model that best fits the experimental kinetic data (Table 8). This kinetic model was the most suitable for describing the adsorption process due not only to its high coefficient of determination (R^2 = 0.99999) but also to consistently displaying the lowest error values across all evaluated error functions. The interpretations of adsorption mechanisms via kinetic models lack robust theoretical underpinnings and cannot be discerned solely through straightforward curve fitting techniques [52]. However, it can be indicated that the adsorption of the Safranine-T dye by LTA zeolite follows a physical mechanism, which should be corroborated through the corresponding isothermal study. The q_e (2.271 mg/g) and K_1 (16.913 L/min) values were consistent with those previously documented for the removal ST dye using other zeolitic materials [32].

Table 9
Experimental results from the isothermal study for the adsorption of the ST dye on LTA zeolite.

C_0 (mg/L)	C_e (mg/L)	Removal (%)	q_e (mg/g)
10	0.665 ± 0.065	93.35 ± 0.65	0.434 ± 0.003
15	0.610 ± 0.020	95.93 ± 0.13	0.669 ± 0.001
20	0.630 ± 0.010	96.85 ± 0.05	0.901 ± 0.000
25	0.710 ± 0.010	97.16 ± 0.04	1.130 ± 0.000
40	0.885 ± 0.045	97.79 ± 0.11	1.819 ± 0.002
50	0.940 ± 0.020	98.12 ± 0.04	2.282 ± 0.001
60	1.445 ± 0.055	97.59 ± 0.09	2.723 ± 0.003
75	2.470 ± 0.070	96.71 ± 0.09	3.373 ± 0.003
80	2.970 ± 0.030	96.29 ± 0.04	3.583 ± 0.001
85	3.675 ± 0.045	95.68 ± 0.05	3.783 ± 0.002
90	5.565 ± 0.005	93.82 ± 0.01	3.927 ± 0.000
100	8.425 ± 0.105	91.58 ± 0.10	4.259 ± 0.005

C_0: inicial dye concentration; C_e: dye concentration at the equilibrium and q_e: zeolite sorption capacity at equilibrium.

Table 8
Parameters of the kinetic models and corresponding error functions values.

Model	R^2	Error Functions						
		ERRQS	EABS	ARE	HYBRID	MPSD	X^2	CND
PFO	**0.99999**	**0.0001**	**0.0000**	**0.0000**	**0.0003**	**0.0004**	**0.0000**	**0.0000**
PSO	0.99993	0.0003	0.0099	0.0436	0.0016	0.0022	0.0001	0.0001
ID	0.17808	3.8161	0.0000	7.3849	4.8810	6.4457	0.4393	0.8219
Elovich	0.98831	0.0549	0.0018	0.0097	0.2686	0.3547	0.0242	0.0117

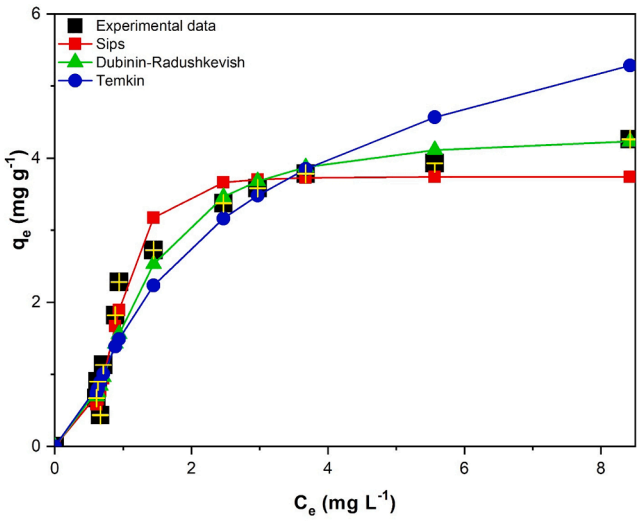

Fig. 5. Isothermal experimental data compared with the isothermal models for ST dye adsorption onto waste-based LTA zeolite.

Sorption isothermal results

Isothermal experiments were conduced at room temperature (22 ± 1 °C), using the dye solution at the pH resulting of its preparation and with 1 min of contact time (optimal contact time according to the kinetic study). Furthermore, the agitation rate and zeolite dosage were 147 rpm and 21.5 g/L, respectively, parameters that were determined through the CCRD. The concentration influence for Safranine-T dye adsorption was studied within the range of 10–100 mg/L (Table 9).

It was observed that the adsorption capacity (q_e) increased from 0.434 to 4.259 mg/g when the initial dye concentration was increased from 10 to 100 mg/L. However, this led to a decrease in the removal efficiency, reducing from 98.12 % to 91.58 %. According to Yadav et al. [22], elevated concentrations of dye ions generate a driving force to overcome mass transfer between liquid and solid phases, but at exceedingly high concentrations, binding sites reach saturation, leading to a decline in adsorption efficiency. The waste-based LTA zeolite employed demonstrates high porosity, a significant CEC, and an anionic surface over a broad pH range [23]. This suggests that the uptake of dye molecules by this material could occur through both adsorption and ion exchange mechanisms [28]. Adsorption isotherm models depict the distribution of adsorbed species between the liquid and the adsorbent using graphs constructed based on a set of assumptions. These models are associated with the heterogeneity or homogeneity of the adsorbent, the coverage type, and the potential for interaction among the adsorbates [41]. To determine the mechanisms involved in the adsorption process and the maximum adsorption capacity, different isothermal models (Table 3) were applied. Fig. 5 shows the experimental isothermal data compared to the best-fit isothermal models (considering models with $R^2 > 0.9$). The isothermal parameters and corresponding error function values are shown in Table 10.

When comparing the R^2 values for all the analyzed isotherms, the fit follows the following sequence: Dubinin-Radushkevich > Sips > Temkin > Toth > Langmuir > Redlich-Peterson > Freundlich > Linear. Hence, the Dubinin-Radushkevish (R^2 = 0.96580) and Sips (R^2 = 0.96320) isotherms were the ones that yielded the most accurate fits. Although the D-R model showed a slightly higher R^2 than the Sips model, it doesn't serve as a suitable means to pinpoint the adsorption mechanism. According to Puccia and Avena [53], the use of the D-R equation at the the solid–liquid systems has been incorrect, because substituting concentrations in molar units results in a "chemical" binding, whereas using units in mg/L leads to a "physical" binding. Moreover, considering the other error functions, it can be seen that with the exception of the *Average Relative Error* (ARE) and the *Coefficient of Nondetermination* (CND) functions, all the others presented lower values for the Sips model. Thus, the Sips model can be considered the isothermal model that best fits the experimental data and best describes the adsorption behavior of the textile dye on the zeolite, concurring with the kinetic studies. The Sips model suggests that, when adsorbate concentrations are low, it adopts the Freundlich form, characterized by the existence of weak physical interactions (van der Waals forces) between the adsorbate and the adsorbent [41]. Given that 50 mg/L can be regarded as a relatively low concentration for textile dyes, the involvement of physisorption processes in the adsorption mechanism can be expected. Physisorption is a reversible adsorption process in which adsorbate molecules adhere to the surface of the adsorbent, forming multiple layers. As the adsorption process unfolds and layers increase, a gradual decrease in interaction between adsorbent and adsorbate molecules is observed, culminating in the completion of the adsorption process [41]. This mechanism is confirmed by assessing the values of n in the Freundlich model and the adsorption energy (E) in the D-R model. In this context, when n exceeds unity, as in this study where n = 1.07, it is interpreted that the adsorption process is physical, heterogeneous, and multilayered. Furthermore, the value of E, which is 1.24 kJ/mol, reaffirms that the adsorption mechanism at the active sites of the zeolite is of a physical nature, as E < 8 kJ/mol, indicating weak and reversible interactions in the adsorption process [54]. The fact that the interactions are attributed to weak intermolecular forces suggests

Table 10
Parameters of the isothermal models and corresponding error functions values.

Model	Parameters		R^2	Error Functions						
				ERRQS	EABS	ARE	HYBRID	MPSD	X^2	CND
Linear	K_d	0.9963	0.7341	25.5960	0.0000	7.0243	60.7299	74.1543	7.2876	0.2659
Langmuir	q_{max}	7.1344	0.8824	3.4163	2.0163	4.7640	16.8028	71.0435	2.0163	0.1176
	K_L	0.2524								
Freundlich	K_F	1.3311	0.7693	6.3935	4.5733	0.0000	25.2883	85.4151	3.0346	0.2307
	n	1.6975								
Dubinin-Radushkevish	q_{max}	4.3357	0.9658	2.5156	1.2876	0.0001	10.7300	38.6504	3.0346	0.0342
	K_{ads}	0.3239								
Sips	q_{max}	3.7413	**0.9632**	**1.0036**	**0.6312**	**0.4206**	**5.2597**	**23.6249**	**0.6312**	**0.0368**
	K_S	1.3051								
	m	3.9516								
Toth	K_T	56.3653	0.8969	2.8217	1.9066	5.5489	15.6065	71.6528	1.8728	0.1031
	a_T	8.0918								
	t	0.6046								
Redlich-Peterson	K_R	1.4761	0.8600	2.3037	1.5512	3.9906	12.8690	57.2457	2.1278	0.1400
	a_R	0.0272								
	n	2.0393								
Temkin	A_T	2.5170	0.9228	2.8141	0.0000	3.8366	11.2402	41.6778	1.3488	0.0772
	b_T	1.4177								

that the ST molecules adsorbed on the surface of the saturated zeolite can be easily desorbed. This would facilitate the reuse of the zeolite and the recovery of the textile dye.

The q_{max} (3.74 mg/g) obtained by applying the Sips model presented an intermediate value between the values (q_{max} = 1.3 mg/g and q_{max} = 7.0 mg/g) reported by Atun et al. [29] and Das et al. [31], respectively, using different zeolitic materials for ST adsorption. Nevertheless, the differences between the corresponding values can be attributable to the dissimilar experimental conditions used for the different authors, i.e, adsorbent dosage, adsorbate concentration, etc. According to Sieren et al. [4] the adsorption of the Safranine-T cations is restricted to the outer surface of the zeolites due to the larger size of ST^{+} compared to the dimensions of the zeolite channels, which could account for variations in dye removal. Atun et al. [29] attribute the lower q_e values obtained for the adsorption of Safranine-T dye to its larger molecular size compared to the other basic dyes used on the same synthetic zeolite. Ayar et al. [30] found that the removal capacity of the ST dye is related to the pore sizes and cation exchange capacities (CEC) of the adsorbents, using both a natural zeolite and a synthesized one (a mixture of Analcime and Sodalite). With the natural Clinoptilolite zeolite, twice the ST removal was achieved compared to the synthetic zeolite. This difference can be attributed to the lower affinity of Analcime and Sodalite mixture present in the synthetic zeolite towards ST cations, owing to the smaller pore size and reduced catio-exchange capacity (CEC). The waste-based zeolite used in this study has a high CEC (170meq/100g), but has a very limited pore diameter (3.8 nm) compared to the large size of the ST dye molecules, which may have influenced the adsorption process, corroborating Sieren et al. [4] who state that adsorption is limited to the zeolite surface area.

Thermodynamic analysis and comparison of the Safranine-T dye adsorption using different zeolite types

The spontaneity of ST adsorption by the waste-based zeolite was determined by calculating the Standard Gibbs free energy changes (ΔG^0), standard entropy changes (ΔS^0) and standard enthalpy changes (ΔH^0), using Equation (4) and Equation (5), presented below.

$$\Delta G^0 = -RTln\left(\frac{q_e}{C_e}\right) \quad (4)$$

$$\Delta G^0 = \Delta H^0 - T\Delta S^0 \quad (5)$$

in which R = universal gas constant (8.314 J/(mol K)), T = absolute temperature (K), q_e is zeolite sorption capacity at equilibrium (mg/g) and C_e is equilibrium sorbate concentration (mg/L). The thermodynamic parameters calculated are presented in Table 11.

According to Kaur et al. [50], the negative ΔG^0 suggests that the adsorption of ST onto the LTA zeolite occurs spontaneously and feasibility. The negative ΔH^0 signifies the exothermic character of adsorption process, indicating a preference for lower temperatures. Additionally, the negative ΔS^0 values indicate substantial disorderliness at the solid–liquid interface, with no notable alteration in the internal zeolite structure and its affinity toward the dye.

Application of different zeolites on the Safranine-T removal

In addition to the waste-based LTA zeolite, Safranine-T removal was tested using different zeolite types, including a waste-based NaP zeolite, a natural Mordenite zeolite and a commercial LTA zeolite. The results are presented in Table 12 and Fig. 6. It was found a removal efficiency of 94.40 ± 0.16 % for the waste-based NaP zeolite, 93.11 ± 0.11 % for the natural Mordenite and 82.95 ± 0.17 % for the commercial LTA zeolite. These values are lower than the removal efficiency of LTA zeolite used in this study (98.12 ± 0.04 %). The final concentration of the textile effluent after the adsorption process varied between 0.94 ± 0.02 mg/L and 8.53 ± 0.09 mg/L for the waste-based LTA and commercial LTA zeolites, respectively. The NaP zeolite, also synthesized from aluminum waste [33], was the second best performer in ST adsorption, in terms of removal efficiency, adsorption capacity and lowest final dye concentration. While the waste-based LTA zeolite showed an adsorption capacity q_e of 2.282 ± 0.001 mg/g, the waste-based NaP achieved a q_e of 2.195 ± 0.004 mg/g. These results can be attributed, especially, to structural, textural and cation exchange capacity (CEC) differences between the zeolites [30]. Regarding cation exchange capacity (CEC), although the waste-based NaP zeolite has a CEC of 2.73 meq/g, its performance in adsorbing the ST dye was lower than that of the waste-based LTA (CEC of 1.70 meq/g). In terms of surface area, the commercial LTA zeolite, which showed the lowest adsorption capacity, was also the one with the lowest SBET (7.37 m^2/g) [55], compared to 19 m^2/g for Mordenite [56], 14.2 m^2/g for waste-based NaP and 19.7 m^2/g for the waste-based LTA used in this study. This indicates the important influence of this parameter on the adsorption capacity of the materials tested.

Table 11
Thermodynamic parameters for the adsorption of Safranine-T onto waste-based LTA zeolite.

ΔH (kJ/mol)	ΔS (J/(mol K))	ΔG (kJ/mol)			
		295 K	308 K	318 K	328 K
−13.32	−38.31	−16.55	−14.45	−13.88	−13.82

Table 12
Adsorption capacity of the different types of zeolites applied to the removal of ST dye.

Zeolite Type	Ce (mg/L)	Removal (%)	q_e (mg/g)
Waste-based LTA	0.94 ± 0.02	98.12 ± 0.04	2.282 ± 0.001
Waste-based NaP	2.80 ± 0.08	94.40 ± 0.16	2.195 ± 0.004
Natural Mordenite	3.45 ± 0.06	93.11 ± 0.11	2.165 ± 0.003
Commercial LTA	8.53 ± 0.09	82.95 ± 0.17	1.929 ± 0.004

Environmental considerations and future challenges

The LTA zeolite, obtained from hazardous waste in the terciary aluminum industry, has proven to be a highly effective adsorbent for the rapid removal of Safranin-T (utilized as a model for cationic dyes), achieving an efficiency >98 % in synthetic waters within extremely short times (<1 min). This methodology not only prevents the discharge of industrial wastewater contaminated with dyes into natural basins but also addresses issues associated with the disposal of hazardous waste in soil, generating a symbiosis between two polluting industries: the terciary aluminum industry and the textile industry.

The development of this methodology is a significant finding as it overcomes limitations related to the extended durations of conventional adsorption processes [4,12,29–30], making it feasible for the decontamination of waters from the textile industry or other sectors employing dyes.

The promising results, characterized by short times and maximum efficiency, offer the possibility of developing a continuous process for the recovery of contaminated water and spent dye by reusing the zeolite until exhaustion. This continuous process will allow the recovered water to be reused in the same process, ensuring the protection of natural water by reducing industrial water consumption. Furthermore, it will reduce dye consumption by enabling the reuse of the recovered dye, thereby providing environmental and economic benefits to dye-consuming industries.

This industry-promoted approach advocates for greater environmental protection. Additionally, the fully spent zeolite could be reused in other infustrial processes, thus establishing a zero-waste process.

Therefore, the removal of dyes from contaminated waters in the textile industry through adsorption on zeolite derived from hazardous

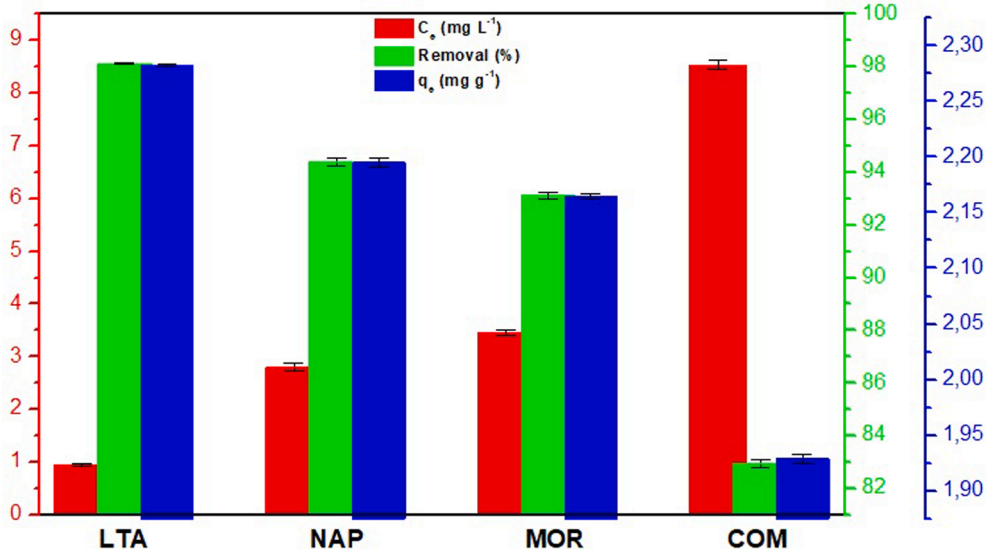

Fig. 6. Comparison between different zeolites on ST adsorption.

waste in the aluminum industry, represents an economical, efficient, and fully sustainable process.

Conclusion

The waste-based LTA zeolite showed an excellent removal efficiency, reaching a remarkable 98.12 % for the Safranine-T dye, demonstrating its promising potential as an effective treatment agent for dye-contaminated wastewater. The sorption process was extremely fast and efficient, requiring just 1 min of contact time for virtually complete removal of the dye. The utilization of thermodynamic and adsorption isothermal models revealed that the process of adsorption was spontaneous, displaying an exothermic nature, and occurred via physical mechanism between the Safranine-T molecules and the surface of LTA zeolite.

The optimal experimental conditions, determined statistically, consisted of a zeolite dosage of 21.5 g/L and agitation at 147 rpm. However, it is noteworthy that the zeolite dosage was the sole variable, expressed in linear and quadratic forms, exerting a significant influence on ST removal. The obtained R^2 value of 0.9927 indicates a high degree of correlation between experimental and predicted values. Furthermore, the ANOVA demonstrated the model validity at a 95 % confidence level without the need for adjustments.

The utilization of different zeolites in the ST adsorption process demonstrated that the waste-based LTA zeolite was the most efficient (98.1 %), exhibiting a removal capacity even higher than the commercial LTA zeolite (82.9 %). These findings can significantly contribute to sustainability and the circular economy. Furthermore, the application of the LTA zeolite synthesized using hazardous waste from the aluminum industry in the adsorption of textile dyes enables a mutual benefit (symbiosis) between these two industrial sectors, allowing for the co-recycling of aluminum waste while simultaneously treating wastewater with a high pollutant potential.

The results of this research can greatly contribute to sustainability and the circular economy. The highly promising adsorbent properties of the waste-based LTA zeolite applied to the treatment of dye-containing effluents provides a sustainable alternative to the use of materials produced with commercial reagents, thus reducing the consumption of resources, while helping to improve the water quality and mitigating environmental pollution.

CRediT authorship contribution statement

Magali Teresinha Ritter: Investigation, Data curation, Software, Formal analysis, Writing – original draft. **María Ángeles Lobo Recio:** Conceptualization, Writing – review & editing. **Isabel Padilla:** Methodology, Supervision, Writing – review & editing. **Maria Eliza Nagel Hassemer:** Funding acquisition and review. **Maximina Romero:** Funding acquisition, Writing – review & editing. **Aurora López Delgado:** Conceptualization, Supervision, Writing – review & editing.

Declaration of competing interest

The authors declare that they have no known competing financial interests or personal relationships that could have appeared to influence the work reported in this paper.

Acknowledgements

This research was supported by Eduardo Torroja Institute for Construction Sciences (IETcc-CSIC), the Brazilian National Council of Scientific and Technologic Development (CNPq) and the Coordination for the Improvement of the Higher-Level Personnel (CAPES)-finance code 001.

References

[1] R. Al-Tohamy, S.S. Ali, F. Li, K.M. Okasha, Y.-A.-G. Mahmoud, T. Elsamahy, H. Jiao, Y. Fu, J. Sun, A critical review on the treatment of dye-containing wastewater: Ecotoxicological and health concerns of textile dyes and possible remediation approaches for environmental safety, Ecotoxicol Environ. Saf. 231 (2022) 113160, https://doi.org/10.1016/j.ecoenv.2021.113160.

[2] A. Gholami, S.B. Mousavi, S.Z. Heris, M. Mohammadpourfard, Highly efficient treatment of petrochemical spent caustic efluente via electro-Fenton process for COD and TOC removal: optimization and experimental, Biomass Convers. Biorefinery. https://10.1007/s13399-023-03772-2.

[3] M.M. Kamel, I.H. Alsohaimi, M.S. Alhumaimess, H.M.A. Hassan, M.S. Alshammari, M.Y. El-Sayed, A glassy polyvinyl alcohol/silica gel hybrid composite for safranin removal: Adsorption, kinetic and thermodynamic studies, Res. Chem. Intermed 47 (3) (2021) 925–944, https://doi.org/10.1007/s11164-020-04309-2.

[4] B. Sieren, J. Baker, X. Wang, S.J. Rozzoni, K. Carlson, A. McBain, D. Kerstan, D. Allen, L. Liao, Z. Li, Sorptive removal of color dye Safranin O by fibrous clay minerals and zeolites, Adv. Mater. Sci. Eng. (2020) 1–12, https://doi.org/10.1155/2020/8845366.

[5] A. Tkaczyk, K. Mitrowska, A. Posyniak, Synthetic organic dyes as contaminants of the aquatic environment and their implications for ecosystems: A review, Sci. Total Environ. 717 (2020) 137222, https://doi.org/10.1016/j.scitotenv.2020.137222.

[6] S. Mishra, A. Maiti, The efficacy of bacterial species to decolourise reactive azo, anthroquinone and triphenylmethane dyes from wastewater: a review, Environ.

Sci. Pollution Res. 25 (9) (2018) 8286–8314, https://doi.org/10.1007/s11356-018-1273-2.
[7] C.R. Holkar, A.J. Jadhav, D.V. Pinjari, N.M. Mahamuni, A critical review on textile wastewater treatments: Possible approaches, J. Environ. Manag. 182 (2016) 351–366, https://doi.org/10.1016/j.jenvman.2016.07.090.
[8] B. Sarwar, A.U. Khan, M. Aslam, A. Bokhari, M. Mubashir, A.A. Alothman, M. Ouladsmane, S.A. Aldossari, W.S. Chai, K.S. Khoo, Comparative study of ZIF-8-materials for removal of hazardous compounds using physio-chemical remediation techniques, Environ. Res. 220 (2023) 115168, https://doi.org/10.1016/j.envres.2022.115168.
[9] UNEP – UN Environment Programme. UN Environ. 2018 Annual Report. https://www.unep.org/resources/unenvironment-2018-annual-report, 2018 (accessed on May 10, 2023).
[10] W. Li, Z. Xie, S. Xue, H. Ye, M. Liu, W. Shi, Y. Liu, Studies on the adsorption of dyes, Methylene blue, Safranin T, and Malachite green onto polystyrene foam, Separ. Purif. Technol. 276 (2021) 119435, https://doi.org/10.1016/j.seppur.2021.119435.
[11] R. Shu, Q. Qiao, F. Guo, K. Dong, S. Liu, L. Xu, Y. Bai, N. Zhou, Controlled design of Na–P1 zeolite/ porous carbon composites from coal gasification fine slag for high-performance adsorbent, Environ. Res. 217 (2023) 114912, https://doi.org/10.1016/j.envres.2022.114912.
[12] Y. Shi, X. Wang, X. Wang, K. Carlson, Z. Li, Removal of toluidine blue and safranin O from single and binary solutions using zeolite, Crystals 11 (10) (2021) 1181, https://doi.org/10.3390/cryst11101181.
[13] V.K. Gupta, A. Mittal, R. Jain, M. Mathur, S. Sikarwar, Adsorption of Safranin-T from wastewater using waste materials - activated carbon and activated rice husks, J. Colloid Interface Sci. 303 (1) (2006) 80–86, https://doi.org/10.1016/j.jcis.2006.07.036.
[14] S. Saha, S.K. Shukla, H.R. Singh, K.K. Pradhan, S.K. Jha, Production and purification of bioflocculants from newly isolated bacterial species: a comparative decolourization study of cationic and anionic textile dyes, Environ. Technol. 42 (23) (2021) 3663–3674, https://doi.org/10.1080/09593330.2020.1737737.
[15] M. Suleman, M. Zafar, A. Ahmed, M.U. Rashid, S. Hussain, A. Razzaq, N. A. Mohidem, T. Fazal, B. Haider, Y.-K. Park, Castor leaves-based biochar for adsorption of Safranin from textile wastewater, Sustainability 13 (12) (2021) 6926, https://doi.org/10.3390/su13126926.
[16] R. Jialiang, W. Chu, Z. Yueping, C. Haiyan, Biodegradation of Safranine T by an isolated bacterium Pseudomonas aeruginosa WZS-A, In World Automation Congress, IEEE, 2012, pp. 1-4.
[17] I. Ghosh, S. Kar, T. Chatterjee, N. Bar, S.K. Das, Adsorptive removal of Safranin-O dye from aqueous medium using coconut coir and its acid-treated forms: Adsorption study, scale-up design, MPR and GA-ANN modeling, Sustainable Chem. and Pharm. 19 (2021) 100374, https://doi.org/10.1016/j.scp.2021.100374.
[18] S. Sharafinia, A. Farrokhnia, E.G. Lemraski, The adsorption of cationic dye onto ACPMG@ZIF-8 core-shell, optimization using central composite response surface methodology (CCRSM), Colloids Surf. a: Physicochem. Eng. Aspects 634 (2022) 128039, https://doi.org/10.1016/j.colsurfa.2021.128039.
[19] A. Srivastava, R.M. Rani, D.S. Patle, S. Kumar, Emerging bioremediation technologies for the treatment of textile wastewater containing synthetic dyes: a comprehensive review, J. Chem. Technol. Biotechnol. 97 (1) (2021) 26–41, https://doi.org/10.1002/jctb.6891.
[20] A.C.J. Tacas, P.-W. Tsai, L.L. Tayo, C.-C. Hsueh, S.-Y. Sun, B.-Y. Chen, Degradation and biotoxicity of azo dyes using indigenous bacteria-acclimated microbial fuel cells (MFCs), Process Biochem. 102 (2021) 59–71, https://doi.org/10.1016/j.procbio.2020.12.003.
[21] M. Ashrafivala, S.B. Mousavi, S.Z. Heris, M. Heidari, M. Mohammadpourfard, H. Aslani, Investigation of H2O2/UV advanced oxidation process on the removal rate of coliforms from the industrial effluent: A pilot-scale study, Int. J. Hydrogen Energy 47 (78) (2022) 33530–33540, https://doi.org/10.1016/j.ijhydene.2022.07.231.
[22] S. Yadav, A. Yadav, N. Bagotia, A. Sharma, S. Kumar, Novel composites of Pennisetum glaucum with CNT: preparation, characterization and application for the removal of safranine O and methylene blue dyes from single and binary systems, Biomass Convers. Biorefinery (2022), https://doi.org/10.1007/s13399-021-02240-z.
[23] M.Á. Lobo-Recio, C. Rodrigues, T.C. Jeremias, F.R. Lapolli, I. Padilla, A. López-Delgado, Highly efficient removal of aluminum, iron, and manganese ions using Linde type-A zeolite obtained from hazardous waste, Chemosphere 267 (2021) 128919, https://doi.org/10.1016/j.chemosphere.2020.128919.
[24] V.P. Mallapur, J.U.K. Oubagaranadin, A brief review on the synthesis of zeolites from hazardous wastes, Trans. Indian Ceramic Soc. 76 (1) (2017) 1–13, https://doi.org/10.1080/0371750X.2016.1231086.
[25] F. Collins, A. Rozhkovskaya, J.G. Outram, G.J. Millar, A critical review of waste resources, synthesis, and applications for Zeolite LTA, Micropor. Mesopor. Mater. 291 (2020) 109667, https://doi.org/10.1016/j.micromeso.2019.109667.
[26] S. Lin, X. Jiang, Y. Zhao, J. Yan, Zeolite greenly synthesized from fly ash and its resource utilization: A review, Sci. Total Environ. 851 (2022) 158182, https://doi.org/10.1016/j.scitotenv.2022.158182.
[27] A. López-Delgado, J.I. Robla, I. Padilla, S. López-Andrés, M. Romero, Zero-waste process for the transformation of a hazardous aluminum waste into a raw material to obtain zeolites, J. Clean. Production 255 (2020) 120178, https://doi.org/10.1016/j.jclepro.2020.120178.
[28] M.R. Abukhadra, A.S. Mohamed, Adsorption removal of Safranin dye contaminants from water using various types of natural zeolite, SILICON 11 (3) (2019) 1635–1647, https://doi.org/10.1007/s12633-018-9980-3.
[29] G. Atun, G. Hisarli, A.E. Kurtoglu, N. Ayar, A comparison of basic dye adsorption onto zeolitic materials synthesized from fly ash, J. Hazard. Mater. 187 (1–3) (2011) 562–573, https://doi.org/10.1016/j.jhazmat.2011.01.075.
[30] N. Ayar, G. Keçeli, A.E. Kurtoglu, G. Atun, Cationic dye adsorption onto natural and synthetic zeolites in the presence of Cs + and Sr 2+ ions, Toxicol. Environ. Chem. 97 (1) (2014) 11–21, https://doi.org/10.1080/02772248.2014.949264.
[31] S. Das, S. Barman, R. Thakur, Studies on removal of Safranine-T and Methyl Orange dyes from aqueous solution using NaX zeolite synthesized from fly ash, J. Environ. Sci. Eng. 2 (4) (2013) 735–747.
[32] P.M. Pereira, B.F. Ferreira, N.P. Oliveira, E.J. Nassar, K.J. Ciuffi, M.A. Vicente, R. Trujillano, V. Rives, A. Gil, S. Korili, E.H. Faria, Synthesis of zeolite A from metakaolin and its application in the adsorption of cationic dyes, Appl. Sci. 8 (4) (2018) 608, https://doi.org/10.3390/app8040608.
[33] R. Sánchez-Hernández, A. López-Delgado, I. Padilla, R. Galindo, S. López Andrés, One-step synthesis of NaP1, SOD and ANA from a hazardous aluminum solid waste, Micropor. Mesopor. Mater. 226 (2016) 267–277, https://doi.org/10.1016/j.micromeso.2016.01.037.
[34] R.F. Nascimento, A.C.A. Lima, C.B. Vidal, D.Q. Melo, G.S.C. Raulino, Adsorção: Aspectos Teóricos e Aplicações Ambientais, Fortaleza: Imprensa Universitária, Brazil, 2014, pp. 1-258.
[35] G.E.P. Box, W.G. Hunter, J.S. Hunter, Fractional factorial design at two levels. Statistics for experimenters: an introduction to design, data analysis, and model building, John Wiley & Sons Inc, New Jersey, 1978, pp. 374–418.
[36] S. Lagergren, About the theory of so-called adsorption of soluble substances, K. Sven. Vetenskapsakademiens Handl. 24 (1989) 1–39.
[37] Y.S. Ho, G. Mckay, Pseudo-second order model for sorption processes, Process Biochem. 34 (5) (1999) 451–465, https://doi.org/10.1016/S0032-9592(98)00112-5.
[38] W.J. Weber, J.C. Morris, Kinetics of adsorption on carbon from solution, J. Sanit. Eng. Div. 89 (1963) 31–59, https://doi.org/10.1061/JSEDAI.0000430.
[39] S.Y. Elovich, O.G. Larinov, Theory of adsorption from solutions of non-electrolytes on solid (I) equation adsorption from solutions and the analysis of its simplest form, (II) verification of the equation of adsorption isotherm from solutions, Izv. Akad. Nauk. SSSR, Otd. Khim. Nauk. 2 (1962) 209–216.
[40] J. Wang, X. Guo, Adsorption kinetic models: Physical meanings, applications, and solving methods, J. Hazard. Mater. 390 (2020) 122156, https://doi.org/10.1016/j.jhazmat.2020.122156.
[41] K.Y. Foo, B.H. Hameed, Insights into the modeling of adsorption isotherm systems, Chem. Eng. J. 156 (1) (2010) 2–10, https://doi.org/10.1016/j.cej.2009.09.013.
[42] N. Ayawei, A.N. Ebelegi, D. Wankasi, Modelling and interpretation of adsorption isotherms, J. Chem. (2017) 1–11, https://doi.org/10.1155/2017/3039817.
[43] H.M.F. Freundlich, Over the adsorption in solution, J. Phys. Chem. 57 (1906) 385–471.
[44] I. Langmuir, The constitution and fundamental properties of solids and liquids, J. Am. Chem. Soc. 38 (1916) 2221–2295.
[45] M.M. Dubinin, L.V. Radushkevich, The equation of the characteristic curve of the activated charcoal, Proc. Union Sov. Social. Republics Acad. Sci. 55 (1947) 331–337.
[46] R. Sips, Combined form of Langmuir and Freundlich equations, J. Phys. Chem. 16 (1948) 490–495.
[47] J. Toth, State equations of the solid gas interface layer, Acta Chim. Acad. Sci. Hungar. 69 (1971) 311–317.
[48] O. Redlich, D.L. Peterson, A useful adsorption isotherm, J. Phys. Chem. 63 (1959) 1024–1026.
[49] M.I. Temkin, V. Pyzhev, Kinetics of ammonia synthesis on promoted iron catalyst, Acta Phys. Chim. USSR 12 (1940) 327–356.
[50] S. Kaur, S. Rani, R.K. Mahajan, M. Asif, V.K. Gupta, Synthesis and adsorption properties of mesoporous material for the removal of dye safranin: Kinetics, equilibrium, and thermodynamics, J. Ind. Eng. Chem. 22 (2014) 19–27, https://doi.org/10.1016/j.jiec.2014.06.019.
[51] D. Núñez-Gómez, F.R. Lapolli, M.E. Nagel-Hassemer, M.Á. Lobo-Recio, Optimization of acid mine drainage remediation with central composite rotatable design model, Energy Procedia 136 (2017) 233–238, https://doi.org/10.1016/j.egypro.2017.10.248.
[52] Q. Hu, S. Pang, D. Wang, In-depth insights into mathematical characteristics, selection criteria and common mistakes of adsorption kinetic models: A critical review, Separ. Purif. Reviews 51 (3) (2021) 281–299, https://doi.org/10.1080/15422119.2021.1922444.
[53] V. Puccia, M.J. Avena, On the use of the Dubinin-Radushkevich equation to distinguish between physical and chemical adsorption at the solid-water interface, Colloid Interface Sci. Commun. 41 (2021) 100376, https://doi.org/10.1016/j.colcom.2021.100376.
[54] S. Hosseini Nami, S.B. Mousavi, Nitrate removal performance of different granular adsorbents using a novel Fe-exchanged nanoporous clinoptilolite, Ind. Eng. Chem. Res. 62 (2023) 3659, https://doi.org/10.1021/acs.iecr.2c03308.
[55] P. Wang, Q. Sun, Y. Zhang, J. Cao, Synthesis of zeolite 4^{a} from kaolin and its adsorption equilibrium of carbono dioxide, Materials 12 (9) (2019) 1536, https://doi.org/10.3390/mai2091536.
[56] O. Korkuna, R. Leboda, J. Skubiszewska-Zieba, T. Vrublevska, V.M. Gunko, J. Ryczkowski, Structural and physicochemical properties of natural zeolites: clinoptilolite and mordenite, Micropor. Mesopor. Mater. 87 (3) (2006) 243–254, https://doi.org/10.1016/j.micromeso.2005.08.002.